MATHEMATICAL MODELLING OF FIXED-BED REACTORS

o-O-o

A thesis submitted for the degree of

Doctor of Philosophy

in

The University of Leeds

by

David Leslie Cresswell, B.Sc. (Leeds)

under the direction of

C. McGreavy, B.Sc. (Leeds), D.Eng. (Yale), A.M.I.Ch.E., C.Eng., F.B.C.S.

o-O-o

Department of Chemical Engineering
Houldsworth School of Applied Science
University of Leeds

January 1969

D L Cresswell

ABSTRACT

Consideration is given to the solution of the highly exothermic fixed bed catalytic reactor problem taking into account heat and mass transfer resistances inside the catalyst pellets and across the external fluid film, as well as radial temperature and concentration gradients in the fluid phase.

Comparison of the model with the simpler quasi-homogeneous represenation is made. In the region where the quasi-homogeneous case predicts temperature "run-away", the added refinements assume some importance. Very significant differences in behaviour are predicted. Indeed no temperature "run-away" is apparent.

Including simply a film mass and heat transfer resistance is no guarantee that temperature "run-away" will not be predicted. In fact, it is the particle diffusive resistance which is the main factor limiting the temperature effects. Since the region of temperature "run-away" is often in the practical range it is essential to use a more detailed model for design such as the one described here, especially if optimal operating conditions are being sought.

Even on large digital computers, the computation time is excessively long if the sets of differential equations are solved simultaneously. By examining the intraparticle equations in detail for a practical range of physical properties and operating conditions, it is shown that they may be reduced to a lumped parameter form. While still retaining the characteristics of the general problem, the lumped parameter approximation can be solved in a substantially shorter time, thus making its use in optimization and control studies feasible.

ACKNOWLEDGMENTS

I am indebted to many colleagues for their assistance at some time during this work, but particularly to Dr. McGreavy for his continued encouragement and timely suggestions. I am particularly grateful to J. M. Thornton and K. Turner for their interest and assistance with some of the computations.

Only those who have typed such a manuscript as this will properly appreciate the care and patience of my typists, Miss Bennion and Mrs. Manning, who interpreted my scribblings to produce an excellent typescript.

My thanks are also due to the Science Research Council for making this project possible.

Finally, but by no means least, I am indebted to my parents for their drive and determination to see my research to its conclusion. Their sighs of relief at finally seeing the thesis in print are only exceeded by my own.

LIST OF CONTENTS

LIST OF FIGURES

LIST OF TABLES

To Jean

whose understanding and good humour
are as perfect as her proofreading.

o O o

CHAPTER 1

INTRODUCTION TO THE DESIGN OF PACKED BED REACTORS : RESEARCH OBJECTIVES

1.1 Introduction

The packed bed chemical reactor is a long established method in the chemical industry of contacting gaseous reaction mixtures with solid catalysts. Commercial applications are numerous and varied, e.g., the oxidation of SO_2, the synthesis of ammonia, a multitude of hydrocarbon transformation processes ranging from the cracking reactions of the petroleum industry to the important partial oxidation reactions such as the manufacture of phthalic anhydride from o-xylene or naphthalene. Such reactors normally consist of a cylindrical tube packed with catalyst particles. The reactants are passed through the tube and converted into products in an amount which is governed by parameters of the system such as feed concentration and temperature, flow rate, tube length etc.

Many gas-solid reactions of industrial importance are accompanied by the liberation of large amounts of heat. A highly exothermic reaction raises the temperature of the system as conversion progresses which is desirable from the point of view of reducing the size of the reactor, but for other reasons is undesirable. Too high a "hot spot" temperature in the reaction mixture may lead to the promotion of unwanted side reactions or cause damage to the catalyst or the tube itself. In these cases provision is made for removing heat from the system in order to keep the "hot spot" temperature within a reasonable bound. Conventionally, this is achieved by building up the reactor with a number of small diameter tubes (1" is not uncommon) encased in a single body through which is circulated a cooling medium. Some novel innovations in design have been undertaken in an attempt to achieve better control

over the "hot spot" temperature. PARIS and STEVENS[124] proposed a jacket design comprising several sections, with different rates of cooling in each. CALDERBANK, CALDWELL and ROSS[125] studied the effect of mixing pellets of catalyst and inert material in such a way as to achieve a particular optimum temperature profile. An important consideration in the design of reactors to carry out highly exothermic reactions is, therefore, the "hot spot" temperature.

It is well known in practice that such reactors sometimes go out of control. Thus, the temperature at some point may rise rapidly after a minor upset and burn out a tube. Or a system may be set into strong thermal oscillation due to temperature perturbations and rapidly deactivate the catalyst. Recognition of the circumstances which can cause such effects and knowledge of how to prevent them are important aspects of reactor design. With the increasing importance of exothermic reactions in industry the need for a reliable method of designing packed bed reactors is apparent.

1.2 Design methods : experimental vs. theoretical

The most obvious basis for design of a commercial reactor is the pilot scale model. Experiments can be carried out on the model to determine the region of "safe" operation. The commercial reactor is then built and operated within this region. This technique is usually successful but is both time-consuming and expensive. Also, scale-up problems may be troublesome.

In view of the disadvantages of this method a theoretical treatment is required. The approach adopted in the thesis is a theoretical one.

At present the field of reactor design is in a period of transition between the extremes of pilot plant experimentation and theoretical analysis. The state of affairs in existence requires the following strategy:-

(1) A mathematical model is set up which contains what are believed to be the important mechanisms necessary to give an accurate description of a commercial reactor. Some of the parameters of the model might be reasonably estimated from existing correlations. Others have to be obtained experimentally.

(2) Laboratory scale units are constructed which are designed to measure the unknown parameters. The basic postulates of the mathematical model are made use of in formulating an experimental programme. Since the assumed controlling processes are identified individually they can be measured in isolation from the remainder. Thus a series of experiments is set up in which one particular effect is studied. These experiments may be designed, for example, to procure surface kinetic data, thermodynamic data, mass and heat transfer data, etc.

(3) The data, some measured, some estimated, are then used in the mathematical model and theoretical predictions of the reactor performance are obtained by solving the energy, momentum and material balance equations.

(4) As a final stage the experimental reactor is run under reaction conditions so as to confront the mathematical results with actual experimental data. This confrontation is very important in establishing the validity of the mathematical treatment. Depending on the outcome it may be necessary to return to the first stage and update the mathematical model.

The ideal situation, of course, is one in which a reliable mathematical model is available, and all the relevant kinetic, thermodynamic and transport data are at hand. In practice, this ideal is rarely in existence and is unlikely to be for some years.

Most design problems involve only a steady state model, but the increasing importance of optimization and control has emphasized the

need for dynamic models. A pre-requisite for the latter is certainly a good steady state model, and because time constants on large plants tend to be relatively large, the transient can often be approximated by a sequence of pseudo steady states. A reliable steady state model is therefore a useful step forward.

1.3 Theoretical design methods : current status

No review can be undertaken without acknowledgement of HOUGEN'S[47] classic presentation which outlines the status of engineering aspects of solid catalysis (1961). More recently, CARBERRY[122] (1966) reviews in depth some of the problems confronting the designer. A further invaluable review article is presented by FROMENT[90] (1967). Recent books in the fields of catalysis and reactor design include SATTERFIELD and SHERWOOD[15] (1963), PETERSEN[27] (1965), THOMAS and THOMAS[126] (1967).

A summary of the more significant advances in theoretical design methods is given at this point in order to set in perspective the objectives behind this research.

The need for external cooling of exothermic reactors was stressed in Section 1.1. In these circumstances it is inevitable that temperature gradients must appear perpendicular to the direction of flow. Since the extent of conversion is dependent on temperature, radial concentration gradients must also appear. Gradients in the axial direction must, of course, exist due to the convective flow. It follows, therefore, that a mathematical model of the non-isothermal reactor must be <u>at least</u> two-dimensional. However, a preliminary design is often based on a one-dimensional approximation in which only longitudinal gradients in concentration and temperature are considered. It is assumed that radial transport of heat and mass in the reactor itself is instantaneous and that resistance to heat transfer may be lumped at the tube wall. With the assumptions of no resistance to heat or mass transfer within the

packing or between fluid and packing and no axial diffusion or conduction, BARKELEW[127] (1959) studied the stability of packed bed reactors and developed some empirical correlations on the basis of steady state equations.

The general availability of high-speed digital computers in the last decade was undoubtedly instrumental in providing a new incentive to these mathematical studies. Thus, FROMENT[37] (1962) considered a two-dimensional model in which radial transport of heat and mass were assumed to occur by conduction and diffusion-like processes. Again, however, no allowance was made for transport between the phases or within the catalyst pellets. He demonstrated that serious radial gradients may occur and, when this is the case, the one-dimensional model cannot be accurately applied. Further, he observed the phenomenon of "parametric sensitivity", a type of behaviour which exists when small changes in a parameter induce large changes in steady state conditions. A similar behaviour was observed earlier by BARKELEW, and BILOUS and AMUNDSON[128]. LIU and AMUNDSON[76-78] (1962-3) studied the stability problem by analyzing the transient response of the system to some fluctuation, but were restricted to a one-dimensional dynamic model by computational limitations. However, they did account for transport between the phases, albeit in an elementary manner, by lumping the heat and mass transfer resistances at the particle surface with the only intra-particle effect being that of chemical reaction. CARBERRY and WENDEL[10] (1963) considered a one-dimensional steady state model including axial dispersion of heat and mass for a complex reaction scheme, $A \rightarrow B \rightarrow C$. Their treatment of the processes occurring between the fluid and the internal 'active' surface of the catalyst was the most ambitious yet attempted at that time. Intraparticle diffusion of reacting species as well as interparticle heat and mass transport was

taken into account, but the existence of a temperature gradient inside the porous catalyst was ignored, probably to simplify the solution. The results showed that axial dispersion of heat and mass exerts a negligible effect on performance unless the bed is extremely shallow. By far the most important detriment to high yield of desirable intermediate B was due to "pore" diffusion. MICKLEY and LETTS[92] (1963-4) extended the two-dimensional model to the case of multiple reactions with arbitrary rate expressions and stoichiometry.

The developments described above have one common denominator; they lead to continuum models, i.e., the dependent variables of the system are continuous functions of the reactor axial and radial coordinates. Even the analyses of LIU and AMUNDSON, CARBERRY and WENDEL which introduce the idea of discrete particles into the physical model lead to a mathematical system which itself is a continuum model. While the physical picture is rather simple, the actual calculations are complicated, especially for the non-isothermal reactor. The main reason is that the mathematical models which simulate the physical situation lead to a simultaneous system of partial differential equations which have to be integrated numerically in a two-dimensional network, at least for the more realistic models.

In order to overcome the difficulties of solving boundary-value partial differential equations DEANS and LAPIDUS[12] (1960) proposed an altogether different type of primary representation of the reactor. It is based on the fundamentally heterogeneous nature of the packed bed; particle diameter becomes the natural measure of length, and the void volume associated with a particle is taken as the volume element for the balances. Known as the "finite stage model", this representation views all transport in the fluid phase other than by the bulk flow to occur as a result of a sequence of mixing events in a two-dimensional

array of perfect mixers. The steady state equations, written for each stage, are algebraic and seemingly altogether more tractable than the case of nonlinearly coupled partial differential equations. McGUIRE and LAPIDUS[39] (1965) used this model to study the stability of a detailed packed bed reactor which included transport mechanisms both within the packing and between the fluid and the external surface of the packing. They concentrated attention on a very limited range of conditions and found computation times to be excessive unless the bed was made very short (e.g., 15 particle diameters). Recently, VANDERVEEN, LUSS and AMUNDSON[129] (1968) studied the stability of adiabatic packed bed reactors using first a simple cell model and then one with coupling between the particles. With a cell approach they were able to gain more insight into the stability problem than with the continuous model proposed earlier (76). Of further interest is the fact that the computation time was decreased by a factor of twenty. CALDERBANK, CALDWELL and ROSS[125] (1968) explored the possibilities of the dilution of the catalyst by inert particles for the control of the temperature profile in an exothermic reactor. Their two-dimensional mathematical model can be considered to be a refinement of the mixing cell system of DEANS and LAPIDUS. Here, the continuous mixing and splitting of streamlines, which is essentially the origin of radial dispersion in fixed beds, is simulated by a sequence of triangular matrices of mixing cells representing the sequence of single layers of close-packed spherical particles.

1.4 Research objectives

A characteristic feature of the so called "quasihomogeneous" model, detailed by FROMENT[37] and others, is its tendency to exhibit "parametric sensitivity". Small changes in the temperature of the feed or the jacket may produce temperature "run-aways" or "hot spots". A similar tendency may occur with small adjustments in the heat transfer data

which may be required over a period due to changes in the heat transfer characteristics of the bed and the tube wall itself. Much research has been undertaken to recognize the conditions under which "parametric sensitivity" can occur. Novel innovations such as the "diluted-catalyst" reactor of CALDERBANK et al[125] and, complementary to it, the work of PARIS and STEVENS[124] on jacket design have been introduced in an attempt to overcome the problem of temperature "run-aways".

This critical region, in which temperature "run-away" occurs, is a very important one from a commercial standpoint. For a conventional reactor displaying constant conditions along the tube wall, a high conversion can only be obtained if at the same time a "hot spot" is accepted. As a compromise the reactor is usually operated in a sub-critical region in which conversion is lowered and the temperature is such that the catalyst does not deactivate too rapidly or have its selectivity adversely affected. It is conceivable someday that economic considerations will dictate that a reactor be operated in the critical region with a tight control system to prevent "run-away". The problem of regeneration of the catalyst is a serious one. Often the catalyst is too valuable to discard. Frequent shut-down and start-up of the reactor is an expensive procedure. Even if regeneration can be carried out with the catalyst in place, continuous operation demands auxiliary reactors which adds to the initial cost of installation.

With these economic factors in mind the following consideration is relevant, namely:

1. What level of sophistication is needed in a model of the packed bed reactor to describe all essential characteristics quantitatively, while still using well-defined physical parameters to represent the phenomenological processes?

Heretofore, no practical mathematical modal has been available for

combining the environmental and reaction phenomena. To carry out the first objective a number of models of increasing sophistication are constructed, ranging from the quasihomogeneous representation to a detailed model including both finite rates of heat and mass transfer inside the particles and between the fluid and the external surface of the particles. This then leads on to the following consideration:

2. Is the detailed model suitable in terms of available high-speed digital computers for evaluation of solutions?

If it is to be of practical as well as academic interest the model must be mathematically tractable. Solutions must be obtainable either analytically or by numerical means at acceptable cost and in a fairly short time.

Looking further ahead to the use of mathematical models in optimization and control, a further profitable avenue of research is opened up in the development of model reduction techniques. Clearly a sound basis for this is a detailed knowledge of the properties of the basic model.

The requirement of a satisfactory model reduction technique is that it should lead to a simpler model which permits the retainment of the essential features of the system, but removes much of the mathematical complexity associated with the detailed model.

The enquiry made here, in this respect, forms the first step in a research programme designed to eventually integrate mathematical models of the packed bed reactor into optimization and computer control strategies.

CHAPTER 2

FORMULATION OF THE GENERALIZED MODEL

In formulating a generalized model of a packed-bed reactor particular attention must be paid to its compatibility within the framework of current knowledge in the field. If the model is to be of practical value it must only contain parameters which are well-defined in the sense that they may be determined from independent experiments or from correlations available in the literature. Consequently, attention will be confined to a restricted set of equations but one which is sufficiently general so as to contain all the mechanisms believed to be necessary to accurately describe the behaviour of a commercial reactor.

2.1 Conceptual problems

Fixed bed processes are inherently discrete in character and as such do not lend themselves readily to rigorous mathematical modelling.

In a real bed of particles the concentrations and temperatures do not vary smoothly throughout the confines of the bed, but rather there are concentration and temperature structures around and within each particle with a scale of the order of a particle itself. This short range structure is superimposed upon a longer range structure which more closely approximates the progress of the reaction as the reacting gases pass through the bed. A rigorous mathematical description of this type of behaviour, which is typical of all fixed-bed processes, is intractable. Instead, a statistical description appears to offer more promise.

As the statistical description depends on some kind of averaging to represent the properties of the bed as functions of position, the property is averaged over a representative region of the bed having the same order of magnitude as a particle of packing. For the solid, this region is simply the volume of a particle. For the fluid, the region

is more obscure but may be thought of as being bounded by constrictions in the passages among the particles, or, more vaguely, as simply a "hole" in the packing. In practice, these regions vary in both size and shape throughout the bed, so that at best the average of a property is only approximately a smooth function of position.

The formulation of the equations is based on the assumption that it is possible to choose the size of the differential volume sufficiently large to contain a considerable number of particles, and yet be consistent with the requirement of uniformity of temperature and concentrations within the differential volume. While these two assumptions are to some degree self-contradictory, similar assumptions in the field of turbulence theory have met with notable success. It is to be hoped that knowledge of the structure of packed beds will develop sufficiently to allow consideration of spatially fluctuating properties. At the present time understanding in this area is minimal.

2.2 The mathematical model

For the purpose of illustrating the physical significance of the various terms which make up the design equations, this section will be broken down into 3 parts. The first sub-section will deal with the mathematical description of the global (fluid) phase. This section will be followed by a discussion of the transport and reactive processes occurring in the particulate phase. Finally, something will be said about transport between the two phases. Wherever applicable, definitive statements will be corroborated by experimental findings. Further discussion of the physical properties of porous catalysts and the phenomenological parameters of packed beds is to be found in Chapters 3 and 9.

2.2.1 Model of transport in the fluid phase

Consider a differential volume of a packed bed reactor. Then the Fourier-Poisson equations for heat transfer and mass transfer of species i in the fluid phase are given by

$$\partial/\partial\theta(\varrho c_f T_f) = -\text{div}(-k' \text{ grad } T_f) - \text{div}(\vec{G} c_f T_f) - \varrho_B(-\Delta H_j)\,\eta_j R_j^* \qquad (2.1)$$

$$\partial C_{fi}/\partial\theta = -\text{div}(-D \text{ grad } C_{fi}) - \text{div}(\vec{V} C_{fi}) + \varrho_B \eta_i R_i^* \qquad (2.2)$$

(i = 1, 2,....N, where N is the number of chemical species present)

The actual velocity $\vec{V}$ at any point in the bed may be expressed as the vector sum of the superficial velocity $\vec{V}_o$ and a fluctuating velocity $\vec{v}$, characteristic of the point in question and caused largely by deflections of the fluid by catalyst particles. Then

$$\vec{V} = \vec{V}_o + \vec{v} \qquad (2.3)$$

Similarly, the actual point concentration C_{fi} is expressed in terms of the concentration averaged over the differential volume $\overline{C}_{fi}$, and a concentration fluctuation, c_{fi}, due to the fluctuating velocity.

$$C_{fi} = \overline{C}_{fi} + c_{fi} \qquad (2.4)$$

Using equations (2.3) and (2.4) in equation (2.2) and averaging over the differential volume and assuming steady state, it follows that

$$-\text{div}(-D \text{ grad } \overline{C}_{fi}) - \text{div}(\vec{V}_o \overline{C}_{fi}) - \text{div } \overline{\vec{v} c_{fi}} + \varrho_B \eta_i \overline{R}_i^* = 0 \qquad (2.5)$$

since the average of gradients of velocity and concentration fluctuations disappear.

The term $-\text{div } \overline{\vec{v} c_{fi}}$ is the one which gives rise to the flux due to the fluctuations caused by the catalyst particles. The axial component

of this flux may be generally neglected compared with the much larger flux due to the convective flow. An assessment of the lateral flux follows from methods analagous to those used in the elementary kinetic theory of gases[1, 27].

Consider three parallel planes perpendicular to the lateral direction, the distance between the planes being $\lambda/2$, where λ is a suitable mean free path. Suppose the central plane is situated at a lateral position r and assume that material crossing this plane in a positive (or negative sense) originated from the plane at $r - \lambda/2$ (or $r + \lambda/2$). Let v_l denote the average of the absolute values of the lateral velocity fluctuations. The flux originating from any plane is proportional to $v_l . \overline{C}_{fi}$. Thus the flux crossing the central plane in a positive sense is proportional to $(v_l . \overline{C}_{fi})_r - \lambda/2 . \text{grad}_l (v_l . \overline{C}_{fi})$, while the flux crossing the central plane in a negative sense is proportional to $(v_l . \overline{C}_{fi})_r + \lambda/2 . \text{grad}_l (v_l . \overline{C}_{fi})$ where terms of second and higher orders in λ are neglected. Hence, the net flux due to fluctuations is

$$\overline{\vec{v}\, c_{fi}} \propto - \lambda \, \text{grad}_l (v_l \, \overline{C}_{fi}),$$

or since $v_l \propto V_o$ and assuming that the mean free path is proportional to pellet diameter

$$\overline{\vec{v}\, c_{fi}} = -K . l . \text{grad}_l (V_o \, \overline{C}_{fi}), \qquad (2.6)$$

where K is a constant characteristic of the packing only. Substituting equation (2.6) into (2.5), it follows that

$$-\text{div}(-D \, \text{grad}_l \, \overline{C}_{fi}) \; -\text{div}(-K . l . \text{grad}_l (V_o \, \overline{C}_{fi})) \; -\text{div}(\vec{V}_o \, \overline{C}_{fi})$$

$$+ \varrho_B \, \eta_i \, \vec{R}_i^* = 0 \qquad (2.7)$$

A similar treatment of equation (2.1) leads to

$$-\text{div}(-k' \, \text{grad}_l \, \overline{T}_f) \; -\text{div}(-K . l . \text{grad}_l \, (G_o \, c_f \, \overline{T}_f)) \; -\text{div}(\vec{G}_o \, c_f \, \overline{T}_f)$$

$$- \varrho_B (-\Delta H_j) \, \eta_j \, \vec{R}_j^* = 0 \qquad (2.8)$$

Equations (2.7) and (2.8) each consist of four terms and an appreciation of the physical significance of each term is presented below in order to solidify a mental image of the processes involved.

$$-\text{div}(-k' \text{grad}_1 \bar{\bar{T}}_f),\ -\text{div}(-D \text{ grad}_1 \bar{\bar{C}}_{fi}) ;$$

These terms represent, respectively, lateral fluxes of heat and mass in the fluid within the differential volume of the packed bed owing to molecular conduction and diffusion processes. k' and D represent the molecular thermal conductivity and diffusivity of the fluid. Subscript $_1$ indicates lateral flux component, and - over a symbol denotes a space - averaged property. T_f and C_{fi} designate fluid temperature and point molar concentration (on volume fluid basis) of component i.

$$-\text{div}\left\{-K.l.\text{grad}_1(G_o c_f \bar{T}_f)\right\},\ -\text{div}\left\{-K.l.\text{grad}_1(V_o \bar{C}_{fi})\right\} ;$$

Accumulation of heat and mass may also occur by a transverse flux due to the fluctuations caused by the catalyst pellets. This lateral flux results from an eddy diffusion process, a process so named because of the apparent similarity in the mathematical forms of the eddy diffusive and molecular diffusive fluxes. It is generally understood that transverse eddy diffusion results from a random walk of elements of fluid through the passages in the bed[1], or equivalently, from mixing of converging streams[2, 3]. Experimental data are available[4, 5] which substantiate the usefulness of the eddy diffusion concept. It will suffice for present understanding to say that K is a constant characteristic of the packing only, and l represents some characteristic pellet length. The determination of these quantities is discussed in the text of PETERSEN[27]. G_o and V_o represent the superficial mass flow rate and velocity. c_f is the mean specific heat of the reaction mixture in the differential volume of the bed.

Axial fluctuations in the direction of flow lead to an effective axial diffusion term. This term arises primarily from the stagewise mixing in the interstices of the bed[6, 7], with a contribution due to the variation in mass velocity with radial position[8, 9]. It is usual to neglect this diffusive flux in comparison with the much larger axial flux due to the convective flow. While this rule of thumb is undoubtedly a good one, it is important to be aware of the conditions under which it will fail. CARBERRY and WENDEL[10] considered the consecutive reaction $A \rightarrow B \rightarrow C$ in a tubular packed-bed reactor operating adiabatically. They showed the influence of axial dispersion of heat and mass upon conversion and the "hot spot" to be negligible so long as the bed depth is greater than about 50 particle diameters. Similar conclusions are drawn from the isothermal case[11]. The neglect of axial mixing effects seems to be permitted in industrial reactors where the flow velocity is high and where the ratio of tube to particle diameter is sufficiently large to have nearly uniform velocity profiles. Furthermore, while axial mixing effects may be thought of as generally being unimportant, the extra effort needed to account for them is large.

In cases where axial mixing must be taken into account e.g., short beds, the cell model of DEANS and LAPIDUS[12] provides a useful representation of the behaviour of a packed bed. It also obviates the conceptual difficulties of the continuum model. Little more will be said about this alternative formulation since, as a generality, axial mixing rarely requires consideration. Under these conditions it is the practice to find the time required to compute individual cases to be substantially reduced if the continuum model is used in preference to the cell model. In addition, the conceptual difficulties mentioned earlier rarely lead to differences in predicted performance greater than the inherent errors in the kinetic data.

$$-\mathrm{div}(\vec{G}_o \cdot c_p \cdot \bar{T}_f),\ -\mathrm{div}(\vec{V}_o \cdot \bar{C}_{fi})\ ;$$

The most commonly encountered transport mechanism, and generally the most important, is caused by convective flow. Material and energy may be transferred from point to point by convective processes in an amount equal to the product of some scalar intensive property and the component of the superficial velocity vector $\vec{V}_o$ in the direction of flow between the two points. Note that $\vec{G}_o = \rho\vec{V}_o$.

$$-\rho_B\,(-\Delta H_j)\,\eta_j\,\vec{R}_j^{*},\ \rho_B\,\eta_i\,\vec{R}_i^{*}\ ;$$

The final terms of equations (2.8) and (2.7) represent accumulation rates due to chemical reaction. The reaction rate, $\vec{R}_i^{*}$, denotes the rate of production of species i by chemical reaction per unit mass of catalyst, and ρ_B represents the mass of catalyst per unit volume of bed (assumed constant). More will be said in the ensuing section with regard to the definition of $\vec{R}_i^{*}$ and $(-\Delta H_j)$. It is sufficient here to say that the heat release due to chemical reaction is based upon the j'th component, the choice of which is arbitrary.

In many cases, knowledge of ρ_B, $\vec{R}_i^{*}$ $(i = 1, 2, \ldots N)$ and $(-\Delta H_j)$ alone is insufficient because the pseudo-rate, $\vec{R}_i^{*}$, is based upon the bulk phase properties such as temperature and concentrations. The magnitude of these properties at the reaction site on the 'internal' surface of the catalyst may, in general, be different from the bulk values because of gradients in these properties owing to finite resistances to the transport of energy and mass. Thus, in these circumstances, the pseudo-rate used in the design calculations must be modified to account for the effects of finite transport rates between the bulk phase and the reaction site.

The concept of the pseudo-rate is so appealing that it is customary to retain it and account for finite transport rates between the bulk

fluid and reaction site by defining a quantity, η , known as the effectiveness factor. By definition, the effectiveness factor is the ratio of the actual rate of reaction on a catalyst pellet to the rate at which reaction would occur if the temperature and concentrations throughout the pellet were constant and equal to their respective values in the bulk phase. By the very nature of the definition the actual reaction rate is obtained by multiplying the pseudo-rate (i.e., observed rate) by the effectiveness factor. In the limiting case of infinite overall transport rates, the actual reaction rate per unit mass of catalyst and the pseudo-rate become equal and the effectiveness factor is unity. This special case may be identified with the "quasi-homogeneous" formulation so widely used in design studies at present.

In order to proceed further it is necessary to elevate the definition of effectiveness factor to a quantitative level. This will require the formulation of a model describing transport between the phases and a model characterizing the transport and reactive processes occurring within the particulate phase.

A further form of energy transport which has been neglected is due to conduction through one particle to the next. SINGER and WILHELM[4] have shown this form of transport to be insignificant for porous catalyst particles.

2.2.2 Model of transport and reaction in the particulate phase

For surface catalysis to be effective, the reactants present in the ambient fluid must be transported to the surface of the solid, and reaction products then transported back from surface to fluid. The diffusion path may be broken down into two parts: bulk fluid to outer surface of the particle, and particle surface to active 'internal' surface of the porous solid. This section deals with the resistance to transport between particle surface and active internal surface.

The structure of a catalyst particle is characterized by a complex system of interconnected channels that is formed by compacting microscopic particles. The microscopic particles, themselves, may be porous and contain pores much smaller than the macro-pores among the particles. It is, therefore, a common occurrence to find catalysts possessing a bimodal distribution of pore sizes.

It is impossible to describe the transport of material within such a porous structure by rigorous mathematical means. Instead, idealized models have been proposed in order to render the problem amenable to analysis. It will become apparent later that even with the crudest of models the mathematical problem is difficult to handle.

The importance of internal transport in the field of catalysis has been recognized for a number of years. THIELE[13] and ZELDOWITSCH[14] simultaneously laid the analytical foundations in 1939, and since that time many applications of simultaneous mass transport and reaction have been reported[15]. It has become apparent that the process of mass transport within a porous solid is unquestionably related in some way to the nature of the porous structure itself. Attempts to describe this relationship have resulted in the concept of an "effective" diffusivity definition which is then used in the normal diffusion equation.

Several workers have tried to relate in quantitative fashion the "effective" diffusivity to properties associated with the porous matrix [16, 17, 18]. For catalysts having a bimodal pore size distribution, MINGLE and SMITH[19] and HARRIOTT[20] developed a mathematical model which views diffusion as occurring in the main macropore from which micropores branch out along the wall. Diffusion in the micropores is predominantly of the Knudsen type, while that in the macropores is either in the bulk or transition range. This model has been used in a considerable amount of work dealing with catalytic effectiveness and selectivity[21, 22], but

the relationship of "effective" diffusivity to the individual pore structure is not defined by the model.

Experimental results seem to indicate that the main mechanisms of gas transport in small pores are those to be expected on classical grounds. However, DACEY[23] points towards an additional mode of transport due to surface migration of species becoming important if sufficient surface is available. Surface transport rates may be sufficiently large at low temperatures to obscure the results of counter-diffusion experiments designed to measure "effective" diffusion coefficients[24, 25]. Recently, FOSTER and BUTT[26] carried out a theoretical investigation of the influence of surface diffusion on catalytic activity. They showed surface transport of mass to affect both rate and temperature dependence of rate in diffusionally-influenced systems, even though measured values of surface diffusivity may be small in comparison to gas phase transport coefficients.

The question of mechanism will not be belaboured any further. In the analysis which follows, transport by surface migration of physically adsorbed layers is ignored. This assumption seems reasonable at high temperatures. Although such transport may be of importance, there is clearly an optimum to be met between the level of sophistication inherent in the model and the requirement to solve the equations rapidly, since in the overall design procedure these equations must be solved many times during the progress of the computation. The final results, of course, must be viewed with a certain degree of suspicion. It is often the case that analysis of a simplified version of the problem proves invaluable in deciding on a suitable strategy of attacking a more complex version of basically the same problem. Reference to the paper of FOSTER and BUTT[26] reveals that even for their grossly idealized system the mathematical formulation is highly complex and seemingly intractable if the intention is to synthesize it into design studies.

Consideration is given to a simple reaction scheme of the type

$$\sum_{i=1}^{i=N} a_i A_i = 0 \qquad (2.9)$$

where, by convention, $a_i < 0$ is a reactant and $a_i > 0$ is a product.

The rate expression may be written as a function of the N-dimensional vector of scalar intensive concentrations and the temperature.

Thus

$$\bar{R}_i = R_i(\vec{\bar{C}}_s, \bar{T}_s) \qquad (2.10)$$

where $\vec{\bar{C}}_s$ of equation (2.10) is given by

$$\vec{\bar{C}}_s = \left[\bar{C}_{s1}, \bar{C}_{s2}, \ldots\ldots \bar{C}_{sN} \right] \qquad (2.11)$$

From the stoichiometric equation (2.9)

$$\bar{R} = \frac{\bar{R}_i}{a_i} = \frac{\bar{R}_j}{a_j} \qquad (2.12)$$

where $\bar{R}$ represents the specific rate of reaction per unit area of pore surface. The bar superscript again indicates a space-averaged quantity. The averaging is carried out over a region small with respect to the size of the catalyst pellet but large with respect to the dimensions of the passages within the porous solid. Subscript s indicates a solid phase scalar property. Thus, $\bar{C}_{si}$ represents the space-averaged molar concentration of component i in the solid phase and $\bar{T}_s$ denotes the temperature.

The mathematical model which follows is based on a homogeneous pore structure. That is to say if the pellet were divided into many thin sections then all sections would be identical, independent of the direction or location of the slice. It is also supposed that the pore structure is completely random, with no preferred directions. Let Ω

be the interior of the catalyst pellet, and $\sum$ its external surface.

The steady state equations describing mass and heat transfer in the porous solid are given by

$$-\text{div}(-D_i \text{ grad } \bar{C}_{si}) + S_v.\bar{R}_i = 0 \qquad (2.13)$$

$$(i = 1, 2, \ldots . N)$$

and

$$-\text{div}(-K_p \text{ grad } \bar{T}_s) - (-\Delta H_j).S_v.\bar{R}_j = 0 \qquad (2.14)$$

for $r \in \Omega$, where r is the position vector.

The first term of equations (2.13) and (2.14) represents the rate of accumulation due to "effective" diffusion and conduction processes respectively. D_i is the "effective" diffusivity of species i, or that value which gives the true flux of i in the porous solid through a unit of geometric area when multiplied by the actual concentration gradient of i. The definition of K_p, the "effective" conductivity, follows by parallel reasoning. A discussion of these two properties of porous catalysts is given in Chapter 5 of Peterson's text. At the design stage, the relationship of these properties to the pore structure, the properties of the transported species, temperature and pressure is assumed to be known.

The second term of equations (2.13) and (2.14) represents the rate of accumulation due to chemical reaction. S_v is the available pore surface per unit volume of porous solid. ΔH_j is the enthalpy of reaction based upon the conventional stoichiometric equation in which the j th species appears as a reactant. Thus, ΔH_j is based upon a_j moles of the j th species and, in accordance with convention, it is numerically negative for an exothermic reaction.

Equations (2.13) and (2.14) are of general applicability in the Knudsen diffusion region, i.e. whenever the mean free path between

molecular collisions is large in comparison with pore radius, irrespective of volume change during reaction. When the mean free path is considerably less than the pore radius (bulk diffusion region), the equations are strictly applicable only to reacting systems without volume change i.e., $\sum_{i=1}^{i=N} a_i = 0$. Systems which do not conform to this condition are subject to a second transport process due to Poiseuille flow. In many commercial catalysts, Knudsen diffusion prevails up to gas pressures of about 10 atmospheres[28] so, within the framework of the assumptions already made, equations (2.13) and (2.14) are of some generality in describing transport in most catalysts.

2.2.3 Model of transport between the phases

Transport resistances external to the catalyst pellet give rise to differences between the bulk and external surface values of the temperatures and concentrations. When these resistances are accounted for it becomes necessary to include equations describing the processes occurring external to the pellet. These equations, in effect, couple together the transport/reaction models describing the behaviour of the fluid and particulate phases. The particular form of these coupling equations is the subject of much conjecture at the present time.

The various film theories which have been put forward as a basis for the analysis of transport between phases in flow systems are appealing because of their simplicity. While, in principle, the practice of correlating heat and mass transfer coefficients between fluids and non-reacting boundaries is correct, the extension of this idea to reacting boundaries is, in general, not feasible since the convective properties are inextricably related to the kinetics of the surface reaction. Nevertheless, this approach has been used successfully by ACRIVOS and CHAMBRÉ[29] to predict overall reaction rates well within the accuracy of the kinetic information. Since the method lacks a firm fundamental basis the results may be somewhat fortuitous.

Strictly speaking, the analyses of flow systems using film theories or more fundamental concepts, for that matter, have considered the particle to be non-porous. The employment of such theories to porous catalyst pellets is therefore questionable. Fortunately, the conditions under which external transport dominate the overall rate lead to the reaction being confined to the external surface, so that in effect the pellet is behaving as though it were non-porous. Furthermore, as the thickness of the reaction zone decreases to its limiting value, the effects of curvature of the surface are minimized. Both the mass and thermal fluxes normal to the surface become independent of position on the surface and independent of the geometry of the pellet. In fact they approach the values on a flat slab of similar material. Each element of external surface is uniformly accessible to reactants - a vitally important condition, since FRANK-KAMENETSKII[30] demonstrated that when this condition is fulfilled external transport phenomena are not influenced by the complexity or the non-linear character of the rate expression. Film coefficients determined in the absence of reaction may then be exactly utilized to predict the performance of a similar system in which reaction is occurring.

The fundamental inadequacies of the various film theories direct attention towards a more rigorous treatment of the processes involved. A difficulty of a different kind is now encountered - that of solving the resulting fluid mechanical problem. One class of problems which has yielded to fundamental treatment is that of laminar boundary-layer flows around streamlined catalytic surfaces. Even for this idealized case the resulting equations are of the partial differential type, and bearing in mind that these equations only form boundary conditions between distributed parameter models of the fluid and particulate phases, this approach is likely to prove too time-consuming. It is also limited in application to systems wherein the fluid mechanical problem can be solved.

There seems little alternative, therefore, but to adopt a simplified treatment which is powerful, in general, and likely to lead to an answer, albeit an approximate one.

Following FRANK-KAMENETSKII[30], local coefficients of heat and mass transfer may be defined. Thus, for mass transfer, the normal component of the surface flux per unit external surface area is equated to the product of a film resistance, k_i, and a concentration driving force, $(\overline{C}_{fi} - \overline{C}_{si})$, i.e.,

$$\vec{n}.(D_i \text{ grad } \overline{C}_{si}) = k_i.(\overline{C}_{fi} - \overline{C}_{si}) \qquad (2.15)$$

$$(i = 1, 2, \ldots . N) \qquad r \in \sum .$$

By parallel reasoning, a similar equation may be written for heat transfer:

$$\vec{n}.(K_p \text{ grad } \overline{T}_s) = h.(\overline{T}_f - \overline{T}_s) \qquad (2.16)$$

$$r \in \sum$$

where h is the heat transfer coefficient between fluid and solid.

Flow in a direction parallel to the surface is neglected. This is in accord with the assumption of a uniformly accessible surface. It will be demonstrated quantitatively at a later stage that this condition is met in external transport-influenced systems.

The definition of effectiveness factor may now be put on a quantitative basis. Noting the qualitative definition given in Section 2.2.1, it follows from equation (2.15) that

$$\eta_i = \frac{-\iint_{A_p} D_i \text{ grad } \overline{C}_{si}.\vec{n} \, dA_p}{\varrho_p . V_p . \vec{R}_i^*} \qquad (2.17)$$

$$(i = 1, 2, \ldots . N)$$

where A_p and V_p represent the external surface area and volume of the pellet respectively. ϱ_p is the apparent density of the catalyst pellet.

The success of the synthesis of the particulate problem, posed by equations (2.13) and (2.14) subject to boundary conditions (2.15) and (2.16), into the overall design procedure will depend among other things upon the requirement of the boundary layer to fully develop and destroy itself in a length scale of the order of a particle diameter. Axial dispersion data[31] indicate that this requirement is met in gas-solid fixed bed systems.

CHAPTER 3

AN APPLICATION OF THE GENERALIZED MODEL

It is true to say that while the general problem may be formulated, successful applications are limited to idealized systems in which the reactor and particle geometries are such that:

(a) The relevant phenomenological parameters are well-defined.

(b) The mathematical difficulties involved, coupled with available computing facilities, allow a solution to be obtained in a reasonable time. Preferably, this time should be sufficiently short so that calculations can be made on a routine basis.

The specific application considered in this chapter is, therefore, but a gross simplification of the events as they actually occur in a real bed of particles. Nevertheless, in comparison with the corresponding and widely used "quasi-homogeneous" model, the representation proposed is highly sophisticated and considerably more complex in mathematical detail.

One of the objectives of this research is to illustrate clearly the importance of physical rate-influencing factors without, at the same time, introducing undue mathematical difficulties which tend to obscure the issue. To achieve this aim certain practically based assumptions are made which render the problem amenable to mathematical analysis without significant loss in generality.

3.1 The simplifying assumptions

1. Consideration is given to the conventional tubular-type reactor packed with spherical catalyst particles, as shown in Fig. 3.1. The individual particles of packing are of uniform diameter and are both physically and chemically identical (see Fig. 3.2). They are assumed to pack together to produce a homogeneous assembly with no preferred flow directions.

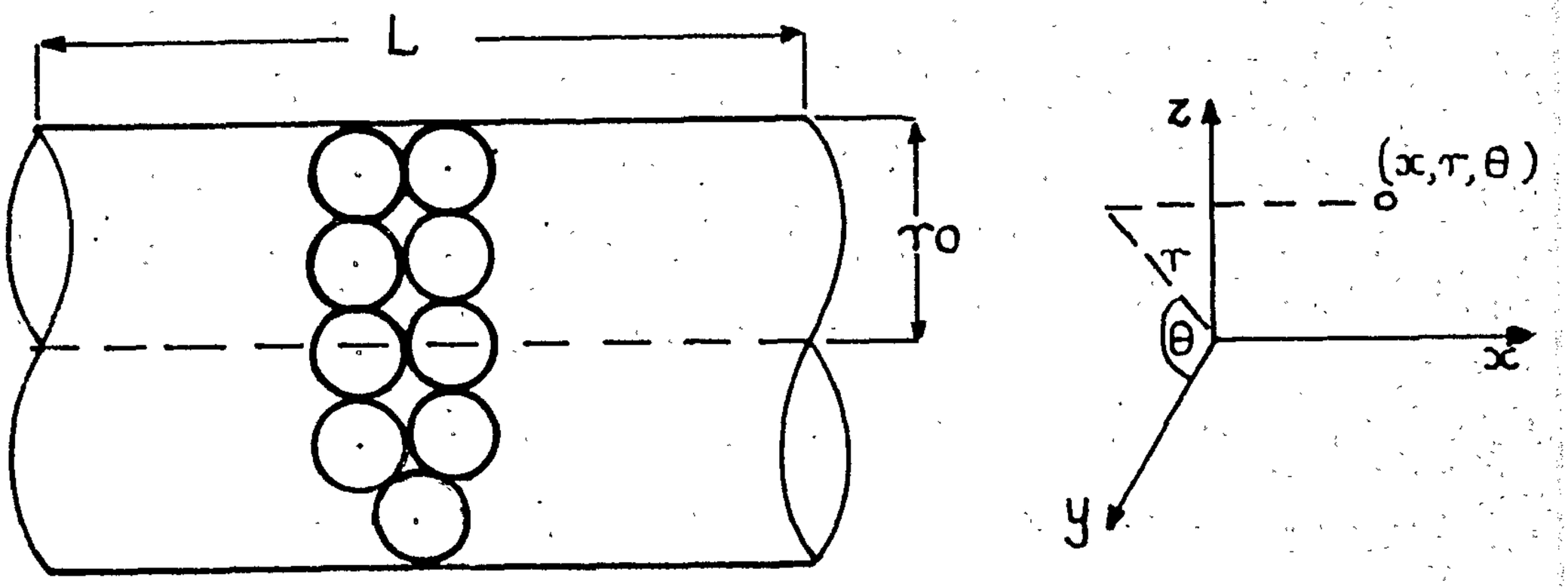

FIG. 3.1 Two-dimensional fixed bed-reactor of cylindrical shape.

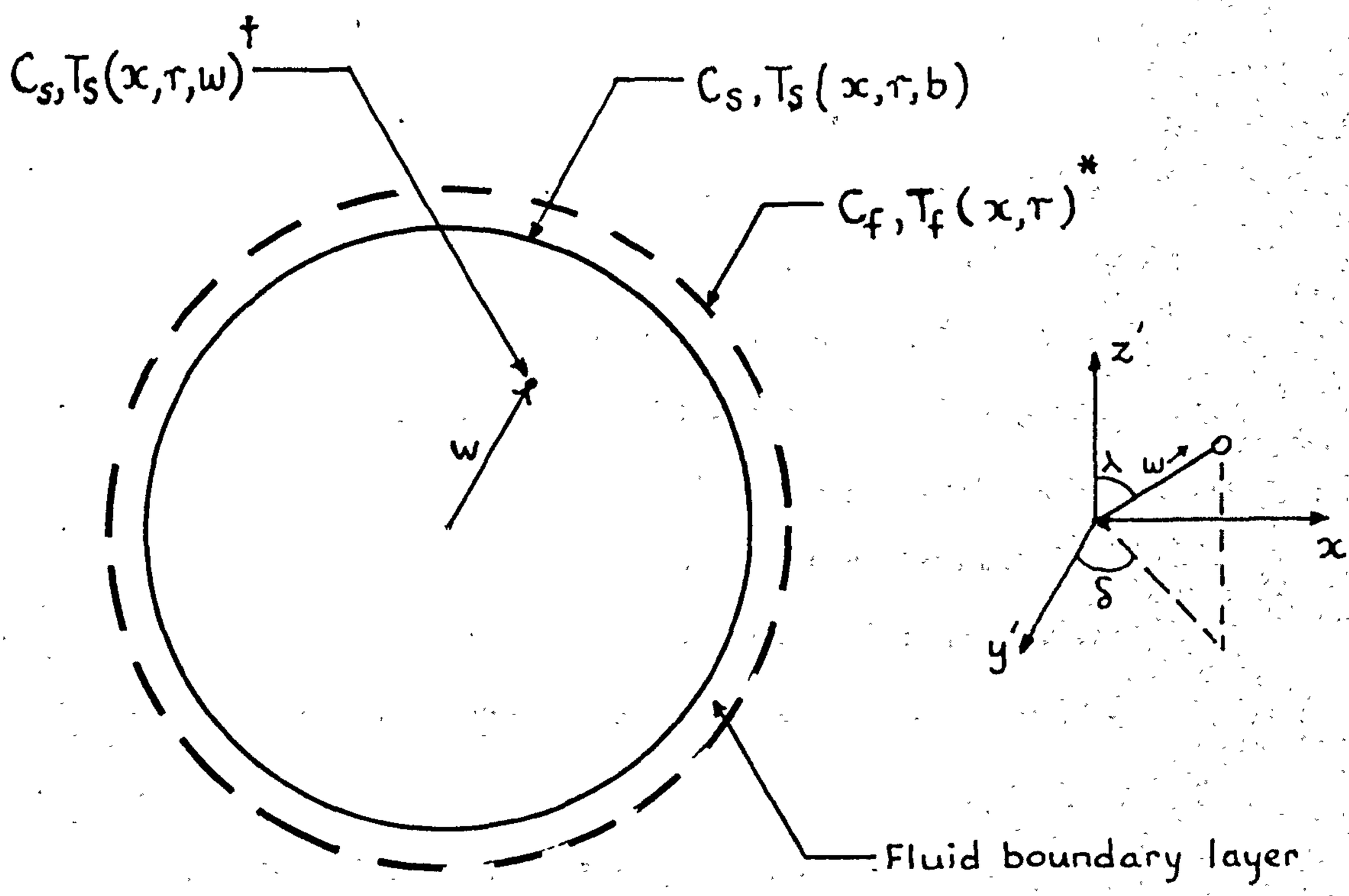

* see Assumption 2
† see Assumption 6

FIG. 3.2 One-dimensional catalyst particle of spherical shape.

2. The reactor is immersed in a coolant bath at constant temperature.

3. Molecular transfer processes transverse to the direction of flow may be neglected in comparison with eddy diffusive processes. For the range of flow rates typical of industrial operation, this assumption is based on sound experimental evidence[32, 33].

4. $\vec{G}_o$ has only one non-vanishing component, namely the superficial mass velocity in the direction of flow (x - axis), and from continuity

$$\text{div } \vec{G}_o = 0.$$

For reactions in which $\sum_{i=1}^{i=N} a_i \neq 0$, G_o is not constant everywhere in the system. Although G_o is invariant with conversion, radial conversion profiles tend to set up radial pressure gradients. Then secondary flows occur to relieve these gradients. Despite this possibility, it is the usual practice to assume constancy of G_o since a more detailed analysis is impracticable at the present time.

5. Both fluid and packing properties, heat of reaction are considered to be insensitive functions of temperature and concentration, at least when compared with the reaction rate.

Probably the weakest assumption made here is the neglect of the radial variation in fluid density and its axial derivative caused by variations in temperature and reaction rate, especially where the reaction is proceeding with a nett change in the number of moles present. The possibility of significant radial variation in gas density tends to invalidate assumption 4, thereby introducing further complications.

6. The external surface of the catalyst particles is uniformly accessible to reactants. This requirement has been considered in some detail in Chapter 2.

7. An irreversible reaction of the form $a_A A \rightarrow B$ ($a_A = 1, 2, \ldots$) is

occurring on the pore walls. The specific reaction rate, R, is defined by an Arrhenius type rate law,

$$R = \alpha . \exp(^{-E}/_{R_g T_s}) . C_s^{\,n} \qquad (3.1)$$

where α = Arrhenius frequency factor.

E = activation energy of reaction.

R_g = gas constant.

n = order of reaction.

C_s and T_s represent the concentration of reactant, A, and temperature respectively averaged over a neighbourhood of some point in the solid. For convenience, bar superscripts on space-averaged quantities will be omitted from now onwards, and it will be taken as understood that the concentrations, temperatures and reaction rates which appear in the design equations are space-averaged rather than point quantities.

Consideration of an irreversible reaction in which there is only one reactive component in no way limits the generality of the design methods, since it may be shown (see Appendix 1) that the system equations pertinent to the reaction scheme given by equation (2.9) may be written in terms of the concentrations of an arbitrarily chosen limiting reactant. It is traditional, however, to base the choice upon the reactant which is present stoichiometrically in least amount in the reaction mixture.

The rate expression given by equation (3.1) is absolved of adsorption influence. It is true to say that treatments which ignore surface occupancy of reactants and products are of limited utility in the analysis and design of catalytic systems. However, in view of the large number of parameters required to characterize typical surface rate laws of the Langmuir-Hinshelwood, Hougen-Watson type, it is not surprising to find the simple power-law model being in such wide usage. For the present, the use of a power law model is in keeping with the

exploratory nature of the design study. More realistic rate models might perhaps be most conveniently studied at a later stage in the overall research programme when the sophistication of the model has been reduced to a level which includes all important effects. That is, of course, assuming such a process of model reduction is possible without significant loss in generality.

It follows as a consequence of assumptions (4) and (5) that plug flow conditions prevail throughout the volumetric confines of the reactor. Radial variations in velocity have been noted experimentally by SMITH and co-workers[34, 35, 36], but the experimental work does not, as yet, lead to a satisfactory prediction of the velocity profile in a given situation. SCHWARTZ and SMITH[35] show that plug flow conditions are approached for ratios of pipe diameter to pellet diameter of more than 30. This simple rule of thumb is often used to justify the use of a plug flow model in a particular application but, in reality, the only justification for ignoring the actual radial variation in velocity is that the uncertainty about the velocity distribution is as large as the correction that would be made by accounting for it in the model.

In addition, axial variation in velocity is ignored. Although this assumption is divorced from reality in some instances (e.g., reactions for which $\sum_{i=1}^{i=N} a_i \neq 0$), its relaxation may introduce an extensive increase in the complexity of the design equations, thereby making their solution more difficult (see, for example, the paper by CARBERRY and WENDEL[10]). Such a step may be ultimately necessary in a specific case but prior work on a simplified model, one which nevertheless possesses many of the features common to the complex model, may allow some of the issues to be resolved without the introduction of overtaxing mathematical problems. It will become evident later that the complexity of the

simplified model is still sufficient to produce mathematical problems which can only be described as acute, if not entirely unmanageable.

3.2 Particular form of the design equations

As a result of applying assumptions (1) to (7) to the generalized set of equations (2.8), (2.7), (2.13) to (2.16) the following system of equations is obtained:

Fluid:

$$-G_o \cdot c_f \frac{\partial T_f}{\partial x} + K_f \cdot \left(\frac{\partial^2 T_f}{\partial r^2} + \frac{1}{r} \frac{\partial T_f}{\partial r} \right) - (-\Delta H) \cdot (1-e) \cdot \eta \cdot R_A'(C_f, T_f) = 0 \qquad (3.2)$$

$$-V_o \cdot \frac{\partial C_f}{\partial x} + D_f \cdot \left(\frac{\partial^2 C_f}{\partial r^2} + \frac{1}{r} \frac{\partial C_f}{\partial r} \right) + (1-e) \cdot \eta \cdot R_A'(C_f, T_f) = 0 \qquad (3.3)$$

Solid:

$$D_A^* \cdot \left(\frac{\partial^2 C_s}{\partial w^2} + \frac{2}{w} \frac{\partial C_s}{\partial w} \right) + R_A'(C_s, T_s) = 0 \qquad (3.4)$$

$$K_p \cdot \left(\frac{\partial^2 T_s}{\partial w^2} + \frac{2}{w} \frac{\partial T_s}{\partial w} \right) - (-\Delta H) \cdot R_A'(C_s, T_s) = 0 \qquad (3.5)$$

Interface:

$$D_A^* \cdot \left. \frac{\partial C_s}{\partial w} \right|_{w=b} = k_A \cdot (C_f - C_s|_{w=b}) \qquad (3.6)$$

$$K_p \cdot \left. \frac{\partial T_s}{\partial w} \right|_{w=b} = h \cdot (T_f - T_s|_{w=b}) \qquad (3.7)$$

C_f and C_s refer to local concentrations $C_f(x,r)$ and $C_s(x,r,w)$ of reactant A in the fluid and solid phases respectively. $C_s|_{w=b}$ and $T_s|_{w=b}$ are the catalyst external surface values of C_s and T_s, i.e., $C_s|_{w=b} = C_s(x,r,b)$; $T_s|_{w=b} = T_s(x,r,b)$. The bed voidage, e, has been introduced into the fluid conservation equations by use of the relationship

$\varrho_B = (1-e).\varrho_p.R_A'$ is a modified reaction rate, based upon unit gross volume of catalyst pellet. It is related to the previously defined rate (equation 2.12) by the equation $R_A' = S_v.R_A = a_A.S_v.R$, where R is given by equation (3.1). Thus, R_A' may be expressed as a function of C_s and T_s by the equation

$$R_A' = a_A.k_v C_s^n \qquad (3.8)$$

where k_v, the intrinsic reaction rate constant per unit of gross volume of catalyst pellet, is given by

$$k_v = \alpha.S_v.\exp\left(\frac{-E}{R_g T_s}\right) \qquad (3.9)$$

The parameters K_f and D_f, which appear in equations (3.2) and (3.3) respectively, represent radial eddy conductivity and diffusivity coefficients. Since the transport of heat and mass are by the same mechanism, it is not surprising to find a direct relationship between K_f and D_f. Available data for radial mass transfer rates are correlated in the form of Pe_M - Re plots, where the Peclet number for mass transfer, Pe_M, is defined by $Pe_M = V_o.dp/D_f$, dp being particle diameter. For turbulent diffusion being the dominant mode of radial transport of heat and mass (see assumption 3), the Peclet numbers based upon heat and mass transfer are identical and are related to the constant K, introduced in Chapter 2, by the equation

$$Pe_M = Pe_H = {}^1/K \qquad (3.10)$$

where the Peclet number for heat transfer, Pe_H, is given by $Pe_H = G_o c_f dp/K_f$. From the definition of Pe_M and Pe_H and equation (3.10), it follows that $K_f = \varrho_f.c_f.D_f$.

Experimental measurements reveal a considerable decrease in K_f near the tube wall, probably as a result of variation in fluid properties,

system geometries and flow velocities. To account for this behaviour, all the variations that affect heat transfer close to the wall are lumped together in the form of an apparent wall heat transfer coefficient. On the other hand, material transport close to the wall is not very important, because the diffusion barrier at the wall makes the radial variation in concentration small.

3.3 Boundary conditions

The specification of the design problem is completed by defining a pertinent set of boundary conditions.

It is clear that assumption (2) renders the boundary conditions on equations (3.2) and (3.3) independent of the angle θ, thereby leading to a two-dimensional representation of the continuous fluid phase. Events in the particulate phase are one-dimensional as a consequence of assumption (6), which leads to boundary conditions independent of the angles δ and λ.

Boundary conditions on equations (3.2) and (3.3) are thus:

$$T_f = T_{fo}; \quad x = 0, \quad 0 \leq r \leq ro. \tag{3.11}$$

$$C_f = C_{fo}; \quad x = 0, \quad 0 \leq r \leq ro. \tag{3.12}$$

$$\left.\begin{aligned} \frac{\partial T_f}{\partial r} &= 0; \quad r = 0 \qquad (3.13) \\ -K_f \cdot \frac{\partial T_f}{\partial r} &= U.(T_f\big|_{r=ro} - T_a); \quad r = ro \qquad (3.14) \end{aligned}\right\} 0 \leq x \leq L.$$

$$\left.\begin{aligned} \frac{\partial C_f}{\partial r} &= 0; \quad r = 0 \qquad (3.15) \\ & \quad r = ro \qquad (3.16) \end{aligned}\right\} 0 \leq x \leq L.$$

Condition (3.11) idealizes the situation somewhat since, in practice, a certain radial temperature profile may be established in the pre-heat section. So as not to obscure the results in the reactor, abstraction

of the pre-heat section has been made. Conditions (3.13) and (3.15) indicate rotational symmetry of the profiles about the axis, (3.16) expresses the requirement of zero mass flux at the tube wall, and (3.14) gives the conditions of heat transfer with the reactor surroundings. U is an overall heat transfer coefficient that contains the apparent wall heat transfer coefficient, h_w, introduced to account for the variation in K_f near the wall, the conductivity of the wall itself and the outside film coefficient.

Boundary conditions on the particulate problem, posed by equations (3.4) and (3.5), are already given at the interface by equations (3.6) and (3.7). Additional conditions arise from symmetry. Namely,

$$\left.\begin{aligned} \frac{\partial C_s}{\partial w} &= 0; \quad w = 0 \\ \frac{\partial T_s}{\partial w} &= 0; \quad w = 0 \end{aligned}\right\} \quad 0 \leq x \leq L,\ 0 \leq r \leq ro \qquad (3.17)\ (3.18)$$

The effectiveness factor, η, appearing in equations (3.2) and (3.3), is obtained by simplifying the general definition given by equation (2.17). Thus,

$$\eta = \frac{-D_A^* \cdot \left(\frac{\partial C_s}{\partial w}\right)_{w=b} \cdot 4\pi b^2}{4/3\,\pi b^3 \cdot R_A'(C_f, T_f)} = \frac{-3 \cdot D_A^* \cdot \left(\frac{\partial C_s}{\partial w}\right)_{w=b}}{b \cdot R_A'(C_f, T_f)} \qquad (3.19)$$

where $\varrho_p \bar{R}_i^* = R_A'$.

3.4 The technique of solution : Initial considerations

The development has now reached the stage where consideration must be given to the implementation of an effective means of solution. A few preliminary observations indicate some of the difficulties likely to be involved.

Non-linear kinetic schemes and non-isothermality within the catalyst demand approximate solution or digital/analogue simulation. Often the

two avenues of approach are supplementary. Digital/analogue simulation techniques will generally provide the design engineer with accurate solutions, but often only at the expense of much programming effort and machine time. On the other hand, approximate methods of solution will allow answers to be obtained quickly, but the degree of approximation is impossible to predict without some knowledge of the "accurate" solution. Evidently, an optimum overall strategy, which falls somewhere between the two extremes, is sought.

In the special case, $\eta = 1$, the model reduces to the "quasi-homogeneous" representation. Digital simulation, based upon finite difference methods, has been successfully employed by FROMENT[37] to obtain solutions to this limiting case. If all derivatives are replaced by their difference approximations, a two-dimensional array of mesh points results. The initial-value character of the problem in the x-direction facilitates a step-wise solution along the axis, whereas the boundary-value character in the r-direction requires a simultaneous evaluation of the radial temperature and concentration profiles.

Inclusion of kinetic and physical interactions within the packing introduces another dimension, since it is required to now evaluate η at each mesh point by solving the equations for the associated sphere. Inspection of equations (3.4), (3.5), (3.8) and (3.9) reveals that this evaluation is likely to prove difficult. Not only is the particulate problem distributed in character, but also it is non-linear and of coupled form. Furthermore, the boundary conditions, (3.6), (3.7), (3.17) and (3.18), are such that it is two-point boundary value in character.

Experience in the adsorption field[38] suggests that analogue simulation is unattractive for problems as complex as the one at hand. Unfortunately, it is impossible even to estimate the time requirements for a numerical solution of the design equations, since the stability

(and rate of convergence where iteration is required) of applicable procedures cannot be predicted. Certainly, the introduction of a third dimension will aggravate the stability and/or convergence requirements. Moreover, the coupling between the two fields may necessitate their simultaneous solution, thereby introducing storage limitation as a potentially important consideration.

Evidence obtained by McGUIRE and LAPIDUS[39] lends support to the idea that the particulate problem forms the major obstacle to the advancement of sophisticated models in design and subsequent optimization and control studies. If the current research is to be elevated from a purely academic level to one with practical implications, this hurdle must be overcome.

The following two chapters will be concerned, therefore, with a detailed study of the behaviour of a single particle bathed by the continuous phase. Initial attention will be centred upon an accurate assessment of the issues involved by the use of digital simulation techniques. From the information obtained attempts will be made to develop lumped-parameter analogues, which approximate real behaviour but also lend themselves to rapid evaluation, with a view to implementation in the design procedure.

CHAPTER 4

THE SINGLE PARTICLE PROBLEM :

(1) ANALYSIS OF RATE-INFLUENCING PHENOMENA

4.1 Introduction

Following on from the early analyses of mass transfer in an isothermal catalyst particle, WHEELER[16] and subsequently PRATER[40] have observed that substantial temperature gradients can sometimes occur. Experimental verification of such gradients has recently been reported by CUNNINGHAM et al[41], MILLER and DEANS[42], IRVING and BUTT[43].

There have been a number of publications describing mathematical analysis of this effect. TINKLER and METZNER[44], CARBERRY[45], WEISZ and HICKS[46] give families of curves correlating the effectiveness factor or the maximum temperature rise with other parameters for flat plate and/or spherical geometries in which first order and/or second order irreversible reaction is occurring. Their analyses, however, have largely been restricted to the class of problems for which rate alteration is due only to gradients in concentration and temperature within the intraphase. In practice, gradients must also be established within the fluid interphase regime by virtue of finite transport rates of heat and mass between the bulk fluid phase and the catalyst external surface. Recent evidence[47, 48, 49] suggests that these gradients may not be insignificant in comparison with those present in the intraphase.

Current conception of the issues involved in determining the overall rate of reaction may, therefore, be somewhat limited. In the light of the above findings a more unified treatment is sought, capable of accounting for rate-influencing factors in the interphase as well as the intraphase regime. The following study is designed to elucidate the question of rate-controlling mechanism(s) in this situation, particular attention being paid to physically realizable systems.

4.2 Description of the System

Equations (3.4) and (3.5), combined with (3.8) and (3.9), are written in dimensionless form for a single particle in isolation by defining the reduced variables

$$y = {}^{w}/_{b} \; ; \; c = {}^{C_s}/_{C_f} \; , \; t = {}^{T_s}/_{T_f} \; ,$$

Thus,

$$\frac{d^2c}{dy^2} + \frac{2}{y}\frac{dc}{dy} + a_A . \phi^2 exp \left\{ \gamma (1 - {}^{1}/_{t}) \right\} c^n = 0 \quad (4.1)$$

$$\frac{d^2t}{dy^2} + \frac{2}{y}\frac{dt}{dy} - a_A \beta \phi^2 exp \left\{ \gamma (1 - {}^{1}/_{t}) \right\} c^n = 0 \quad (4.2)$$

where the definition of β, γ and ϕ follows on the lines proposed by WEISZ and HICKS,

$$\beta = {}^{C_f (-\Delta H) . D_A^*}/_{K_p . T_f} \; ; \; \gamma = {}^{E}/_{R_g T_f} \; ;$$

$$\phi = b \sqrt{{}^{k_{v_f} . C_f^{\,n-1}}/_{D_A^*}} \; ; \; k_{v_f} = \alpha . S_v . exp \; ({}^{-E}/_{R_g T_f}) \; ;$$

Boundary conditions on equations (4.1) and (4.2) are obtained from equations (3.17), (3.18), (3.6) and (3.7).

$$\left.\begin{aligned} \frac{dc}{dy} &= 0 \\ \frac{dt}{dy} &= 0 \end{aligned}\right\} \; y = 0 \qquad (4.3), \; (4.4)$$

$$\left.\begin{aligned} \frac{dc}{dy} &= \frac{Sh'(1-c)}{2} \\ \frac{dt}{dy} &= \frac{Nu'(1-t)}{2} \end{aligned}\right\} \; y = 1 \qquad (4.5), \; (4.6)$$

Sh' and Nu' represent modified Sherwood and Nusselt numbers defined by

$$Sh' = 2 . k_A b / D_A^* \text{ and } Nu' = 2 \; hb / K_p .$$

The effectiveness factor, η, is related to the concentration gradient at the external surface and the reaction-diffusion modulus, ϕ, by the equation

$$\eta = \frac{-3 ({}^{dc}/_{dv})}{a_A \phi^2} \quad y = 1 \qquad (4.7)$$

Inspection of the boundary conditions brings to light an interesting point regarding the behaviour of the equations describing the system. By an analysis similar to that of PRATER, it may be shown (Appendix 1) that a direct link exists between local values of temperature and concentration. This relationship may be stated in the form

$$t = 1 + \beta Sh'/Nu' - \beta c - \beta c_s \ (Sh'/Nu' - 1) \qquad (4.8)$$

where c_s refers to the value of c at the external surface (y = 1).

Equation (4.8) enables the maximum permissible temperature rise between the pellet and the bulk fluid to be predicted. A knowledge of this upper bound is clearly important in relation to the physical temperature limit of the pellet. For systems of practical origin, evidence is presented in Section 4.5 which suggests the ratio $Sh'/Nu' \gg 1$. In this instance, the maximum temperature rise will be approached as c_s tends to zero. The upper bound is then given by

$$\Delta t_{max} = t_{max} - 1 = \beta . Sh'/Nu' \qquad (4.9)$$

The class of problems considered in the literature may be identified with the special case, $Sh' = Nu' = \infty$, and $Sh'/Nu' = 1$ or, equivalently, with an alternative statement of the boundary conditions given by equations (4.5) and (4.6) for the former special case

i.e. c = 1, t = 1, at y = 1

For this case, PRATER has shown the maximum temperature rise to be

$$\Delta t'_{max} = \beta \qquad (4.10)$$

This is also true when $Sh'/Nu' = 1$.

From (4.9) and (4.10),

$$\Delta t_{max}/\Delta t'_{max} \ (= Sh'/Nu') \gg 1 \qquad (4.11)$$

While equation (4.11) indicates that a much larger maximum temperature rise is to be anticipated in the presence of fluid film transport, the question at issue must be concerned with establishing whether or not such conditions can prevail in practice. The precise influence of the

phenomena involved on the rate of reaction and the temperature rise remains undefined until the problem posed by equations (4.1) to (4.6) is solved.

4.3 Mathematical Considerations

An assessment of the relative importance of the factors involved in the diffusion-reaction case in a non-isothermal particle requires, even in the most favourable circumstances, the solution of two simultaneous ordinary differential equations involving conditions at two points. The non-linear dependence of the reaction rate on both concentration and temperature precludes analytical integration. In the first instance numerical methods have, therefore, to be employed.

Bearing in mind that the local regime is coupled and distributed throughout the reactor, the evaluation of bed behaviour demands integration of the single particle problem many times over. In choosing a numerical technique for the latter particular attention must be paid, therefore, not only to the obvious stability requirement but also to the speed of computation. Computing times will be influenced by several variables among which the most important are likely to be (a) the type of integration procedure used and where appropriate (b) the logic behind the iterative strategy of the method. The sophistication of the logic determines the rate of convergence of the iterations. Additional factors such as the storage requirement and the flexibility of the numerical scheme, with regard to integration into the overall computational framework, also require consideration.

4.3.1 Current Methods

There are a number of numerical methods for finding the solution of two ordinary differential equations describing a simple reaction in porous particles. For the class of problems, $Sh' = Nu' = \infty$, (and $Sh'/Nu' = 1$) reported in the literature the analysis is relatively simple,

because, as shown by PRATER, the concentration of reactant can be expressed as a function of temperature so that only one equation - i.e. the energy balance, has to be solved. SCHILSON and AMUNDSON[50] first solved this equation by an iterative integral technique which required fairly accurate initial approximations (one or two straight lines) of the heat generation function. Further publications on the same problem were given by TINKLER and METZNER, who employed analogue simulation and CARBERRY[45] who developed a relaxation solution of simultaneous difference equations. WEISZ and HICKS later simplified the numerical computations by transforming the boundary-value problem into an initial-value one. LIU[51] obtained solutions for the consecutive reaction A → B → C by integrating the corresponding transient equations. Being interested in only the steady state solution he was able to accelerate the dynamics by using positive arbitrary capacity terms, few nodes and large time increments.

The efficiency of the elegant "quasi linearization" technique of BELLMAN and KALABA[52] is illustrated by LEE[53] for the backmixing-reactor in the continuous fluid phase. The marked similarity of backmixing or dispersion-reaction in the fluid phase and diffusion-reaction in the particulate phase provides a basis for fruitful application of this procedure in the field of catalysis.

4.3.2 Proposed Strategies

It might seem at first sight that an obvious step to take is to use equation (4.8), the counterpart of PRATER'S relationship, to decouple equations (4.1) and (4.2) and so produce a single differential equation. This move is unwise, for the resulting equation contains c_s as an unknown in the non-linear reaction rate. In theory, the problem is soluble by combining iteration on an initial assumed value for (dc/dy) at $y = 1$, with a backward integration scheme. The iteration is terminated when a value of $(dc/dy)\ y = 1$ is found which produces a computed

boundary condition (at y = 0) satisfying equation (4.3). Numerical experiments show that an approach of this type is beset by severe stability difficulties, a finding endorsed by COSTE, RUDD and AMUNDSON[54] for Taylor diffusion-reaction in the continuous phase. Faced with the task of having to solve simultaneously the material and energy balance equations, it is difficult to see how the simple transformation proposed by WEISZ and HICKS can be utilised to produce a more tractable initial-value problem. An indirect solution, involving some form of iteration scheme, seems the only alternative.

(a) Boundary iteration approach

Perhaps the most obvious basis for iteration is at one of the boundaries. The strategy here is to assume additional conditions at one boundary (in this instance c and t, at y = 0), use some initial-value integration technique to integrate to the other boundary, and then in some logical way adjust the assumed conditions so that the requirements at the latter boundary are ultimately satisfied. The method used here is an adaptation of that given by McGINNIS[55] for the non-isothermal partially mixed reactor. To improve the original estimates a Newton iteration process, hence second-order convergence, is used. A complication which arises concerns the evaluation of the partial derivatives appearing in the Newton algorithm. Rather than court the dangers inherent in numerical differentiation, the derivatives are found exactly by solving two additional equations which are derived from the material and energy balance equations.

This type of approach has several attractive features:

(1) It allows the use of an explicit integration formula, and, of course, there are several such techniques with low truncation error. In this study use was made of B-Library 3003, Leeds University Electronic Computing Laboratory. This procedure integrates an n-dimensional set

of 1st order ordinary differential equations using the fourth-order Runge-Kutta-Merson process, with facility for automatic step length adjustment.

(2) Storage requirements are low, since only information at the boundary, y = 1, is used in the updating of the assumed conditions.

(3) Convergence occurs by a second-order process. That is to say, for the convergent case, the error in the (k + 1) st iteration tends to be proportional to the square of the error in the k th iteration.

On the other hand, computing time and programming effort appear to be doubled by virtue of solving the two additional derived equations. In fact, this is not true. The derived equations are of the same general form as the conservation equations, and simplifications result so that the programming and computing effort is reduced. More specifically, the same explicit numerical technique can be used to solve all four equations, and the non-linear terms in the derived equations are simply related to those in the conservation equations.

There is no a priori reason to expect that convergence of the process will occur. This is particularly likely in the event of the computed boundary conditions exhibiting sensitivity to small changes in the assumed conditions. In non-linear systems especially, accuracy at one point does not necessarily imply the same accuracy at other points. If convergence is conditioned by the choice of initial estimates, the method is not directly applicable, in general. Presumably it would form part of a hybrid scheme supplementing the initial search for accurate estimates in the two-dimensional "assumed conditions" space. However, in this situation an alternative philosophy, free from such a crippling constraint, is demanded.

Further details of the method are given in Appendix 2.

(b) Finite difference approach

An alternative method, used by CARBERRY and WENDEL, has received considerable attention in the literature[10,45,56], and would seem to be of broad applicability to boundary-value problems involving simultaneous transport of heat and mass with chemical reaction. The approach works on the principle of replacing the differential equations by their central difference approximations, and including the boundary conditions in differenced form in the respective matrix of finite difference equations. Two sets of equations arise, each having a tridiagonal coefficient matrix. It is well known that inversion of such a matrix is easily accomplished by the Thomas[57] method. Non-linear terms in the equations are included in the coefficient matrices and are approximated so as to allow an iterative matrix inversion procedure. The solution is obtained by iteration upon initial assumed concentration and temperature distributions.

While the technique of handling the non-linearities is somewhat crude, the efficiency of the Thomas method of solution compensates to some extent for the iterative procedure required. It is generally necessary to use a small integration step size to keep the truncation error down to a tolerable level. Because of this requirement, and the fact that the logic behind the iterative scheme draws on knowledge concerning the entire distributions of concentration and temperature, more information must be stored than is the case with the boundary-iteration method. The increased storage, while inconsequential for the single particle problem, may be important in relation to the use of this type of approach for the particulate field in a digital simulation of the design problem.

Further details are given in Appendix 2.

4.4 The Policy

In planning the approach at this stage it is important to bear in

mind both the immediate and the long term objectives. The immediate concern is that of gathering together information regarding the interactions of the physical and chemical processes occuring both within, and at the external surface of the catalyst particle. As a result it is hoped that simplifications will be permitted which allow the particulate problem to be integrated into the design programme so that calculations may be carried out on a routine basis. Whilst a quantitative appraisal of any approximation rendered to the single particle model is relatively straightforward, it is difficult to see how such effects interact in the general multi-particle design problem without having, as a basis, a solution obtained by digital simulation. Since the efficiency of the numerical strategy is likely to be critically influenced by the approach adopted for handling the pellet, a fruitful avenue of research lies in assessing the relative merits of techniques suitable for solving the particle model with a long term objective of implementing one into design calculations.

Consequently, solutions are to be obtained by utilising both the boundary-iteration method and that of CARBERRY and WENDEL. Agreement between such contrasting strategies, supplemented by asymptotic checks on the model, would seem to provide a satisfactory way of establishing the validity of the solutions. In addition, an early indication of the philosophy most suited for the particle simulation in the design procedure is facilitated.

4.5 Range of parameters

A description of the non-isothermal simple reaction-diffusion event in a catalyst particle, subject to finite rates of supply of reactant and removal of heat, requires the specification of five parameters. It is assumed that the required kinetic information is available by the time the design stage is reached. Three of these parameters, β, γ

and ϕ , are common to the previous analyses and results are reported for variations of these groups probably well beyond the range of applicability to real systems.[46] The additional parameters, Sh' and Nu', are introduced by virtue of allowing for finite mass and heat transfer rates across the fluid film separating the continuous fluid phase from the particulate phase. It is instructive, at this stage, to examine the expected range of variation of the additional parameters in physically realizable systems.

In practice, Sh' and Nu' are related through the j-factor correlation - i.e.,

$$\psi = \frac{Nu'}{Sh'} = \rho_f . c_f . \frac{D_A^*}{Kp} \left(\frac{Sc}{Pr}\right)^{2/3} = \rho_f . c_f . \frac{D_A^*}{Kp}$$

for gases and vapours. For most porous catalysts

$D_A^* = 10^{-2}$-10^{-3} $cm^2/sec.$,[15] and $Kp = 10^{-3}$-10^{-4} cal/cm. sec.^oC;[58,59,60] therefore, D_A^*/Kp = 1-100. Taking as a typical case a gas of molecular weight 50, at 500^oK., 1 atmosphere, then

$$\psi = 5 \times 10^{-4} \text{ for } \frac{D_A^*}{Kp} = 1$$

$$\psi = 5 \times 10^{-2} \text{ for } \frac{D_A^*}{Kp} = 100$$

On the other hand, for a hydrogen-rich gas

$$\psi = 1.7 \times 10^{-4} \text{ for } \frac{D_A^*}{Kp} = 1$$

$$\psi = 1.7 \times 10^{-2} \text{ for } \frac{D_A^*}{Kp} = 100$$

The absolute values of Sh' and Nu', however, are of particular importance.

Consider, by way of illustration, the following example taken from a paper by BEEK[61].

G_o (molar) = 4.3×10^{-3} gm. moles/cm.^{2}sec.

T_{fo} = 500^oK

Av.molecular wt. = 104.7 gm./mole

Inlet gas pressure = 10 atmospheres

Bed voidage, e = 0.4

Spherical catalyst particles, dp = 0.5 cm.

$D_A^* = 0.16\ D = 9.78 \times 10^{-4}$ cm^2/sec.

$Kp = 6 \times 10^{-4}$ cal/cm.$^\circ$C.

Schmidt number, Sc = 1.339.

Prandtl number, Pr = 0.771.

Reynolds number $Re \left(= \frac{G_o dp}{\mu_{molar}} \right) = 1090$

For the first row of particles in the bed it follows, from the correlation postulated by CARBERRY[62], that $k_A = 0.8$ cm/sec., and $h = 1.73 \times 10^{-2}$ cal./cm.^{2} $^\circ$C. Substituting the values of k_A and h into the definitions of Sh' and Nu' gives

$$Sh' = \frac{k_A . dp}{D_A^*} = 408 \ , \ Nu' = \frac{h . dp}{Kp} = 14.4,$$

with $\psi = 3.5 \times 10^{-2}$

Suppose now that the reactor were fed with a gas largely laden with hydrogen under the same conditions of temperature, pressure and molar flow rate. Assuming $(Sc)_{H2} = Pr = 0.67$, and taking $D^*_{H2} = 0.16\ D_{H2} = 2.3 \times 10^{-2}$ cm^2/sec., Re = 34, then $k_{H2} = 7.12$ cm/sec., and $h = 1.22 \times 10^{-2}$ cal./cm^2. $^\circ$C.

Consequently,

Sh' = 155, Nu' = 10.2, with $\psi = 6.6 \times 10^{-2}$

The comparison of Sh' and Nu' and estimates of their absolute magnitude suggests that the interphase region may be the seat of appreciable heat transfer resistance. Furthermore, neglect of fluid film considerations on the basis of negligible interphase concentration gradients could well be a dangerous practice. A fine example of this "faux pas" is to be found in a recent publication by IRVING and BUTT[43]. For the hydrogenation of benzene on $\frac{1}{2}$" cylindrical pellets, formed by compressing a nickel on kieselguhr powder, the authors measured interphase

temperature gradients as large as 70°C. even though j-factor correlations and generalizations for mass and heat transfer in multi component systems indicated a change in concentration across the fluid film of less than 1%.

4.6 Discussion

To facilitate an understanding of the interaction of the processes involved it is desirable, in the first instance, to examine each effect separately, when permissible, and demonstrate its influence on the solution by undertaking a series of "parametric sensitivity" tests. It is instructive to begin with the simplest situation which can arise - i.e. reaction - diffusion in the absence of reaction heat release. Thermal effects, which tend to complicate an appreciation of the interaction between mass transfer and chemical rates, are therefore removed at present from the sphere of rate-influencing phenomena.

4.6.1 Isothermal Case : Interphase versus Intraphase mass transfer rate-limitation

In the isothermal case $\beta=0$, and the effectiveness factor, for a given reaction and reaction rate expression, is determined solely from a knowledge of the two parameters ϕ and Sh'. Evaluation of effectiveness factor for zero and first order kinetics follows from analytical integration of the equation corresponding to (4.1). For second order kinetics, the equation is non-linear in c and has, therefore, to be solved numerically.

Two questions immediately arise : (1) For what range of values of ϕ and Sh' is the reaction essentially kinetically controlled? (2) Under what conditions does interphase mass transfer become important in relation to "pore" diffusion in significantly influencing the overall reaction rate? The answers to these questions, among others, have particular importance in design synthesis and in guiding the experimentalist interpreting rate data from an experimental reactor. In fact, the uses of the

effectiveness factor concept are discussed in an article by McGREAVY and CRESSWELL[68].

The first point is considered by HUDGINS[69] who presents a general criterion for absence of diffusion control in an isothermal catalyst pellet, regardless of the form of the kinetic rate expression. If it is required that the overall rate be within 5 per cent of the rate obtained if the particle were completely accessible to the external concentration, then

$$\phi < 1 \quad \text{(1st order reaction)}$$

$$\phi < 0.5 \quad \text{(2nd order reaction)}$$

Inspection of Figs. 4.1 and 4.2 confirms the usefulness of the criterion. Note that in these regions any lowering of effectiveness factor is almost entirely due to "pore" diffusion, as shown by coincidence of the curves for finite and infinite values of the Sherwood number.

An assessment of the importance of "pore" diffusion in limiting the reaction rate is found by solving the special case - i.e. $Sh' = \infty$. By way of illustration, the effectiveness factor for a first-order reaction is given by

$$\eta = \frac{3}{\phi^2}\left(\phi \coth \phi - 1\right) \qquad (4.12)$$

When η is plotted as a function of ϕ, the curve corresponding to $Sh' = \infty$ in Fig. 4.1 results. For finite values of Sh', rate limitation is caused by both "pore" and gas-film mass transfer. In this instance, the effectiveness factor becomes a function of Sh' as well as ϕ. Analytical integration for the first order reaction gives

$$\eta = \frac{3.Sh'.(\phi \coth \phi - 1)}{2\phi^2\left[\phi \coth \phi + \left(\frac{Sh'}{2} - 1\right)\right]} \qquad (4.13)$$

Curves are presented in Fig. 4.1 for finite values of Sh' as low as 100, a very low value for gas-film mass transfer. It is evident that the lowering in effectiveness factor due to gas-film transport is always less

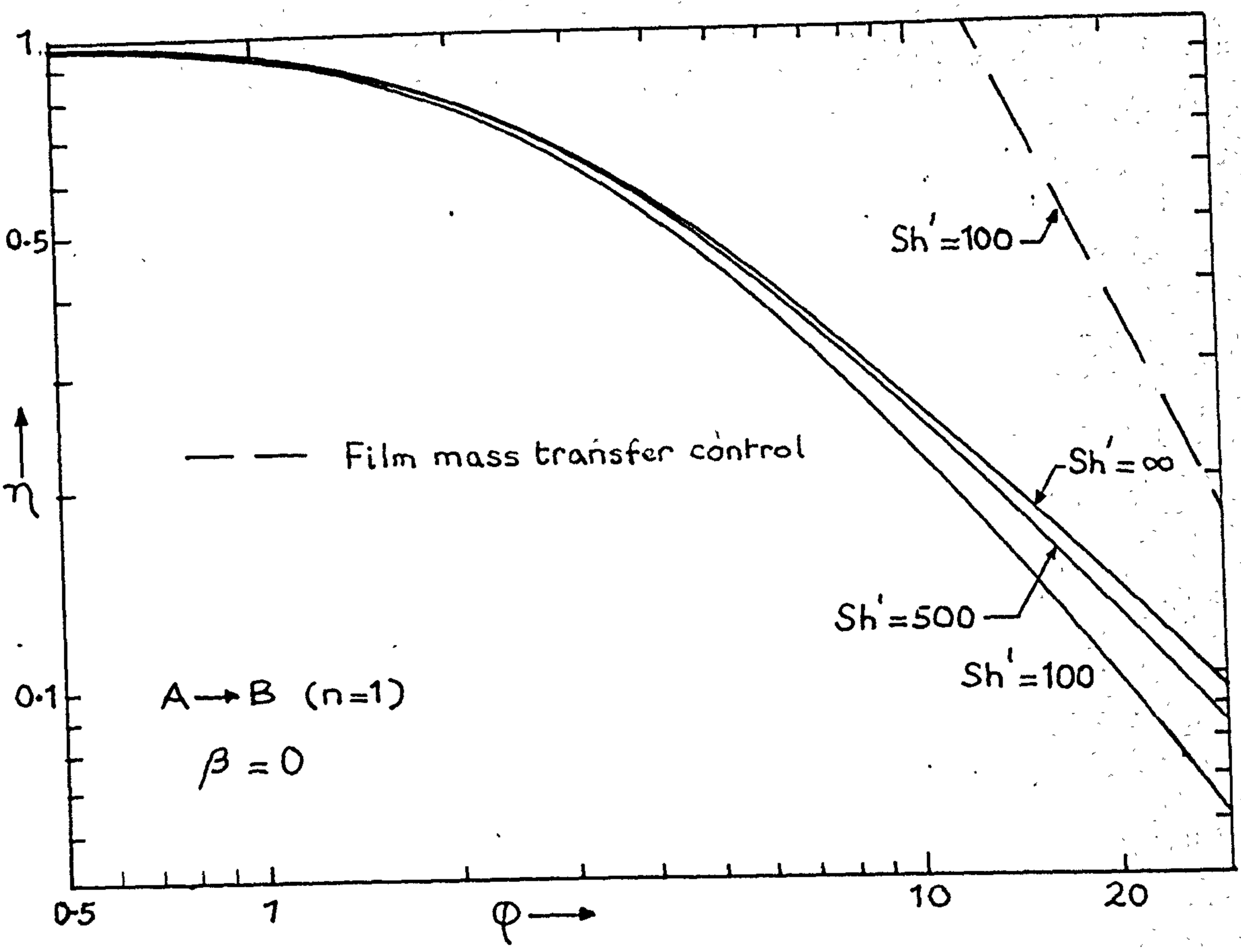

FIG. 4.1 Isothermal Case : Influence of parameters Φ and Sh' on effectiveness factor . First order reaction .

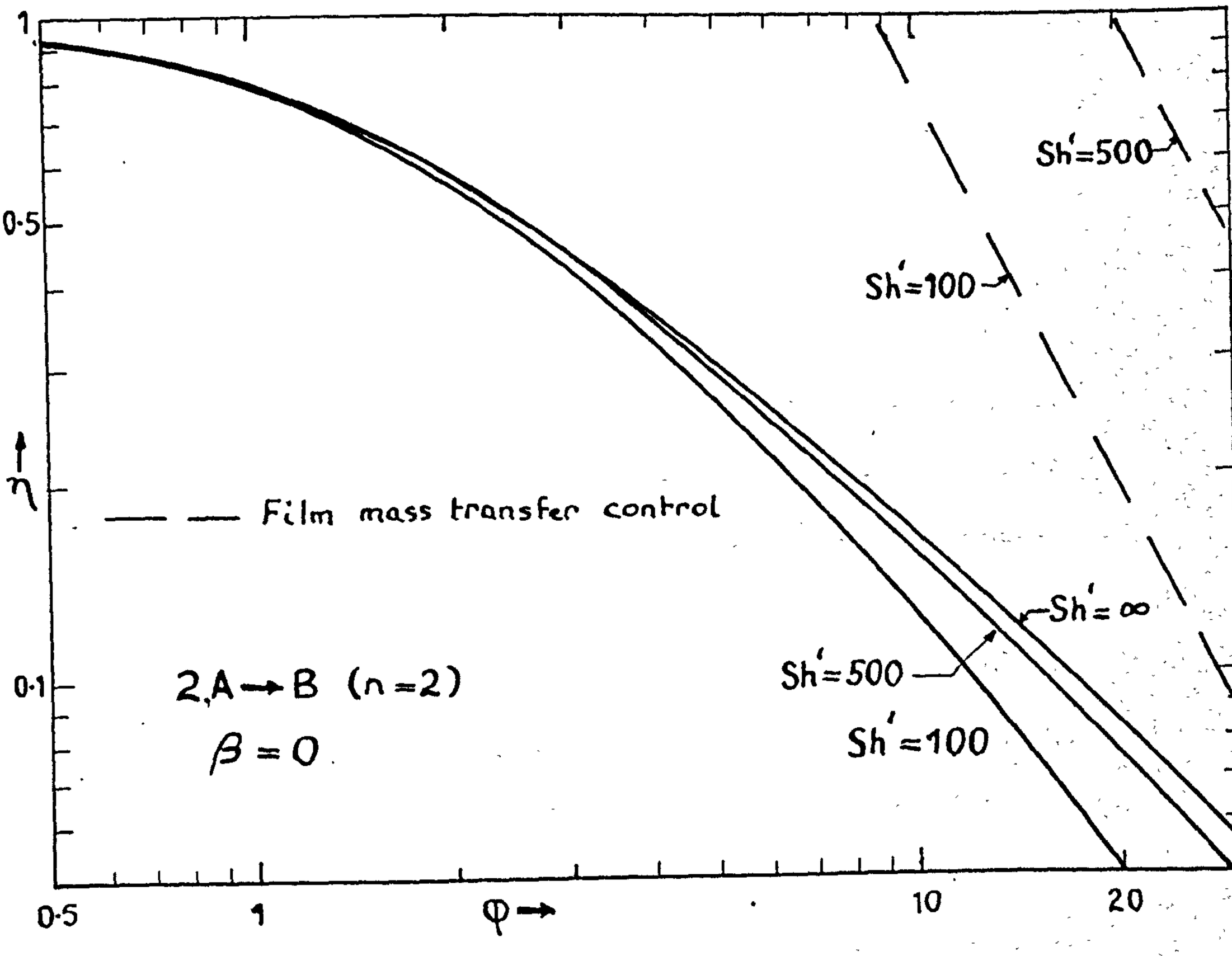

FIG. 4.2 Isothermal Case : Influence of parameters Φ and Sh' on effectiveness factor . Second order reaction

than that produced by "pore" diffusion. This means, in effect, that if mass transfer to the external surface influences the reaction rate, then "pore" diffusion must also influence the rate and an analysis which includes both effects is required. The dotted lines in Figs. 4.1 and 4.2 represent bounds on the effectiveness factor obtained by considering the overall reaction rate to be completely dominated by gas-film mass transfer. Significant deviation of the actual curves from the asymptotes is indicative of appreciable "pore" diffusion influence, and this behaviour is present over a range of ϕ values probably well beyond that applicable to real systems. Nevertheless, it is clear that interphase mass transfer can appreciably influence the overall rate in an isothermal system and an indication of when it must be considered is desirable in answer to question (2).

Dividing equation (4.13) by (4.12), noting that for practical purposes $Sh'/2 - 1 \simeq Sh'/2$, the following equation arises

$$\eta^* = 1/\left[\, 1 + \left(\frac{2}{Sh'}\right) \phi \coth \phi \,\right] \qquad (4.14)$$

A suggested criterion for the absence of gas-film mass transfer effect is obtained from equation (4.14),

$$\text{i.e.,} \quad \frac{2}{Sh'} \cdot \phi \coth \phi \leq 0.1 \qquad (4.15)$$

Thus, setting $Sh' = 100$, it follows from equation (4.15) that, providing $\phi \leq 5$, interphase mass transfer is unimportant in relation to "pore" diffusion in limiting the overall rate for a first order reaction. It follows that for $Sh' > 100$, which is normally the case, the bound on ϕ increases and in these circumstances since $\coth \phi \cong 1$, equation (4.15) simplifies to

$$\phi \leq 0.05 . Sh'. \qquad (4.16)$$

A similar approach for the second order reaction is, unfortunately, prohibited by virtue of the non-linear form of the kinetic rate expression.

However, in the absence of a more detailed analysis, it is tentatively suggested that the criterion (4.15), developed specifically for the first order reaction, can be applied to give useful results for the second order case. An indication of the accuracy is provided in Table 4.1.

Sh'	ϕ values	
	Equation (4.15)	Actual
100	≤ 5	≤ 4
500	≤ 25	≤ 20

Table 4.1 An indication of the accuracy of equation (4.15) in predicting ϕ values for the reaction $2A \rightarrow B$ below which gas film transport need not be considered.

The need for caution in generalizing criteria developed for a specific system cannot be overstated. An excellent example is provided by the shortcomings of the Weisz-Prater[70] criterion for diffusion control in intraparticle reaction when applied to reactions involving strong product inhibition [71,49,72]; and, more recently, by the application of Petersen's asymptotic solution to the carbon-carbon dioxide reaction, involving product inhibition for an external atmosphere of pure carbon dioxide[71,73,69,74].

4.6.2. Temperature sensitivity effects

The more interesting and relevant cases are accompanied by reaction heat release (or abstraction). Attention will be focussed here on exothermic reactions ($\beta > 0$) for it is these cases which bring into play the interactions between the physical transport phenomena and the surface kinetics.

Removing the restriction that $\beta = 0$ now means that the rate of reaction is governed by 5 parameters γ, β, ϕ, Sh' and Nu'. Moreover,

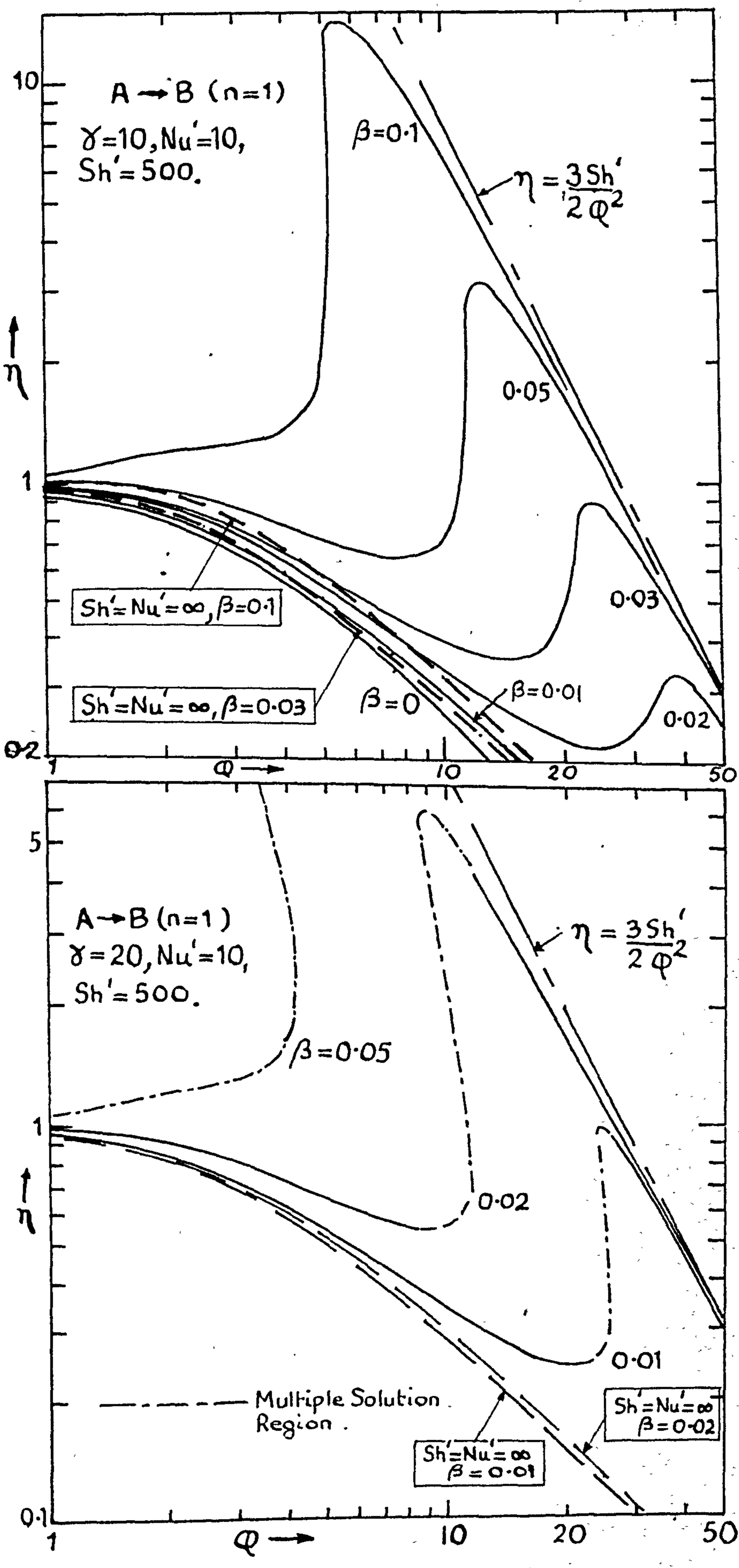

FIG. 4.3 Influence of β on effectiveness factor

the non-linear relationship of kinetic rate to temperature excludes analytical integration of the balance equations. Rather than try to cover all the potential ranges of interest attention will be focussed on a number of cases from which, it is hoped, some generalizations can be drawn.

In figure 4.3 are summarized the results of effectiveness calculations for two cases (γ= 10, 20) for a range of β values up to 0.1, which represents a probable bound for most systems of interest. The calculations are carried out for a 1st order reaction under practically realizable values of the film parameters, Nu' and Sh'. Also shown by dotted curves are the corresponding profiles in a system free from film transport limitations (Nu' = Sh' = ∞).

Catalyst effectiveness :

The novel aspects in this work arise from the influence of film transport limitations upon the overall rate of reaction and the temperature rise accompanying reaction.

The curves shown in Fig. 4.3 are of a type not previously reported and inspection shows them to be made up of three regions, schematically represented in Fig. 4.4. Region I corresponds to kinetic control and $\eta \simeq 1$. As $\emptyset$ increases further, mass transfer in the pellet leads to rate retardation in region II until eventually film mass transfer is the dominant resistance in region III, which actually results from a large film heat transfer resistance. This large heat transfer resistance prevents the heat of reaction being removed sufficiently rapidly, so that the temperature rises to such an extent that the reaction essentially takes place in the surface layers of the catalyst at a rate that maintains the concentration at a value approaching zero. Clearly, the limiting rate at which reactant can be supplied is determined by the maximum concentration driving force across the fluid film under a given bulk

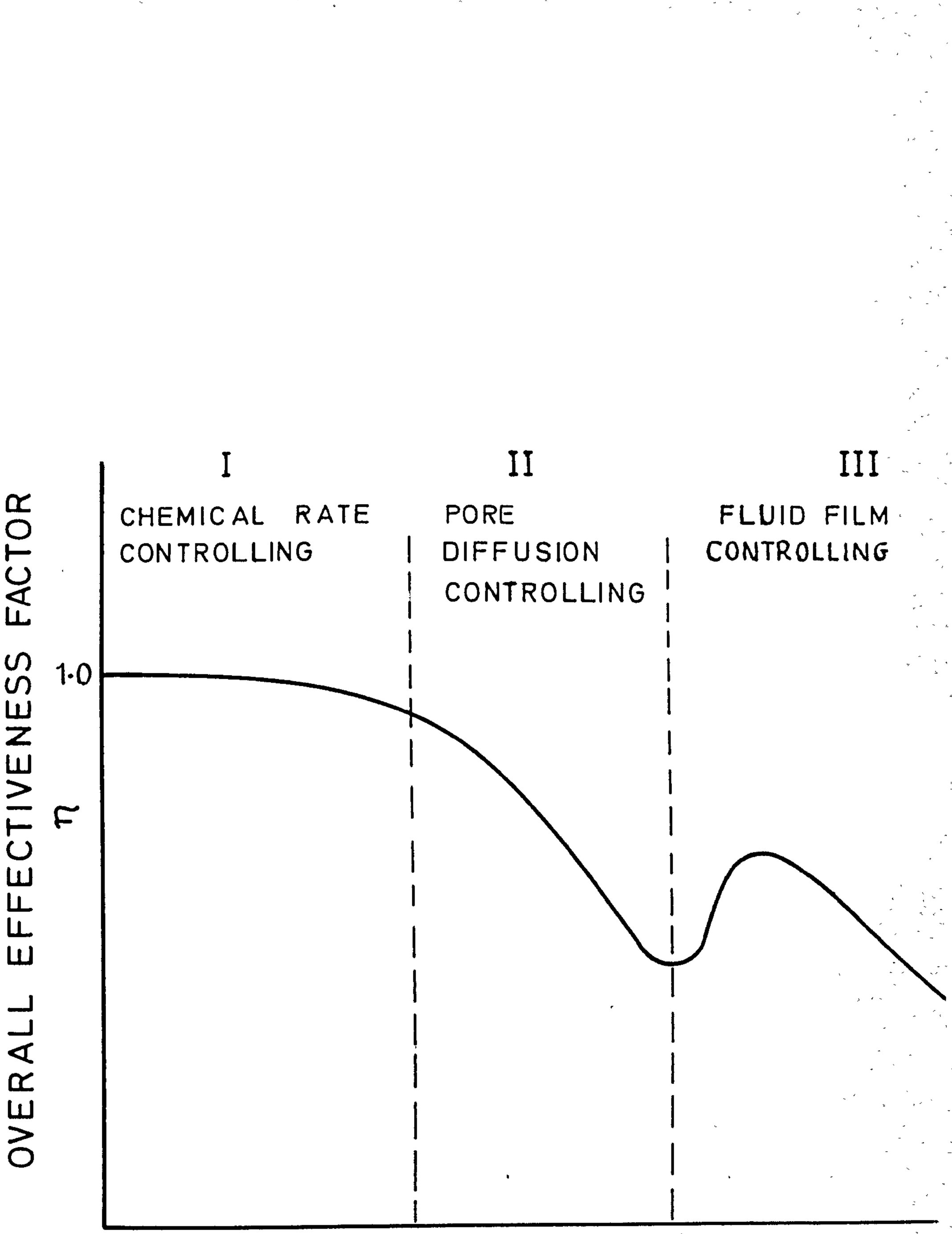

FIG. 4.4 Schematic diagram of a 'typical' effectiveness factor curve.

fluid concentration. For this condition an explicit expression for effectiveness factor follows from combining equations (4.5) and (4.7), setting c = 0 :-

$$\text{i.e., } \eta = {}^{3\,Sh'}/_{2\phi^2} \qquad (4.17)$$

for a 1st order irreversible reaction.

Equation (4.17) represents the asymptote of all curves, irrespective of γ, β and Nu', since ultimately the overall rate of reaction will depend only upon the external surface area of the catalyst, the bulk fluid concentration and the film mass transfer coefficient. The agreement of equation (4.17) with the exact solutions in Fig. 4.3 is seen to be very good in region III. Since this is likely to be a practically important range for highly exothermic reactions, equation (4.17) is particularly useful in leading to a rapid evaluation of effectiveness factor.

A quantitative interpretation of the relative importance of the various rate-influencing phenomena is provided in Table 4.2, where a typical curve (γ=20, β=0.02, Sh'=500, Nu'=10) is broken down into a number of special cases.

TABLE 4.2 Analysis of rate-influencing factors

ϕ	β =0 Nu'= ∞ Sh'= ∞ (1)	β=0.02 Nu'= ∞ Sh'= ∞ (2)	β=0.02 Nu'= ∞ Sh'=500 (3)	β=0.02 Nu'=10 Sh'=500 (4)	Equation (4.17) (5)
	Effectiveness factor values (A→B;n=1)				
1	0.939	0.960	0.959	0.983	750
5	0.480	0.516	0.507	0.651	30
7	0.367	0.395	0.384	0.565	15.3
15	0.187	0.200	0.188	2.87	3.33
20	0.143	0.153	0.141	1.69	1.88
50	0.059	0.064	0.052	0.289	0.3
100	0.030	0.034	0.023	0.074	0.075

KEY

(1) "Pore" diffusion influence

(2) "Pore" diffusion + thermal conduction influences

(3) "Pore" diffusion + thermal conduction + film mass transfer influences

(4) "Pore" diffusion + thermal conduction + film mass and heat transfer influences

(5) Film mass transfer controlling

The first column represents the retardation from kinetic control (η=1) due to "pore" diffusion only. In the second column an increase in the rate is observed due to the existence of a temperature gradient in the pellet. The increase is generally small. In the third column allowance is made for fluid film mass transfer. A comparison of results in the third and first columns reveals that by far the greatest single effect in limiting the rate of reaction is <u>"pore" diffusion</u>. The interesting results really arise in Column (4), where an influential film heat transfer resistance is in evidence. Here, the rate is significantly enhanced, the effect being particularly pronounced in a critical region between $\emptyset$=8.5 and $\emptyset$=11.5 (see Fig. 4.3), where a change in the rate-controlling mechanism of <u>"pore" diffusion</u> to <u>film mass transfer</u> occurs. Column (5) shows effectiveness factor values predicted from equation (4.17) on the basis of a fluid film mass transfer controlled process. Agreement of the results with those in column (4) is satisfactory beyond $\emptyset$=15.

These findings conform rather well with the experimental results of CROSSER and FULTON[48] for the hydrogenation of ethylene on a nickel/alumina catalyst. It was found that a three-fold increase in particle diameter through a critical size range (0.03 - 0.09 cm. diameter) produced a 30-fold increase in reaction rate per unit external surface area.

Such a steep rise in reaction rate could only be due to thermal effects. From calculations, the internal (ΔT) max is less than $0.01^{o}C$. If these effects are not internal, then they must be external.

Temperature distribution:

The analysis presented in Section 4.2 revealed that a much larger maximum temperature rise is to be expected in the presence of fluid film transport; the ratio of temperature rises for the Neumann and Dirichlet $(Nu'=Sh'=\infty)$ cases being given by equation (4.11) - i.e., $\Delta t_{max}/\Delta t'_{max} = Sh'/Nu'$, where $\Delta t'_{max} = \beta$.

CARBERRY'S[122] illuminating treatment of this problem suggests that while the largest concentration difference will exist in the catalyst phase the gas film will probably be responsible for the major portion of overall temperature rise. Insight into the distribution of overall temperature rise between the catalyst particle and the gas film can be gained from Table 4.3. In the kinetically controlled region ($\phi \leq 1$) the temperature rise is small and mainly confined to the catalyst pellet. At higher values of ϕ, the temperature rise is more pronounced.

TABLE 4.3 Fluid film and overall temperature rises

ϕ	Δt_{ex}	Δt_{ov}
1	0.0013	0.0045
5	0.0217	0.0411
7	0.0369	0.0562
15	0.860	0.862
20	0.902	0.904
$\Delta t_{maximum} = 1$		

KEY Overall temperature rise, $\Delta t_{ov} = t\ (y=0) - 1$

Film temperature rise, $\Delta t_{ex} = t\ (y=1) - 1$

$\gamma = 20, \beta = 0.02, Sh' = 500, Nu' = 10$

and now tends to reside more across the film rather than within the pellet. In the critical region, between $\emptyset = 8.5$ and $\emptyset = 11.5$, the temperature experiences a dramatic rise and a switch from "pore" diffusion to film mass transfer control occurs. The entire temperature rise occurs across the film and the reactant is largely consumed on the external surface of the pellet.

Such extreme conditions can only be interpreted in terms of an influential film heat transfer resistance. There is no tendency for a sudden temperature rise to occur when the limitation on heat transfer across the film is removed.

4.6.3 The critical region : its relevance in reactor design

The curves in Fig. 4.3 pass through a maximum which may be considerably in excess of unity, depending upon the values of γ and β. For a given reaction occurring in a specific catalyst at set operating conditions changing the pellet size sufficiently might force the system into this critical region. The actual picture is by no means as clear as that shown in Fig. 4.3, however. Increasing the pellet size will increase $\emptyset$ but also Nu' and Sh', since it can be shown from j-factor correlations that both Nu' and Sh' $\propto dp^{q} (q < 1)$. Actually finding an optimum pellet size, if one exists, is therefore extremely difficult.

Because of the sharply peaked nature of the maxima a slight decrease in the magnitude of $\emptyset$, due to changes in fluid temperature for example, will cause a large reduction in reaction rate. Operation at a maximum rate is therefore equally difficult. Furthermore, the large temperature rises which occur between the catalyst and the bulk fluid may cause degradation or promote unwanted side reactions. Obviously design conditions must be well removed from the regions of these maxima. No evidence is available for giving general rules. Much more information on specific systems needs to be collected.

4.6.4 Hydrodynamic effects

In practice, the film transport parameters, k_A and h, are determined from j-factor correlations, a review of which is given by NUSSEY[123]. For illustration, consider the correlation given by CARBERRY[62]:-

$$j_H = j_M = 1.15(Re')^{-\frac{1}{2}}$$

where $j_H = \frac{h}{G_i.c_f}(Pr)^{\frac{2}{3}}$, $j_M = \frac{\rho_f k_A}{G_i}(Sc)^{\frac{2}{3}}$

and $Re' = {}^{G_i.dp}/_{\mu^*}$.

Substituting the definitions of h and k_A, given above, into the parameters Nu' and Sh' gives

$$Nu' = \frac{1.15\ c_f}{Kp(Pr)^{\frac{2}{3}}}\sqrt{G_i.dp.} \qquad (4.18)$$

$$\text{and} \quad Sh' = \frac{1.15}{\rho f.D_A^*\,(Sc)^{\frac{2}{3}}}\sqrt{G_i.dp.} \qquad (4.19)$$

For a given reaction, occurring in a specific catalyst under a specified bulk fluid concentration and temperature, the magnitude of the parameters Nu' and Sh' is influenced only by

(a) the particle diameter

(b) the mass flow rate past the particle.

The ratio $\psi = {}^{Nu'}/_{Sh'}$ is uninfluenced by either (a) or (b)

(i) <u>influence of mass flow rate</u>

Implicit in the curves of Fig. 4.5 is the effect of mass flow rate on the overall rate of reaction. Changing the flow rate has little, if any, effect in the kinetically controlled region ($\phi<1$), as is to be expected. However, in region II of Fig. 4.4 decreasing the flow velocity may produce a significant increase in reaction rate. The most noticeable increase is demonstrated by curve 1 where Nu' and Sh' values are in the region where transport processes in the fluid film are

* Section 9.1.2.

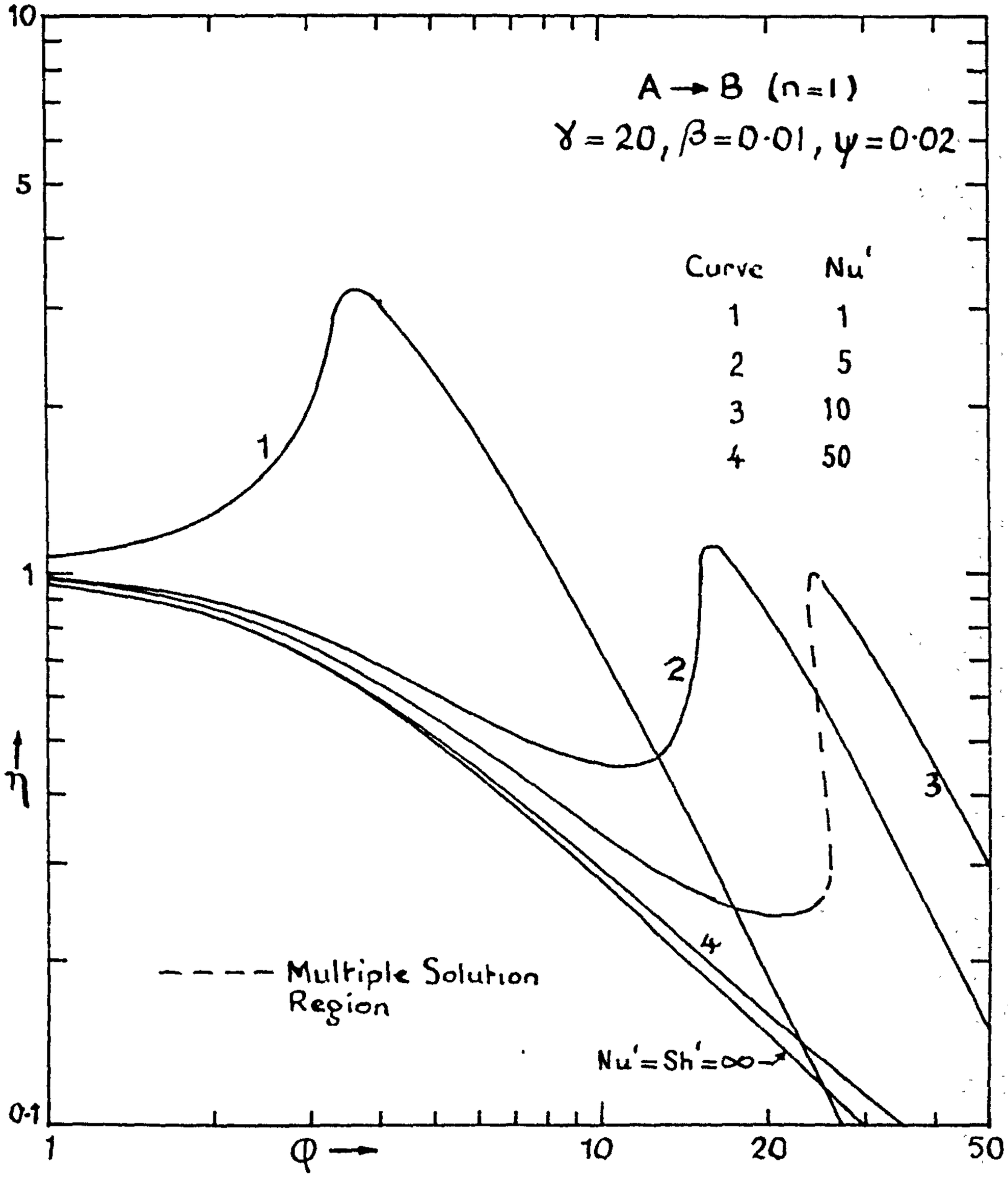

FIG. 4.5 Effect of changing the parameters Nu' and Sh' on the effectiveness factor, keeping their ratio ψ constant.

Note : The locus of the maximum is not a monotonically decreasing curve.

dominated by molecular conduction and diffusion. Here, the rate retarding influence of "pore" diffusion is not apparent, rather rate enhancement is in evidence. This can only be explained in terms of the low value of the Nu' number. All the curves in region III are parallel and of slope -2. They can be predicted accurately from equation (4.17).

(ii) <u>influence of particle size</u>

Changing the particle size will alter not only the magnitude of the film parameters Nu' and Sh' but also the modulus ϕ. A general picture is, therefore, not easily constructed. Instead, consider the following example taken from an article by BEEK[61].

Conditions around the pellet:

$T_f = 500^oK$; $G_i = 0.449$ gm./cm.^{2}sec. ;

Total pressure = 10 bar ; Mole fraction of reactant in the mixture = 0.5 ;

Properties of the gas :

Avge.mol.wt. = 104.7 gm/mole ; $c_f = 2.45$ j/gm. deg; $\mu = 2.06 \times 10^{-4}$ gm/cm.sec. ; $K' = 6.55 \times 10^{-4}$ j/cm.sec.deg. ; $D = 6.11 \times 10^{-3}$ cm^2/sec. ;

Properties of the catalyst :

$Kp = 2.51 \times 10^{-3}$ j/cm.sec.deg. ; $D_A^* = 9.78 \times 10^{-4}$ cm^2/sec. ;

Description of the chemical process :

1st order irreversible reaction, $A \rightarrow B$ ($a_A = -1$, $n = 1$)-$\Delta H =$ 2.054×10^5 j/mole ; $E = 8 \times 10^4$ j/mole ;

k_{vf} is exaggerated from 0.133 sec.$^{-1}$ to 1 sec^{-1}.

From these data,

$\gamma = 19.24$, $\beta = 0.019$, $Pr = 0.771$

and $Sc = 1.339$. Furthermore,

$\phi = 16.dp$

$Nu' = 12.84 \sqrt{dp}$

$Sh' = 369.7 \sqrt{dp}$

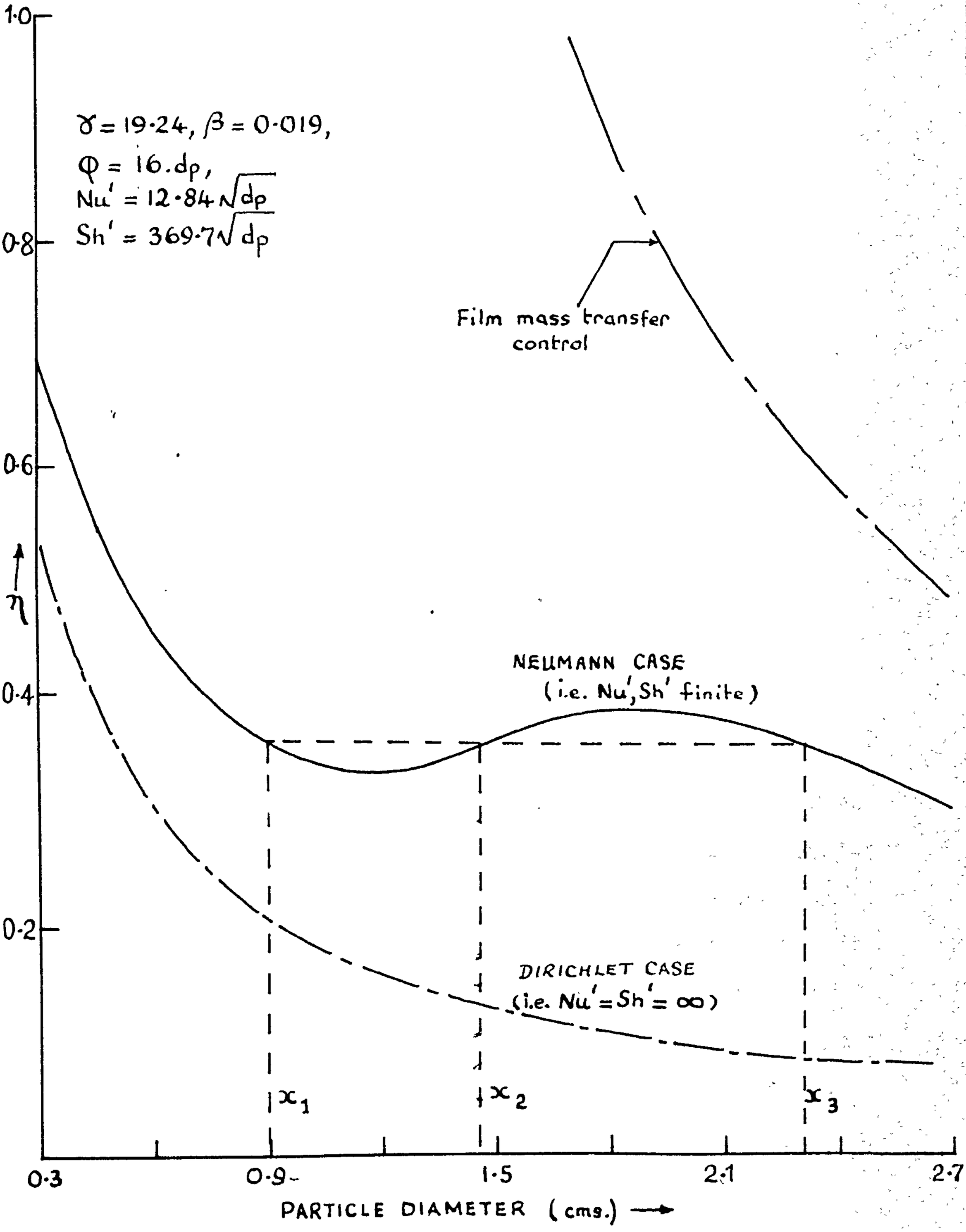

FIG. 4.6 Influence of particle size on effectiveness factor.

where Nu' and Sh' are obtained from equations (4.18) and (4.19). Now consider the effect on the overall rate of reaction of increasing the particle size from 0.3 cm. to 2.7 cm. diameter in steps of 0.3 cm. The relevant values of ϕ, Nu' and Sh' are given below in Table 4.4.

dp	ϕ	Nu'	Sh'
0.3	4.8	7.03	203
0.6	9.6	9.95	286
0.9	14.4	12.2	351
1.2	19.2	14.1	405
1.5	24	15.7	453
1.8	28.8	17.2	496
2.1	33.6	18.6	536
2.4	38.4	19.9	573
2.7	43.2	21.1	607

TABLE 4.4 Values of parameters ϕ, Nu' and Sh' for the investigation of the influence of particle size on overall rate of reaction.

Some observations:

(a) as an aid to the experimentalist.

The bottom curve of Fig. 4.6 shows what happens to the effectiveness factor, and thus the overall rate of reaction, as the particle diameter is increased from 0.3 cm. to 2.7 cm. for the case in which there are no film transport restrictions (Nu' = Sh' = ∞). The rate of reaction is seen to fall progressively with increase in particle size as a result of increasing internal mass diffusion. Although not evident here, it is possible for this curve to display a maximum value of effectiveness factor greater than unity for a more severe value of β (say ≥ 0.2)*. On

* Weisz, P.B., Hicks, J.S., C.E.S. 17 265 (1962)

this basis, therefore, a useful guide for indicating whether a simple reaction is diffusion-influenced is to observe the rate of reaction for three particle sizes under identical reaction conditions. If the rates of reaction/unit mass or vol. of catalyst are the same, then transport properties are not influencing the overall rate. This criterion is, in fact, a well established one in catalytic studies.

The intermediate curve shows what happens when the mathematical model is generalized to include film transport limitations. A completely different situation is in evidence. Now the effectiveness factor can exhibit a minimum and a maximum for values less than unity. It is possible to choose three particle sizes: x_1, x_2 and x_3 of Fig. 4.6 which give the same overall rate of reaction even though the rate is seriously influenced by either internal or film mass transfer. The possible existence of two maxima has not been isolated for the range of γ and β values considered to be practically realizable. It would seem, therefore, that, in theory, one more experiment is necessary to confirm whether or not the reaction is influenced by transport limitations. In practice, the situation is unlikely to be so simple. If experimentation is carried out in the region between particle sizes x_1 and x_3 then, due to experimental errors, this region may be flattened to an extent that no matter how many particle sizes between x_1 and x_3 are used the rate is essentially the same, hence the inference of kinetic control. Clearly, much experimentation is necessary to identify the bounds of this region.

An attempt might be made to remove the film resistances from further considerations by, say, increasing the fluid flow around the catalyst pellet. This would seem to be the obvious step to take, of course. Achieving this objective may not be as straightforward as is imagined, especially for a highly exothermic reaction. A good example is provided

by IRVING and BUTT[43]. Using a newly developed experimental technique these authors claim to be able to measure the temperature at the particle external surface. They give the surface temperature as a function of the temperature upstream of the catalyst for a highly exothermic reaction, the hydrogenation of benzene on $\frac{1}{2}$" cylindrical pellets. It is evident from this plot that surface temperatures were considerably higher than gas stream temperatures. For an upstream temperature above 80°C a pronounced dependence of surface temperature on flow rate was found to exist, indicating the presence of a fluid film resistance. Increasing the superficial flow velocity to over 1 ft/sec. had little effect in removing this resistance. Both simplified j-factor correlations and generalizations for mass and heat transfer in multicomponent systems indicated a concentration difference across the film of <u>less</u> than 1%.

It is not sufficient, therefore, to demonstrate that interphase concentration gradients are negligible, for though this may be the case an appreciable film heat transfer resistance can be present. Great care is needed in interpreting rate data from an experimental reactor. Clearly, the interpretation can become considerably more difficult if film transport effects tend to mask themselves in the manner described above.

If the particular system under study is troublesome in these respects it is suggested that an attempt be made to operate the experimental reactor <u>isothermally</u> by diluting the feed with inert. The problem then becomes easier, in a sense, since only mass transfer effects can affect the rate of reaction. This procedure lowers the overall rate of reaction thereby reducing the extent of conversion in the reactor. In the extreme, practical difficulties may be encountered associated with the measurement of a small conversion.

(b) relevance in reactor design.

It is apparent from Fig. 4.6 that at low values of dp(=0.3 cms) rate retardation is largely due to internal mass transfer, but at high values (= 2.7 cms) the intermediate curve tends towards the asymptote given by the upper curve and film mass transfer is controlling the overall rate. Between these extremes of particle size there is a gradual transition in rate-controlling stage with both a weak minimum and maximum in evidence. For more extreme conditions around the pellet - e.g., pure reactant feed ; a higher temperature:- Fig. 4.3 indicates that over a narrow range of particle size the reaction rate can vary dramatically. Further, the curve may possess a <u>non-unique</u> region in which, for a given particle size, there exist <u>three</u> reaction states. It is important to be aware of the conditions under which catalyst particles exist in non-unique states, and there is an urgent need for criteria which will inform the designer whether such a phenomena can exist in a detailed packed-bed reactor and, if so, under what conditions. Further thoughts on this problem are presented in Chapter 11.

Conclusions

1. For the isothermal case the predominant mass transfer process leading to rate retardation is "pore" diffusion. Film mass transfer can be influential but never predominant.

2. The results obtained for the non-isothermal case demonstrate that the reverse situation can occur. Now, film mass transfer can be the rate-controlling mechanism resulting from high film resistance to heat transfer. Analysis of the temperature distribution shows that the film is responsible for the major portion of overall temperature rise. Thus, the assertion that the pellet itself is isothermal is relevant to experience. This finding is of considerable significance in the development of lumped parameter anaolgues for use in design synthesis (cf. Chapter 5).

3. Following on from the second conclusion, the effectiveness factor curves are generally of the form shown schematically in Fig. 4.4. Three regions are apparent:-

REGION I Kinetic control

REGION II "Pore" diffusion control

REGION III Film mass transfer control, resulting from a high film heat transfer resistance.

The transition from region II to region III can be accompanied by a dramatic increase in the overall rate of reaction and the temperature rise accompanying reaction. The transition region may even be non-unique (cf. Fig. 4.3), in which case three steady states are potentially attainable although not all are stable. In region III the overall rate and the temperature rise can be evaluated explicitly in terms of measurable quantities.

No criteria are available for distinguishing between the three regions. More work is required on this problem.

4. The observations made in Section 4.6.4 (ii) reiterate the need for caution in interpreting rate data from an experimental reactor, particularly the assurance that film heat transfer as well as mass transfer effects are absent.

5. The preferred approach of solving the balance equations is to use a finite difference method, in conjunction with iteration on the concentration and temperature profiles, rather than a method which relies on boundary iteration. Some improvement in the present technique is envisaged by

(a) increasing the rate of convergence by, perhaps, adopting the "quasilinearization" algorithm of BELLMAN and KALABA[52].

(b) using a non-uniform step method tailored towards a more accurate approximation of the steep gradients near the particle surface.

CHAPTER 5

THE SINGLE PARTICLE PROBLEM :
(2) DEVELOPMENT OF APPROXIMATION METHODS

Evidence presented in Appendix 3 suggests that while the particulate problem may be successfully solved by numerical methods the speeds of computation are not conducive to similar approaches being used in the reactor simulation. Furthermore, the type of numerical procedure best suited to the particle is one which could lead to excessive storage requirements if implemented into design calculations. There is, therefore, a need for approximate methods of analysis which allow a rapid prediction of catalyst effectiveness and temperature rise without the encumbrance of numerical integration.

The essential feature of any simplified treatment must, of course, be concerned with ultimate accuracy of prediction. This requirement is inherently related to the validity of assumptions made in the course of obtaining the solution. Commensurate with the accuracy objective is the need for rapid evaluation of the effectiveness factor. As ever, flexibility of application is a prime consideration.

5.1 Previous treatments

Since current ideas are largely centred about the analysis of intraparticle mass diffusion and thermal conduction effects on activity and selectivity it is hardly surprising to find that much of the literature concerned with simplified methods is directed towards the special case - i.e., $Sh' = Nu' = \infty$. The limited utility of the intraphase event in explaining activity in real systems, in which appreciable interphase influence is present leads to the conclusion that current approximation techniques are certainly not applicable, without modification to the general problem i.e., Sh' and Nu' finite. A brief description of the more important techniques

at present available is presented below.

SCHILSON and AMUNDSON[50] (1961) evaluated the heat generation function over the maximum temperature variation permissible between pellet centre and pellet surface. They then proceeded to replace the function by either a single line or two lines, according to its shape, and integrated the resulting linear equation(s) analytically. In the case of the two-line approach, the position in the particle corresponding to the temperature at which the two lines intersect is found by solving a non-linear algebraic equation derived by equating temperature gradients at the unknown point. Agreement with their rigorous method is satisfactory providing the actual temperature at the particle centre is near to the maximum value predicted from the PRATER relationship. BEEK[61] (1961) approximated the reaction rate by its Taylor series about the reference rate in the bulk fluid phase, taking the expansion as far as terms linear in concentration and temperature. The method is very similar to the single line approach of SCHILSON and AMUNDSON, and is of quantitative value over a limited range of parameters. Indeed, its range of usefulness for exothermic reactions is restricted to $\eta \cong 1$.

TINKLER and PIGFORD[63] (1961) set up a perturbation solution for the effectiveness factor using the heat effect parameter ϵ (= $\gamma\beta$ in present notation) to form the perturbation series. The zeroth perturbation, η_0, corresponds to the isothermal effectiveness factor of THIELE. A correction for heat effects is added by evaluation of the first perturbation function. Subsequent terms prove to be time-consuming to calculate and in order not to violate the objective of a rapid method of analysis the series is terminated at η_1, the first perturbation. Consequently, the perturbation technique is found to be useful in allowing for heat effects when the temperature

difference across the pellet is small but not regarded as negligible.

By far the most powerful technique was developed by PETERSEN (1962). His asymptotic method has received usage in many engineering applications[27]. The physical basis of the asymptotic approach is centred upon the assumption that reaction is confined to a thin surface layer of catalyst under conditions of strong diffusional resistance to the transport of reactant through the porous matrix. In this situation, the mathematical complexities of the model are greatly reduced. More particularly, the concentration of reactant at the centre of the particle drops effectively to zero, thereby permitting the specification of an additional boundary condition. Furthermore, all pellet shapes may be treated as slabs because the curvature of the important part of the reaction zone is small. The problem now becomes initial value, and the calculation of effectiveness factor requires, at worst, the evaluation of the exponential integral. Solutions appear satisfactory for spherical catalyst geometry beyond $\phi = 6$, and become asymptotically rigorous as $\phi \rightarrow \infty$.

More recently, GUNN[65] (1966) obtained analytical expressions for temperature and concentration profiles in terms of Airy functions when the reaction velocity constant is a linear function of the particle radial variable. A comparison of the effectiveness factors calculated in this way with other work shows that for reactions of low to moderate exothermicity, the linear approximation is adequate. For reactions of stronger exothermicity appreciable disagreement is found.

In order to gain some idea of the accuracy of the various methods consider Fig. 5.1. Curves are presented of η vs. ϕ for an exothermic ($\gamma\beta = 6$) first order irreversible reaction. It is clear

FIG. 5.1 Comparison of approximation methods for special case ($Nu' = Sh' = \infty$)

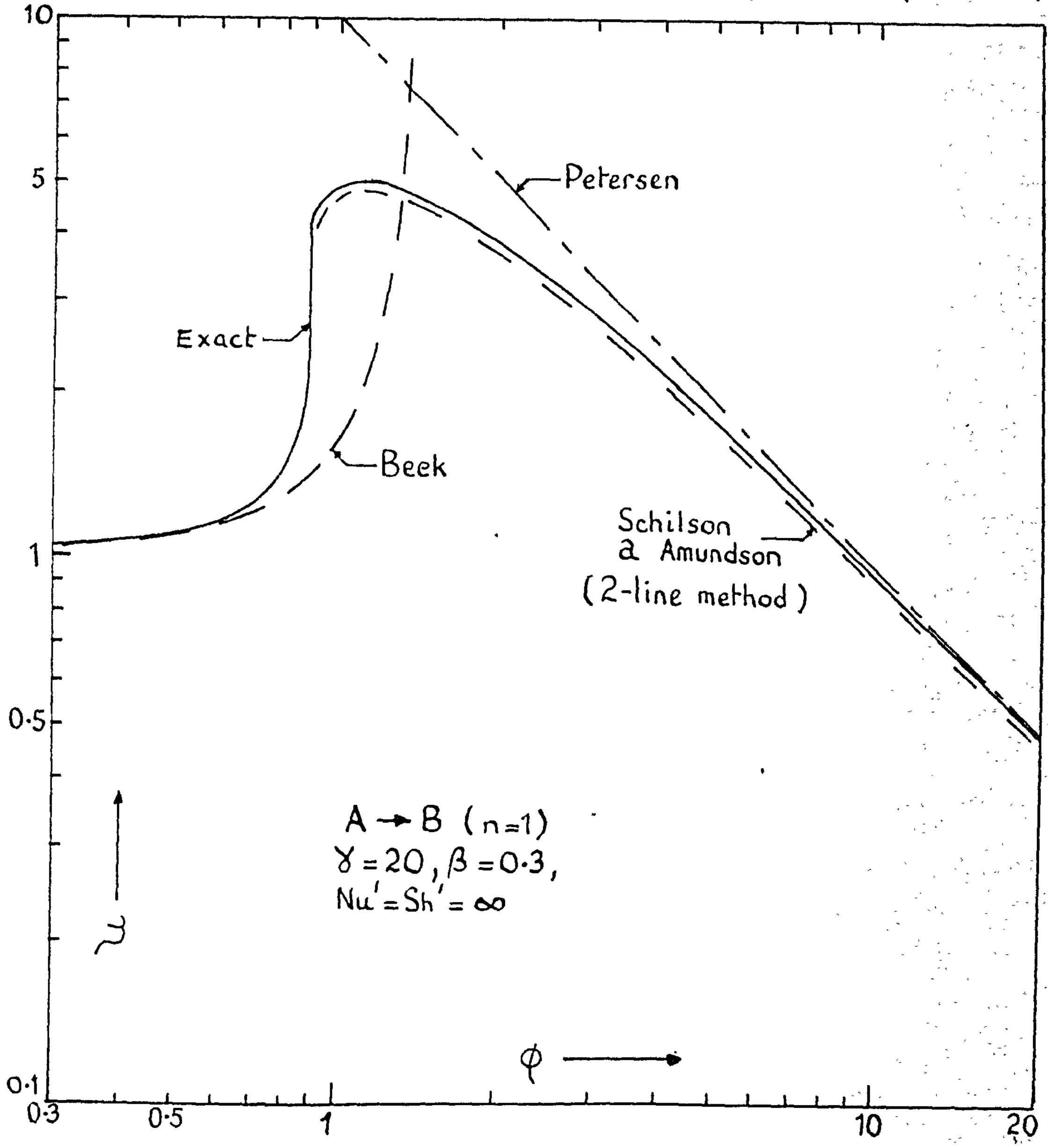

that no one method gives an entirely satisfactory estimation of η over the range of ϕ values extending from the chemically rate-controlled situation ($\eta \rightarrow 1$) to the diffusive-dominated region ($\eta << 1$). The technique due to PETERSEN is seen to converge asymptotically to the exact solution for increasing ϕ values. On the other hand, poor agreement is found in the kinetically-controlled region. However, in this region the approach of BEEK gives a satisfactory representation of the solution. The method developed by SCHILSON and AMUNDSON is the most flexible technique considered, but this advantage is appreciably offset by a computational load considerably in excess of that of either of the two previous methods. There appears to be no easy route to the solution in the region of steep rise in η , associated with the onset of an appreciable thermal gradient.

A few comments about the computational aspects of the methods considered may be in order. In the computation of effectiveness factor from the PETERSEN approach employing the exact form of Arrhenius rate law, the integral is replaced by the difference of two exponential integrals. Computer-oriented approximations of the exponential integral are given in the literature[66]. The particular one used in the present case is of the form

$$x.e^{x}.E_1(x) = \frac{x^4 + a_1 x^3 + a_2 x^2 + a_3 x + a_4}{x^4 + b_1 x^3 + b_2 x^2 + b_3 x + b_4} + \xi(x)$$

$$(1 \leq x < \infty); \left| \xi(x) \right| < 2 \times 10^{-8};$$

An automatic procedure is used to locate the optimal point of intersection of the two-line approximation to the heat generation function in the method of SCHILSON and AMUNDSON. The point of intersection is found by minimising a function, identical to the

integral of the square of the error between the heat generation function and its two-line approximation, taken over the domain of maximum temperature rise attainable within the pellet. The unimodality of the function in question suggests the use of a sequential search plan of the Fibonacci type. In general, a precise knowledge of the optimum is not required since deviations of the order of ± 5% have little effect on the magnitude of the effectiveness factor. As a rule of thumb, between 5 to 10 experiments are sufficient to locate the minimum using a Fibonacci search.

5.2 The physical basis of approximation methods for the general case

It is indeed difficult to conceive of any one approximation method extending over the diverse operating states compatible with kinetic control as one extreme and interphase mass transfer control of the overall rate as the other. This is by no means a disastrous circumstance, but clearly much effort is required in building up a file of methods, each one being applicable over a certain range of specified conditions.

Evidence presented in Chapter 4 points to the fact that interphase temperature gradients may be more common than hitherto anticipated. In brief, an appreciable portion of the overall temperature rise is found in the interphase, the result being that the catalyst is operating in a quasi-isothermal state. Furthermore, the presence of the influential thermal resistance across the film accentuates the withdrawal of reactant to the surface layers of the catalyst leading to a reaction zone of essentially slab-type geometry and a reactant concentration of effectively zero at the centre of the particle. An illustration of this behaviour is given in Fig. 5.2.

Two approximation techniques are presented in the following

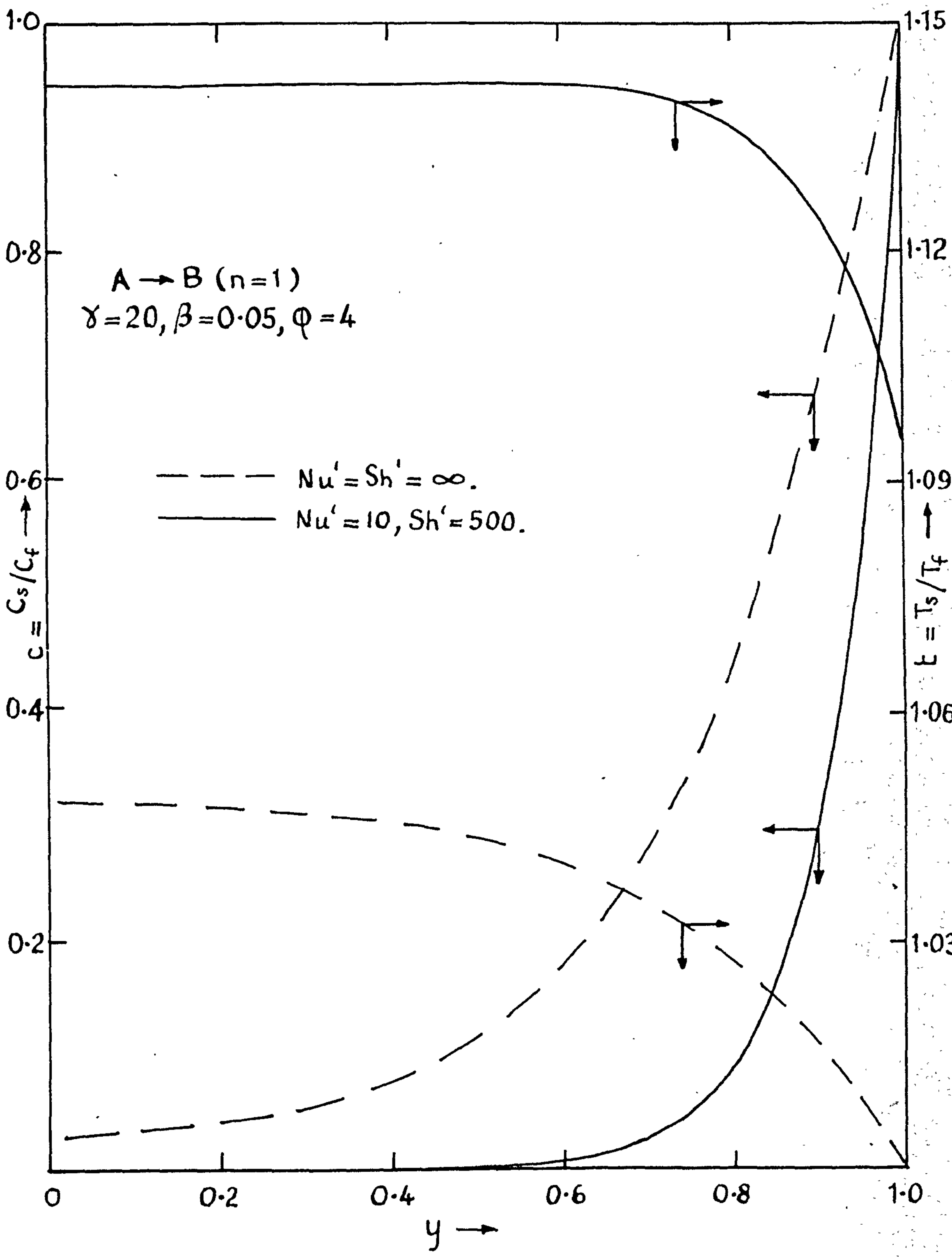

FIG. 5.2 Influence of Nu' and Sh' groups on intraparticle concentration and temperature profiles.

section. The first method, applicable directly only to the first order reaction and termed the "lumped thermal resistance" method, views the catalyst particle as being at a uniform temperature, and therefore conduction within it is neglected. The resistance to heat transfer is assumed to lie entirely in the surface film. Both interphase and intraphase mass transfer resistances are accounted for in the model. Effectiveness factors calculated from this model must display the desired characteristics at the two extremes of kinetic or interphase mass transfer domination of the rate process as a result of the physical basis of the formulation. In regions intermediate between these extremes a certain rate-influencing temperature gradient may exist within the particle. This gradient is, in general, appreciably less than that across the interphase and its effect on the reaction rate can be accounted for by extending the technique due to BEEK[61], basing the linearization of the reaction rate about the external surface value.

A second approach is considered which is capable of handling reactions of arbitrary order. It is fundamentally an application of PETERSEN'S[64] method to the inter-intraphase event, and as such displays the desired characteristics over a wide range of operating conditions, ranging from the onset of intraphase mass and heat transfer influence through to eventual film mass transfer control.

5.3 Approximation methods

5.3.1 Lumped thermal resistance model

Employing the nomenclature used in Chapter 3, the material and energy balance equations may be written for a first order irreversible reaction as

$$D_A^* \cdot \left(\frac{d^2 C_s}{dw^2} + \frac{2}{w} \cdot \frac{dC_s}{dw} \right) - \alpha \cdot S_v \cdot \exp\left(\frac{-E}{R_g T_s} \right) C_s = 0 \qquad (5.1)$$

$$h.(T_f-T_s) + \frac{(-\Delta H)}{b^2}.\alpha.S_v.\exp\left(\frac{-E}{R_g\ T_s}\right)\int_o^b w^2.C_s\ dw = 0 \qquad (5.2)$$

For ease of comparison with the fully distributed model, equations (5.1) and (5.2) are written in dimensionless form by using reduced variables given in Chapter 4. The following equations arise:

$$\frac{d^2c}{dy^2} + \frac{2}{y}.\frac{dc}{dy} - \phi^2.\exp\left(\gamma_{(1\ -\ \frac{1}{t})}\right).c = 0 \qquad (5.3)$$

$$\frac{Nu'}{2}.(1-t) + \beta.\phi^2.\exp\left(\gamma_{(1\ -\ \frac{1}{t})}\right).\int_o^1 y^2.c.dy = 0 \qquad (5.4)$$

Boundary conditions on equation (5.3) are given by equations (4.3) and (4.5) i.e.,

$$dc/dy = 0, \quad y = 0 \qquad (4.3)$$

$$dc/dy = \frac{Sh'}{2}(1-c), \quad y = 1 \qquad (4.5)$$

As a further aid to comparison with the more complex model equation (5.4) has been derived by dividing equation (5.2) by the effective thermal conductivity, Kp. This operation separates the groups Nu' and β, familiar to the fully distributed model, from a single group given by $C_f(-\Delta H).D_A^*/h.b.T_f$.

This set of equations may be solved in a straight forward manner, since equation (5.3) is linear in c; although t is unknown, it is constant. Note, however, that for a second order reaction the material balance equation analogous to (5.3) is non-linear and cannot be solved analytically. The simplicity of the "lumped thermal resistance" model is not carried over to the second order case.

The solution of equation (5.3) subject to equations (4.3) and (4.5) is

$$c_y = \frac{1}{y} \cdot \frac{\left(\frac{Sh'}{2}\right).\sinh \Delta y}{\Delta.\cosh \Delta.\left[1 + \left(^{Sh'}/_{2} - 1\right).\tanh \Delta/\Delta\right]} \qquad (5.5)$$

$y > o,$

where

$$\Delta^2 = \phi^2.\exp\left\{\gamma\left(1 - \frac{1}{t}\right)\right\}$$

is an unknown constant. Substitution of equation (5.5) into (5.4) gives

$$\frac{Nu'}{2}.(t-1) = \frac{\beta.\left(\frac{Sh'}{2}\right)\left[1 - \frac{\tanh\Delta}{\Delta}\right]}{1 + \left(\frac{Sh'}{2} - 1\right).\frac{\tanh\Delta}{\Delta}} \qquad (5.6)$$

The left hand side of equation (5.6) is proportional to the rate at which heat can be released from the particle surface, while the right hand side is proportional to the rate at which heat is generated in the particle. When the right hand side is plotted as a function of t, a sigmoidal shaped curve as shown in Fig. 5.3 is obtained whose intersections with the heat release curve gives the temperature of the steady-state particle. It is evident that there may be combinations of parameters which lead to the possibility of multiple steady states.

The effectiveness factor, η, is found by differentiating equation (5.5) using the result in equation (4.7). Thus,

$$\eta = \frac{3.Sh'}{2\phi^2}.\left[\frac{1 - \frac{\tanh\Delta}{\Delta}}{1 + \left(\frac{Sh'}{2} - 1\right).\frac{\tanh\Delta}{\Delta}}\right] \qquad (5.7)$$

At large values of Δ, equation (5.7) predicts the desired characteristic - i.e., $\eta \rightarrow 3\ Sh'/2\phi^2$, associated with interphase mass transfer dominance. In this circumstance, equation (5.6) reduces to

$$(\Delta t) = t - 1 \rightarrow \frac{\beta}{Nu'}\frac{Sh'}{};$$

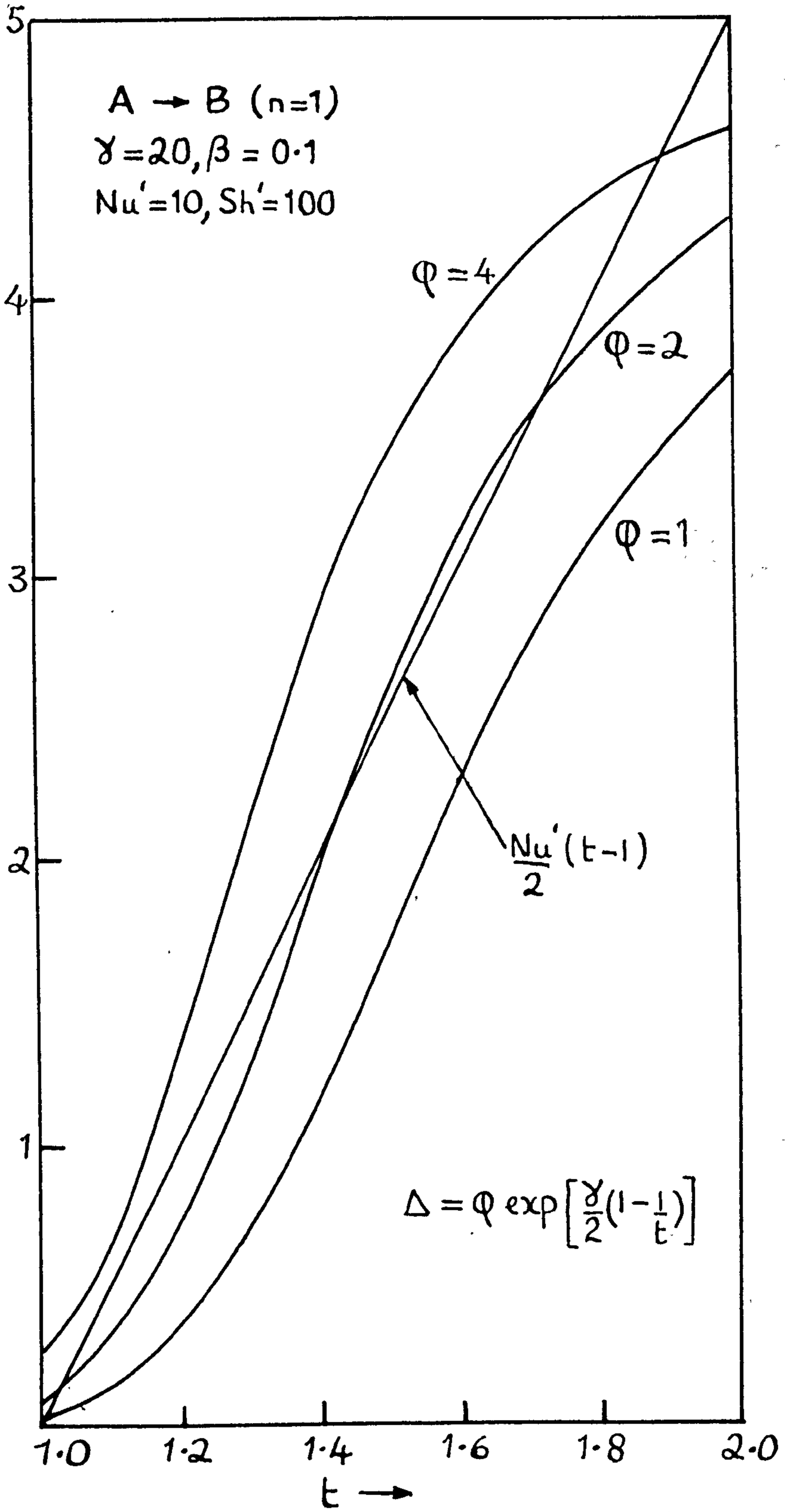

FIG.5.3 Graphical representation of Eqn.(5.6) showing multiple intersections.

the maximum temperature rise. At the other extreme, Δ very small, equation (5.6) shows that $t \rightarrow 1$, so that, in fact, $\Delta \rightarrow \emptyset$. From (5.7), the $\underset{\emptyset \rightarrow 0}{\text{Lim}}\, \eta \rightarrow 1$ after some manipulation, which is the chemical rate controlled situation.

The solution of the non-linear algebraic equation given by (5.6) is found by iteration upon an assumed value of t. Convergence of the Newton-Raphson algorithm, for an assumed value of t in the domain $1 \leq t \leq \left(1 + \frac{\beta . Sh'}{Nu'}\right)$, is unconditional in the region of unique solutions. In the multiple solution region the final root depends upon the assumed value of t. Thus, the lower steady state is isolated by approaching from the lower bound $t = 1$, while the upper state is found by starting with $t = 1 + \frac{\beta Sh'}{Nu'}$. The intermediate state is shown to be metastable by AMUNDSON and RAYMOND[67], and since every steady state is the result of a transient state the intermediate state will never be attained in a natural way.

Knowing the value or values of t satisfying equation (5.6), the evaluation of effectiveness factor follows directly from (5.7). The concentration distribution within the pellet, if required, follows from equation (5.5). At the pellet centre ($y = 0$), $\underset{y \rightarrow 0}{\text{Lim}} \left(\frac{\sinh \Delta y}{y}\right) \rightarrow \Delta$ and

$$c(y = 0) = \frac{\left(\frac{Sh'}{2}\right)}{\cosh \Delta \left[1 + \left(\frac{Sh'}{2} - 1\right) . \tanh \Delta / \Delta\right]}$$

A consideration of the bounds of the unique regions of solutions is important in relation to reactor stability and a discussion is presented in Section 11.4.

5.3.2 General solution for Petersen's assumptions

Extensive computations on the problem in which there are no fluid film transport limitations led PETERSEN[64] to the conclusion

that in the region of appreciable mass and heat transfer resistances - a region of particular importance to the design engineer - the penetration of reactants is restricted to the surface layers of the catalyst, which in turn means that all pellet shapes may be treated as slabs since the curvature of the important part of the reaction zone is small. Restriction in penetration is a consequence of a large particle, a rapid reaction or a slow diffusion of reactants.

The presence of an influential thermal barrier at the particle surface serves to heighten this effect as a result of rate-enhancement over the film transport-free case. An approach similar to that due to PETERSEN[64] is suggested.

(a) <u>The assumption of slab geometry</u>

Putting $\xi = \phi.(1-y)$; neglecting the effect of curvature on the reaction rate, then equations (4.1) to (4.6) are written as

$$d^2c/d\xi^2 + r'(c,t) = 0 \qquad (5.8)$$

$$d^2t/d\xi^2 - \beta.r'(c,t) = 0 \qquad (5.9)$$

$$\left.\begin{aligned} dc/d\xi &= 0 \\ dt/d\xi &= 0 \end{aligned}\right\} \quad \xi = \phi \qquad \begin{matrix}(5.10)\\(5.11)\end{matrix}$$

$$dc/d\xi = \frac{Sh'}{2\phi}.(c-1), \quad \xi = 0 \qquad (5.12)$$

$$dt/d\xi = \frac{Nu'}{2\phi}.(t-1), \quad \xi = 0 \qquad (5.13)$$

where $r'(c,t)$ is given by

$$r'(c,t) = a_A.\exp\left\{\gamma\left(1 - \frac{1}{t}\right)\right\}.c^n \qquad (5.14)$$

Manipulation of equations (5.8) to (5.13) by an approach detailed in Appendix 1 leads to a relationship between t and c of the form previously stated - i.e.,

$$t = 1 + \beta.Sh'/Nu' - \beta c - \beta c_s.(Sh'/Nu' - 1) \qquad (4.8)$$

where c_s refers to the value of c at $\xi = 0$. Letting $t_m = 1 + \beta.Sh'/Nu' - \beta.c_s.(Sh'/Nu' - 1)$, equation (4.8) may be written as

$$t = t_m - \beta c \qquad (5.15)$$

Using equation (5.15) in equation (5.14), there results the relationship

$$r'(c,t) \equiv r^*(c,c_s) = a_A.\exp\left[\frac{\gamma.f(c,c_s)}{1+f(c,c_s)}\right] c^n \qquad (5.16)$$

where $f(c,c_s) = t_m - 1 - \beta c = \frac{\beta.Sh'}{Nu'} - \beta c_s.(\frac{Sh'}{Nu'} - 1) - \beta c$ (5.17)

Writing $p = dc/d\xi$; making use of equation (5.16), equation (5.8) is expressed as

$$p.\, dp/dc + r^*(c,c_s) = 0 \qquad (5.18)$$

Equation (5.18) may be integrated easily to give

$$p^2 = 2\int_{c_o}^{c} -r^*(x,x_s)dx,$$

where equation (5.10) has been used and c_o refers to the value of c at $\xi = \emptyset$. Using the definition of p, the concentration gradient at any ξ, $0 \leq \xi \leq \emptyset$, is given by

$$dc/d\xi = -\sqrt{2}.\left[\int_{c_o}^{c} -r^*(x,x_s)dx\right]^{\frac{1}{2}} \qquad (5.19)$$

An implicit solution for the unknown c_s follows from equation (5.19) by setting $\xi = 0$, and using the boundary condition (5.12).

$$c_s = 1 - \frac{2\sqrt{2}.\emptyset}{Sh'}\left[\int_{c_o}^{c_s} -r^*(x,x_s)dx\right]^{\frac{1}{2}} \qquad (5.20)$$

Equation (5.20) cannot be solved without a knowledge of the unknown c_o. In theory, c_o may be obtained by integrating equation (5.19) to obtain the implicit equation for the concentration profile

$$\xi = \frac{1}{\sqrt{2}} \cdot \int_{c}^{c_s} \left[\int_{c_o}^{z} -r^*(x,x_s)dx \right]^{-\frac{1}{2}} dz \qquad (5.21)$$

Setting $\xi = \emptyset$, equation (5.21) gives an implicit value of c_o,

$$\emptyset = \frac{1}{\sqrt{2}} \cdot \int_{c_o}^{c_s} \left[\int_{c_o}^{z} -r^*(x,x_s)dx \right]^{-\frac{1}{2}} dz \qquad (5.22)$$

Assuming for now that the integrals in equation (5.20) and (5.22) are easily evaluated, two equations arise which are simultaneous in c_o and c_s. In general, it is to be expected that these equations can only be solved by iteration. Having extracted the pertinent values of c_o and c_s, the problem is solved completely.

The effectiveness factor, η, is found in terms of c_s by transforming equation (4.7) in terms of the new co-ordinate, ξ, and using equation (5.12) to give

$$\eta = -\frac{3.Sh'}{2a_A.\emptyset^2}.(1-c_s) \qquad (5.23)$$

In principle, no other computation is necessary on the particle problem for it to be implemented in design. However, the design engineer is also interested in the temperature rise occurring within the pellet from the point of view of physical stability, deactivation or process selectivity in complex reactions. An assessment of the fluid film temperature rise and the overall temperature rise between bulk fluid phase and the centre of the particle follows from equations (5.24) and (5.25) - i.e.,

$$(\Delta t)_{ex} = t_s - 1 = \frac{\beta Sh'}{Nu'}.(1-c_s) \qquad (5.24)$$

$$(\Delta t)_{ov} = t_o - 1 = \frac{\beta\, Sh'}{Nu'} - \beta\, c_o - \beta c_s\left(\frac{Sh'}{Nu'} - 1\right) \quad (5.25)$$

where t_s and t_o refer to particle temperature at $\xi = 0$ and $\xi = \phi$ respectively.

Evaluation of the integrals in equations (5.20) and (5.22) analytically can only be achieved in a few cases. While the integral in equation (5.20) can be found for particular forms of the rate equation, the second integral in equation (5.22) cannot be usually found analytically. Thus, although in principle equations (5.20) and (5.22) solve the problem, solutions are not easily obtained because of integration difficulties. Evidently, further simplification is necessary.

(b) <u>The assumed boundary condition</u>

FRANK-KAMENETSKII[30] considers an n^{th}-order reaction occurring in a semi-infinite pore (or slab). In this circumstance, equation (5.10) is replaced by

$$c(\infty) = \frac{dc(\infty)}{d\xi} = 0$$

For the case of a finite particle subject to a reaction zone which is largely confined to the surface layers, it is inferred that the concentration of reactant A, c_o, at $\xi = \phi$ is small. While c_o can never equal zero, computations show that it may fall to less than 10^{-37} in practical cases. The condition imposed by FRANK-KAMENETSKII is approximately valid in these cases.

Equation (5.10) is therefore supplemented by the condition,

$$c \equiv c_o = 0, \quad \xi = \phi \quad (5.26)$$

This assumption makes equation (5.22) redundant, thereby removing the major source of difficulty. The problem is solved by extracting c_s from the modified form of equation (5.20) - i.e.,

$$c_s = 1 - \frac{2\sqrt{2}.\phi}{Sh'}\left[\int_0^{c_s} -r^*(x, x_s)dx\right]^{\frac{1}{2}} \quad (5.27)$$

If required, the concentration profile is given by the implicit equation

$$\xi = \frac{1}{\sqrt{2}} \cdot \int_{c}^{c_s} \left[\int_{o}^{z} -r^*(x, x_s)dx \right]^{-\frac{1}{2}} dz$$

The effectiveness factor, η, and fluid film temperature rise, $(\Delta t)_{ex}$, are given by equations (5.23) and (5.24) as before. A simplified form of equation (5.25) may be written as

$$(\Delta t)_{ov} = (\Delta t)_{ex} + \beta . c_s \qquad (5.28)$$

(c) Particular forms of the integral: $\int_{o}^{c_s} -r^*(x, x_s)dx$

The integral appearing in equation (5.27) is written as

$$I(c_s) = -a_A \cdot \frac{\gamma^{n+1}}{\beta^{n+1}} \cdot \exp(\gamma) \int_{q_o}^{q_s} \exp(-q) \cdot \frac{1}{q^2} \cdot \left(\frac{1}{q_o} - \frac{1}{q}\right)^n dq \qquad (5.29)$$

where $q = \gamma/(1+f)$, $q_o = \gamma \Big/ \left[1 + \frac{\beta Sh'}{Nu'} - \beta c_s \left(\frac{Sh'}{Nu'} - 1\right)\right]$

and $q_s = \gamma \Big/ \left[1 + \frac{\beta Sh'}{Nu'}(1 - c_s)\right]$; f is defined by equation (5.17).

Equation (5.29) cannot be evaluated for arbitrary values of n, however for n = 0 and integer values, solutions can be readily obtained. Thus, for the first order case A → B,

$$I(c_s) = \frac{\gamma^2}{\beta^2} \exp(\gamma) \left[\left(\frac{1}{2q_s} - \frac{1}{2} - \frac{1}{q_o}\right) \cdot \frac{e^{-q_s}}{q_s} + \frac{1}{2}\left(1 + \frac{1}{q_o}\right) \cdot \frac{e^{-q_o}}{q_o} \right.$$

$$\left. -\left(\frac{1}{2} + \frac{1}{q_o}\right) \left\{E_1(q_o) - E_1(q_s)\right\} \right] \qquad (5.30)$$

where $E_1(\alpha) = \int_{\alpha}^{\infty} \frac{\exp(-v)}{v} dv$

Using equation (5.29) in equation (5.27) produces an implicit equation in c_s, given by

$$c_s = 1 - \frac{2\sqrt{2}\,\phi}{Sh'}\cdot\sqrt{I(c_s)} \qquad (5.31)$$

The speed of solution of equation (5.31), where for the moment it is assumed $I(c_s)$ can be obtained in closed form, is one of the essential issues if an approach of this kind is to prove useful in design. Granted that iteration is necessary as a result of the implicit form of (5.31), a method of solution is needed that combines speed with simplicity.

To illustrate the difficulties involved equation (5.31) is written as

$$F(c_s) = 1 - c_s - \frac{2\sqrt{2}\,\phi}{Sh'}\cdot\sqrt{I(c_s)} = 0 \qquad (5.32)$$

It is the normal practice to solve an equation of the form, $f(x) = 0$, by the Newton-Raphson method. This process is highly efficient, in general, and only moderately complex in computation. A successful application of this method depends on a number of factors, one of the most important being the availability of the first derivative, $^{df}/_{dx}$. Inspection of equation (5.30) for the first order reaction shows $I(c_s)$ to be a complex function of c_s. Such complexity when introduced into equation (5.32) prohibits the evaluation of the gradient, $^{dF}/_{dc_s}$, for use in the Newton-Raphson algorithm. It appears to be the case that this algorithm cannot be used to solve equation (5.32).

There are of course many alternatives but for various reasons the great majority are unattractive. The regula-falsi or simple interpolation procedures, which do not require specifically a knowledge of the derivative, are easy to implement but often slow to converge. Other methods are available which utilise an approximation of the derivative, but again convergence is generally slower than the Newton Raphson method.

In short, the form of the integral is such that the solution of equation (5.32), while obtainable, is only likely to be reached after considerable computing effort. This is a particularly unfortunate circumstance from the viewpoint of the long term objectives of the analysis.

There are two alternatives available for overcoming this problem.

(i) Retain the exact form of the integral and examine critically existing root-finding procedures with a view to implementation.

(ii) Dispense with the exact form of the integral, replacing it by an approximate form based upon the physical picture built up in Chapter 4.

The second alternative is particularly attractive in the present instance.

(d) Approximate forms of the integral: $\int_0^{c_s} -r^*(x,x_s)dx$

Suppose equation (5.14) for the reaction rate, $r'(c,t)$, is expressed as

$$r'(c,t) = a_A.\exp\{f(t)\}.c^n \qquad (5.33)$$

where $f(t) = \gamma.(1 - \frac{1}{t})$. The quasi-isothermal state of the catalyst pellet under surface transport-limitation of the overall rate of reaction suggests that the function $f(t)$, being analytic for all possible ranges of t, can be approximated without significant loss in accuracy by a suitably truncated Taylor series about $f(t_s)$. Two approximations are put forward. The first is simply $f(t) = f(t_s)$, while a second and more accurate estimate is

$$f(t) = f(t_s) + (t - t_s).\, f'(t_s) \qquad (5.34)$$

Carrying out the required algebra between equations (5.33) and (5.34), an approximate rate is obtained from

$$r'(c,t) = a_A.\exp\left\{\gamma.(1 - \frac{2}{t_s})\right\}.\exp(\frac{\gamma\, t}{t_s^2})c^n \qquad (5.35)$$

After some manipulation of (5.35), the integral corresponding to equation (5.29) is written as

$$I^*(c_s) = -a_A.\exp\left\{\gamma\left(1 - \frac{1}{t_s}\right)\right\}. \int_0^{c_s} \exp\left(\frac{c_s - c}{p_s}\right) c^n.dc \qquad (5.36)$$

where $p_s = t_s^2/\gamma\beta$;

Particular forms of the integral, $I^*(c_s)$, are given in Table 5.1.

The virtue of using the approximate form of the integral given by (5.36) lies in the simplification introduced into the function $F(c_s)$ of equation (5.32). An analytical form for dF/dc_s can be found for use in the Newton-Raphson algorithm.

Stoichiometric Equation	Reaction order, n	I^*
$A \rightarrow B(a_A = -1)$	0	$P_s.Q_s$
"	$\frac{1}{2}$	$p_s^{\frac{1}{2}}.\exp(c_s/p_s).P_s.\gamma(\frac{3}{2}, \frac{c_s}{p_s})$
"	1	$P_s(p_s.Q_s - c_s)$
"	2	$P_s\left[2p_s^2.Q_s - c_s(c_s+2p_s)\right]$
$2A \rightarrow B(a_A = -2)$	2	$2P_s\left[2p_s^2.Q_s - c_s(c_s+2p_s)\right]$

Table 5.1 Particular forms of the integral I^*;

$P_s = p_s.\exp\left\{\gamma(1 - 1/t_s)\right\}$, $Q_s = \exp(c_s/p_s) - 1$; γ is the incomplete gamma function, $\gamma(a,x) = \int_0^x e^{-v}.v^{a-1}dv$ $(a>1)$.

(e) <u>The error introduced into the effectiveness factor by the use of the approximation, $I^*(c_s)$</u>

A quantitative assessment of the error in the effectiveness factor arising from the use of the approximate form of the integral is difficult to obtain without actually performing computations using the

exact integral. However, some knowledge can be gained regarding the bound on the error for the most unfavourable circumstance which can arise - i.e., for the case in which the entire temperature rise is forced to reside within the pellet ($Nu' = \infty$).

For the special case ($Sh' = Nu' = \infty$), the calculation of effectiveness factor is explicit. By way of illustration, exact and approximate forms of effectiveness factor for the first order reaction are given by

$$\eta_1 = \frac{3\sqrt{2}.\gamma^{\frac{1}{2}}.\exp(\gamma/2)}{\beta\phi}\left[-(\beta+\tfrac{1}{2}+\tfrac{\gamma}{2}).\frac{\exp(-\gamma)}{\gamma}+(\beta+1).\right.$$

$$\left.\frac{(\beta+1+\gamma)}{2}.\frac{\exp\left(\frac{-\gamma}{1+\beta}\right)}{\gamma}-(\beta+1+\frac{\gamma}{2})\int_{\left(\frac{\gamma}{1+\beta}\right)}^{\gamma}\frac{\exp(-v)dv}{v}\right]^{\frac{1}{2}}$$

and $$\eta_2 = \frac{3\sqrt{2}.\exp(\gamma\beta/2)}{\gamma\beta.\phi}\left[1-\exp(-\gamma\beta)\{1+\gamma\beta\}\right]^{\frac{1}{2}}$$

respectively for $|\beta| > 0$ (c.f. Petersen, E.E., C.E.S. 17 987 (1962)).

Table 5.2 shows the influence of the parameters γ and β on the % error in effectiveness, defined by error = $(\eta_1-\eta_2) \times 100/\eta_1$. In the great majority of practical cases, $\beta < 0.1$, and it is reasonable to expect a bound of 5% on the percentage error in effectiveness factor. In view of other uncertainties generally involved in reactor design, the approximation is deemed more than adequate.

γ	β	error
10	0.1	-1
20	0.1	-2.5
40	0.1	-7.5
20	0.05	-0.5
20	0.1	-2.5
20	0.2	-14

Table 5.2 Influence of the parameters γ and β upon the error introduced into the effectiveness factor for a first order reaction by the use of the integral, $I^*(c_s)$.

Summary

Lumped parameter analogues of the distributed parameter problem, describing simultaneous heat and mass transfer with simple chemical reactions in porous catalysts, have been developed for the general case in which film transport limitations to heat and mass are present.

Calculations carried out in Chapter 4 show that when the reaction rate is influenced by transport restrictions within the catalyst and across the interphase, the following conditions arise:

(i) The reaction is confined to a thin surface layer of catalyst.

In these circumstances it is reasonable to assume that all pellet shapes can be treated as slabs since the curvature of the important part of the reaction zone is small.

(ii) As a consequence of (i) the reactant concentration at the particle centre is, effectively, zero.

(iii) The pellet is near-isothermal; most of the overall temperature rise being appropriated by the fluid film.

For the specific case of a 1st order irreversible reaction observation (iii) is used to develop a simplified mathematical model which views the particle as being isothermal with the entire temperature rise lying across the external film. Evaluation of the effectiveness factor and the temperature rise follows from the solution of a non-linear algebraic equation. Asymptotic agreement is found with the fully distributed model at the extremes of 'pure' kinetic rate control on the one hand and film mass transfer control on the other.

A more generalized treatment for arbitrary reaction rate forms is considered by making use of observations (i) and (ii). To reduce the computational effort an approximate form of Arrhenius kinetics is utilised by developing the temperature dependence of the intrinsic reaction rate in terms of a truncated Taylor series expansion, the

expansion being based on the reference value at the external surface of the particle. The mathematics produces an integral equation for the unknown concentration, c_s, at the external surface of the particle. For integer order reactions the integral equation can be reduced to a non-linear algebraic equation. For certain non-integer values (e.g. $\frac{1}{2}$, $\frac{1}{3}$, $^1/5$), the integral may be reduced to a standard form which is tabulated[66].

CHAPTER 6

THE SINGLE PARTICLE PROBLEM :

(3) COMPARISON OF DIGITAL SIMULATION AND APPROXIMATION METHODS

This chapter is concerned with providing information on several issues which require consideration prior to the design synthesis stage.

A comparison is given of some results from the lumped parameter analogues and digital simulation of the distributed parameter model. Accuracy and speeds of computation are assessed, together with any other features of the simplified methods which might be of importance in the design stage - e.g., convergence requirements on the iterative algorithms for computing effectiveness factor.

6.1 Accuracy

Although it is to be expected that Nu'/Sh' will be less than 0.05 in practical cases, as shown in Section 4.5, the accuracy is first examined for Nu'/Sh' values considerably greater than this figure, thereby giving an initial impression of the utility of the methods in a set of circumstances divorced from those in which the underlying assumptions are based. The comparison is made for a fairly typical value of $\gamma = 20$ and for $\beta = 0.1$, which represents an upper bound for most systems of interest. Three cases are considered in Fig. 6.1 for $Nu' = 10$ and $Sh' = 25$, 50, 100 which correspond to $\psi = 0.4$, 0.2 and 0.1 respectively. Calculations are carried out over a range of Thiele modulus ϕ sufficient to demonstrate such important characteristics as

(i) a maximum in the effectiveness factor.

(ii) a region of multiple solutions.

(iii) the onset of film mass transfer control.

Examining the lumped thermal resistance approach first of all, it is evident that this model displays the expected asymptotic behaviour at the

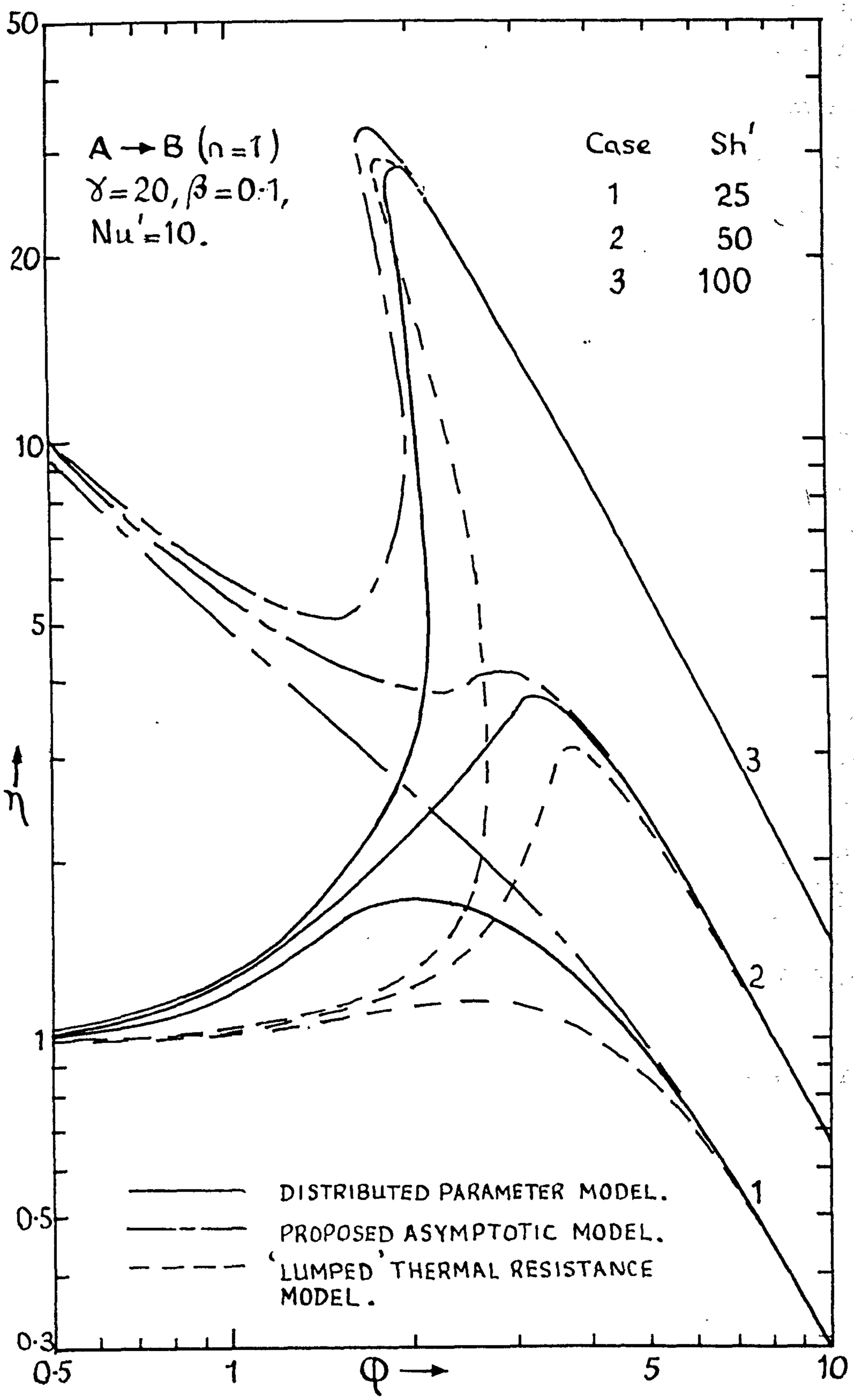

FIG. 6.1 Comparison of simplified models of the catalyst particle with the distributed parameter model.

two extremes of kinetic control (say, $\phi < 0.5$) on the one hand, and film mass transfer control ($\eta = 3Sh'/2\phi^2$) on the other hand. Not surprisingly the discrepancy is appreciable in the region intermediate between the two extremes as a result of appreciable intraparticle temperature gradients. Even so, the simplified model predicts the maximum value of η and the corresponding value of ϕ with good accuracy for cases 2 and 3. Further, the prediction of the multiple solution region for case 3 is in good agreement with the one determined from the distributed parameter problem. The more generalized treatment considered in Section 5.3.2 is seen to diverge badly in the region of kinetic control, as expected. However, it gives a good prediction of the position and magnitude of the maximum value of η. For the multiple solution case its prediction of the bounds on ϕ values for which multiple states can occur is extremely good.

The stringency tests carried out above indicate that the gross features of the simplified analyses are correct but not necessarily accurate in detail. Consider now a more realistic case typified, for example, by $\gamma = 20$, $\beta = 0.02$, $Nu' = 10$, $Sh' = 500$ with $\gamma = 0.02$. Table 6.1 compares effectiveness factor values from the simplified analyses with those from digital simulation. Also shown are the values predicted from PETERSEN's[64] asymptotic solution on the basis $Nu' = Sh' = \infty$. Table 6.2 compares film and overall dimensionless temperature rises. The calculations are extended over a range of ϕ values sufficient to cover all potential regions of interest.

ø	(1)	(2)	(3)	(4)
1	0.98	0.96	3.34	3.21
2	0.92	0.86	1.74	1.61
3	0.82	0.75	1.22	1.07
5	0.65	0.60	0.81	0.64
8	0.55	0.50	0.63	0.40
15	2.86	2.86	2.87	0.21
20	1.69	1.69	1.69	0.16

TABLE 6.1 Comparison of effectiveness factors for a 1st order irreversible reaction

KEY

(1) Distributed parameter model

(2) Lumped thermal resistance model

(3) Proposed asymptotic model

(4) Petersen's asymptotic model

6.1.1 The asymptotic model

Looking first at the asymptotic model (column 3) the results for effectiveness factor show an appreciable discrepancy at least until film mass transfer becomes the dominant rate controlling process ($\phi \simeq 15$). The relative distribution and magnitude of the temperature rise between the fluid film and the catalyst particle is, however, satisfactorily predicted in regions II and III of the schematic diagram, Fig. 4.4.

The deviation of the asymptotic solution to the spherical pellet from the exact solution may be caused by three factors:-

(i) the assumption of slab geometry.

(ii) the assumption of zero concentration of reactant at the pellet centre.

ø	(1)	(2)	(3)
1	.004 (.001)	.001	.024 (.004)
2	.015 (.005)	.005	.029 (.009)
3	.026 (.010)	.009	.034 (.015)
5	.041 (.022)	.020	.046 (.027)
7	.056 (.037)	.034	.062 (.043)
15	.862 (.860)	.859	.862 (.860)
20	.904 (.902)	.902	.904 (.902)

TABLE 6.2 Comparison of temperature rises.

KEY (1) Distributed parameter model

(2) Lumped thermal resistance model.

(3) Proposed asymptotic model

.004 (.001) signifies the overall and fluid film temperature rises; where overall temp. rise = $(T_c-T_f)/T_f$, and fluid film temp. rise = $(T_s-T_f)/T_f$. T_c, T_s, T_f represent the temperatures at the centre of the pellet, the surface of the pellet and in the bulk fluid phase respectively.

(iii) the use of the approximate form of the integral, given by equation (5.36), rather than the exact form, equation (5.29).

From examination of the overall and film temperature rises in Table 6.2 and from Section 5.3.2.(e) it is concluded that assumption (iii) does not introduce a significant error in the solution.

Intraparticle concentration profiles presented in Fig. 6.2 throw some light on the source of the error. At low ø values neither assumption (i) nor (ii) is satisfied; both are contributing to the overall error but their relative effects are difficult to assess.

FIG. 6.2 Intraparticle concentration profiles
$\gamma = 20, \beta = 0{\cdot}02, Nu' = 10, Sh' = 500$

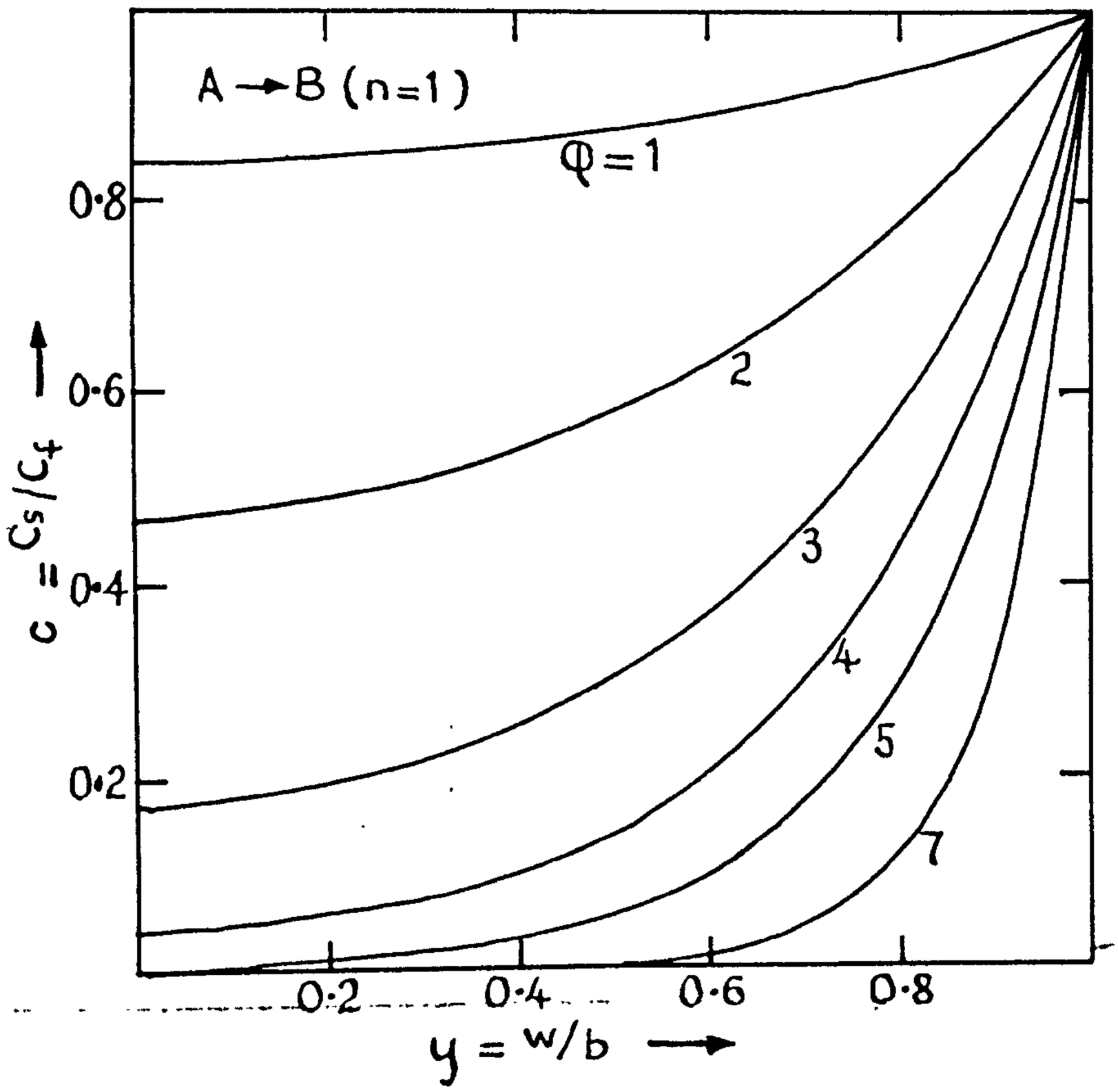

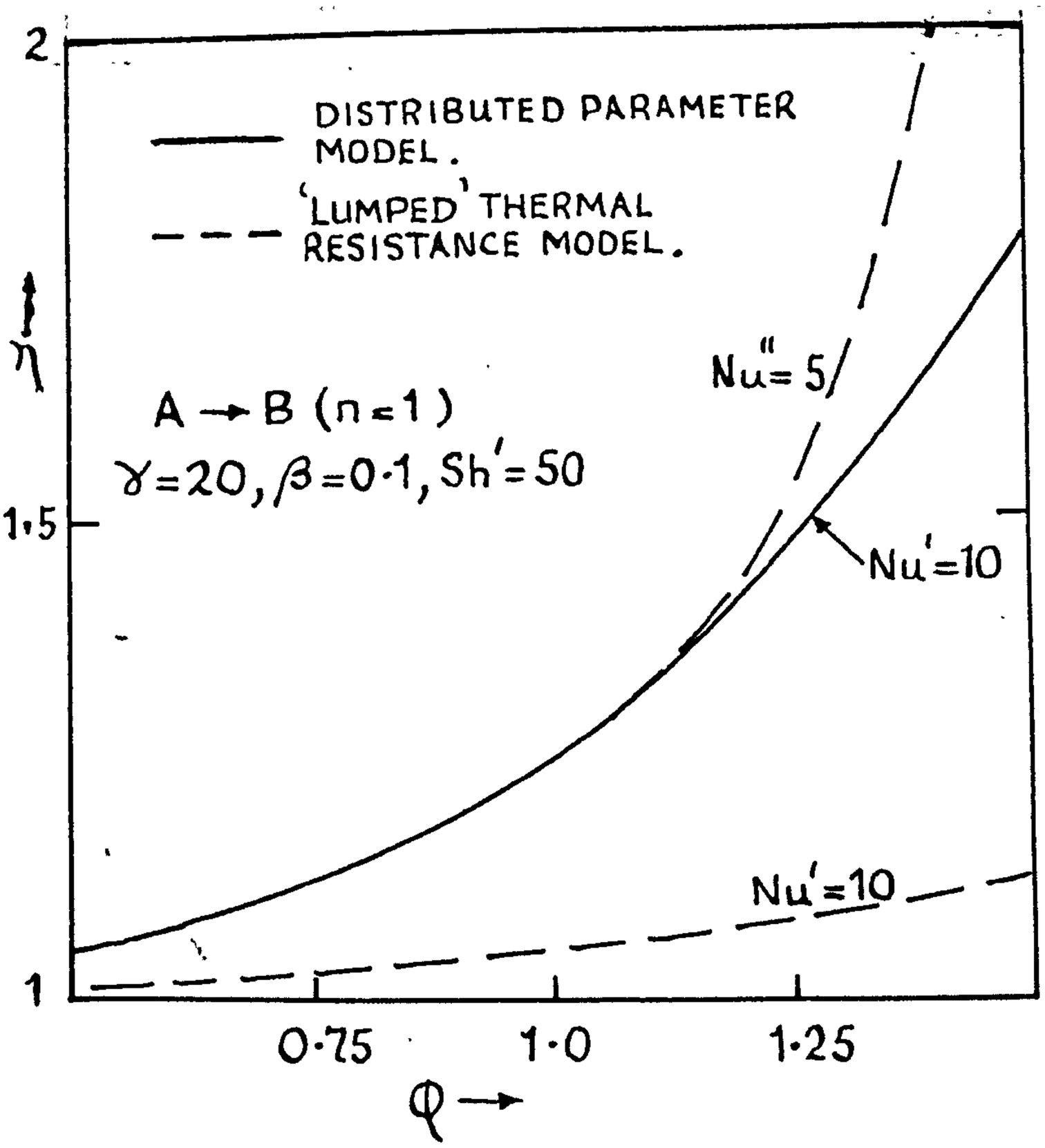

FIG. 6.3 The modified Nusselt number, Nu"

As ϕ is increased the concentration of reactant at the centre of the pellet falls progressively until at $\phi=7$ it is for practical purposes effectively zero. Any error present in the solution must now be largely due to assumption (i). At $\phi=7$, in fact, the exact and approximate values of η are 0.565 and 0.658 - an error of more than 16%. Assumption (i) does, therefore, seem to be of particularly doubtful validity unless the overall rate is dominated by film mass transfer i.e., operation is in region III of Fig. 4.4. In this region the simplified methods become redundant, for the effectiveness factor and the overall temperature rise are found with good accuracy from the explicit equations (4.17) and (4.9).

A correction for the terms $-\frac{2}{\phi(1-\xi/\phi)}\cdot dc/d\xi$ and $-\frac{2}{\phi(1-\xi/\phi)}\cdot dt/d\xi$, omitted from equations (5.8) and (5.9), can be found by considering the asymptotic solution as the first term in a perturbation series solution. Experience with the computationally simpler special case, in which $Nu'=Sh'=\infty$, showed that the effort required to obtain the second term in the series is appreciable. In view of the important requirement of speed of computation, as well as accuracy, this approach hardly seems worth extending to the more general case. It is evident that PETERSEN'S solution, shown in Column 4 of Table 6.1, does not display the correct asymptotic behaviour for the general case, in which Nu' and Sh' are finite, as might be expected.

6.1.2 The lumped thermal resistance model

The prediction of effectiveness factor using the lumped thermal resistance model is within 10% of the exact value shown in Table 6.1 over a range of ϕ values covering all potential regions of interest. Similar agreement has been found with other cases of practical origin. In view of such uncertainties in practice as the definition of pellet geometry and the measurement of effective diffusivity in porous catalysts, the error is not deemed excessive.

It is true that the simpler model mentioned above only leads to an estimate of the temperature rise across the fluid film (compare Columns 1 and 2 of Table 6.2) and does not provide any information concerning the excess temperature in the pellet, which may be unacceptable for reasons of selectivity or catalyst stability. Normally, however, the excess temperature inside the pellet is small in relation to the temperature rise across the film, especially when the overall temperature rise is appreciable, so this shortcoming is unimportant.

A method of correcting for a small temperature gradient inside the pellet which does not defeat the objective of a rapid method of analysis is presented in Appendix [illegible] The technique adopted lumps the distributed internal heat transfer resistance into a hypothetical solid film at the external surface of the catalyst pellet. Equations (5.1) and (5.2) are still applicable, but now T_s refers to the mean catalyst temperature and h is no longer a fluid film heat transfer coefficient, rather it is an overall coefficient made up of terms which include the fluid film heat transfer coefficient and the particle thermal conductivity. The final result is expressed in the form

$$Nu'' = \frac{10.Nu'}{(10+Nu')}$$

where Nu'' is a new Nusselt number including the modified heat transfer coefficient, h_{ov}. Figure 6.3 demonstrates the usefulness and limitation of the modification for case 2 (Fig. 6.1), in which a significant intra-particle temperature gradient is present, at least for a part of the range of ϕ values considered. Clearly, the simple modification is useful below ϕ=1.25, when the assumption of a parabolic intraparticle temperature profile is approximately valid. At higher ϕ values, with the onset of an appreciable fluid film heat transfer effect, the method seriously over-estimates the overall heat transfer resistance and leads to a prediction of the overall rate of reaction far in excess of the true value.

Since the region in which the discrepancy occurs is one to be avoided in design (cf. Section 4.6.3), the disparity is of theoretical rather than of practical interest.

6.2 Computing times

Computing times for the different procedures are closely related to several factors and it is difficult to obtain valid a priori estimates of the advantages of a particular technique over any other in a given situation. The numerical integration methods of Chapter 4 are compared in Appendix 3, and it was found that the integration step size and the rate of convergence depend to a large extent on the region of the schematic diagram, Fig. 4.4 in which the calculations are being carried out. Roughly speaking, the following times are indicative of the three regions for the method of solution used by CARBERRY and WENDEL[10].

Region	Compute time/iteration
I	$^1/_5$ second
II	1 second
III	2 seconds

The number of iterations required in region I is generally less than 4, but in region II is usually between 6 and 10 for the initial conditions.

$$c = t = 1, \quad 0 \leq y \leq 1.$$

The choice of initial conditions is arbitrary and convergence of the solution outside the multiple solution region does not depend on this assumption. Convergence in region III can be accelerated by altering the initial conditions to $c=0$, $t=1+\beta Sh'/Nu'$; $0 \leq y \leq 1$.

To picture more clearly the problems involved with the simplified techniques consider the case of a single irreversible first order reaction. Looking at the more generalized treatment of Section 5.3.2, equation (5.31) is combined with the value of the respective integral appearing in Table 5.1 to produce a non-linear algebraic equation for the

unknown, c_s. Putting $x = 1-c_s$, the following equation arises after some manipulation

$$\frac{Sh'}{2\phi}.x = G(x) \qquad (6.1)$$

where $G(x) = \frac{\sqrt{2}.}{\gamma\beta}(1+\lambda x).^2 \exp\left(\frac{\gamma.\lambda.x}{(2(1+\lambda x))}\right).$

$$\left[\exp\left(\frac{\gamma\beta(1-x)_2}{((1+\lambda x)^2)}\right) - 1 - \frac{\gamma\beta(1-x)_2}{(1+\lambda x)^2}\right]^{\frac{1}{2}}, \beta > 0$$

and $\lambda = \beta Sh'/Nu'$.

The right hand side of equation (6.1) is plotted as a function of x in Fig. 6.4 for the three cases considered in Fig. 6.1. The left hand side of equation (6.1) is a linear function of x whose intersection(s) with the G(x) curve give the root(s) of equation (6.1). Two observations concerned with the properties of the function G(x) are of considerable importance.

1. For exothermic reactions the function G(x) exhibits a maximum in the range $0 \leq x \leq 1$.*

2. The G(x) curve may exhibit three intersections with the left hand side of (6.1) - e.g., the curve for $\lambda = 1$ and the line F of Fig. 6.4.

With respect to these observations it is clear that the Newton-Raphson iteration process for finding the roots of equation (6.1) cannot be used without care. Depending on the initial estimate $x^{(o)}$ convergence may or may not occur to the desired root. Changing the initial value $x^{(o)}$ will remove this problem. Within the framework of the design synthesis procedure this difficulty has not arisen for two reasons:

(a) only unique particle states have been studied in which the point of intersection always lies to the left of the maximum.

* It is readily shown that no such maximum exists for endothermic reactions ($\beta < 0$).

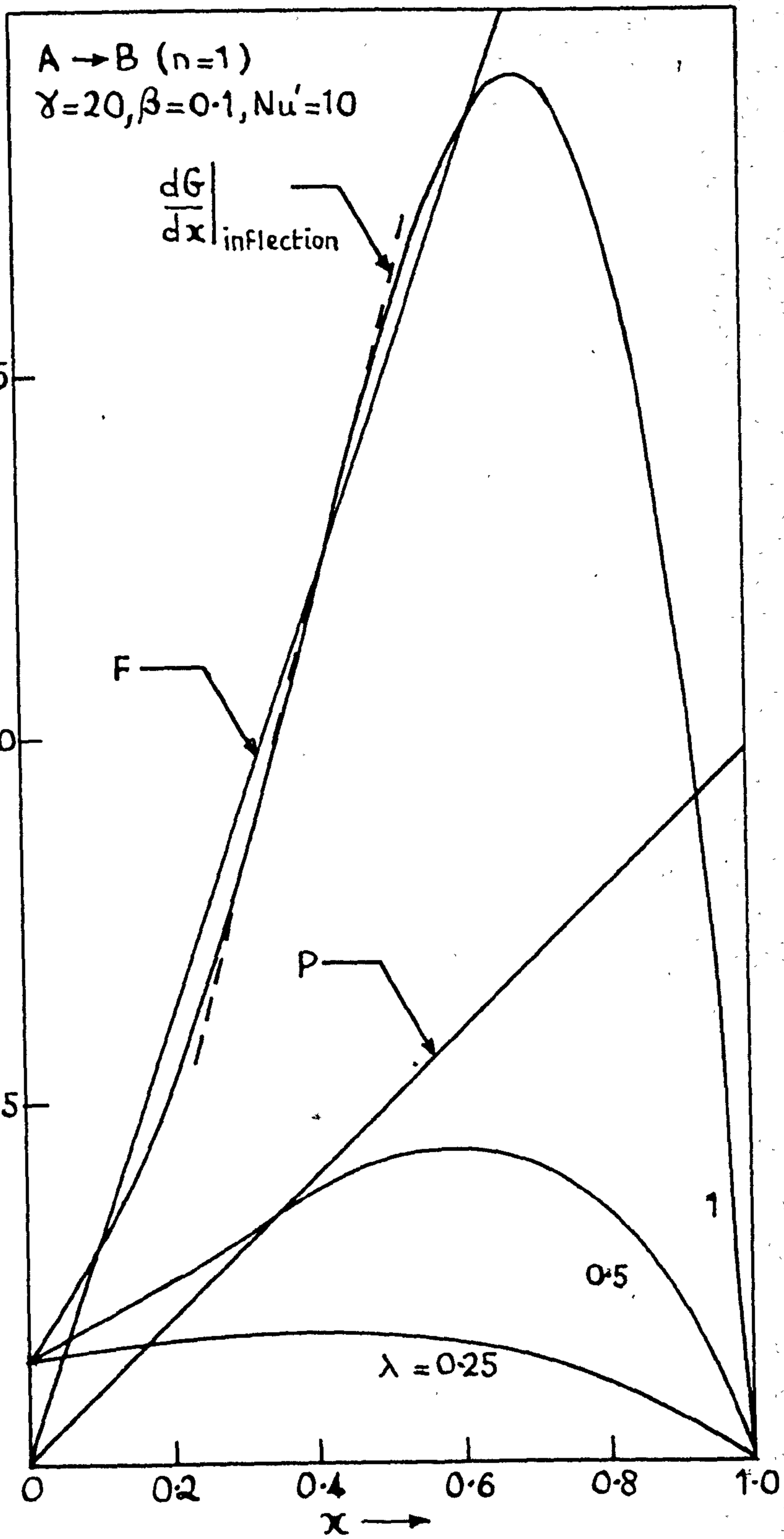

FIG. 6.4 The asymptotic model. Plot of the function $G(x)$ showing multiple intersections with the line $y = Sh'.x\,/\,2Q$

(b) good estimates of the root have been obtained by making use of the stepwise integration procedure in the two-dimensional finite difference network covering the reactor.

In regions I and II of Fig. 4.4 both the lumped thermal resistance model and the asymptotic model display rapid convergence, as might be expected from the geometric background of the Newton-Raphson procedure. Generally, only 3 iterations are required to establish a relative error between successive iterations $x^{(n)}$, $x^{(n+1)}$ of less than 0.01% starting from the initial condition $x^{(o)} = 0$. More accurate initial estimates do not noticeably improve the rate of convergence. In region III convergence is again extremely rapid starting from $x^{(o)} = 1$.

The average compute time/iteration for over 200 calculations covering regions I to III is of the order of 0.1 second for <u>both</u> simplified models.

<u>Summary</u>

Some illustrative results demonstrate the limited utility of the asymptotic approach as a reliable means of analysis. The method, while asymptotically exact in region III of Fig. 4.4, may show appreciable discrepancy in the important region of "pore" diffusion influence (region II). The main cause of the discrepancy in this region is believed to be due to the effects of particle geometry. While a correction can be obtained for this effect, the effort required is considerable and the objective of a rapid method of analysis is defeated.

The lumped thermal resistance model generally leads to a prediction of the overall rate within 10% of the true value. A method of correcting for a small temperature gradient inside the pellet is suggested which seems to improve the agreement when the assumption of a parabolic intra-particle temperature profile is valid.

However, there seems no obvious way in which a priori estimation of

the error involved in the model can be found. Further, the method of solution is directly applicable only to reaction networks involving zero or first order reactions. It might be added here that early indications point to the usefulness of the model for the consecutive reaction scheme $A \rightarrow B \rightarrow C$ in which overall exothermicity is present.

In the region of utility (i.e. region II) of the lumped thermal resistance model, the saving in computational effort/iteration is ten-fold compared with that required to solve the distributed parameter problem.

CHAPTER 7

DESIGN SYNTHESIS:

(a) IMPLEMENTATION OF APPROXIMATION TECHNIQUES INTO DESIGN; NUMERICAL DIFFICULTIES AND PROPOSED STRATEGY

To date, attention has been largely concentrated on understanding the factors which influence 'local' catalyst behaviour. Following on from this analysis it is legitimate to inquire how the local regime is coupled and distributed throughout the reactor. Integration of the local regime will provide an overall picture of the temperature and conversion distributions throughout the confines of the bed.

Such a technique of design synthesis has received rare usage. It appears that there has been only one attempt (by LIU[75]) to solve the problem posed in Chapter 3 by using an "effectiveness factor" approach, and valuable though the work undoubtedly is from the theoretical standpoint, the assumption of Dirichlet boundary conditions at the external surface of the particle seriously restricts its practical application.

The reasons behind the apparent neglect are obvious. It is difficult to justify the employment of complex models in design in the absence of suitable data. Moreover, the procurement of catalytic surface rate models and, perhaps to a lesser extent, transport coefficients presents a formidable problem both in the design of laboratory scale equipment and the interpretation of experimental data. Further, computational feasibility is very important and must be investigated. Even though the advent of high-speed digital computers has alleviated this problem, the use of efficient numerical analysis has assumed considerable importance, especially in view of the highly non-linear form of the equations but also by complications introduced by some of the boundary conditions.

7.1 The Policy

In an attempt to overcome this difficulty, approximate methods of analysis were developed in Chapter 5 which permit a rapid assessment of the "local" behaviour without the need to solve the distributed set of equations for the catalyst particle. While it is relatively straightforward to obtain an indication of the accuracy of the prediction of "local" behaviour by comparison with "exact" numerical integration, it is difficult to see how the "local" errors, introduced by the approximation to η, interact and distribute through the computed solution for the entire bed, without having as a basis a solution of the fully distributed problem given in Chapter 3. In order to check the underlying assumptions of the simpler models, numerical solutions of the fully distributed problem are also obtained.

7.2 Decision making

The concept of decision-making as applied to model discrimination lies outside the scope of this research. Nevertheless, it represents a vitally important issue in the optimization of design strategy.

Having a reasonably accurate detailed model it should be possible to develop semi-empirical simpler models which retain the essential features of the system, albeit over a limited range. Knowing the range over which it may be applied, when conditions change sufficiently the semi-empirical model can be updated i.e., used adaptively. Such a technique of model reduction is valuable in design, on-line optimization and control studies, since the storage and computing times can be drastically cut, yet all the important detail is retained. If an approach of this kind is to have generality, it can only follow as a result of exhaustive computations on all factors and functions governing local and overall activity, and selectivity (yield).

In the design syntheses which follow, the idea of approximation methods for handling computations of "local" behaviour is introduced into

design strategy, but no decisions are yet taken, within the framework of the computation, as to the type of approximation method to be used.

7.3 Lumped parameter analogues for use in design synthesis

Approximation methods were developed in Chapter 5 as a result of ideas originating from the analysis in Chapter 4. Two methods were considered, the "lumped thermal resistance" model and a treatment extending PETERSEN'S[64] asymptotic solution. The former is tailored specifically to the first order reaction and is asymptotically exact in both the kinetic and interphase mass transfer controlled regions. The latter technique, while more flexible in handling reactions of arbitrary order, diverges badly from the true solution in the region of chemical kinetic rate control.

To illustrate the use of approximation methods in design synthesis, attention is focused on the more important first order reaction. In order to cover a representative number of case histories, the more flexible "lumped thermal resistance" model is chosen as a basis for synthesis into the design procedure.

7.3.1 Comparisons with previous work

Since the present synthesis extends most others in combining the internal particle problem with the 2-dimensional external field, it is important to ascertain the effects of the added complexity. Consequently, the alternative and simpler "surface reaction model" is set up to allow a computational comparison. A one-dimensional form of this model has been used in a series of papers by LIU, ARIS and AMUNDSON[76-78] to investigate stability in packed beds of catalyst. Basically, the simpler model lumps heat and mass transfer resistances at the particle surface and considers chemical reaction as the only intraparticle effect. In general, the descriptive equations form a coupled system of non-linear algebraics.

7.3.2 The surface-reaction model

Although it is not necessary, the reaction is assumed to be first order. More complicated reactions can be treated but no new features are introduced. In accordance with the physical basis of the model, the relevant material and energy balance equations are

$$\frac{\beta}{b} \cdot k_A(C_f - C_s) - \alpha \cdot S_v \cdot \exp(^{-E}/R_g T_s) C_s = 0 \qquad (7.1)$$

$$\frac{\beta}{b} \cdot h \cdot (T_f - T_s) + (-\Delta H) \cdot \alpha \cdot S_v \cdot \exp(^{-E}/R_g T_s) C_s = 0 \qquad (7.2)$$

Obviously, the external field equations for this model are the same as previously defined (equations (3.2) and (3.3)).

An assessment of the factors influencing the "local" rate process follows readily from equation (7.1). By manipulation,

$$C_s = \frac{k_A \cdot a_v \cdot C_f}{(k_A \cdot a_v + k_s)} \qquad (7.3)$$

where a_v $(= \frac{\beta}{b})$ is the surface to volume ratio of the catalyst particle, and k_s $(= \alpha \cdot S_v \cdot \exp(^{-E}/R_g T_s))$ is the surface reaction rate constant.

The rate of reaction per unit gross volume of catalyst, $k_s \cdot C_s$, may be written from (7.3)

$$k_s C_s = \frac{k_s \cdot k_A \cdot a_v}{(k_A \cdot a_v + k_s)} C_f = k_E \cdot C_f,$$

where k_E is an "effective" rate constant, reflecting both surface reaction kinetic and film mass transfer influence, given by

$$k_E = k_s \cdot k_A \cdot a_v / (k_A \cdot a_v + k_s) \qquad (7.4)$$

Analysis of equation (7.4) demonstrates "surface reaction kinetic" control when $k_s / k_A \cdot a_v \ll 1$, and conversely "film mass transfer" control if $k_A \cdot a_v / k_s \ll 1$. Intermediate values are in what may be called a "mixed" regime and the overall rate is a function of both the kinetic and transport characteristics.

7.3.3 The quasi-homogeneous model

Clearly, the simplest model that can be envisaged for the catalyst pellet is one in which the overall rate is governed only by surface reaction kinetics. The disregard of possible heat and mass transfer rate-influencing factors both within and external to the catalyst pellet means, in effect, that $\eta(x,r) = 1$ throughout the reactor, and an appreciation of the temperature and conversion distributions follows simply from integration of the external field equations given by (3.2) and (3.3). The term quasi-homogeneous arises by virtue of the close similarity of the descriptive equations with those for the "empty" tubular reactor in which homogeneous reaction is occurring. Hidden in the equations, however, is the influence of the catalyst assembly on the dispersion, conduction and reaction rate coefficients.

Since both "surface reaction" and "quasi-homogeneous" models are special cases of the more general "lumped thermal resistance" model, attention will be concentrated on the latter. In examining solutions the "surface reaction" model can be obtained by allowing the solid diffusional resistance to approach zero (i.e., $D_A^* \rightarrow \infty$). The "quasi-homogeneous" representation follows by, in addition, letting $k_A \rightarrow \infty$ and $h \rightarrow \infty$.

7.4 The synthesized model

The set of descriptive equations covering the transport processes in the external field and the transport/reaction processes within the solid catalyst pellets is given by equations (3.2), (3.3) and the "lumped thermal resistance" model, (5.1) and (5.2), written for the general n^{th} order reaction. In dimensionless form these equations are written as

$$-\frac{\partial T_f^*}{\partial z} + c_1\left(\frac{\partial^2 T_f^*}{\partial s^2} + \frac{1}{s}\cdot\frac{\partial T_f^*}{\partial s}\right) - c_2\cdot\eta\cdot r^*(C_f^*, T_f^*) = 0 \qquad (7.5)$$

$$- \frac{\partial C_f^*}{\partial z} + c_3\left(\frac{\partial^2 C_f^*}{\partial s^2} + \frac{1}{s} \cdot \frac{\partial C_f^*}{\partial s}\right) - c_4 \cdot \eta \cdot r^*(C_f^*, T_f^*) = 0 \qquad (7.6)$$

$$\frac{\partial^2 C_s^*}{\partial y^2} + \frac{2}{y} \cdot \frac{\partial C_s^*}{\partial y} - \Phi_o^2 \cdot r^*(C_s^*, T_s^*) = 0 \qquad (7.7)$$

$$(T_f^* - T_s^*) - \beta_1 \Phi_o^2 \cdot \int_o^1 y^2 r^*(C_s^*, T_s^*) dy = 0 \qquad (7.8)$$

where the boundary conditions follow from a consideration of equations (3.11) - (3.17) and equation (3.6).

$$T_f^* = 0 \quad ; \quad z = 0, \quad 0 \leq s \leq 1 \qquad (7.9)$$

$$C_f^* = 0 \quad ; \quad z = 0, \quad 0 \leq s \leq 1 \qquad (7.10)$$

$$\partial T_f^*/\partial s = 0 \quad ; \quad s = 0, \quad 0 \leq z \leq 1 \qquad (7.11)$$

$$\partial T_f^*/\partial s = \lambda \cdot (1 - T_f^*); \quad s = 1, \quad 0 \leq z \leq 1 \qquad (7.12)$$

$$\partial C_f^*/\partial s = 0 \quad ; \quad s = 0 \qquad (7.13)$$

$$s = 1 \qquad (7.14)$$

$\Big\}$ $0 \leq z \leq 1$

$$\partial C_s^*/\partial y = 0 \quad ; \quad y = 0 \qquad (7.15)$$

$$\partial C_s^*/\partial y = \frac{Sh'}{2} \cdot (C_f^* - C_s^*); \quad y = 1 \qquad (7.16)$$

$\Big\}$ $0 \leq z \leq 1, \; 0 \leq s \leq 1$

In these equations the following reduced variables are used:

$$z = \frac{x}{L}, \quad s = \frac{r}{r_o}, \quad y = \frac{w}{b}, \quad C_f^*(C_s^*) = \frac{C_{fo} - C_f(C_s)}{C_{fo}}$$

and $T_f^*(T_s^*) = \frac{T_f(T_s) - T_{fo}}{T_a - T_{fo}}$, respectively.

The coefficients in the external field equations, (7.5) and (7.6), are given by

$$c_1 = \frac{K_f L}{G_o c_f ro^2} \left(\equiv \frac{dp\ L}{ro^2} \cdot \frac{1}{Pe_H} \right) , \quad c_2 = \frac{(-\Delta H).L.(1-e)k_{v_{fo}} C_{fo}^{n}}{G_o c_f (T_a - T_{fo})} ,$$

$$c_3 = \frac{D_f L}{V_o ro^2} \left(\equiv \frac{dp\ L}{ro^2} \cdot \frac{1}{Pe_M} \right) , \quad c_4 = \frac{L.(1-e).k_{v_{fo}}.C_{fo}^{n-1}}{V_o}$$

Φ_o (appearing in equations (7.7) and (7.8))may be regarded as a reaction-diffusion modulus based upon an "imaginary" specific reaction rate of the feed stream - i.e.,

$$\Phi_o = b \sqrt{\frac{k_{v_{fo}}.C_{fo}^{n-1}}{D_A^*}} , \text{ where } k_{v_{fo}} = \alpha.S_v.\exp(^{-E}/R_g T_{fo})$$

Other dimensionless groups and functions appearing in the particulate field equations are defined by

$$\beta_1 = \frac{(-\Delta H) C_{fo} D_A^*}{h.b.(T_a - T_{fo})} \quad ; \quad r^*(C_s^*, T_s^*),$$

a dimensionless reaction rate, is equal to

$$a_A \exp\left[\gamma.\theta.T_s^* / (1+\theta T_s^*) \right].(1-C_s^*)^n; \quad \gamma = {}^{E}/R_g T_{fo}; \quad \theta = (T_a - T_{fo})/T_{fo}.$$

The specification of coefficients is completed by examination of the boundary conditions (7.9) to (7.16). Two groups arise which are defined below:

$$\lambda = U.ro/K_f; \quad Sh' = 2\ k_A\ b/D_A^* \quad \text{(see Section 4.2)}$$

Finally, the effectiveness factor, η, appearing in equations (7.5) and (7.6) is obtained from equation (3.19) expressed in terms of dimensionless quantities by

$$\eta = \frac{3.(\partial C_s^*/\partial y)_{y=1}}{\Phi_o^2 . r^*(C_f^*, T_f^*)} \qquad (7.17)$$

7.4.1 Classification of the equations

A most vital part of the overall programme, and one which cannot be overemphasized, is concerned with solving the descriptive equations. It is desirable, furthermore, to be able to justify the answers which result, assuming, of course, that the equations can be solved.

To move towards this objective requires consideration of the basic properties of the equations comprising the system. Often this step is ignored, sometimes with disastrous consequences (e.g., indiscriminate use of finite difference methods for hyperbolic equations). Although the equations are written for single particles and the interstitial fluid, once the equations are formulated, the model no longer reflects the idea that there are single particles in the bed. The mathematical system, in other words, is a continuous representation of a physical model which is essentially discrete.

Equations (7.5) to (7.8) represent an interesting problem in mixed types of equations; equations (7.5) and (7.6), describing the interstitial fluid field, are partial differential equations in 2-dimensions, of parabolic form[79], boundary-value in the s-dimension and complicated by non-linear kinetics. The equations describing the particulate phase are given by (7.7) and (7.8) and are coupled to the external field equations at each point (z,s) of the external field either directly, as in (7.8), or through the boundary condition (7.16) describing mass transport through the surface film. Equation (7.7) denotes the mass transport/reaction situation inside a catalyst pellet and, at some point (z,s) of the external field, is viewed as an ordinary differential equation, boundary-value in the y-dimension and non-linear

for $n \neq 0,1$. Coupled to this equation is the energy balance equation (7.8) which is both algebraic and non-linear in T_s^* as a consequence of the exponential temperature dependence of the reaction rate. Of further interest is the integral in equation (7.8) which arises from the presence of an intraparticle concentration gradient.

The presence of non-linear functions of the dependent variables prevents an analytical solution. Either digital simulation or semi-analytic methods appear to offer the only route to the solution. Both avenues of approach are investigated in this chapter with the intention of going someway towards establishing the kind of philosophy best suited to solving problems of this kind.

7.5 The special case of first order kinetics

A numerical strategy capable of handling reactions of any order has been summarized[80]. Illustration of the method is given for the first order reaction. It is not the intention, here, of repeating that work. Rather, attention will be focused on developing the special property of the "lumped thermal resistance" model for the first order reaction.

The method of solution of the particulate field problem and the simplifications brought about, thereupon, are presented in Section 5.3.1. For the first order reaction, equation (7.7) is linear in C_s^* and may be integrated analytically since T_s^*, although unknown, is independent of y. From equations (7.7), (7.15) and (7.16), the intraparticle concentration profile is given by

$$C_s^* = 1 - \frac{1}{y} \cdot \frac{\frac{Sh'}{2} \cdot (1-C_f^*) \sinh \Delta y}{\left[\Delta \cosh \Delta + (\frac{Sh'}{2} - 1) \sinh \Delta\right]} \qquad (7.18)$$

$y > 0$, where $\Delta^2 = \Phi_o^2 \exp\left(\frac{\gamma \theta T_s^*}{1+\theta T_s^*}\right)$

Substituting equation (7.18) in equation (7.8) and integrating gives

$$(T_f^* - T_s^*) + \beta_1 . \frac{Sh'}{2} . f(C_f^*, T_s^*) = 0 \qquad (7.19)$$

where $$f(C_f^*, T_s^*) = \frac{(1-C_f^*).(1 - \tanh \Delta / \Delta)}{\left[1 + (\frac{Sh'}{2} - 1) \frac{\tanh \Delta}{\Delta}\right]} \qquad (7.20)$$

Differentiating equation (7.18), setting y = 1 and using $(\partial C_s^* / \partial y)_{y=1}$ in equation (7.17), there results the equation

$$\eta . r^*(C_f^*, T_f^*) = - \frac{3\ Sh'}{2\ \Phi_o^2} . f(C_f^*, T_s^*) \qquad (7.21)$$

The simplification produced by this approach is considerable in many respects. Using the more general method described elsewhere[80], an appreciation of "local" activity, η, requires the simultaneous sclution of equations (7.7) and (7.8) at each point (z,s) of the external field. This is not easily accomplished numerically, and it is found that inclusion of a third dimension, y, aggravates the stability problem, increases storage and dramatically increases computing times. The method presented here, in effect, removes the third dimension by replacing equations (7.7) and (7.8) by a non-linear algebraic equation (7.19). It is to be expected that this approach will lead to considerable reduction in compute times, a factor of paramount importance particularly in optimization and control studies.

Unfortunately, the n^{th} order reaction ($n \neq 0,1$) presents more difficulty since the equation corresponding to (7.7) is non-linear in C_s^*. Similar simplificoations cannot be evoked by using the "lumped thermal resistance" model. More detailed analysis is called for on a level similar to that in Chapter 5 before the n^{th} order reaction can be confidently handled by methods which lead to the simplifications described above.

7.6 Numerical difficulties

Granted the simplifications brought about in the previous section, it is still apparent that, because of non-isothermality in the external field, analytical integration of the equations is not feasible. Numerical methods which rely on the use of finite difference approximations are subject to certain complications introduced through the boundary conditions.

Firstly, a discontinuity in $\partial T^*_f / \partial s$ exists between equations (7.9) and (7.12) at the point (0,1). Methods of obtaining numerical solutions to partial differential equations by the use of finite difference schemes are inaccurate in the neighbourhood of a singularity. Nevertheless, it is widely believed for equations of parabolic type that the errors die away fairly rapidly in a step by step process. Recent evidence[81] indicates that this is not necessarily the case, and PARKER and CRANK[82] have shown that the errors can persist for certain types of boundary conditions.

A further source of difficulty can arise even if there is no discontinuity present. KEAST and MITCHELL[83] demonstrated that the use of certain apparently stable difference formulae (e.g., Crank/Nicolson[84]) can lead to serious instability for certain boundary conditions, of which (7.11) and (7.12) enter this category.

The foregoing remarks apply to the linear parabolic equation. In relation to the non-linear problem at hand there seems little that can be achieved in the way of conventional numerical stability analyses. No quantitative results on either persistent or accumulating error seem obtainable. All that can be inferred is that if such effects show up in the numerical solution of the isothermal (i.e., linear) problem, then it is reasonable to expect their appearance, possibly on a much larger scale, in the non-linear case.

The need for extreme caution in assessing the accuracy of results is

apparent, especially in view of what has been said above. A common method with stable finite difference formulae is to demonstrate the convergence by reducing the integration step sizes until the solution stops changing, although there is no guarantee that this is the correct answer[85]. It is, in otherwords, a necessary but insufficient condition. Nevertheless, this approach is usually the most satisfactory way of checking one particular technique. A further check can be made by employing an alternative technique and seeing if it gives the same answer. In the present instance this philosophy is not easily put into practice, since any alternative non-analytic strategy must also suffer the effects of the discontinuity. Instead, a semi-analytic method is developed (see Appendix 5) which is applicable over the entrance region of the bed. Although a complete check on accuracy is not possible, the results from numerical integration can at least be approximately assessed over the most critical phase of the computation - i.e., in the region of the discontinuity.

Instability of the differential system, itself, is also manifest when the individual particles can exist in more than one state. A possibility of this kind should be borne in mind when considering the significance of the instability of finite difference approximations of such systems.

7.7 Numerical methods of approach

The fundamental way of approaching this problem is not in dispute. It is obvious that the solution is to be projected from the region where the dependent variables in the fluid field are known (i.e., $z = 0$) stepwise into the region where they are unknown (i.e., $z > 0$). What is in dispute, however, is the numerical strategy to be adopted to advance the solution.

It is the general practice to employ finite difference methods to

solve problems of this kind. Of immediate concern is the extent to which finite difference approximations are to be used in replacing the derivatives appearing in equations (7.5) and (7.6). If only the radial derivatives are replaced by finite differences, a set of 2M + 2 differential-difference equations is obtained, where M is the no. of radial increments. These equations may be solved by standard low truncation error integration formulae - e.g., Runge-Kutta. The treatment of non-linearities is explicit - i.e., no iteration is required. An alternative approach is to employ finite difference approximations in both the axial and radial space dimensions, and so produce a set of 2M + 2 algebraic equations at each z step. If explicit methods are used the equations are linear, whereas the more commonly adopted implicit methods lead to simultaneous non-linear equations.

It must be stressed that the choice of numerical scheme requiring the least total amount of work is only likely to follow as a result of trial and error. No general principles can be laid down for non- linear systems regarding the choice of method. However, in seeking methods of integration some guidance is permitted from a study of linear systems. At present, the most reasonable outlook is to seek highly stable techniques for linear problems and hope that stability is carried over (with conveniently large steps) to the non-linear problem. Following this philosophy it is immediately evident that explicit schemes such as the Euler and Runge-Kutta formulae are unlikely to prove fruitful. In both methods stability can impose much more severe penalties in computing time than truncation error alone[38, 86, 87]. The obvious alternative is to examine implicit processes.

7.7.1 Implicit methods

As mentioned earlier, implicit methods lead to simultaneous algebraic equations. In general, these equations are non-linear and can only be

solved by a method of successive approximation. Besides the obvious requirement of seeking a finite difference scheme which combines high stability with low truncation error, there arises the additional problem of handling the non-linearities in a way which does not impose a further restriction on step size.

Considering the former requirement first of all, it is concluded that there is no single method in wide usage which combines the dual virtues of high stability and low truncation error. The nearest approach to the ideal is probably the technique due to CRANK and NICOLSON[84]. For linear problems this technique solves the problem of stability completely†. In a sense, however, it only just solves it, and in certain applications instability can appear when the method is extended to a non-linear problem. A considerable improvement in the stability property is brought about by using LAASONEN'S[88] implicit formula, but the truncation error is larger and this in itself can impose fairly severe restrictions on the axial step size.

There is a voluminous literature on stability of numerical methods but much of it stops short of what is needed in practical applications to non-linear equations.

Direct applications of the Crank Nicolson method in reactor design and stability studies are to be found in papers by von ROSENBERG[89], FROMENT[37, 90], LIU and AMUNDSON[78], and LEE[91]. The Laasonen formula is used by MICKLEY and LETTS[92].

7.7.2 Treatment of non-linearities

The benefits which accrue from the use of implicit methods can be severely offset by inefficient handling of the non-linear terms. There are many ways of dealing with the non-linearities in problems of this

† Excepting the remarks made by PARKER and CRANK[82], KEAST and MITCHELL[83].

kind and each approach offers something over the others in a particular set of circumstances. Only by extensive computing experience will it be possible to develop a unified treatment of this problem. However, certain requirements must be satisfied by any technique if it is to be used at all successfully. Particular attention is paid to the following points:

(a) actual computing time,

(b) flexibility of application,

(c) storage requirement.

Fundamentally there would seem to be two categories under which all developments can be classified:-

(i) <u>non-iterative methods</u>

Non-iterative finite difference methods are based upon explicit evaluation of non-linear terms and implicit expressions for linear terms. For mild conditions this approach is to be preferred over an iterative method since the balance between computational effort per step and the no. of steps required is favourable compared with the more tedious iterative process. For highly non-linear equations the situation is reversed and iterative methods provide the pay-off. In looking for flexible techniques iterative schemes are pursued.

(ii) <u>iterative methods</u>

Iterative processes are centred on the concept of prediction and correction. The "predictor" can be viewed as a technique of the type classified in the previous paragraph. Its purpose is to provide an estimate of the true solution. The "corrector" improves the estimate recursively until the sequence of updated solutions is deemed to have converged to the true solution. Only then is the computation allowed to proceed to the next step in the integration. Obvious features of any such method include a predictor scheme which provides accurate estimates of the true solution, in order to guarantee convergence of the iterations,

without at the same time imposing further restriction on the allowable axial step, and a corrector scheme which rapidly forces the iterations to converge. It is extremely difficult, if not impossible, to predict the stability and rate of convergence of such methods without performing actual computations. Some guidance on these matters is permitted by reference to the literature.

The concept of prediction and correction for non-linear parabolic equations was introduced by DOUGLAS et al[93-95]. Application to the 1-dimensional dynamic "surface reaction" model is to be found in the work of LIU and AMUNDSON[78]. Predictions of the true solution to the interstitial fluid equations at the (n + 1) st time step are found by allowing the partial pressure and temperature of the particulate phase to lag 1 time step, treating the linear terms implicitly. The predicted solution is improved by successive applications of Crank Nicolson's method. Integration of the particle equations proceeds over a time step by use of a set of predictor-corrector formulas based on Euler's formula and the trapezoidal rule.

The shortcomings of this method of integration are highlighted by LEE[91] by direct comparison with an alternative technique due to BELLMAN and KALABA[52]. Known as the generalized Newton-Raphson method (or the quasi linearization technique), this process represents the non-linear equation by a sequence of linear equations. Actual computational experience has shown that if the iterative process converges, the rate of convergence is quadratic in the sense that the error of any iteration is approximately the square of the error of the preceding iteration. The value of the method lies in its rapid convergence to the solution, quite often from poor starting values. Because of its broad applicability this technique is gaining frequent use in a variety of applications[96-100].

Recently LIU[51, 75] has applied predictor-corrector methods to two-

point boundary value problems of the kind studied in Chapter 4, and to simultaneous non-linear parabolic equations describing radial mixing-reaction in a packed tubular reactor. His technique based upon one by SAUL'YEV[101] combines the best features of the implicit and explicit methods. It avoids solving simultaneous equations but retains stability. The truncation errors may be lowered by alternating the direction of integration in the radial direction at successive axial steps or by averaging the two at the same axial step[101, 102]. Although no direct comparison is made with the quasilinearization technique the computation time indicated[75] must rate the method a serious competitor.

CHAPTER 8

(b) NUMERICAL SOLUTION OF THE DESCRIPTIVE EQUATIONS

Summary

A generalized implicit finite difference scheme combined with the quasilinearization technique is employed to solve the system of equations describing the synthesized model. An alternative semi-analytic method is discussed in Appendix 5 and is applied to the special case of the 2-dimensional "surface reaction" model. Analytical solutions are developed for the most general linear form of the rate equation which maintains the coupling between the material and energy balance equations.

The numerical approach developed here can be conveniently broken down into three steps.

(i) Construction of the linearized sequence of partial differential equations approximating equations (7.5) and (7.6) by application of quasi-linearization.

(ii) Reduction of the linearized equations into difference form by the use of a generalized implicit scheme.

(iii) Solution of the simultaneous difference equations.

Each step is considered in some detail in the following sections.

8.1 Construction of the linearized sequence

The procedure for constructing the sequence of differential equations is initiated by linearization of equation (7.21).

Equation (7.21) is written in the form

$$\eta . r^*(C_f^*, T_f^*) = g(C_f^*, T_s^*) \qquad (8.1)$$

where g is a non linear function given by

$$g(C_f^*, T_s^*) = -(3Sh'/2\beta_o^2) . \; f(C_f^*, T_s^*), \qquad (8.2)$$

$f(C_f^*, T_s^*)$ being defined by equation (7.20). The right hand side of equation (8.1) can be linearized by use of the generalized equation

$$\underline{f}(\underline{U}_{k+1}) = \underline{f}(\underline{U}_k) + \underline{J}(\underline{U}_k) \; (\underline{U}_{k+1} - \underline{U}_k) \qquad (8.3)$$

where $\underline{U}_{k+1}$, $\underline{U}_k$ and $\underline{f}$ are in vector form and represent the vectors $U_{(k+1),1}$, $U_{(k+1),2}$, $\cdots U_{(k+1),m}$; $U_{k,1}$, $U_{k,2}$, $\cdots U_{k,m}$; and f_1, f_2, $\cdots f_m$ respectively. The Jacobian matrix $\underline{J}(\underline{U}_k)$ is defined by

$$\underline{J}(\underline{U}_k) = \begin{bmatrix} \frac{\partial f_1}{\partial U_{k,1}} , \frac{\partial f_1}{\partial U_{k,2}} , \cdots \frac{\partial f_1}{\partial U_{k,m}} \\ \\ \frac{\partial f_m}{\partial U_{k,1}} , \frac{\partial f_m}{\partial U_{k,2}} , \cdots \frac{\partial f_m}{\partial U_{k,m}} \end{bmatrix} \qquad (8.4)$$

Note that the symbols g, C_f^* and T_s^* in equation (8.1) correspond to f_1, $U_{(k+1),1}$ and $U_{(k+1),2}$ in equation (8.3), and the Jacobian matrix in (8.4) reduces to $\underline{J}(\underline{U}_k) = \begin{bmatrix} \frac{\partial f_1}{\partial U_{k,1}} , \frac{\partial f_1}{\partial U_{k,2}} \end{bmatrix}$. If $C^*_{f,k}$ and $T^*_{s,k}$ represent the values of C_f^* and T_s^* at the k'th iteration, equation (8.1) can be linearized into the form

$$\eta \cdot r^*(C^*_{f,k+1}, T^*_{f,k+1}) = g_k + \frac{\partial g}{\partial C^*_{f,k}} \cdot (C^*_{f,k+1} - C^*_{f,k}) + \frac{\partial g}{\partial T^*_{s,k}} \cdot (T^*_{s,k+1} - T^*_{s,k}) \qquad (8.5)$$

From equations (7.19), (8.2) and (8.5)

$$T^*_{f,k+1} - T^*_{s,k+1} = \frac{\beta_1 I_o^2}{3} \left[g_k + \frac{\partial g}{\partial C^*_{f,k}} \cdot (C^*_{f,k+1} - C^*_{f,k}) + \frac{\partial g}{\partial T^*_{s,k}} (T^*_{s,k+1} - T^*_{s,k}) \right] \qquad (8.6)$$

Expressing $T^*_{s,k+1}$ explicitly in terms of interstitial values, it follows from (8.6) that

$$T^*_{s,k+1} = \left(1 - \frac{\beta_1 I_o^2}{3} \cdot a_k\right) \cdot T^*_{f,k+1} - \frac{\beta_1 I_o^2}{3} (b_k \cdot C^*_{f,k+1} + d_k) \qquad (8.7)$$

where

$$a_k = \frac{\partial g/\partial T^*_{s,k}}{\left(1+\frac{\beta_1 \bar{\Phi}_o^2}{3}\cdot\frac{\partial g}{\partial T^*_{s,k}}\right)} \quad , \quad b_k = \frac{\partial g/\partial C^*_{f,k}}{\left(1+\frac{\beta_1 \bar{\Phi}_o^2}{3}\cdot\frac{\partial g}{\partial T^*_{s,k}}\right)}$$

$$\text{and } d_k = \left[\frac{g_k - (\partial g/\partial C^*_{f,k}).C^*_{f,k} - (\partial g/\partial T^*_{s,k}).T^*_{s,k}}{\left(1+\frac{\beta_1 \bar{\Phi}_o^2}{3}\cdot\frac{\partial g}{\partial T^*_{s,k}}\right)}\right] \qquad (8.8)$$

Substituting equation (8.7) into (8.5) and rearranging gives the reaction rate as a linear function of interstitial fluid values $C^*_{f,k+1}$ and $T^*_{f,k+1}$ - i.e.,

$$\eta . r^*(C^*_{f,k+1}, T^*_{f,k+1}) = a_k . T^*_{f,k+1} + b_k . C^*_{f,k+1} + d_k \qquad (8.9)$$

Using equation (8.9) in equations (7.5) and (7.6), the energy and material balance equations for the interstitial fluid can be linearized into the following form:

$$-\frac{\partial T^*_{f,k+1}}{\partial z} + c_1\left(\frac{\partial^2 T^*_{f,k+1}}{\partial s^2} + \frac{1}{s}\cdot\frac{\partial T^*_{f,k+1}}{\partial s}\right) - c_2(a_k . T^*_{f,k+1} + b_k . C^*_{f,k+1} + d_k) = 0 \qquad (8.10)$$

$$-\frac{\partial C^*_{f,k+1}}{\partial z} + c_3\left(\frac{\partial^2 C^*_{f,k+1}}{\partial s^2} + \frac{1}{s}\cdot\frac{\partial C^*_{f,k+1}}{\partial s}\right) - c_4(a_k . T^*_{f,k+1} + b_k . C^*_{f,k+1} + d_k) = 0 \qquad (8.11)$$

The variables with subscript (k+1) are the unknown variables while those with subscript k are considered known. It is to be noted that equations (8.10) and (8.11) form a sequence (k=0,1,2,...) of <u>linear</u> simultaneous partial differential equations which replace the original non-linear equations. The boundary conditions on the linearized system are identical in form to those given previously, (7.9) to (7.16), for the non-linear system.

8.2 Mathematical requirements

8.2.1 Continuity, Boundedness, Convexity (or concavity)

Certain requirements of the function $g(C_f^*, T_s^*)$ have been tacitly assumed in the development of the approximating sequence of linear equations. The function $g(C_f^*, T_s^*)$ must be continuous in C_f^* and T_s^*, possess bounded first and second partial derivatives with respect to C_f^* and T_s^*, and be strictly convex (or concave) for all values of C_f^* and T_s^* within the domain of interest. The last requirement is a mathematical nicety which is seldom satisfied in engineering problems.

A close examination of convexity is not facilitated by the complex form of the function $g(C_f^*, T_s^*)$. In many applications the form of g can be simplified by restricting $\Delta > 3$, in which case $\tanh \Delta \cong 1$. Carrying out a more restrictive examination on this basis leads to the following conclusion:

g is <u>concave</u>, rather than strictly concave, providing

$$G = \left[(1+\theta\, T_s^*) - \frac{\gamma}{4} \cdot \left(\frac{x-1}{x+1}\right) \right] < 0 \qquad (8.12)$$

where $x = \left(\frac{Sh'}{2} - 1\right) \cdot \frac{1}{\Delta}$

A priori, specification of G in equation (8.12) is hindered by the presence of the unknown, T_s^*, whose domain of interest must be computed numerically. However, some information is forthcoming from graphical considerations. If G is plotted as a function of T_s^* for given values of θ, γ, Sh' and $\bar{\phi}_o$, curves of the form shown in Fig. 8.1 ensue. It is evident that as T_s^* is decreased (i.e. T_s is increased) there is a growing tendency for the function g to undergo transition from concave to convex form. The occurrence of the transition region within the domain of admissible T_s^* values can lead to divergence of the linear sequence. This behaviour has been observed in isolated cases, notably when the

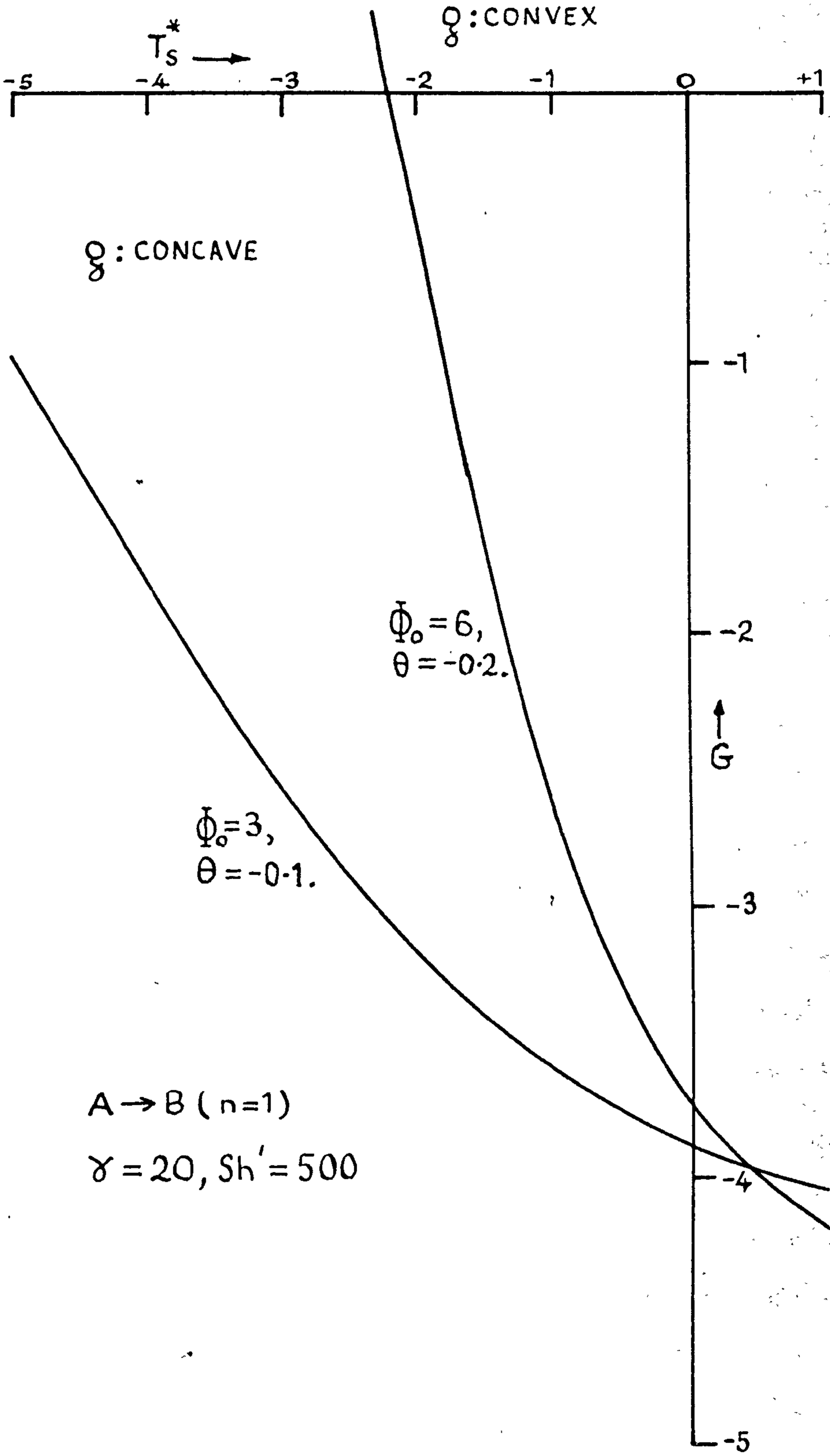

FIG. 8.1 Influence of system parameters on concavity condition.

solution is non-unique. Unfortunately, there seems no easy way of predicting the onset of this phenomenon.

8.2.2 Positivity, monotonicity and quadratic convergence

In connection with the desirability of monotonic convergence of the approximating sequence of linear equations it is further required that the partial differential operator should possess the positivity property. The proof can be quite involved. It is sufficient to state here that this property extends to parabolic partial differential equations.[103]

Granted the desired positivity property and the concavity (convexity) of the function g, theoretical considerations lead to the expectation of monotonic convergence.[103] Furthermore, the geometric background of the Newton-Raphson procedure suggests that convergence will be quadratic if the z-step is sufficiently small. The combination of these two properties produces a powerful technique. Computations on a series of case studies (CHAPTERS 9 and 10) demonstrate the fulfillment of both requirements.

If the initial approximations $C_f^*(k=o)$ and $T_f^*(k=o)$ are chosen arbitrarily, monotonicity is not guaranteed. However, this drawback can be overcome by making use of the stepwise policy of integration in the z-direction to provide fairly accurate starting conditions at any z-step.

A final point concerns the use of equation (8.3) in preference to the simpler Picard type

$$\underline{f}(\underline{U}_{k+1}) = \underline{f}(\underline{U}_k) \qquad (8.13)$$

The arguments in favour of (8.3) over (8.13) are similar to those put forward to justify the use of the Newton-Raphson technique over simple iteration in root-finding problems. Providing the elements of the Jacobian matrix (equation (8.4)) are available in analytic form and providing their evaluation is not time-consuming, then the quadratic rate of convergence combined with modest computing is likely to be a feature of the quasilinearization technique which the Picard algorithm cannot meet.

8.3 Reduction of the quasi-linearized equations into difference form

There are inherent difficulties in equations (8.10) and (8.11) which make their analytical integration exceedingly difficult. These difficulties arise as a result of the complicated form of the coefficients a_k, b_k and d_k which are defined in equation (8.8). Numerical methods of integration have therefore to be employed to provide solutions.

8.3.1 Finite difference analogues

Suppose the domain $\left[0 \leq z \leq 1\right] x \left[0 \leq s \leq 1\right]$ is covered by a 2-dimensional net, and the mesh points are $(j\Delta z, m\Delta s)$ where $j=0,1,2,\ldots J$; $m=0,1,2,\ldots M$; $J\Delta z = 1$, $M\Delta s = 1$ (cf. Figure 8.2). Let V_{k+1}, U_{k+1}, a'_k, b'_k, d'_k (j,m) be the discretized versions of $T^*_{f,k+1}$, $C^*_{f,k+1}$, a_k, b_k, d_k $(j\Delta z, m\Delta s)$. By way of illustration consider finite difference analogues of equation (8.10). Equation (8.11) may be reduced to equivalent difference form by parallel reasoning. Equation (8.10) is written in the form

$$\frac{\partial T^*_{f,k+1}}{\partial z} = c_1\left(\frac{\partial^2 T^*_{f,k+1}}{\partial s^2} + \frac{1}{s}\cdot\frac{\partial T^*_{f,k+1}}{\partial s}\right) - c_2 R_{k+1} \qquad (8.14)$$

where R_{k+1} is a separable function of $T^*_{f,k+1}$ and $C^*_{f,k+1}$ given by

$$R_{k+1} = a_k \cdot T^*_{f,k+1} + b_k\, C^*_{f,k+1} + d_k \qquad (8.15)$$

The procedure adopted here is an implicit one which assigns an arbitrary weighting factor Ⓗ to the right hand side of equation (8.14) expressed at the axial steps (j) and (j+1). Consider the finite difference analogue of (8.14) to be

$$\frac{V_{k+1}(j+1,m) - V(j,m)}{\Delta z} = Ⓗ\cdot\left[\frac{c_1}{(\Delta s)^2}\left(\delta^2 V_{k+1} + \frac{1}{m}\delta V_{k+1}\right) - c_2 \cdot R'_{k+1}(j+1,m)\right] + (1-Ⓗ)\cdot\left[\frac{c_1}{(\Delta s)^2}\left(\delta^2 V + \frac{1}{m}\delta V\right) - c_2 \cdot R'(j,m)\right] \qquad (8.16)$$

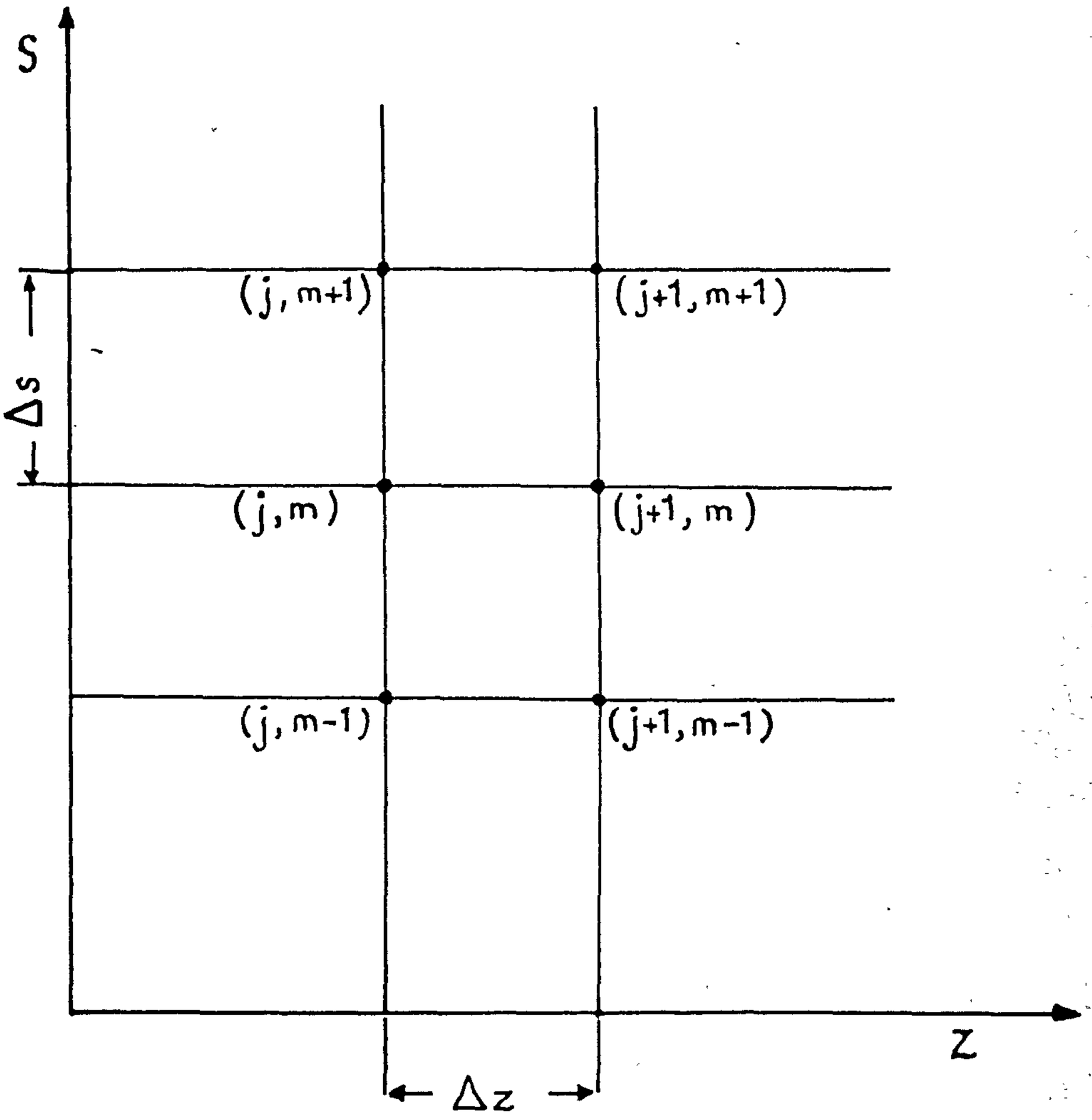

FIG. 8.2 Finite difference network showing node values.

where $0 \leq \Theta \leq 1$, and R' corresponds to the R in equation (8.15) i.e.,

$$R'_{k+1} = a'_k V_{k+1} + b'_k U_{k+1} + d'_k \qquad (8.17)$$

The symbol δ is the usual central difference operator and

$$\delta^2 V_{k+1} = V_{k+1}(j+1,m+1) - 2\,V_{k+1}(j+1,m) + V_{k+1}(j+1,m-1)$$

$$\delta V_{k+1} = \frac{V_{k+1}(j+1,m+1) - V_{k+1}(j+1,m-1)}{2} \qquad (8.18)$$

Since the values of V, U, a', b' and d' at axial step (j) are considered known, the subscript (k+1) which denotes the (k+1)'th iteration has no meaning at the j'th step. Consequently, all quantities at the j'th step are written without the subscript (k+1). Keeping Θ arbitrary in the formulation subsequently facilitates exploration of some interesting special cases, notably $\Theta = 0$, $\frac{1}{2}$ and 1 which correspond to explicit, Crank Nicolson and fully implicit (Laasonen) analogues.

The finite difference replacement (8.16) holds at the internal nodes m=1,2,...M-1, but requires modification at the boundary nodes m=0,M where the boundary conditions

$$\partial T^*_{f,k+1}/\partial s = 0 \qquad s = 0,\ 0 \leq z \leq 1 \qquad (8.19)$$

$$\partial T^*_{f,k+1}/\partial s = \lambda\,(1-T^*_{f,k+1}) \qquad s = 1,\ 0 \leq z \leq 1 \qquad (8.20)$$

apply. In order not to lose the accuracy obtained by using a central difference approximation at the internal nodes, the approximations of the boundary conditions (8.19) and (8.20) should be of such an order that the power of Δs in the error term (cf. Section 8.3.3) remains unchanged. This may be accomplished easily by a method outlined below.

8.3.2 Inclusion of the boundary conditions

At the axis (s=0), equation (8.19) is applicable and the indeterminate term $1/s \cdot \partial T^*_{f,k+1}/\partial s$ can be shown to possess the limit $\partial^2 T^*_{f,k+1}/\partial s^2$. Hence, on the boundary s=0, equation (8.14) becomes

$$\frac{\partial T^*_{f,k+1}}{\partial z} = 2\, c_1 \cdot \frac{\partial^2 T^*_{f,k+1}}{\partial s^2} - c_2 \cdot R_{k+1} \qquad (8.21)$$

In fact, on the boundary the temperature gradient is approximated by a central difference form

$$\partial T^*_{f,k+1}/\partial s = \frac{1}{2\Delta s}\left[V_q(p,m+1) - V_q(p,m-1) \right];$$

$m = 0,M$; $p = j,j+1$; $q = k+1$ if $p = j+1$. This approximation together with equations (8.19), the differenced form of equation (8.21) at $m = 0$, and equations (8.16), (8.20) at $m = M$ enables the boundary conditions to be incorporated into the difference scheme without loss of accuracy.

8.3.3 Truncation error

The difference between the exact solution of the partial differential equation and the exact solution of the finite difference equation is called the truncation error. Normally, the magnitude of this error can only be determined approximately from numerical experiments. However, an indication of the order of magnitude of the error is forthcoming from suitable Taylor series expansions of the partial derivatives[79]. The analysis, which is relatively straightforward but voluminous in content, leads to the statement of the error incurred by replacement of the partial differential equation (8.14) with the difference equation (8.16); viz:-

$$\text{ERROR} = -(\Theta-\tfrac{1}{2}).\Delta z.\frac{\partial^2 T^*_f}{\partial z^2} -(\Theta-\tfrac{1}{3}).\frac{(\Delta z)^2}{2}.\frac{\partial^3 T^*_f}{\partial z^3} -(\Theta-\tfrac{1}{4}).\frac{(\Delta z)^3}{6}.\frac{\partial^4 T^*_f}{\partial z^4}$$

$$-\frac{c_1(\Delta s)^2}{12}.\left(\frac{\partial^4 T^*_f}{\partial s^4} + \frac{2}{s}.\frac{\partial^3 T^*_f}{\partial s^3}\right) - \frac{\Theta.c_1(\Delta s)^2.\Delta z.}{12}\left(\frac{\partial^5 T^*_f}{\partial z \partial s^4} + \frac{2}{s}.\frac{\partial^4 T^*_f}{\partial z \partial s^3}\right)\ldots \qquad (8.22)$$

where the derivatives are taken at $(j\Delta z,\ m\Delta s)$. The important point to note is that for all Θ values, except $\Theta=\frac{1}{2}$, the error is $O\left[(\Delta s)^2+\Delta z\right]$. If, however, the Crank Nicolson analogue ($\Theta=\frac{1}{2}$) is used, the error is reduced to $O\left[(\Delta s)^2+(\Delta z)^2\right]$. This finding implies that larger increments

can be taken in the z-direction for a given accuracy of integration by using the Crank Nicolson scheme rather than the fully implicit form (Θ=1). It is misleading to judge the merits of one scheme as opposed to another prior to computation, particularly in the present case. Other features are in evidence which may lead to serious restrictions in the allowable axial step compared with that incurred by truncation error alone. Notably, the discontinuity in $\partial T_f^*/\partial s$ at (0,1) (see Section 7.6), and the convergence requirement on the starting policy of integration at each z-step (see Section 8.5.1 (ii)).

If the additional restrictions on Δz are severe then the accuracy benefits which accrue from Crank Nicolson's method are largely, if not entirely, lost. In these circumstances more refined computing strategies are worthy of particular consideration:- e.g., hybrid schemes of a semi-analytic/numerical form, varying Δz step methods with an improved starting policy.

8.3.4 The totality of equations

The totality of finite difference equations can be expressed in the form

$$\underline{A}_{l,k}\,\underline{V}_{k+1}(j+1) + \underline{B}_{l,k}\,\underline{U}_{k+1}(j+1) + \underline{D}_{l,k} = 0 \qquad (8.23)$$

by combination of equations (8.16), (8.17) and (8.18) at the internal nodes m=1,2,...M-1, and inclusion of the boundary,conditions at m=0,M in the manner indicated in Section 8.3.2. $\underline{A}_{l,k}$ represents the following (M+1) x (M+1) tridiagonal matrix:

$$\underline{A}_{l,k} = \begin{bmatrix} h_o & b_o & 0 & \cdot & \cdot & \cdot & 0 \\ a_1 & h_1 & b_1 & & & & \cdot \\ 0 & a_2 & h_2 & b_2 & & & \cdot \\ \cdot & & \cdot & \cdot & \cdot & & \cdot \\ \cdot & & & a_m & h_m & b_m & \\ & & & & \cdot & \cdot & 0 \\ & & & & a_{M-1} & h_{M-1} & b_{M-1} \\ 0 & \cdot & \cdot & & 0 & a_M & h_M \end{bmatrix}$$

with $b_o = -4r\Theta c_1$

$h_o = 1+4r\Theta c_1 + \Delta z.\Theta c_2 a'_k(j+1,0)$

and $a_m = -r\Theta c_1(1-{}^1/2m)$

$b_m = -r\Theta c_1(1+{}^1/2m)$

$h_m = 1+2r\Theta c_1+\Delta z.\Theta c_2 a'_k(j+1,m)$] $m=1,2,\ldots M-1$

$a_M = -2r\Theta c_1$

$h_M = 1+2r\Theta c_1(1+\lambda/\Delta s(1+{}^1/2M)) + \Delta z\,\Theta c_2 a'_k(j+1,M)$

$r = \Delta z/(\Delta s)^2$

$\underline{B}_{1,k}$ is a diagonal matrix with the following diagonal elements:

$\text{diagm} = \Delta z.\Theta.c_2.b'_k(j+1,m), \quad m=0,1,2,\ldots M.$

$\underline{V}_{k+1}(j+1)$, $\underline{U}_{k+1}(j+1)$ and $\underline{D}_{1,k}$ are M+1 column vectors defined by

$$\underline{V}_{k+1}(j+1) = \begin{bmatrix} V_{k+1}(j+1,0) \\ V_{k+1}(j+1,1) \\ V_{k+1}(j+1,2) \\ \vdots \\ V_{k+1}(j+1,m) \\ \vdots \\ V_{k+1}(j+1,M) \end{bmatrix}, \quad \underline{U}_{k+1}(j+1) = \begin{bmatrix} U_{k+1}(j+1,0) \\ U_{k+1}(j+1,1) \\ U_{k+1}(j+1,2) \\ \vdots \\ U_{k+1}(j+1,m) \\ \vdots \\ U_{k+1}(j+1,M) \end{bmatrix},$$

$$\underline{D}_{1,k} = \begin{bmatrix} -4(1-\Theta).c_1.r.V(j,1)-\left[1-(1-\Theta)(4c_1r+\Delta zc_2a'(j,0))\right].V(j,0)+p_k(0) \\ \vdots \\ -(1-\Theta)c_1r.(1+{}^1/2m).V(j,m+1)-\left[1-(1-\Theta).(2c_1r+\Delta z.c_2.a'(j,m)\right].V(j,m) \\ -(1-\Theta)c_1r.(1-{}^1/2m).V(j,m-1) + p_k(m) \\ \vdots \\ -\left[1-2(1-\Theta)c_1r.\left[1+\lambda\Delta s(1+{}^1/2M)\right]-\Delta z.c_2(1-\Theta)a'(j,M)\right].V(j,M) \\ -2(1-\Theta)c_1r.V(j,M-1) + p_k(M) - 2.c_1.r.\lambda.\Delta s(1+{}^1/2M) \end{bmatrix}$$

with $p_k(m) = \Delta z.c_2\left[(1-\Theta)\left[b'(j,m).U(j,m)+d'(j,m)\right]+\Theta d'_k(j+1,m)\right]$

, $m=0,1,2,\ldots M.$

By parallel reasoning the material balance equation (8.11) together with the boundary conditions given by equation (8.24) - i.e.,

$$\partial C^*_{f,k+1}/\partial s = 0, \quad s = 0,1 , \quad 0 \leq z \leq 1 \qquad (8.24)$$

can be reduced to a system of M+1 simultaneous equations

$$\underline{A}_{2,k}\underline{U}_{k+1}(j+1) + \underline{B}_{2,k}\underline{V}_{k+1}(j+1) + \underline{D}_{2,k} = 0 \qquad (8.25)$$

where $\underline{A}_{2,k}$ is an (M+1) x (M+1) tridiagonal matrix:

$$\underline{A}_{2,k} = \begin{bmatrix} h'_o & b'_o & 0 & & & & 0 \\ a'_1 & h'_1 & b'_1 & & & & \cdot \\ 0 & a'_2 & h'_2 & b'_2 & & & \cdot \\ \cdot & \cdot & \cdot & \cdot & & & \cdot \\ \cdot & & & a'_m & h'_m & b'_m & \\ \cdot & & & & \cdot & \cdot\cdot \quad \cdot & 0 \\ & & & & & a'_{M-1} \quad h'_{M-1} & b'_{M-1} \\ 0 & \cdot & \cdot & \cdot & & 0 \quad a'_M & h'_M \end{bmatrix}$$

with $b'_o = (c_3/c_1).b_o$

$h'_o = 1+4r\textcircled{H}c_3+\Delta z.\textcircled{H}c_4 b'_k(j+1,0)$

and $a'_m = (c_3/c_1).a_m$

$b'_m = (c_3/c_1).b_m$

$h'_m = 1+2r\textcircled{H}c_3+\Delta z.\textcircled{H}c_4 b'_k(j+1,m)$ $\Big\}$ m=1,2,...M-1

$a'_M = (c_3/c_1).a_M$

$h'_M = 1+2r\textcircled{H}c_3+\Delta z.\textcircled{H}c_4 b'_k(j+1,M).$

$\underline{B}_{2,k}$ is a diagonal matrix with the following diagonal elements:

$$diag_m = \Delta z.\textcircled{H}c_4 a'_k(j+1,m) \ , \ m=0,1,2,..M$$

$\underline{D}_{2,k}$ is an M+1 column vector defined by

$$\underline{D}_{2,k}=\begin{bmatrix} -4(1-\Theta).c_3.r.U(j,1)-\left[1-(1-\Theta)(4.c_3.r+\Delta z.c_4 b'(j,0)\right].U(j,0)+q_k(0) \\ -(1-\Theta).c_3 r.(1+{}^{1}/_{2m})U(j,m+1)-\left[1-(1-\Theta)(2c_3 r+\Delta z.c_4 b'(j,m))\right]. \\ U(j,m)-(1-\Theta)c_3 r.(1-{}^{1}/_{2m}).U(j,m-1)+q_k(m) \\ \left[1-(1-\Theta)(2.c_3 r+\Delta z.c_4 b'(j,M))\right].U(j,M)-2(1-\Theta)c_3 r.U(j,M-1)+q_k(M) \end{bmatrix}$$

with $q_k(m) = \Delta z.c_4\left[(1-\Theta)\left[a'(j,m)V(j,m)+d'(j,m)\right]+\Theta d_k'(j+1,m)\right]$

8.4 Solution of the difference equations

The third and final stage of the analysis is concerned with the solution of the 2M+2 linear algebraic equations given by (8.23) and (8.25). These equations are coupled and must, therefore be solved simultaneously.

8.4.1 Simultaneous solution

From equation (8.25)

$$\underline{U}_{k+1}(j+1) = -\underline{A}_{2,k}^{-1}\left[\underline{B}_{2,k}\underline{V}_{k+1}(j+1) + \underline{D}_{2,k}\right] \qquad (8.26)$$

providing $\underline{A}_{2,k}$ is non-singular. Substituting (8.26) into (8.23) and rearranging gives

$$\underline{V}_{k+1}(j+1) = \underline{E}_k^{-1}.\underline{F}_k \qquad (8.27)$$

where $\underline{E}_k = \underline{A}_{1,k} - \underline{B}_{1,k}.\underline{A}_{2,k}^{-1}.\underline{B}_{2,k}$, and $\underline{F}_k = \underline{B}_{1,k}\underline{A}_{2,k}^{-1}\underline{D}_{2,k} - \underline{D}_{1,k}$.

The matrix $\underline{E}_k$ is tridiagonal and its inverse $\underline{E}_k^{-1}$ is readily found by a method described by BRUCE et al[57]. Post-multiplication of the inverse by the column vector $\underline{F}_k$ gives the vector $\underline{V}_{k+1}(j+1)$ (equation 8.27). Substitution of $\underline{V}_{k+1}(j+1)$ into equation (8.26) produces a column vector $\underline{B}_{2,k}\underline{V}_{k+1}(j+1)+\underline{D}_{2,k}$ which post-multiplies the inverse of the tridiagonal matrix $\underline{A}_{2,k}$ to make known the vector $\underline{U}_{k+1}(j+1)$.

The majority of the computing time required to evaluate the vectors $\underline{V}_{k+1}(j+1)$ and $\underline{U}_{k+1}(j+1)$ is taken up by calculation of the inverse matrices $\underline{A}_{2,k}^{-1}$ and $\underline{E}_k^{-1}$. These matrices are derived from the tridiagonal matrices $\underline{A}_{2,k}$ and $\underline{E}_k$. It is well known that such matrices can be rapidly

inverted if use is made of the Thomas method.[57] A simultaneous solution of the finite difference equations does therefore seem to be relatively straightforward and not too time consuming.

8.4.2 Sequential solution

The sequential type of solution is preferred by LEE.[91,100] By this approach equations (8.23) and (8.25) are decoupled by allowing $\underline{U}_{k+1}(j+1)$ and $\underline{V}_{k+1}(j+1)$ in the respective second terms to lag 1 iteration.

Equations (8.23) and (8.25) now become

$$\underline{\underline{A}}_{1,k}\cdot\underline{V}_{k+1}(j+1) = -\left[\underline{\underline{B}}_{1,k}\underline{U}_k(j+1) + \underline{D}_{1,k}\right] = \underline{d}_{1,k} \qquad (8.28)$$

$$\underline{\underline{A}}_{2,k}\cdot\underline{U}_{k+1}(j+1) = -\left[\underline{\underline{B}}_{2,k}\underline{V}_k(j+1) + \underline{D}_{2,k}\right] = \underline{d}_{2,k} \qquad (8.29)$$

Since the variables with subscript k are known, equations (8.28)and (8.29) can be solved independently by the Thomas method.

It is not evident, a priori, whether the reduction in computation per iteration incurred by this approach is more than offset by the reduced rate of convergence arising as a consequence of decoupling. Results from several case studies show that even with this simplified technique the number of iterations required per axial step is quite small. This state of affairs is admittedly closely related to the type of starting policy which is used to initiate the iterative process at each axial step.

8.5 The computing procedure

8.5.1 Starting policies

There are two starting policies which require consideration. The first is fundamental to the propagation of the integration away from the bed inlet, where only the state of the interstitial fluid is specified. The second policy is applied at each subsequent axial distance step in order to initiate the iterative mode of solution.

(i) Bed inlet (z=0):

From the entrance conditions (7.9) and (7.10) and the energy balance

for the first row of particles (7.19) at z=0, it follows that

$$T_s^* - \frac{\beta_1 . Sh'/2 . (1 - \frac{\tanh\Delta}{\Delta})}{\left[1 + (Sh'/2 - 1)\frac{\tanh\Delta}{\Delta}\right]} = 0 \qquad (8.30)$$

where $\Delta = \Phi_o \exp\left(\frac{1}{2} . \gamma\theta T_s / (1+\theta T_s)\right)$

Equation (8.30) is non-linear and algebraic in the unknown, T_s^*. It may be solved by the Newton-Raphson method. Initial estimation of the root follows from graphical considerations.

Knowing T_s^*, Δ can be calculated and the intraparticle concentration profile follows from equation (7.18) with $C_f^* = 0$. At the centre of the particle,

Lim $\sinh\Delta y / y \rightarrow \Delta$, and
$y \rightarrow 0$

$$C_s^*(y=o) = 1 - \frac{(Sh'/2)}{\cosh\Delta\left[1 + (Sh'/2 - 1)\frac{\tanh\Delta}{\Delta}\right]} \qquad (8.31)$$

The effectiveness factor follows from differentiation of (7.18) followed by substitution into (7.17) at y=1,

$$\eta = \frac{3Sh'/2\Phi_o^2 . (1 - \tanh\Delta/\Delta)}{\left[1 + \left(\frac{Sh'}{2} - 1\right)\frac{\tanh\Delta}{\Delta}\right]} \qquad (8.32)$$

(ii) Prediction of the solution at $z = (j+1)\Delta z$.

To start the iterative procedure at each axial step it is required to specify a starting policy $\left[\underline{V}_{k=0}(j+1), \underline{U}_{k=0}(j+1), \underline{v}_{k=0}(j+1)\right]$

where $\underline{v}_k(j+1)$ represents the M+1 column vector of discrete solid temperatures, $v_k(j+1,m)$, given by

$$\underline{v}_k(j+1) = \begin{bmatrix} v_k(j+1,0) \\ v_k(j+1,1) \\ \vdots \\ v_k(j+1,m) \\ \vdots \\ v_k(j+1,M) \end{bmatrix}$$

There are various ways of implementing such a policy. A scheme which fits conveniently into the formulation already proposed provides a prediction $\left[\underline{V}_{k=0}(j+1),\ \underline{U}_{k=0}(j+1)\right]$ by setting $\textcircled{H}=0$ in equations (8.23) and (8.25). A pair of predictor formulas

$$\left.\begin{aligned} \underline{V}_{k=0}(j+1) &= \underline{d}_1(j) \\ \underline{U}_{k=0}(j+1) &= \underline{d}_2(j) \end{aligned}\right\} \qquad (8.33)$$

arises, where

$$\underline{d}_1(j) = \begin{bmatrix} 4c_1r.V(j,1)+\left\{1-4c_1r-\Delta z.c_2a'(j,0)\right\}V(j,0)-p(0) \\ c_1r(1+1/2m).V(j,m+1)+\left\{1-2c_1r-\Delta z.c_2a'(j,m)\right\}V(j,m)+c_1r(1-1/2m) \\ V(j,m-1)-p(m) \\ \left[1-2c_1r\left\{1+\lambda.\Delta s(1+1/2M)\right\}-\Delta z.c_2a'(j,M)\right].\ V(j,M)+2c_1r.V(j,M-1) \\ -p(M)+2c_1r\lambda\Delta s(1+1/2M) \end{bmatrix}$$

and

$$\underline{d}_2(j) = \begin{bmatrix} 4c_3r.U(j,1)+\left\{1-4c_3r-\Delta z.c_4b'(j,0)\right\}.U(j,0)-q(0) \\ c_3r(1+1/2m).U(j,m+1)+\left\{1-2c_3r-\Delta z.c_4.b'(j,m)\right\}. \\ U(j,m)+c_3r(1-1/2m).U(j,m-1)-q(m) \\ \left\{1-2c_3r-\Delta z.c_4.b'(j,M)\right\}.U(j,M)+2c_3rU(j,M-1)-q(M) \end{bmatrix}$$

$$p(m) = \Delta z.c_2.\left\{b'(j,m).U(j,m)+d'(j,m)\right\}$$

$$q(m) = \Delta z.c_4.\left\{a'(j,m).V(j,m)+d'(j,m)\right\}$$

for $m = 0,1,2,\ldots M$.

An estimate of the solid temperature, $v_{k=0}(j+1,m)$, follows from equation (8.7) where the a'_k, b'_k and $d'_k(j+1,m)$ are replaced by $a'(j,m)$, $b'(j,m)$ and $d'(j,m)$. The totality of equations can be expressed in the form

$$\underline{v}_{k=0}(j+1) = \underline{B}_3\, \underline{V}_{k=0}(j+1) + \underline{B}_4\, \underline{U}_{k=0}(j+1) + \underline{D}_3 \qquad (8.34)$$

where $\underline{B}_3$ and $\underline{B}_4$ are diagonal matrices with the following diagonal elements:

$$\left.\begin{aligned} \underline{B}_3 &: \text{diag}_m = 1 - \frac{\beta_1 \bar{\Phi}_o^2}{3}.a'(j,m) \\ \underline{B}_4 &: \text{diag}_m = -\frac{\beta_1 \bar{\Phi}_o^2}{3}.b'(j,m) \end{aligned}\right\} m=0,1,2,\ldots M$$

$\underline{D}_3$ is an M+1 column vector of elements:-

$$-(\beta_1 \bar{\Phi}_o^2/3).d'(j,m),\ m=0,1,2,\ldots.M.$$

An alternative policy, which is simpler but less accurate, identifies the set of starting conditions in terms of the converged profiles in temperature and concentration from the previous axial distance step - i.e.,

$$\left.\begin{aligned} \underline{V}_{k=0}(j+1) &= \underline{V}(j) \\ \underline{U}_{k=0}(j+1) &= \underline{U}(j) \\ \underline{v}_{k=0}(j+1) &= \underline{v}(j) \end{aligned}\right\} \qquad (8.35)$$

Both types of starting policy were implemented and preliminary experiments indicated that the improvement in the rate of convergence by using (8.33) and (8.34) in preference to (8.35) was negligible. In all the examples presented later, the simple policy given by (8.35) proved satisfactory.

8.5.2 The computer flow diagram

An abbreviated form of the computer flow sheet is presented in Fig. 8.3. to aid understanding of the computing procedure. In the actual program certain innovations were made to remove all unnecessary computation. For example, the non-major diagonal elements of the matrices $\underline{A}_{1,k}$ and $\underline{A}_{2,k}$ require to be set up only once prior to entering the main program loop which updates the axial counter j. Furthermore,

Start

Read data

Starting policy (z=0)
Newton-Raphson solution of (8.30)

j:=0

z:=(j+1)Δz

Starting policy for iterative process
$\underline{V}_{k=0}(j+1) = \underline{V}(j)$
$\underline{U}_{k=0}(j+1) = \underline{U}(j)$
$\underline{v}_{k=0}(j+1) = \underline{v}(j)$

k:=0

Set up the matrices $\underline{A}_{1,k}$, $\underline{A}_{2,k}$ and the vectors $\underline{d}_{1,k}$, $\underline{d}_{2,k}$

Invert the matrix equations (8.28) and (8.29) to find the vectors $\underline{V}_{k+1}(j+1)$ and $\underline{U}_{k+1}(j+1)$

Tolerance requirements satisfied — NO

YES

k=k_{max} — NO

YES

k:=k+1

Print iterates

Print conditions satisfied — NO

YES

$\underline{V}_k(j+1) := \underline{V}_{k+1}(j+1)$
$\underline{U}_k(j+1) := \underline{U}_{k+1}(j+1)$
$\underline{v}_k(j+1) := \underline{v}_{k+1}(j+1)$
Overwrite iterates

Iteration loop

Overwrite stored values
$\underline{V}(j) := \underline{V}_{k+1}(j+1)$
$\underline{U}(j) := \underline{U}_{k+1}(j+1)$
$\underline{v}(j) := \underline{v}_{k+1}(j+1)$

Print conditions satisfied — NO

YES

Simpson integration to find the mean radial values

Print results

j:=j+1

j=j_{max} — NO

YES

END

Figure 8.3. The Computer Flow diagram
Loop forming increment in Δz

the vectors $\underline{d}_{1,k}$ and $\underline{d}_{2,k}$ of equations (8.28) and (8.29) may be written in terms of the sum of two vectors, one requiring re-evaluation at each iteration and the other only at each updating of j.

The print out from such a program could be voluminous if some restriction is not introduced. Consequently, a facility was implemented to output results at a pre-determined subset of the (J+1) x(M+1) node points. In addition, print out of the iterative sequence of solutions is controlled through a counting device.

Convergence of the iterations is deemed to have occurred if the criterion

$$\left| \frac{x_{k+1}(j+1,m) - x_k(j+1,m)}{x_k(j+1,m)} \right| < \varepsilon \qquad (8.36)$$

$m=0,1,2,\ldots M$; $x=V,U$.

is satisfied, where ε is the relative change between successive iterations. Even for $\varepsilon=10^{-4}$ only a few iterations are required. The criterion is applied at a pre-selected number of equi-spaced radial mesh points, and in the event of divergence or slow convergence of the iterations a forced exit is made from the iterative loop after a given number of cycles. Whenever the converged profiles are printed, a procedure is entered which evaluates the integrated radial conversion and temperatures by Simpson's rule.

The program was written in Algol and run on an English Electric KDF9 computer. Storage of the program body, including the required library procedures, requires 6K. Approximately 1K of store per 20 radial bed increments is required in addition during operation, in order to accommodate the matrices, vectors and coefficients of the Thomas procedure.

CHAPTER 9

CASE STUDY No. 1 :- A KINETICALLY CONTROLLED REACTOR

In presenting a set of results the number of parameters involved produces a disturbing but unavoidable state of affairs. Rather than try to cover all the potential ranges of interest of every parameter, a number of case studies are investigated from which, it is hoped, general conclusions can be drawn. It is the particular intention to extend to the global regime (i.e. the reactor) the analysis of local rate-influencing factors and to examine the coupling and distribution of the local regime in order to gain an understanding of how physically imposed limitations on the rate process can influence global behaviour. The benefits which accrue from the analysis have particular relevance to reactor design and the subsequent optimization and control studies.

The first system chosen is a rather innocent one for which the reaction rate is so low that nowhere is it appreciably influenced by physical transport phenomena occurring either within the interphase or intraphase regions. Intuitively, it is to be expected that the more detailed models considered here should bear close correspondence to the simpler, well established, quasihomogeneous model in which interactions between physical transport phenomena and surface reaction kinetics are ignored.

It might be argued, with good reason, that the operating system considered here is inconsequential from a commercial standpoint. After all, the conversion achieved is rather poor and the feed is largely inert. In a circumstance such as this an attempt might be made to improve the performance of the reactor by adjusting certain manipulable variables (e.g., coolant temperature, feed conditions, flow rate) in such a way that the effluent conversion is increased without excessive

temperature rise in the bed accompanying the increase. If simulation studies are carried out using the quasihomogeneous model it is found that the reactor exhibits "parametric sensitivity"[37, 90]. That is to say, the behaviour of the reactor becomes sensitive to small changes in the manipulable variables. There is a tendency for the temperature to rise uncontrollably and "run away". This phenomenon is completely unacceptable for reasons of safe operation, catalyst deactivation and process selectivity.

One objective of the present work is to bring to attention the over-dramatization of "parametric sensitivity" if due account is taken of physically imposed constraints on the rate process. To achieve this objective it is useful to employ the present operating system as a base from which further analyses can be launched.

The basic data are presented in Table 9.1 and the dimensionless groups appearing in the detailed model described in Section (7.4), together with additional data needed for the calculation of transport coefficients, are assembled in Table 9.2. A brief amplification of the origin of the transport data required to describe the micro-(macro-)scopic physical transfer processes occurring within the individual catalyst particles, across the interphase regime and radially through the bed is presented below.

9.1 Correlations for use in design

The literature germane to this area is voluminous and there are numerous reviews available. HOUGEN[47] presents a classic survey of the general aspects of solid catalysis. More recent reviews relating to macroscopic mass and heat transfer in packed beds are given by BEEK[5] and FROMENT[90]. Predictions of interphase transport coefficients from experimentally determined j-factor correlations are reviewed extensively by BARKER[106]. Additional information is to be found in the theses of

TABLE 9.1 Operating conditions : Physical and Chemical variables

Reaction scheme : $A \rightarrow B$ ($a_A = -1$, $n = 1$)	
Reactor length (L)	125 cm.
Tube inside radius (ro)	2.1 cm.
Pellet radius (b)	0.21 cm.
Mass flow rate based on empty tube (G_o)	0.449 gm/cm^2.sec.
Coolant temperature (T_a), Feed temperature (T_{fo})	450, 500^{o}K
Operating pressure	10 atmos.
Mole fraction of reactant in the feed	0.1
Molecular wt. of mixture	28
Feed concentration (C_{fo})	2.44×10^{-5} g.mole/cc
Mass heat capacity (c_f)	0.585 cal/gm.^{o}K
Superficial velocity (V_o)	65.7 cm/sec.
Bed voidage (e)	0.4
Exothermic heat of reaction ($-\Delta H$)	49.1 k.Cal/g.mole
Activation energy (E)	19.1 k.Cal/g.mole
Reference rate (k_{vfo})	0.132 sec.$^{-1}$
Radial effective thermal conductivity (K_f)	1.104×10^{-2} cal/cm.sec.^{o}K
Radial mass diffusivity (D_f)	2.76 cm^2/sec.
Intraparticle effective diffusion coefficient (D_A^*)	3.66×10^{-3} cm^2/sec.
Intraparticle effective thermal conductivity (K_p)	6×10^{-4} cal/cm.sec.^{o}K
Interphase heat and mass transfer coefficients (h, k_A)	1.88×10^{-2} cal/cm^2.sec.^{o}K 3.28 cm/sec.
Overall wall heat transfer coefficient (U)	1.05×10^{-2} cal/cm^2.sec.^{o}K

TABLE 9.2 Parameters used in the computations

Peclet number for heat transfer $Pe_H (= \frac{G_o . d_p . c_f}{K_f})$	10
Peclet number for mass transfer $Pe_M (= \frac{V_o . d_p}{D_f})$	10
$c_1 = d_p . L/ro^2 . Pe_H$	1.191
$c_2 = (-\Delta H) . L . (1-e) k_{vfo} C_{fo} / G_o . c_f . (T_a - T_{fo})$	- 0.9030
$c_3 = d_p . L/ro^2 . Pe_M$	1.191
$c_4 = L(1-e) k_{vfo} / V_o$	0.1507
$\Phi_o = b \sqrt{k_{vfo} / D_A^*}$	1.267
$\beta_1 = (-\Delta H) . C_{fo} . D_A^* / h . b . (T_a - T_{fo})$	-2.2213×10^{-2}
$\gamma = E / R_g . T_{fo}$	19.24
$\theta = (T_a - T_{fo}) / T_{fo}$	-0.1
$\lambda = U . ro / K_f$	2
$Nu' = h . dp / Kp$	13.2
$Sh' = k_A \, dp / D_A^*$	377
Surface reaction model:	
$\delta = k_{vfo} / (3k_A / b)$	2.836×10^{-3}
$\beta_2 = (-\Delta H) C_{fo} k_A / h (T_a - T_{fo})$	-4.185
Additional parameters:	
$Pr = (c_f \mu) / K'$	0.771
$Sc = \mu / \rho_f D$	1.32
$Re = G_o dp / \mu$	915

FULTON[107], RAMASWAMI[108] and HEGGS[131], and the paper of ROWE, CLAXTON and LEWIS[109]. Recently, GILLESPIE, CRANDALL and CARBERRY[110] have provided an illuminating inquiry into local heat transfer rather than overall integral coefficients in an attempt to realize a greater understanding of the detailed structure of heat, mass and momentum transfer in fixed beds. Their data lend support to a theoretically derived j-factor for fixed beds[62, 111]. Diffusion and heat conduction within porous catalyst pellets is covered in detail by SATTERFIELD and SHERWOOD[15] and PETERSEN[27].

9.1.1 Radial transport

The radial Peclet number, assumed to be constant throughout the reactor, is taken to be 10.0 for both mass and enthalpy transport, since the Reynolds number (Re) cf., Table 9.2, clearly puts the flow in the turbulent regime. The assumption that a Peclet number of 10 describes material transport at high Reynolds numbers leads directly to a limiting value of 10 for enthalpy transport, since both heat and mass are then transported radially solely by eddy conduction and diffusion processes. In addition to eddy conduction heat can be transferred radially through the bed by point conduction between adjacent particles, radiation, and convection from the gas stream. The contributions of the parallel and series mechanisms of heat transfer are calculated according to the correlation of BEEK[5] which is a modification of the one given by ARGO and SMITH[112]:-

$$K_f = \underbrace{\frac{G_o . c_f . d_p}{Pe_H}}_{\text{eddy}} + \underbrace{\frac{0.6\ h . d_p . K_p}{2K_p + 0.7 . h . d_p}}_{\text{packing}} + \underbrace{2\ 6_r' . d_p . T^3}_{\text{radiation}} \qquad (9.1)$$

where $6_r'$ is an effective radiation constant. At the high mass velocity studied here, the eddy portion of the conductivity completely dominates K_f: the respective contributions being 1.104×10^{-2},

0.042×10^{-2} and 0.011×10^{-2} cal./cm.sec.^{o}K for a catalyst of emissivity 1 and a mean bed temperature of 475^{o}K.

9.1.2 Interphase transport

Interphase heat and mass transfer coefficients are calculated according to the correlation of CARBERRY[62]:

$$j_H = j_M = 1.15(Re')^{-\frac{1}{2}} \qquad (9.2)$$

where $j_H = \frac{e.h.}{G_o c_f}(Pr)^{\frac{2}{3}}$, $j_M = \frac{e.k_A}{V_o}(Sc)^{\frac{2}{3}}$

and $Re' = G_o.d_p/e\mu.$

Equation (9.2) is shown by CARBERRY to be in substantial agreement with literature data representing a wide range of physical properties and processes.

9.1.3 Heat transfer at the wall

The overall heat transfer coefficient at the tube wall (U) is expressed in terms of the apparent wall heat transfer coefficient (h_w), introduced to account for the variation in K_f near to the wall, the conductivity of the wall itself (K_w), and the outside film coefficient (h_o) by the equation

$$1/U = 1/h_w + A_i/A_m.l/K_w + A_i/A_o.1/h_o \qquad (9.3)$$

where the A_i, A_m and A_o of equation (9.3) represent the inside, mean and outside circumferential area per unit length of tube. The inside film coefficient (h_w) is calculated according to YAGI and WAKAO[113]

- i.e., $j_{HW} = 0.20.(Re)^{-0.2}$ (9.4)

where $j_{HW} = \frac{h_w.}{G_o.c_f}(Pr)^{\frac{2}{3}}$

In addition, K_w = 0.108 cal/cm.sec.^{o}K, h_o is taken to be 0.028 cal/cm^2.sec.^{o}K, and the wall thickness (l) is 0.635 cms.

9.1.4 Intraphase transport

(a) Effective diffusivity

There is insufficient data available to provide a reliable basis for the prediction of diffusion coefficients in porous materials; the great difficulty being how to describe the complicated pore geometry.

In the past, attempts have been made to correct the diffusion coefficient for tortuosity of the flow path and for flow channels of irregular shape and varying cross section by defining a correction factor, τ , but theoretical account of these factors has remained obscure. Experimental data for various catalysts (Ref. 15, Table 1-6) are widely scattered and provide little guidance as to what values of τ are to be used to predict D_A^*.

Recent work by WAKAO and SMITH[17], and FOSTER and BUTT[18] bears more fruitful promise. In both cases a computational model of the pore structure is set up from which mass transport coefficients can be computed in terms of properties associated with the porcus matrix. The random bi-disperse model of WAKAO and SMITH is derived for non-reacting fluids in which counter-diffusion fluxes are set up according to the usual inverse square root of molecular weight relationship. An assessment of the pore volume-pore radius distribution is required. FOSTER and BUTT consider the void volume to be composed of two major arrays of pores, centrally convergent and centrally divergent, interconnected at specified intervals. The shape of the arrays is specified from the volume-area distribution of the porous structure. STEISEL and BUTT[114] compare results from the two models with experimental data for CO oxidation on a NiO/alumina catalyst.

It is not the intention here to become involved in a criticism of pore-structure models, for every model must have certain short-

comings. In view of the importance of pore diffusional limitation of the rate process in the practical range of operation associated with temperature run-away (Chapter 10), a precise estimate of the diffusion coefficient is clearly desirable. In these circumstances, direct measurement provides the only satisfactory basis for estimation, though even here there is still considerable uncertainty as to the conditions under which flow or diffusion measurements through porous catalysts can be used to describe effective diffusion coefficients in the presence of reaction.

For illustration the calculation of effective diffusivity is carried out along the lines suggested by SATTERFIELD and SHERWOOD[15].

The Knudsen diffusion coefficient of reactant A, $D_{K,eff}$, is given by

$$D_{K,eff} = \frac{19{,}400\ \varepsilon_p^2}{\tau \cdot S_v} \sqrt{\frac{T}{M_1}} \qquad (9.5)$$

where ε_p is the catalyst void volume (say, 0.5)

S_v the available pore surface per unit volume of porous solid (120 m^2/cm^3)

T the absolute temperature ($\cong 500^oK$)

M_1 the molecular weight of reactant A (74)

Substituting the data into equation (9.5) gives $D_{K,eff} = 1.05 \times 10^{-2}/\tau$ cm^2/sec.

The effective bulk diffusion coefficient, $D_{12,eff}$, is that for a binary system, and its use in subsequent analysis requires that the reactant-product-inert system be treated as a binary reactant-pseudo product or inert system. On this basis the effective bulk diffusion coefficient of reactant in pseudo-inert is calculated according to the relation

$$D_{12,eff} = \frac{\varepsilon_p \cdot D_{12}}{\tau} \qquad (9.6)$$

where D_{12} is the ordinary diffusion coefficient evaluated using the Lennard-Jones expression for intermolecular forces[115]:-

$$D_{12} = \frac{0.001858.\ T^{3/2}\left[(M_1+M_2)/M_1M_2\right]^{\frac{1}{2}}}{P.6_{12}^{2}.\ \Omega_D} \qquad (9.7)$$

where M_2 is the molecular weight of pseudo-inert (say, 23)

P the total pressure (atmos.)

Ω_D "collision integral" (say, 1.195)

6_{12} force constant in the Lennard-Jones potential function (say 4.5 $\mathring{A}$)

From equations (9.6) and (9.7), $D_{12,eff} = \frac{0.5 \times 2.04 \times 10^{-2}}{\tau}$

$$= \frac{1.02 \times 10^{-2}}{\tau} \text{ cm}^2/\text{sec.}$$

Taking $\tau = \sqrt{2}$, in accordance with WHEELER'S[16, 28] theoretical prediction, it follows that

$D_{K,eff} = 7.43 \times 10^{-3}$ cm^2/sec.

$D_{12,eff} = 7.21 \times 10^{-3}$ cm^2/sec.

Clearly, the diffusion lies in the transition region between the bulk and Knudsen regimes. The theory of the transition region has been discussed by SCOTT and DULLIEN[116]. As a first approximation the additive law for self-diffusion proposed by POLLARD and PRESENT[117] may be used to give the overall effective diffusivity,

$$1/D_A^* = 1/D_{K,eff} + 1/D_{12,eff}$$

$$= 273$$

$$\therefore D_A^* = 1/273 = 3.66 \times 10^{-3} \text{ cm}^2/\text{sec.}$$

(b) Effective conductivity

Theoretical predictions of the apparently low thermal conductivity of typical catalysts have, in general, not provided good agreement with measured values; the reason being due to an inadequate description of the pore structure. The most elaborate theoretical approach so far developed is due to BUTT[118] who, in essence, extended the pore diffusion model of WAKAO and SMITH[17] to the problem of predicting heat transfer rates within catalyst particles. For the few cases considered agreement between theory and practice is encouraging. At present, however, in the absence of direct measurement probably as good an approach as any is to interpolate or extrapolate from published data[58-60].

9.2 Model comparison

This section is devoted to a comparison of results computed from the simplest model considered - i.e., the quasihomogeneous model in which the only intraparticle effect is chemical reaction - to the most complex model involving both fluid film and porous catalyst heat and mass transfer resistances. Basic to all the models studied is a two-dimensional fluid field. The differences lie in the interpretation of the overall rate process for single catalyst pellets. A summary of the interphase and intraparticle effects considered in the models is presented in Table 9.3.

	Interphase effects	Intraparticle effects
MODEL 1 (Quasihomogeneous)	None	Surface reaction
MODEL 2	Mass and heat transfer	Surface reaction
MODEL 3	Mass and heat transfer	Simultaneous mass transfer and surface reaction
MODEL 4	Mass and heat transfer	Simultaneous mass transfer, heat transfer and surface reaction

TABLE 9.3 Summary of interphase and intraparticle effects considered in the models.

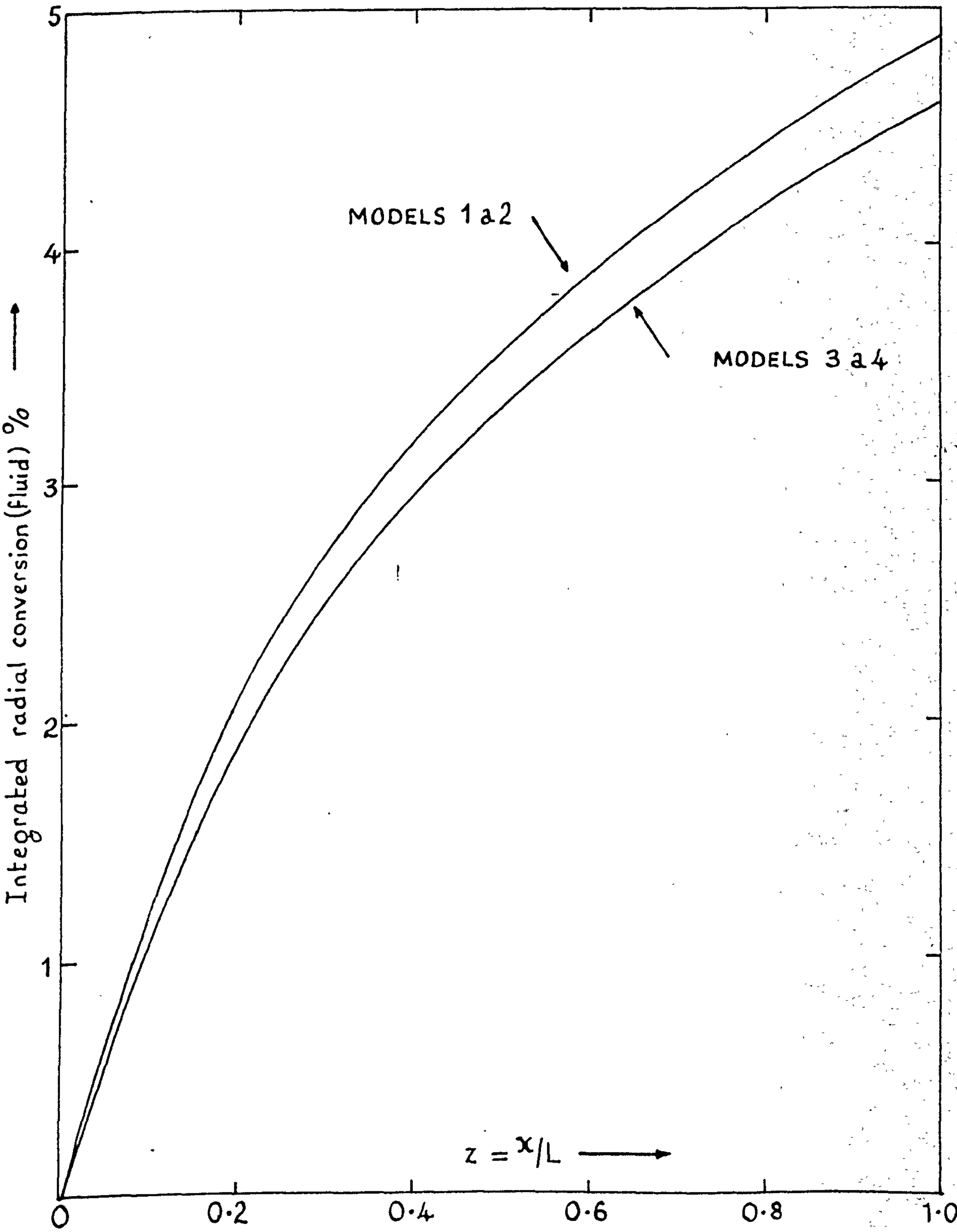

FIG. 9.1 Comparison of reactor models. Integrated radial conversion profiles.

All the models were set up and solved separately for the purposes of comparison. Models 1 to 3 may be looked upon as special cases of Model 4 and can be asymptotically approached by allowing certain transport coefficients to tend to infinity. Such asymptotic checks prove useful in systematic experiments designed to establish the validity of computer programs.

Figure 9.1 compares integrated radial fluid conversion profiles for the four models considered, while Fig. 9.2 shows the temperature profiles along the axis of the reactor. The reaction rate is so low that the reactor exhibits a very weak maximum temperature rise. The closeness of results between the models indicates that nowhere in the bed is there appreciable interaction between surface kinetics and the physical transport processes external to and within the catalyst pellets. For the system under study the refinements of a physically constrained rate process are superfluous. A quantitative analysis of the rate-influencing phenomena is given in the following section.

9.3 Interpretation of the rate process

The maximum temperature difference observed between the centre of the catalyst pellet and the surrounding fluid is 2.5°C. For practical purposes the assumption of local particulate isothermality is valid. Further evidence is provided by the coincidence of curves in Figs. 9.1 and 9.2 for models 3 and 4. Allowing for a pore effectiveness η_p, as a consequence of intraparticle mass transfer, the rate of reaction per catalyst particle is given by $4/3\,\pi b^3 . \eta_p . (k_s C_s)_{w=b}$. This may be equated to the rate of supply of reactant to the external surface of the catalyst, $4\pi b^2 . k_A . (C_f - C_s\big|_{w=b})$

$$\text{i.e.,}\quad 4/3 . \pi b^3 . \eta_p (k_s C_s)_{w=b} = 4\pi b^2 . k_A . (C_f - C_s\big|_{w=b}) \qquad (9.8)$$

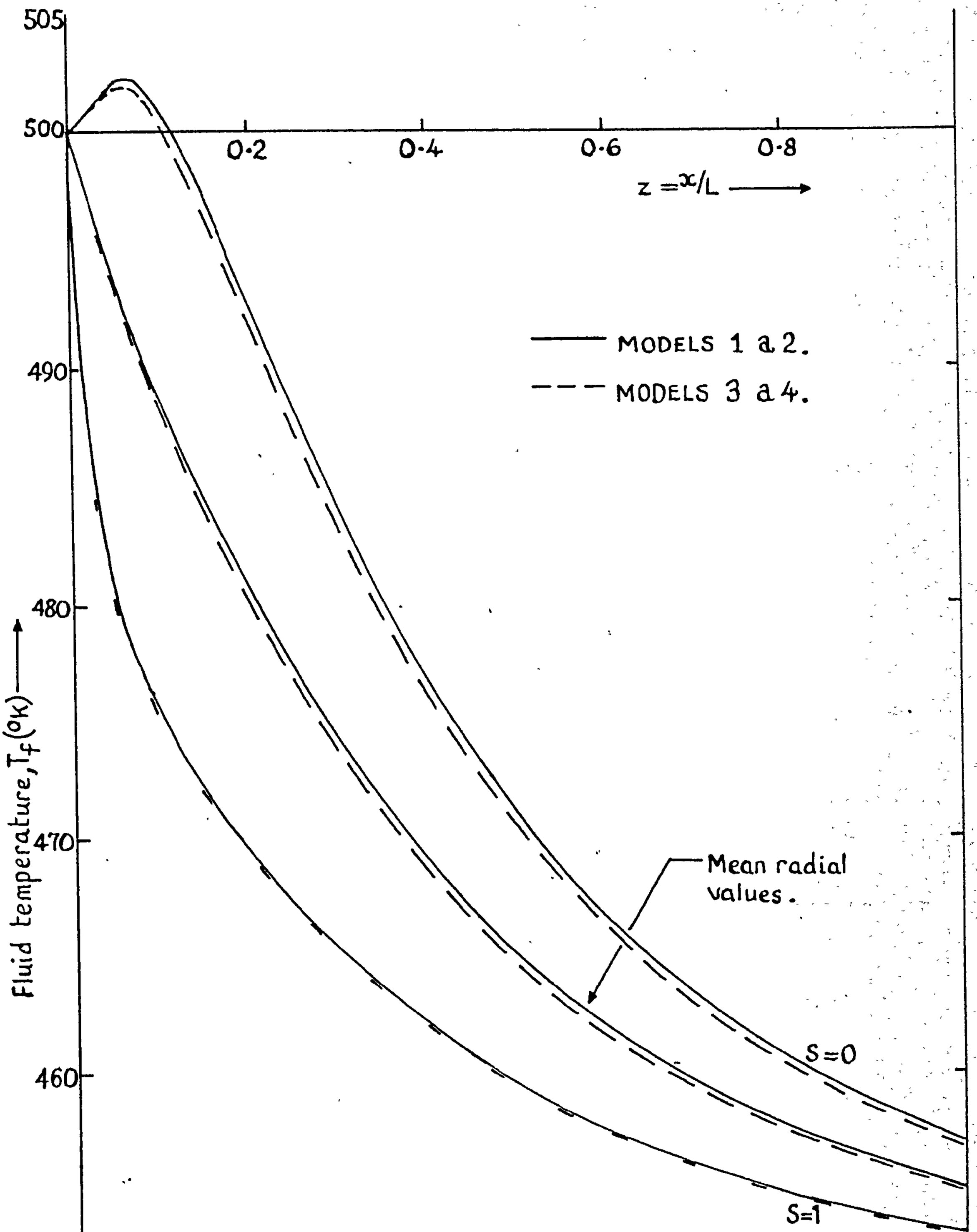

FIG. 9.2 Comparison of reactor models. Longitudinal temperature profiles in the fluid phase.

From (9.8) $$C_s\Big|_{w=b} = C_f/\left(1 + \frac{\eta_p . k_s}{\frac{3}{b} . k_A}\right) \qquad (9.9)$$

Using equation (9.9) in the left hand side of equation (9.8) and dividing by $4/3\,\pi b^3$,

$$\eta_p . (k_s C_s)_{w=b} = \frac{\eta_p . k_s . C_f}{\left[1 + \frac{\eta_p . k_s}{(\frac{3}{b} . k_A)}\right]} = k_e . C_f$$

where $$k_e = \eta_p . k_s \Big/ \left[1 + \frac{\eta_p . k_s}{\frac{3}{b} . k_A}\right] . \qquad (9.10)$$

k_e is an <u>effective</u> rate constant composed of the intrinsic kinetic rate constant (k_s), the film mass transfer rate ($\frac{3}{b} . k_A$) and the pore diffusion contribution (η_p).

It is to be expected that the interaction between the chemical and physical processes will be most pronounced along the axis of the reactor where the chemical rate is a maximum. Table 9.4 compares chemical and effective rates at different longitudinal points along the reactor axis.

z	Chemical rate k_s (sec^{-1})	Effective rate k_e (sec^{-1})	Pore effectiveness η_p
0	0.136	0.123	0.91
0.06	0.147	0.131	0.90
0.10	0.139	0.125	0.90
0.20	0.099	0.092	0.93
0.30	0.069	0.065	0.95
0.50	0.040	0.039	0.97
0.80	0.025	0.025	0.98
1.00	0.022	0.022	0.98
Film mass transfer rate $(\frac{3}{b} . k_A) = 46.9\ sec^{-1}$.			

TABLE 9.4 Analysis of the rate process (s = 0)

Examination of Table 9.4 reveals the following conclusions:-

(i) Even at the point of maximum temperature rise (z = 0.06) the intrinsic chemical rate is over 300 times slower than the rate of mass transfer across the fluid film. Film mass transfer is not influencing the overall rate for any catalyst pellet in the bed.

(ii) In the region of maximum temperature rise the effective rate is some 10% lower than the intrinsic chemical rate. This may be attributed to a mild "pore" diffusion influence. Downstream from the hot spot "pore" diffusion is insignificant.

The behaviour of this particular system is largely characterized by chemical rate control. In the region of the "hot spot" there is a mild "pore" diffusion effect. Radial gradients in the bed are not appreciable and the indications are that a one-dimensional quasi-homogeneous model would be sufficient.

9.4 Computational details

In order to obtain accurate results in a reasonable time several experiments were conducted to ascertain the effects of

(a) increment size

(b) type of finite difference scheme

(c) convergence criteria

upon the accuracy of the numerical solutions and the computation times. Some results are presented in Appendix 6. The influence of the discontinuity upon the solution of the finite difference equations for Model 2 is also discussed in terms of a comparison of the numerical solution with the semi-analytic approach given in Appendix 5.

For the results given in Figs. 9.1, 9.2 and Table 9.4, 100 axial and 20 radial increments were employed in the integration procedures. The Crank-Nicolson scheme ($\theta = \frac{1}{2}$) was employed with

$\varepsilon = 10^{-4}$ in equation (8.36). Results were printed at every 5 axial stages and only the converged radial values were shown at every alternate radial stage. Compute times were:-

MODEL 1 1 min. 30 secs.

MODEL 2 2 mins. 10 secs.

MODEL 3 2 mins. 20 secs.

It is difficult to give a comparable figure for Model 4. The computational situation here is far more complex. No attempt was made to test out different strategies in order to assess the advantages of one particular approach over another. There is no evidence to suggest that the technique employed is necessarily the most efficient for the problem in hand. Experience with the particular method does, however, indicate that, whatever the detailed technique, a policy based on integration of the fully distributed equations described in Chapter 3 will incur, conservatively, a 10-fold increase in computation time compared with the lumped parameter analogue (Model 3). In the region of operation described in Chapter 10, where severe intraparticle gradients are in evidence, a numerical solution of the distributed particulate equations becomes impracticable. In order to maintain accuracy the intraparticle step length must be made small (40 particle increments) in the region of the bed where the intraparticle gradients are severe. Unless sophisticated procedures are introduced to control the mesh size as the integration proceeds the computation time becomes excessive (2-3 hours).

CHAPTER 10

CASE STUDY No. 2 :- A PORE DIFFUSION-INFLUENCED SYSTEM

This system is similar in many respects to the one considered in Chapter 9, except that:

1. The kinetic parameters have been exaggerated so that now, $E = 22.95$ kCals/gm.mole, $-\Delta H = 54$ kCal/gm.mole and $k_{vfo} = 1\ sec^{-1}$.

2. The inlet temperature has been increased from 500°K to 600°K.

3. The coolant temperature has been raised from 450°K to 500°K.

4. The 'effective' pore diffusivity has been lowered almost 4-fold to 9.78×10^{-4} cm^2/sec, so that diffusion is in the Knudsen region.

As a consequence of these modifications certain physical variables and dimensionless groups appearing in Tables 9.1 and 9.2 are altered. The revised values are given in Table 10.1.

These operating conditions put the reactor in the potential "run-away" region where it might be expected that the rate process is appreciably limited by physical transport processes. Curve 1 in Fig. 10.1 shows the peak "hot-spot" attained in the quasihomogeneous reactor model. The explosive increase in the unconstrained reaction rate is accompanied by temperature "run-away" - the maximum temperature rise of 285°K being not far short of the adiabatic temperature rise of 335°K. Curve 2 shows that even with film mass transfer limitation of the rate process it is possible to have temperature "run-away". It is interesting to note that in the first quarter of the bed the reaction rate of Model 2 is in excess of the unconstrained rate of Model 1; the reason being rate enhancement due to a significant interphase heat transfer resistance. Further downstream the effective rate is constrained by interphase mass transfer and actual rate retardation results. The effective rate can still rise to a level which causes severe thermal gradients in the reactor. Curve 3 demonstrates the

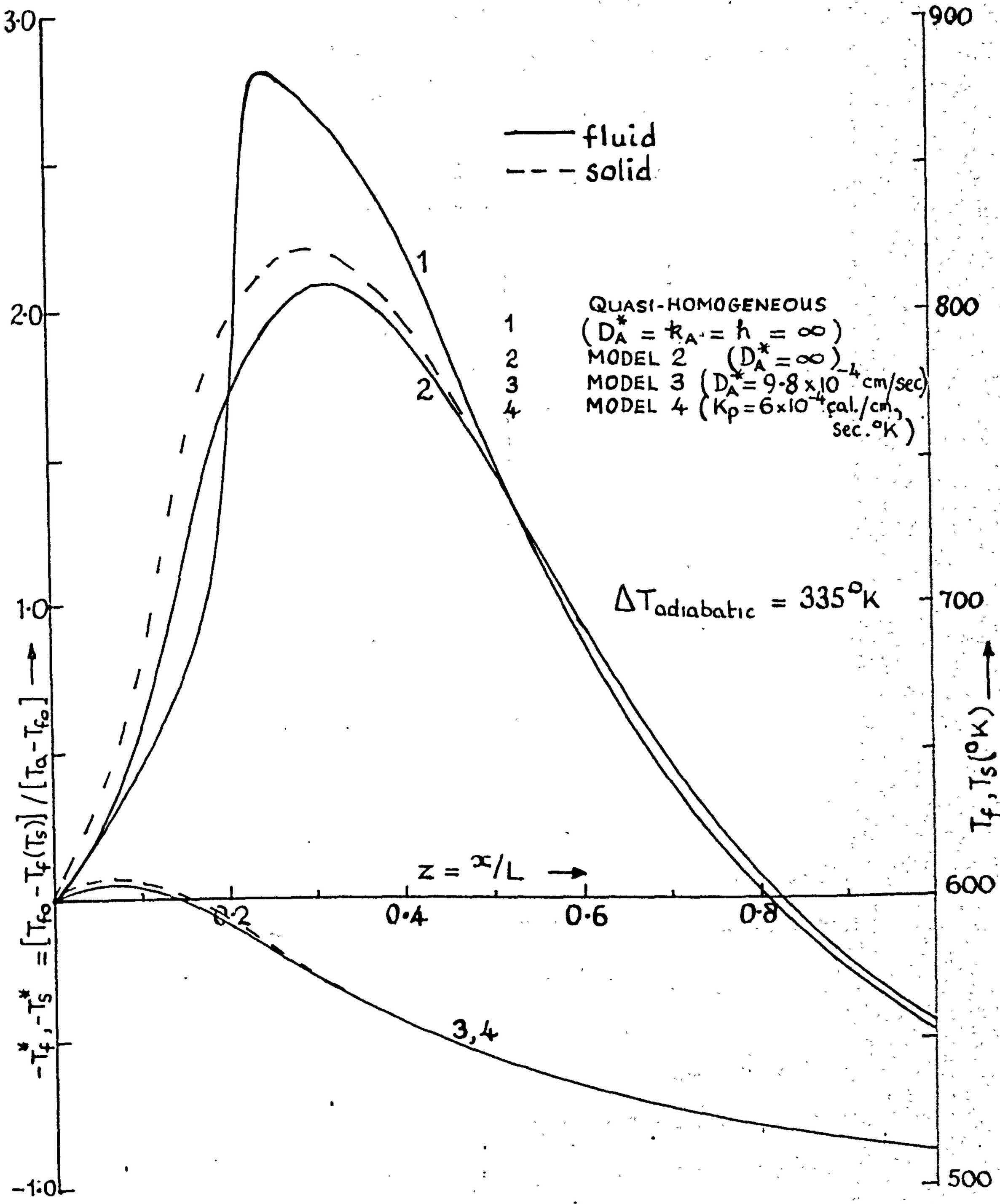

FIG. 10.1 Comparison of reactor models. Longitudinal temperature profiles along the axis (s=0).

Superficial velocity (V_o)	79 cm./sec.
Feed concentration (C_{fo})	2.03×10^{-5} gm.mole/cc
Interphase mass transfer coefficient (k_A)	1.45 cm/sec
Radial mass diffusivity (D_f)	3.32 cm^2/sec

c_2	-3.127
c_4	0.9494
Φ_o	6.715
β_1	-2.718×10^{-3}
γ	19.24
θ	$-1/6$
Sh'	623
Surface reaction model:	
δ	4.828×10^{-2}
β_2	-0.8461
Additional parameter:	
Sc	5.93

TABLE 10.1 Modified data for Case Study No. 2

dramatic influence of "pore" diffusion in constraining the overall rate, thereby preventing uncontrolled temperature rise. Again, local particulate isothermality is apparent as evidenced by the coincidence of curves 3 and 4.

As might be expected, conversions are widespread, particularly between Models 2 and 3. Figure 10.2 shows the distributions in the integrated radial fluid conversion. In the quasihomogeneous model, reaction is essentially completed at $z = 0.4$; the reactor then merely operating as a heat exchanger. The effluent conversion of 97% for Model 2 is to be compared with the corresponding figure of 10% for Model 3.

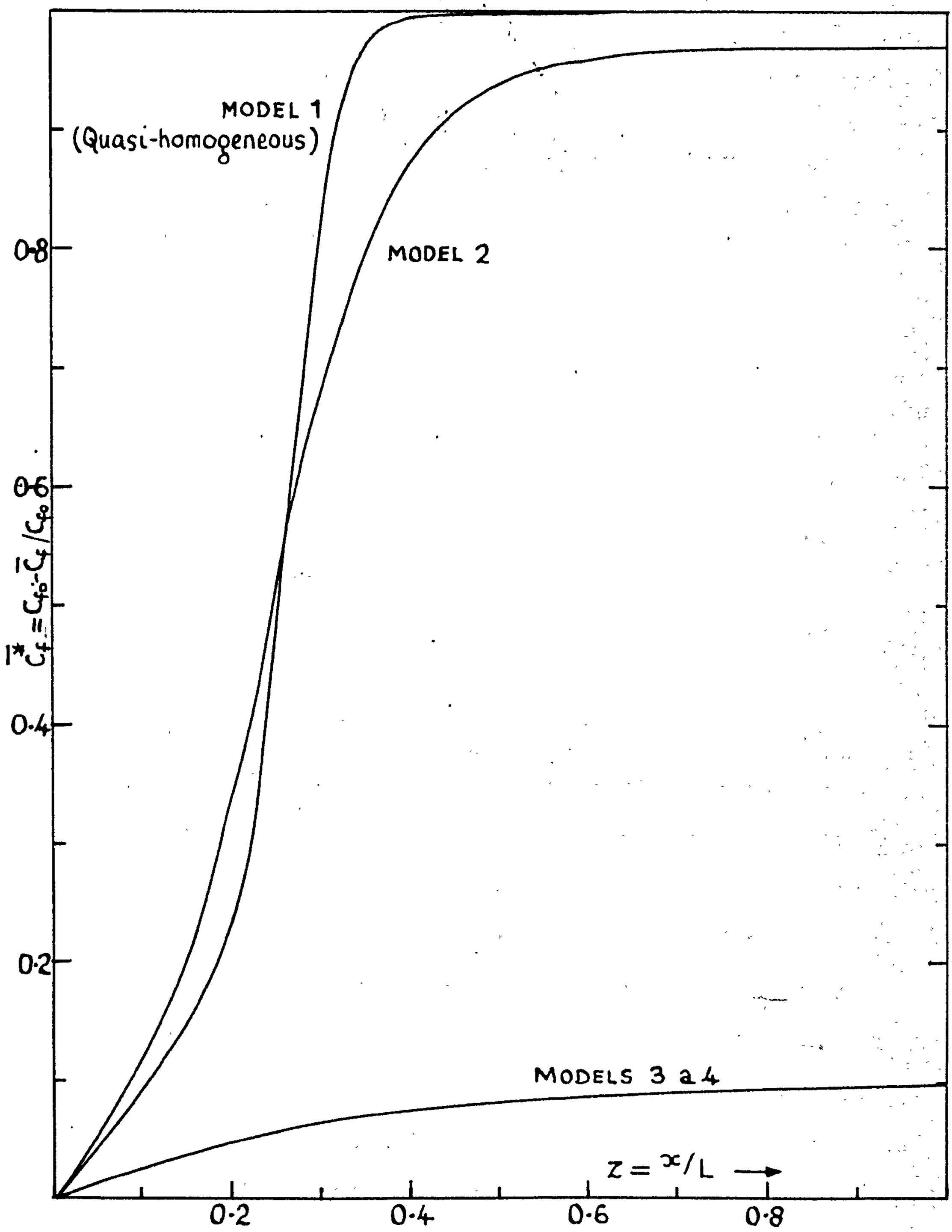

FIG. 10.2 Comparison of reactor models. Longitudinal profiles of mean radial conversion in the fluid phase.

10.1 Analysis of the rate process

To gain an understanding of how local reaction rates, along the axis (s=0), are influenced by physical transport processes, consider Table 10.2.

z	MODEL 1	MODEL 2	MODEL 3
	Unrestricted chemical rate k_s (sec^{-1})	($\eta p=1$) Effective rate k_e (sec^{-1})	Effective rate k_e (sec^{-1})
0	1	1.09	0.384
0.05	1.88	2.34	0.427
0.1	3.74	6.66	0.422
0.2	32.4	17.5	0.313
0.3	396	18.5	0.214
0.4	187	17.7	0.148
0.5	48	14.1	0.105
0.6	11.4	7.88	0.077
0.8	1.06	1.16	0.048
1.0	0.212	0.235	0.036

TABLE 10.2 Comparison of effective rates for Models 1 to 3.

The first column contains values of the unrestricted chemical rate from Model 1. Note the dramatic rise (a 100-fold increase, in fact) in rate between z = 0.1 and z = 0.3. Column 2 shows the effective rate (obtained from equation 7.4) for Model 2. Initially, this rate is larger than the unrestricted rate as a consequence of fluid film heat transfer. However, the effective rate cannot exceed the interphase mass transfer rate of 20.7 sec^{-1}. In the "hot-spot" region the actual rate approaches this maximum very closely, indicating that fluid film mass transfer is controlling. By far the most significant restriction in the rate is shown in Column 3, where "pore" diffusion is introduced. Here, there is immediately placed a serious constraint on the allowable

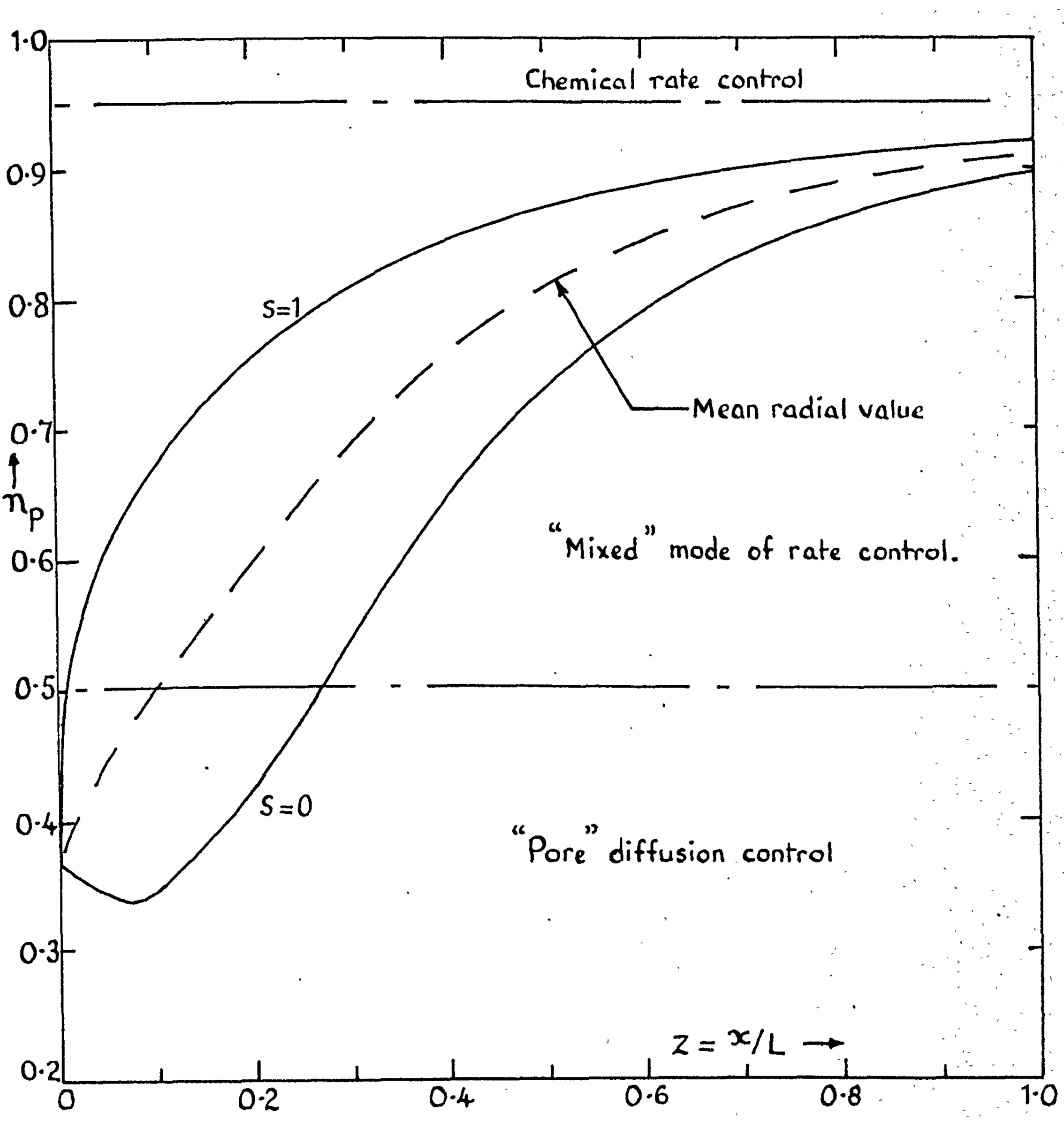

FIG.10.3 Longitudinal profiles of "pore" effectiveness factor.

rate of 0.384 compared with the kinetic rate of 1.05 sec^{-1} (see Table 10.3). There is no tendency for the rate to rise explosively in the manner shown in Column 1. The maximum rate of 0.433 sec^{-1} is almost 50 times slower than the interphase mass transfer rate.

A quantitative appraisal of the various rate-influencing factors in Model 3 is provided in Table 10.3. The points of assessment are again taken on the reactor axis (s=0) to demonstrate the maximum degree of interaction. Effectiveness factor profiles in the reactor are shown in Fig. 10.3.

z	Chemical rate k_s (sec^{-1})	Effective rate k_e (sec^{-1})	Effectiveness factors	
			η_p	η_{ov}
0	1.05	0.384	0.37	0.39
0.05	1.26	0.427	0.35	0.36
0.1	1.24	0.422	0.35	0.36
0.2	0.741	0.313	0.43	0.44
0.3	0.401	0.214	0.54	0.55
0.4	0.231	0.148	0.64	0.65
0.5	0.144	0.105	0.73	0.74
0.6	0.098	0.077	0.79	0.79
0.8	0.056	0.048	0.86	0.86
1.0	0.040	0.036	0.90	0.90
Interphase mass transfer rate = 20.7 sec^{-1}.				

TABLE 10.3 Analysis of the rate process for Model 3.

Over the reactor as a whole it is not possible to identify a single rate-controlling effect, unlike Study No. 1. "Pore" diffusion is dominant in the central core of the bed at, and in the neighbourhood of, the hot spot while a "mixed" form of rate control exists near the tube wall. Towards the tube exit the "mixed" regime is increasingly

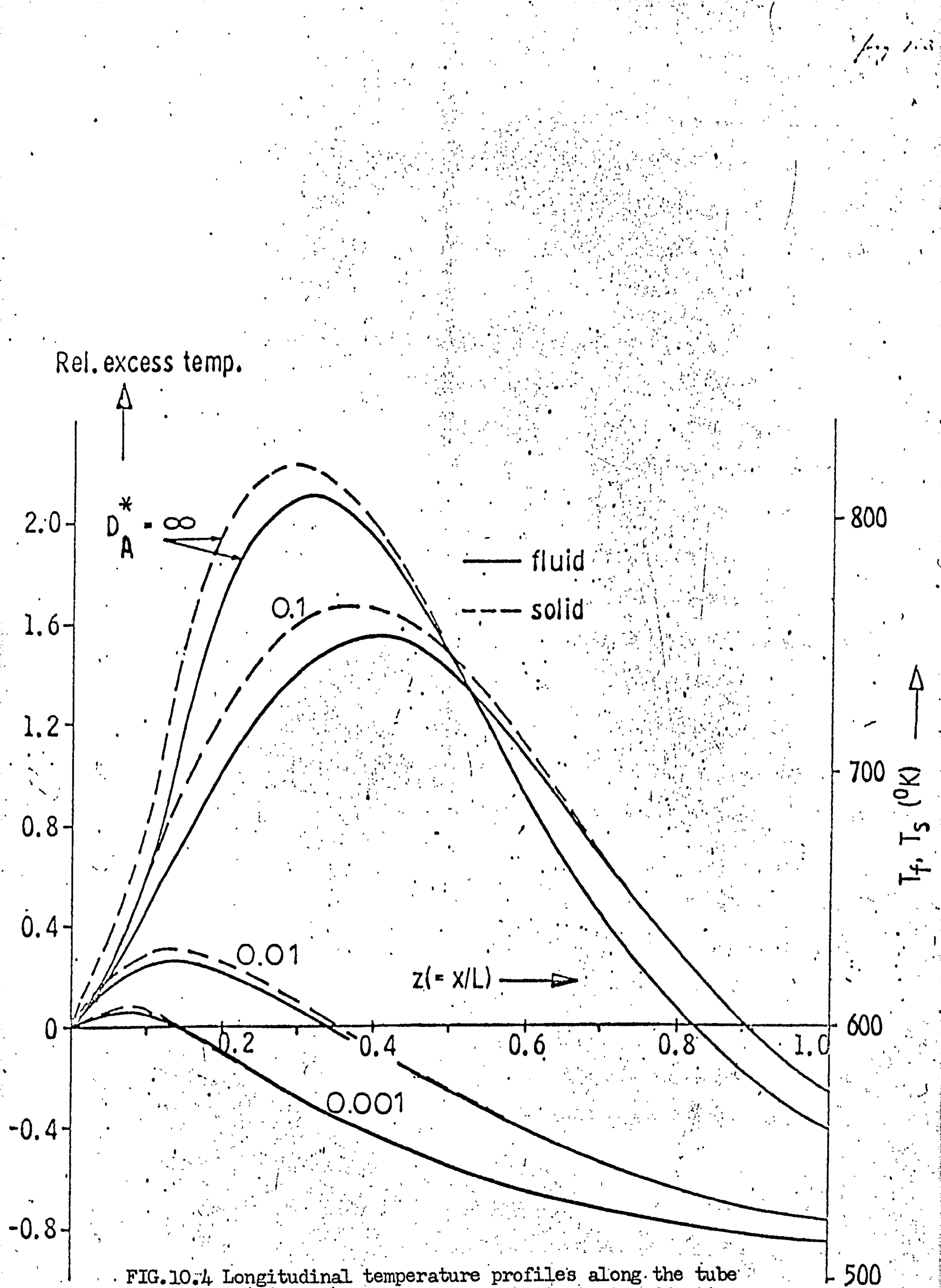

FIG. 10.4 Longitudinal temperature profiles along the tube axis(s=0): Parametric sensitivity to effective diffusion coefficient, D_A^*.

influenced by surface kinetics over the entire reactor cross-section.

Parametric sensitivity of the temperature distribution along the axis (s=0) to "effective" pore diffusivity is shown in Fig. 10.4. The very marked effect of solid diffusional resistance stresses the need for accurate estimates of this parameter.

10.2 Parametric Sensitivity : Influence on design

The particular example considered here has been chosen in a way which demonstrates temperature "run-away". A 4.2 cm. tube filled with 0.42 cm. particles, in which, at the reaction temperature, the reaction proceeds to completion in a length of 50 cms., means for the tube axis a situation which is not very far short from adiabatic conditions. At the same time the wall is cooled so that its temperature is some 300°K lower than the mean reaction temperature in the region of maximum temperature rise. This means that in a zone along the wall the reaction is practically quenched. The reaction system thus balances between extinction starting at the wall and ignition starting from the axis. Radial temperature (and concentration) gradients are very severe in this situation, Fig. 10.5(a).

This design could not, of course, be tolerated in practice. The choice of alternative designs would depend, among other things, upon the type of model used. If the model displays "parametric sensitivity" then the alternative designs may be inappropriate when compared with those based on a more detailed model in which "parametric sensitivity" is not in evidence. For example, more practical conditions for the quasi-homogeneous reactor might be

(i) A ratio much lower than 10:1 for tube and particle diameter e.g., a 1" tube packed with $\frac{1}{4}$" catalyst particles.

(ii) A more dilute reaction mixture.

(iii) A cooling medium at a temperature where the reaction is already reasonably high.

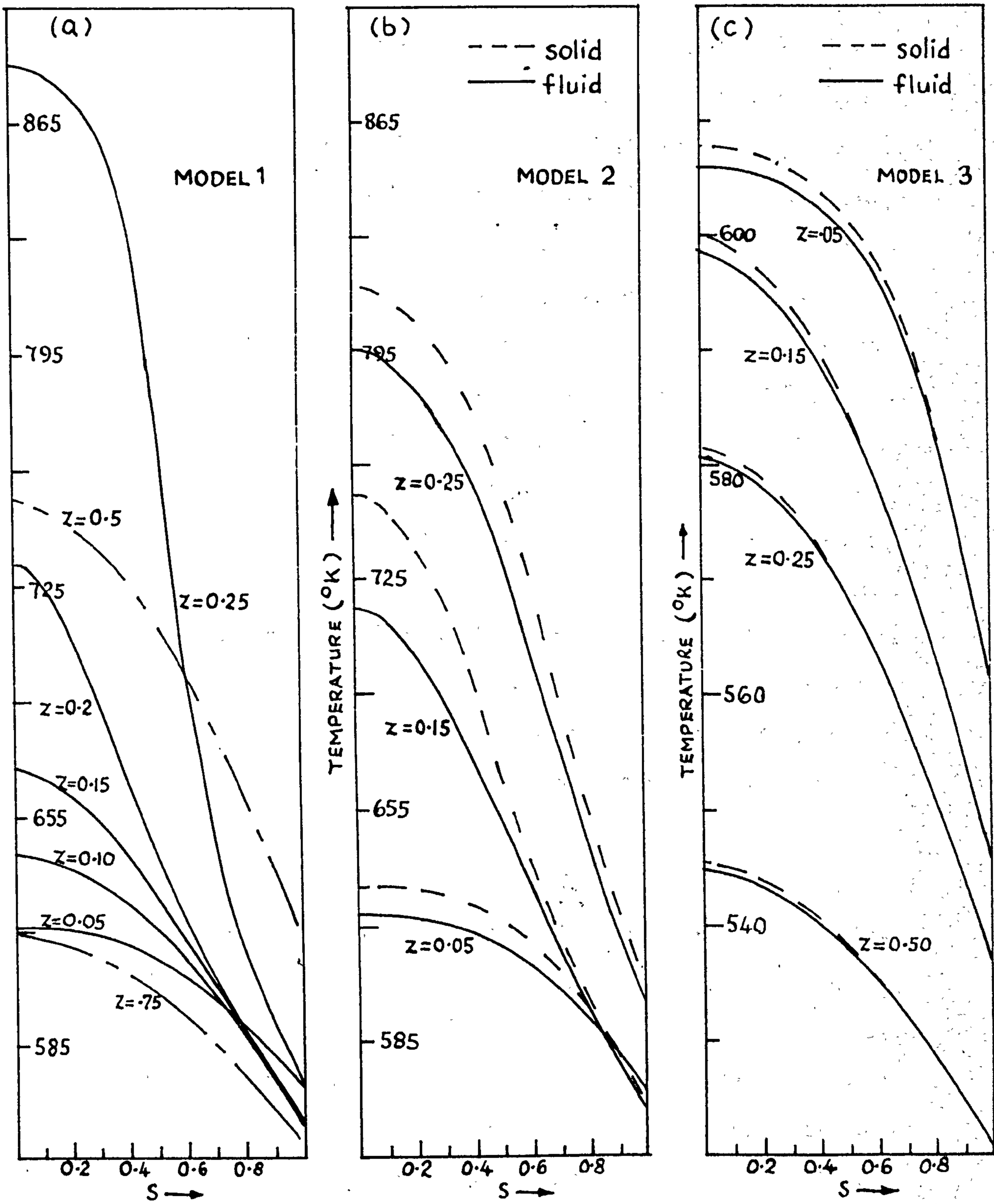

FIG. 10.5 Radial temperature profiles for MODEL'S 1, 2 & 3.

If further measures are necessary a policy of catalyst dilution might be followed in the first part of the tube or a jacket comprised of several sections, with different rates of cooling in each, might be employed.

The delicate balance of the system is not in evidence when the reaction rate is limited by "pore" diffusion, although appreciable radial temperature gradients are still present (Fig. 10.5(c)) as a consequence of too low a cooling temperature. An improved design, based on the detailed model, is facilitated by raising the jacket temperature. Fig. 10.6(a) shows the effect on conversion of increasing the jacket temperature from 500°K to 575°K. Even with a jacket at 575°K, the maximum mean reaction temperature is only some 12°K over the feed temperature while the maximum temperature rise along the tube axis is only 25°K. The large increase in jacket temperature has failed to force the reactor into a region of "parametric sensitivity". Although the kinetic rate is significantly enhanced the increased diffusional limitation within the catalyst pellets constrains the effective rate to a level insufficient to cause appreciable temperature rise within the bed. Effectiveness factor profiles as a function of jacket temperature are shown in Fig. 10.6(b).

Other changes such as an increase in feed concentration or feed temperature have much the same effect. The reactor moves its steady state but the movement is never of the explosive kind found in the quasihomogeneous representation.* Changes of the type mentioned here could not be contemplated from a design based on the quasihomogeneous model. The whole issue of "parametric sensitivity" seems to be over-dramatized as a result of forgetting about transport rate restrictions, especially the restriction imposed by the finite diffusion rate inside porous particles.

* see Chapter 11.

FIG. 10.6 (a) Influence of jacket temperature on mean radial conversion in the fluid phase.

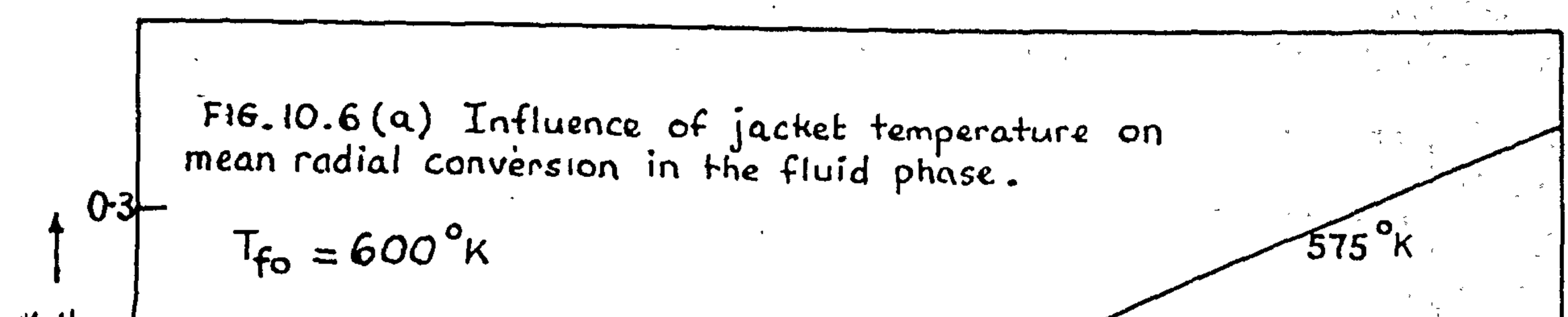

FIG. 10.6 (b) Influence of jacket temperature on mean radial effectiveness factor.

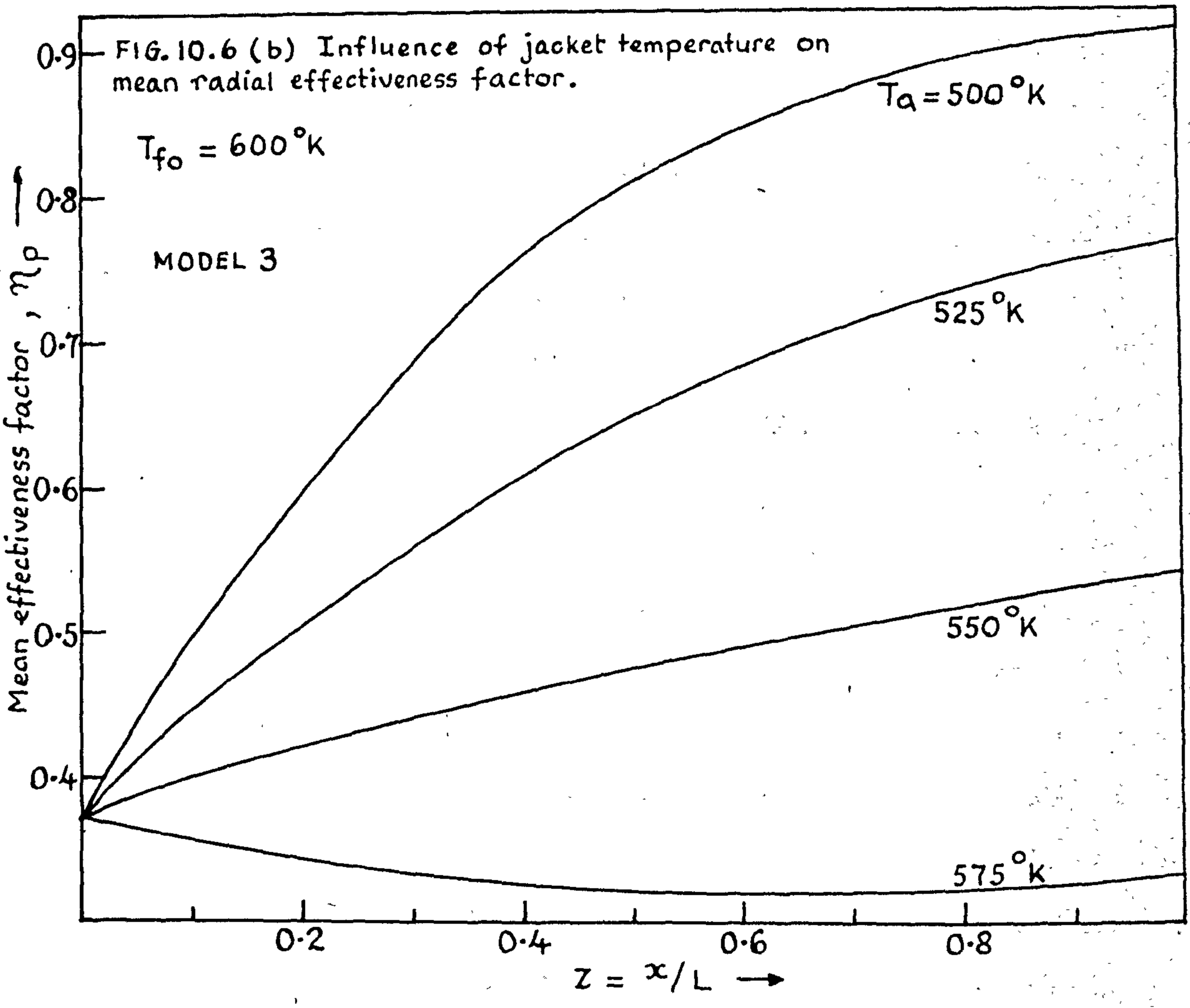

Froment[90] has demonstrated the importance of the heat transfer parameters in influencing the temperature and conversion profiles in a quasihomogeneous reactor. For the air oxidation of o-xylene in a packed bed, an increase of 10% in the values of the effective thermal conductivity or wall heat transfer coefficient had the effect of significantly lowering the maximum mean overtemperature.

Variations in the values of these coefficients of the order of 10% are well within the spread of experimental results, and in this critical situation an accuracy is demanded in the measurement of these parameters which is difficult, if not impossible, to achieve.

Fig. 10.7 shows that such critical situations are not apparent when the reaction rate is constrained by "pore" diffusion. The solid lines represent reactor profiles for a jacket temperature raised to 575°K in an attempt to force a "parametric sensitivity". Both the radial thermal conductivity and the wall heat transfer coefficient are lowered by 10% and the adjustment of the reactor, as shown by the dotted lines, is small. Clearly, this would have important consequences in an experimental programme to determine these coefficients.

10.3 An attempt to improve the quasi-homogeneous model of a diffusion-influenced system

The question might now be asked: Is it possible to modify the magnitudes of the parameters of the quasihomogeneous model in such a way that the prediction matches effectively with that of the complex model (Model 3)? Any corrections to be made can only follow, of course, from a detailed analysis using the complex model. No evidence is available for providing general rules as to when a particular model is appropriate.

The most obvious, and indeed simplest, approach is to examine the distribution of effectiveness factor values in the bed. Providing the spread is not appreciable, it seems reasonable to use a constant mean

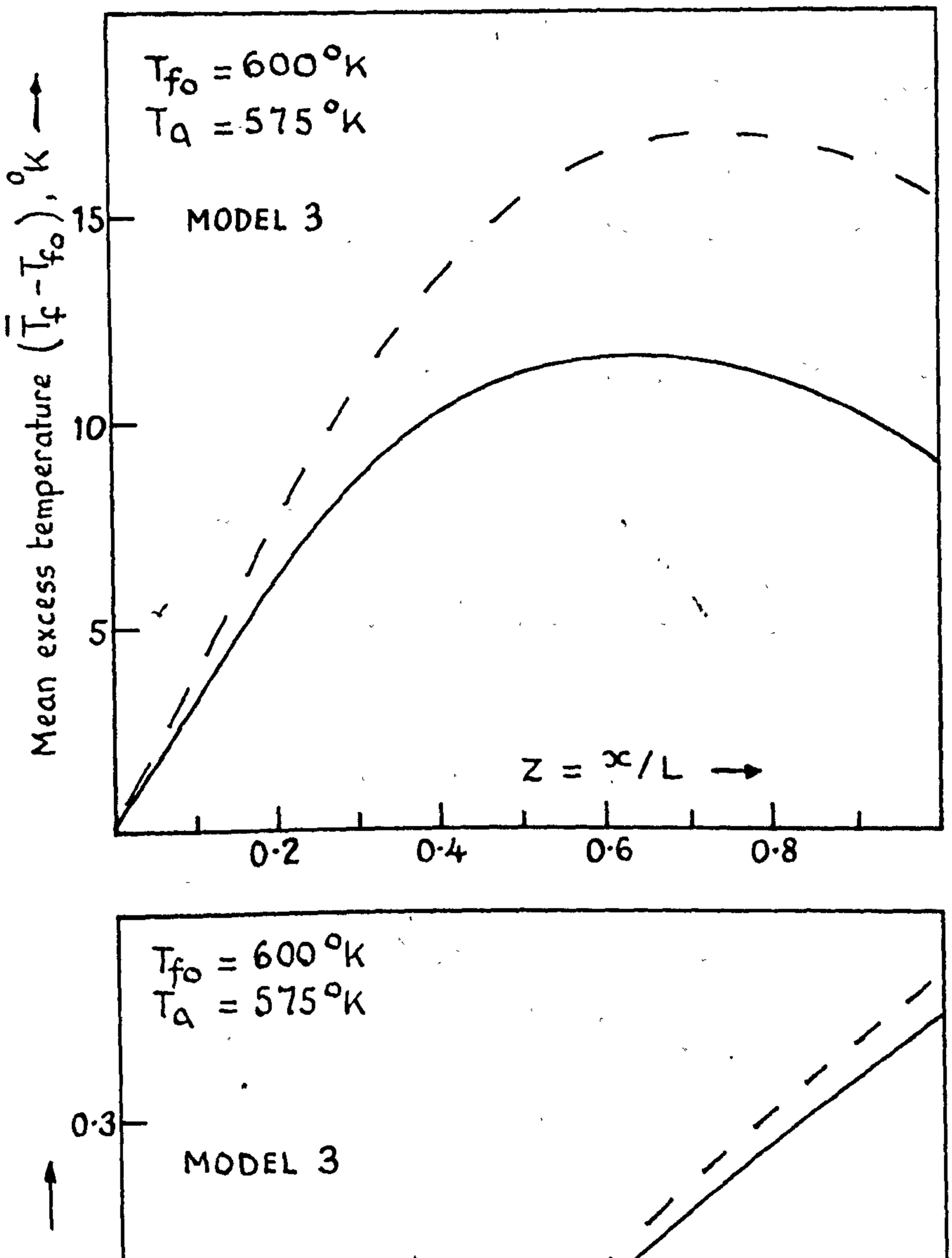

FIG. 10.7 Effect of lowering the effective conductivity and the wall heat transfer coefficient by 10% on mean radial temperature and conversion profiles.

value to adjust the rate data for use in the quasihomogeneous model. An attempt is made here to modify the rate data so as to force the two models to predict essentially the same rate of reaction at the tube inlet. Reference to Table 10.2 shows that, as a consequence of "pore" diffusion, the effective rate in Model 3 is almost one-third of that of Model 1. When film effects are absent the effectiveness factor, as soon as it is lower than say 0.5, is essentially proportional to the reciprocal square root of the chemical rate. For $\phi \gg 1$, it follows from equation (4.12) that for an isothermal pellet,

$$\eta \cong 3/\phi \qquad (10.1)$$

At the reactor inlet, $\phi = b\sqrt{k_{vfo}/D_A^*}$, and the true rate of reaction/ unit vol. of catalyst is given by

$$\text{rate} = \eta . k_{vfo} . C_{fo} \qquad (10.2)$$

where $k_{vfo} = \alpha . S_v . \exp(-E/R_g . T_{fo})$.

From equations (10.1), (10.2) and the definition of ϕ

$$\text{rate} = (\alpha S_v)' . \exp(-E'/R_g . T_{fo}) . C_{fo} \qquad (10.3)$$

where $(\alpha S_v)' = \frac{3}{b} . (\alpha S_v D_A^*)^{\frac{1}{2}}$ and

$$E' = E/2 .$$

Using the modified pre-exponential factor $(\alpha S_v)'$ and the modified activation energy (E') in the quasihomogeneous model, the predicted chemical rate of 0.45 sec^{-1} at the reactor inlet compares favourably with an effective rate of 0.38 sec^{-1}. Table 10.4 compares the predictions of the quasihomogeneous model using a) initial data and b) modified rate data, with the complex model. The improvement is quite dramatic.

	Original rate data $\alpha S_v = 2.27 \times 10^8 \text{ sec}^{-1}$, E = 22.95 kCal/mole	Modified rate data $(\alpha S_v)' = 6.73 \times 10^3 \text{ sec}^{-1}$, E' = 11.48 kCal/mole	
Integrated radial conversion (%) at the tube exit	99.9	15.8	9.93
Max^{m}. temp rise of the fluid over the feed (600^{o}K).	285	8	6.5

TABIE 10.4 Comparison of the Quasihomogeneous Model with the Complex Model

A second case is considered ($D_A^* = 0.05$ cm^2/sec) in which appreciable "pore" diffusion influence becomes only apparent some distance from the reactor inlet, Fig. 10.8. The spread in effectiveness factors is such that it is not possible to use a constant mean value to correct rate data for use in the quasihomogeneous model. A correction based on the effective rate at the point of maximum diffusion retardation ($z = 0.38$, $s = 0$) leads to a serious over-estimation of the actual rate at the inlet with the result that the temperature actually runs away more rapidly (see Fig. 10.9).

Since the predicted performances of Models 1 and 3 are so strikingly different, it is essential to use the more general model in optimization strategies when the reactor is operating in the critical region. The simpler models are useful for indicating roughly where this region is located, but cannot be satisfactorily used there.

There seems no obvious way of modifying the parameter values of the quasihomogeneous model which guarantees a close prediction with the complex model. Indeed, it is necessary to utilize the detailed model before any idea of the modifications can be appreciated.

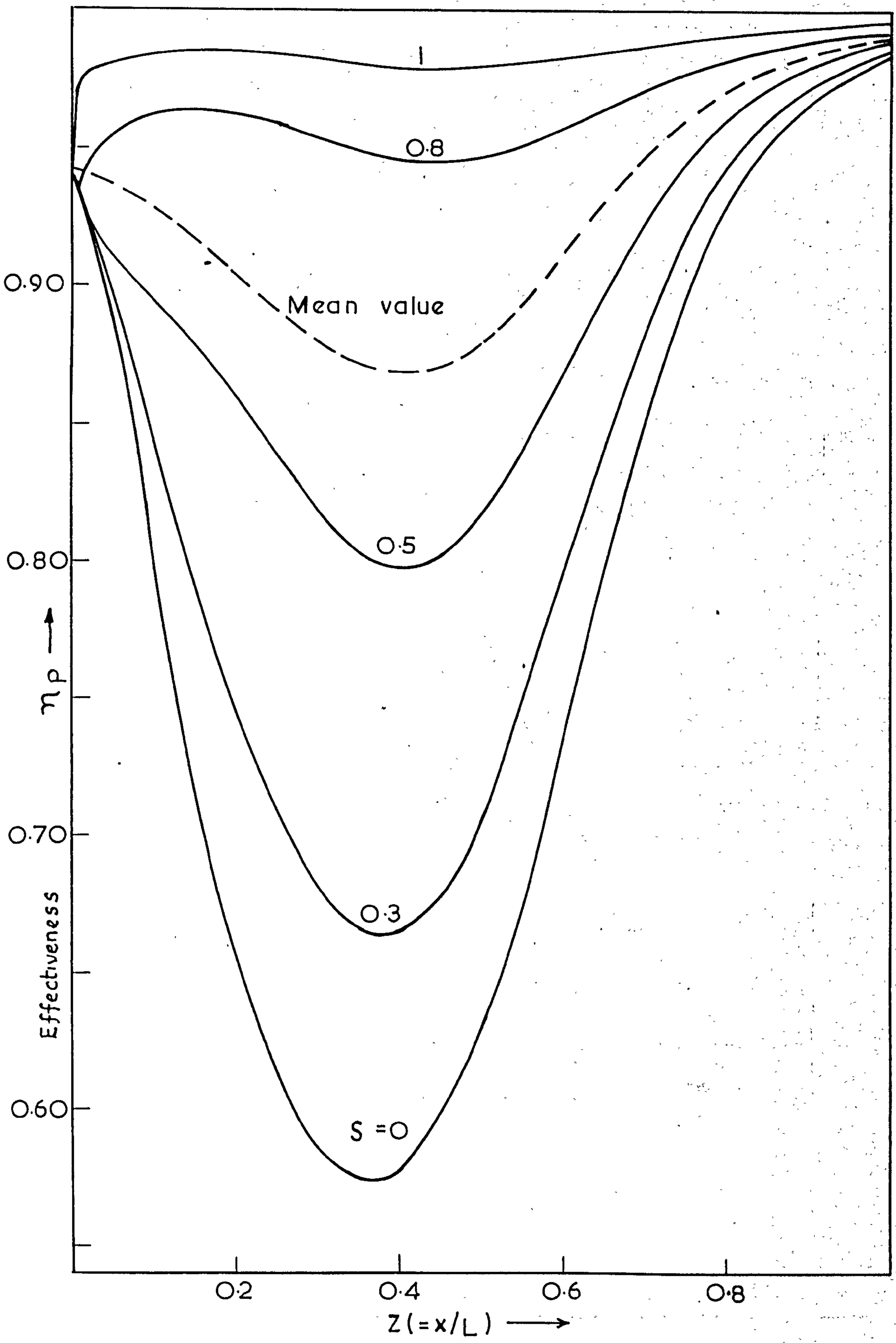

FIG.10.8 AXIAL PROFILES OF EFFECTIVENESS FACTOR FOR CASE 2 WITH $D_A^* = 0{\cdot}05$ cm²/sec.

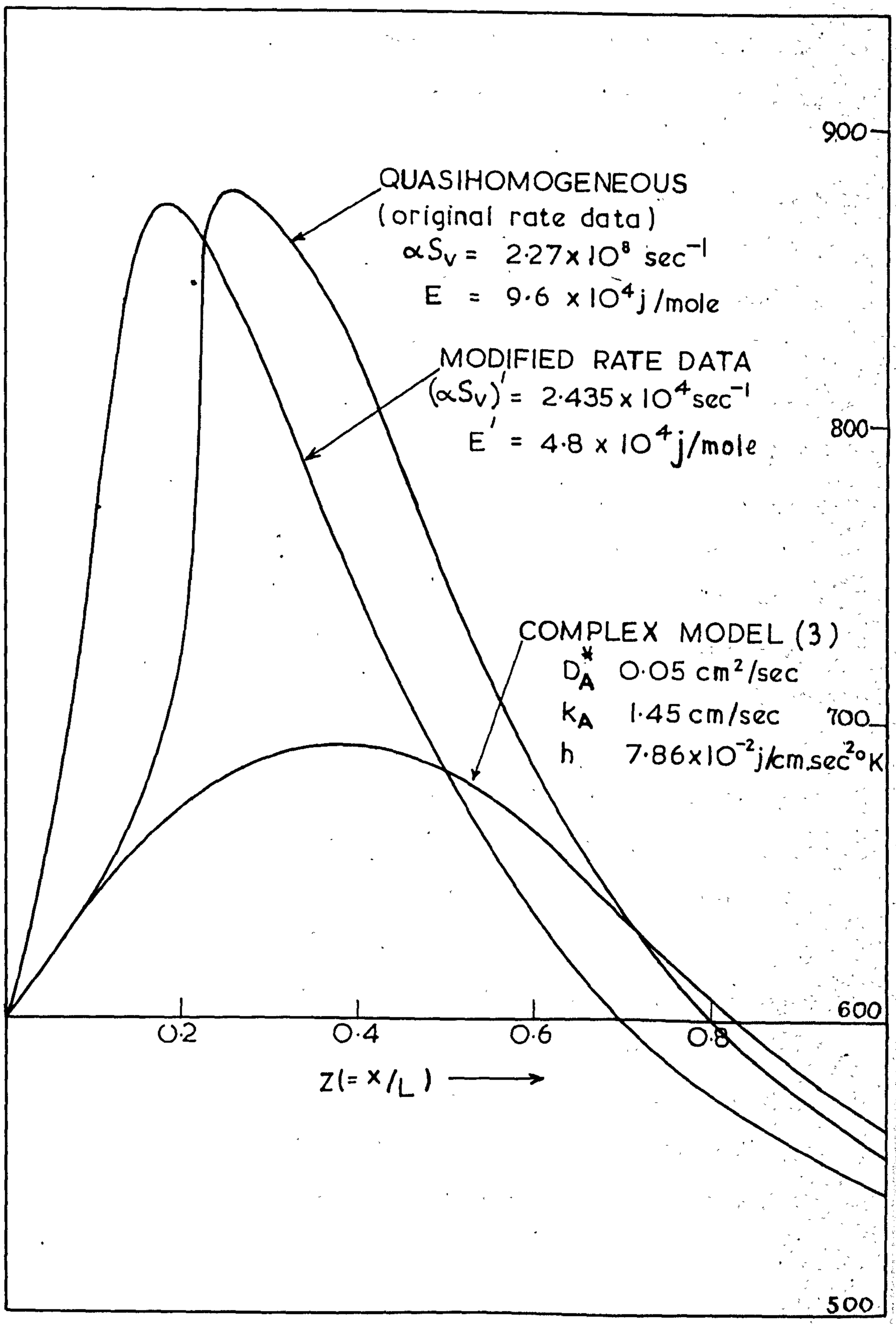

FIG. 10.9 A COMPARISON OF TEMPERATURE PROFILES FOR ACTUAL AND MODIFIED DATA

10.4 Conclusions

For operating conditions far removed from the critical region it is generally unnecessary to consider models more elaborate than those already available in the literature.

The highly exothermic nature of many catalytic reactions infers that these systems are likely to operate in the critical region. On this basis it seems that the only procedure for obtaining valid packed bed reactor profiles is to use a formulation of the detail of Model 3. This model includes many of the important mechanisms necessary to an accurate description of the transport phenomena occurring in such reactors.

Of primary concern in the results obtained is the fact that the use of simplifying assumptions to remove some of the complexity in the model can lead to misleading results. Thus, predicted conversion and temperature profiles are vastly different from those indicated by the simpler quasihomogeneous model. No temperature "run-away" or potential instability is apparent.

Including simply a film mass and heat transfer resistance is no guarantee that temperature "run-away" will not be predicted. In fact, it is the particle diffusive resistance which is the main factor controlling the temperature effects.

Granted the non-isothermality of the continuous domain of packed bed reactors, local isothermality can exist in the particulate phase. Thus, analysis based on a lumped parameter analogue, in which the temperature rise occurs across the fluid film, proves relevant to experience. This assumption permits considerable simplification in the numerical procedure.

CHAPTER 11

MULTIPLE SOLUTIONS

When due account is taken of the finite rates of intraparticle material and heat transfer, the solution of the material and energy balance equations may be non-unique for certain combinations of the transport, thermodynamic and kinetic parameters. Allowance for fluid film mass and heat transfer limitations tends to exaggerate this phenomenon.

The possible onset of multiple solutions in a packed bed reactor is important for two reasons:-

(a) It complicates computation of the steady state by causing severe temperature and concentration gradients. These gradients are caused by adjacent catalyst pellets existing in different reaction states.

(b) It produces a profound effect on dynamical analyses aimed at stability in packed beds.

It is important, therefore, to be aware of such a possibility occurring and, if so, under what conditions.

11.1 Multiple solutions : relation to reactor stability

In recent years dynamical analyses of packed beds by AMUNDSON and co-workers[76-78] have shown theoretically that reactor stability is characterized in terms of various stable and unstable conditions inside porous catalyst particles. The rather elementary treatments considered allowed a priori prediction of non-unique reactor temperature and conversion profiles from analysis of the steady state.

As soon as allowance is made in the mathematical model for radial gradients in the interparticle field and for gradients plus reaction in the intraparticle field, a simple extension of the stability analysis of LIU and AMUNDSON does not seem practicable.

McGUIRE and LAPIDUS[39] drew similar conclusions from transient

integrations of a detailed packed bed reactor model containing both interparticle and intraparticle gradients. They showed that the final profiles of temperature and conversion depend upon how the reactor is started up. If all the particles in the bed have initially a unique state, the reactor is stable to feed perturbations. However, if some of the particles exist in a non-unique initial state, particularly those along the tube axis, the reactor is unstable to feed perturbations of large magnitude. The instability is associated with particles along the tube axis moving from a low reaction state to a high reaction state.

The conditions under which catalyst pellets exist in a unique steady state is, therefore, a fundamental issue in theoretical analyses of reactor stability.

11.2 Uniqueness conditions for a catalyst pellet

The analyses of AMUNDSON and co-workers[119-120, 121, 130] applied to single catalyst pellets have revealed some interesting theoretical results. Much of the work, however, has been applied to the class of problems for which $Sh' = Nu' = \infty$. This special case is rather far removed from the practical situations in which Sh' and Nu' are finite. Furthermore, the analyses are purely "local" rather than "global" when related to a packed bed reactor. In this situation the internal and film phenomena are not the only transport processes of importance; there is also the external field mixing and heat transfer in both axial and radial directions of the bed proper.

If consideration is given to the local regime only, it is possible to arbitrarily choose conditions in the bulk fluid phase which force the catalyst pellet to exhibit multiple states. The point at issue is that in a packed bed reactor the choice of local fluid conditions is not arbitrary; rather, the admissable values only follow as a result of solving the differential equations describing the entire system - both

intraparticle and interparticle fields - for specified boundary conditions. Whether this constraint is now sufficient to remove the combinations of fluid concentration and temperature which lead to multiple states in porous catalyst particles is a point of conjecture which can only be answered by analysis of the entire reactor rather than consideration of a single particle. Because of the extreme complexity of the mathematics it is unlikely that a general analysis will be readily forthcoming.

11.3 Global uniqueness : some observations

Progress can be made on this difficult problem but the complete solution is still evasive.

A description of a catalyst pellet at some arbitrary point in the reactor requires the specification of five parameters: β , γ , ϕ, Sh' and Nu' (c.f. Chapter 4). The first three parameters depend upon the external field concentration and temperature, which are unknowns except at the tube entrance; the latter two parameters are taken to be constant over the reactor volume. Numerical results presented in Chapter 4 show that for given values of Sh' and Nu', the tendency for a catalyst particle to exhibit multiple states is exaggerated by increasing β or γ. Furthermore, the family of curves is bounded by the curves for either $[\beta_{max}, \gamma]$ or $[\beta, \gamma_{max}]$, where β_{max} and γ_{max} represent the maximum values of β and γ considered. At what point in the reactor are the maximum values of β and γ to be expected?

From the definitions of β and γ, maximum values occur when C_f is a maximum and T_f is a minimum. Clearly, this situation will arise at the tube wall for $z = 0$. Maximum values of γ and β can be defined in terms of <u>known</u> variables:-

$$\gamma_{max} = {}^{E}/_{R_g}.T_a \ , \ \beta_{max} = \frac{C_{fo}(-\Delta H)D_A^*}{K_p.T_a}$$

Attempts might now be made to develop sufficient conditions for uniqueness of a catalyst particle by approximate analytical methods[119] or by a numerical method. Utilising the latter approach the effectiveness factor may be computed as a function of modulus ϕ for γ_{max}, β_{max} and the given values of Sh' and Nu'. The resulting curve represents an upper bound on all curves which can be constructed for local values of γ and β downstream from the tube entrance. If this curve contains no multiple solution region then the catalyst pellets at the tube entrance are in a unique state and, moreover, all pellets in the bed must be in a unique state; global uniqueness is guaranteed. This situation is in existence in the systems studied in Chapters 9 and 10.

If the curve contains a region of multiple solutions it is still possible for the catalyst pellets at the tube entrance to exist in a unique state, depending upon the magnitude of ϕ. Whether subsequent particles in the bed are in a unique state, however, remains obscure. Some insight might be gained by plotting trajectories of the catalyst state on an η/ϕ diagram at several or more points within a distributed reactor environment. This would require a discouragingly large collection of such curves and much computation. However, there is likely to be no simple answer to this problem.

It must also be recognized that, in practice, physical stability constraints may prevent mathematical instability by prohibiting the large temperature changes which tend to occur in parts of the bed when the reactor moves from its initial condition to its final state.

11.4 A uniqueness condition for a catalyst pellet : general case $Sh'/Nu' \neq 1$

Some progress can also be made in the study of uniqueness for a single catalyst pellet for the most general type of boundary conditions in which both Sh' and Nu' are finite and their ratio $Sh'/Nu' \neq 1$. This is

generally the situation in practice, but the analyses carried out to date (119-121, 130) have been restricted to the class of problems for which either $Sh' = Nu' = \infty$ or $Sh'/Nu' = 1$. In both of these cases it is possible to combine the material and energy balances for a simple reaction into one differential equation. This procedure is not possible for the general case, $Sh'/Nu' \neq 1$, and the analysis becomes altogether more complicated.

The approach adopted here is relatively straightforward and is based on the observation that when multiple solutions occur over a region of $\emptyset$ values, this region can be accurately predicted by the simpler asymptotic model of Section 5.3.2. An illustration is provided for case 3 of Fig. 6.1.

Examining Fig. 6.4, which gives a graphical representation of equation (6.1), it is apparent that the G(x) curve can, in certain cases, exhibit three intersections with the line $y = Sh'.x/2\emptyset$, corresponding to the left hand side of equation (6.1). Thus, the line F and the G(x) curve for $\lambda = 1$ intersect three times, whereas only one intersection is possible for $\lambda = 0.5, 0.25$ no matter what the gradient of F.

For the case in which multiple solutions can occur an obvious condition for uniqueness is

$$\text{grad. } F > dG/dx \Big|_{\text{inflection}} \qquad (11.1)$$

To simplify the algebra, G(x) is approximated by the equation

$$G(x) = (1 - x).\exp\left[\frac{\gamma\lambda x}{2(1 + \lambda x)}\right], \qquad (11.2)$$

which arises when the exponential term appearing in the square brackets in equation (6.1) is approximated by

$$e^y = 1 + y + y^2/2! \; ; \quad y = \frac{\gamma\beta(1 - x)}{(1 + \lambda x)^2}.$$

This simplification is allowable for $\gamma\beta < 1$, which is generally the case, and is reasonably accurate for $\gamma\beta \simeq 1$, since the square root of the term in square brackets is taken. Differentiating eqn. (11.2)

$$dG/dx = \left[\frac{\gamma\lambda(1-x)}{2(1+\lambda x)^2} - 1\right] \cdot \exp\left(\frac{\gamma\lambda x}{(2(1+\lambda x))}\right) \qquad (11.3)$$

Differentiating equation (11.3), setting $d^2G/dx^2 = 0$

$$x_{\text{inflection}} = \frac{\gamma\lambda - 4\lambda - 4}{\lambda(4\lambda + 4 + \gamma)} \qquad (11.4)$$

Substituting equation (11.4) into (11.3) and rearranging gives

$$dG/dx\Big|_{\text{infl.}} = \frac{1}{e^2} \cdot \left[1 + \frac{8}{\gamma}(1+\lambda)\right] \exp\left(\frac{\gamma\lambda}{(2(1+\lambda))}\right) \qquad (11.5)$$

From equations (11.1) and (11.5) it follows that, for the first order irreversible reaction considered, a unique particle state exists providing

$$\phi < \frac{Sh'}{2} \cdot \frac{e^2}{\left[1 + \frac{8}{\gamma}(1+\lambda)\right]} \cdot \exp\left\{\frac{-\gamma\lambda}{(2(1+\lambda))}\right\} \qquad (11.6)$$

where $\lambda = \beta\, Sh'/Nu'$.

To demonstrate the use of the above derived condition, exact and approximate values of ϕ are compared below which only a unique steady state is possible for spherical particles in which one irreversible first order reaction is occurring. Table 11.1 compares exact and approximate values of ϕ for six cases in which multiple states have been isolated.

γ	β	Sh'	λ	Exact ϕ from num. integration	ϕ from Eqn. (11.6)
10	0.1	500	5	5	5
20	0.02	50	1	0.8	0.7
20	0.02	500	1	7.2	7
20	0.05	500	2.5	0.7	0.6
20	0.1	100	1	1.8	1.4
40	0.1	50	0.4	0.6	0.5

TABLE 11.1 Comparison between the exact and approximate values of ϕ for a spherical catalyst particle in which an irreversible first order reaction is occurring.

According to LUSS[130], a spherical catalyst particle with a single irreversible first order reaction is in a unique state providing $\gamma\beta \leq 4$. This condition is derived on the assumption $Sh' = Nu' = \infty$, and reference to Table 11.1 shows it to be clearly inadequate if applied to the general case.

Condition (11.6) is useful in providing a lower bound on ϕ for those cases in which multiple solutions occur. However, if (11.6) is not satisfied a unique particle state can still exist (cf. intersection of line P with the G(x) curve for $\lambda = 1$ in Fig. 6.4). A complete description requires answers to the following questions:

(i) For given values of γ, β, Sh' and λ is there a region of ϕ values in which multiple states can occur?

(ii) If so, what are the bounds on this region?

Research is presently being undertaken to elucidate these questions.

APPENDIX 1

SIMPLE REACTION, $\sum_{i=1}^{i=N} a_i A_i = 0$: THE INDEPENDENT DESIGN EQUATIONS

The specification of the design problem for the single reaction

$$\sum_{i=1}^{i=N} a_i A_i = 0 \qquad (2.9)$$

involves writing down the conservation of energy equations + N conservation of mass equations for each phase. By analogy with equations (3.2) to (3.5), the pertinent equations are thus:

Fluid

$$-G_o c_f \frac{\partial T_f}{\partial x} + K_f\left(\frac{\partial^2 T_f}{\partial r^2} + \frac{1}{r}.\frac{\partial T_f}{\partial r}\right) - (-\Delta H_j)(1-e)\eta_j R'_j(\vec{C_f}, T_f) = 0 \quad (A1.1)$$

$$-V_o \frac{\partial C_{fi}}{\partial x} + D_f\left(\frac{\partial^2 C_{fi}}{\partial r^2} + \frac{1}{r}.\frac{\partial C_{fi}}{\partial r}\right) + (1-e)\eta_i R'_i(\vec{C_f}, T_f) = 0 \qquad (A1.2)$$

$$(i=1,2,\ldots N)$$

Solid

$$K_p\left(\frac{\partial^2 T_s}{\partial w^2} + \frac{2}{w}.\frac{\partial T_s}{\partial w}\right) - (-\Delta H_j).R'_j(\vec{C_s}, T_s) = 0 \qquad (A1.3)$$

$$D_i\left(\frac{\partial^2 C_{si}}{\partial w^2} + \frac{2}{w}.\frac{\partial C_{si}}{\partial w}\right) + R'_i(\vec{C_s}, T_s) = 0 \qquad (A1.4)$$

$$(i=1,2,\ldots N)$$

Boundary conditions are given by

$$T_f = T_{fo} \quad ; x = 0, \quad 0 \leq r \leq r_o \qquad (3.11)$$

$$C_{fi} = C_{fio} \; ; x = 0, \quad 0 \leq r \leq r_o \qquad (A1.5)$$

$$(i=1,2,\ldots N)$$

$$\frac{\partial T_f}{\partial r} = 0 \quad ; \quad r = 0, \qquad \qquad (3.13)$$

$$-K_f . \frac{\partial T_f}{\partial r} = U.(T_f - T_a) \quad ; \quad r = ro, \qquad \Bigg\} \; 0 \leq x \leq L \qquad (3.14)$$

$$\frac{\partial C_{fi}}{\partial r} = 0 \quad ; \quad \left.\begin{matrix} r = 0 \\ r = ro \end{matrix}\right\} \; 0 \leq x \leq L \qquad \begin{matrix} (A1.6) \\ (A1.7) \end{matrix}$$

$$(i=1,2,\ldots N)$$

$$\frac{\partial T_s}{\partial w} = 0 \quad ; \quad w = 0 \qquad \qquad 0 \leq x \leq L, \qquad (3.18)$$

$$K_p . \frac{\partial T_s}{\partial w} = h \; (T_f - T_s) \; : \; w = b \qquad 0 \leq r \leq ro \qquad (3.7)$$

$$\frac{\partial C_{si}}{\partial w} = 0 \quad ; \quad w = 0 \qquad \qquad 0 \leq x \leq L, \qquad (A1.8)$$

$$D_i . \frac{\partial C_{si}}{\partial w} = k_i (C_{fi} - C_{si}) \quad ; \quad w = b \qquad 0 \leq r \leq ro \qquad (A1.9)$$

$$(i=1,2,\ldots N)$$

The boundary conditions bring to light several points about the behaviour of the equations describing the system. Firstly, it is possible to eliminate all but one of the mass conservation equations (A1.4) for the particulate phase. Furthermore, the form of the resulting equation is such that it may be combined with the energy equation (A1.3) to produce, in total, a single differential equation plus N dependent algebraic equations.

Secondly, all but one of the mass conservation equations for the fluid phase (A1.2) can be eliminated. However, the boundary conditions for the conservation of energy equation differ from those for the conservation of mass equations at $r = ro$, and as a consequence the energy equation cannot be eliminated as a dependent equation. The fluid field reduces, therefore, to a system of two independent differential equations plus N-1 dependent equations.

The overall reduction in the number of differential equations is particularly noticeable for large values of N. In quantitative terms, 2N+2 differential equations (of which N+1 are partial differential equations, the remainder being viewed as ordinary differential equations at a particular point (x,r) in the fluid field) are reduced to 3 differential equations plus 2N-1 dependent equations.

A1.1 The independent equations : Reduction Procedure

Writing equation (A1.4) for species i and j, and noting $R_i' = (a_i/a_j)R_j'$ from stoichiometry, the following equations arise after some manipulation.

$$(a_j/a_i).D_i \left(\frac{\partial^2 C_{si}}{\partial w^2} + \frac{2}{w}.\frac{\partial C_{si}}{\partial w} \right) + R_j'(\overrightarrow{C_s}, T_s) = 0 \qquad \text{(A1.10)}$$

$$D_j \left(\frac{\partial^2 C_{sj}}{\partial w^2} + \frac{2}{w}.\frac{\partial C_{sj}}{\partial w} \right) + R_j'(\overrightarrow{C_s}, T_s) = 0 \qquad \text{(A1.11)}$$

Subtracting equation (A1.11) from equation (A1.10) and integrating twice the resulting differential equation, there arises the relationship

$$C_{si} = C_{si}\Big|_{w=b} + \frac{(a_i.D_i)}{(a_j.D_i)}.(C_{sj} - C_{sj}\Big|_{w=b}) \qquad \text{(A1.12)}$$

$$(i=1,2,\ldots.N; \quad i \neq j).$$

Differentiating equation (A1.12) with respect to w, putting w=b

$$\frac{\partial C_{si}}{\partial w}\Big|_{w=b} = \frac{(a_i D_i)}{(a_j D_i)}.\frac{\partial C_{sj}}{\partial w}\Big|_{w=b} \qquad \text{(A1.13)}$$

From equations (A1.13) and (A1.9),

$$C_{si}\Big|_{w=b} = C_{fi} - \frac{(a_i k_j)}{(a_j k_i)}.(C_{fj} - C_{sj}\Big|_{w=b}) \qquad \text{(A1.14)}$$

$$(i=1,2,\ldots.N \; ; \; i \neq j)$$

Eliminating $C_{si}\Big|_{w=b}$ from equation (A1.12) by using equation (A1.14) and rearranging gives

$$C_{si} = f(C_{fi}, C_{fj}, C_{sj}, C_{sj}\Big|_{w=b})$$

$$= C_{fi} - \frac{(a_i k_i)}{(a_j k_i)} \cdot C_{fj} + \frac{(a_i D_i)}{(a_j D_i)} \cdot C_{sj} + \frac{a_i}{a_j}\left(\frac{k_i}{k_i} - \frac{D_i}{D_i}\right) C_{sj}\Big|_{w=b} \quad (A1.15)$$

$$(i=1,2,....N \; ; \; i \neq j)$$

It may be shown from equations (3.19) and (A1.13) that

$$\eta_i \cdot R_i'(\vec{C_f}, T_f) = (a_i/a_j)\,\eta_j \cdot R_j'(\vec{C_f}, T_f) \quad (A1.16)$$

$$(i=1,2,..N \; ; \; i \neq j).$$

Writing equation (A1.2) for species i and j, eliminating $\eta_i R_i'$ by using equation (A1.16), and rearranging produces the following equations

$$-(a_j/a_i) \cdot V_o \cdot \frac{\partial C_{fi}}{\partial x} + (a_j/a_i) \cdot D_f \cdot \left(\frac{\partial^2 C_{fi}}{\partial r^2} + \frac{1}{r} \cdot \frac{\partial C_{fi}}{\partial r}\right) + (1-e)\eta_j R_j'(\vec{C_f}, T_f) = 0 \quad (A1.17)$$

$$-V_o \cdot \frac{\partial C_{fj}}{\partial x} + D_f\left(\frac{\partial^2 C_{fj}}{\partial r^2} + \frac{1}{r} \cdot \frac{\partial C_{fj}}{\partial r}\right) + (1-e)\eta_j \cdot R_j'(\vec{C_f}, T_f) = 0 \quad (A1.18)$$

Subtracting (A1.18) from (A1.17) and solving the resulting partial differential equation, subject to equations (A1.5), (A1.6) and (A1.7) gives

$$C_{fi} = C_{fio} + (a_i/a_j) \cdot (C_{fj} - C_{fjo}) \quad (A1.19)$$

$$(i=1,2,....N \; ; \; i \neq j)$$

Using equation (A1.19) to remove C_{fi} from equation (A1.15)

$$C_{si} = f_1(C_{fio}, C_{fjo}, C_{fj}, C_{sj}, C_{sj}\Big|_{w=b})$$

$$= C_{fio} - (a_i/a_j) \cdot C_{fjo} + (a_i/a_j)\left(1 - \frac{k_i}{k_i}\right) \cdot C_{fj} + (a_i/a_j) \cdot \frac{D_i}{D_i} \cdot C_{sj}$$

$$+ (a_i/a_j)\left(\frac{k_i}{k_i} - \frac{D_i}{D_i}\right) \cdot C_{sj}\Big|_{w=b} \quad (A1.20)$$

$$(i=1,2,....N \; ; \; i \neq j)$$

Equation (A1.20) states that the composition of the intraparticle fluid with respect to each of the N-1 species, $(i=1,2,...N \; ; \; i \neq j)$, can be calculated from a knowledge of the concentrations of a single species j

in the neighbourhood $0 \leq w \leq b$, at the external surface, $C_{sj}\big|_{w=b}$, and in the surrounding bulk fluid phase, C_{fj}. The entrance conditions, C_{fio} (i=1,2,...N), are specified as boundary conditions by equation (A1.5).

By making use of equation (A1.20) in the reaction rate, $R_j'(\overrightarrow{C_s}, T_s)$, it is possible to express the local reaction rate in the particulate phase in terms of the known N-dimensional vector of inlet concentrations, $\overrightarrow{C_{fo}}$, the local intraparticle fluid concentration of species j, C_{sj}, the local catalyst temperature, T_s, and the concentrations of species j at the external catalyst surface, $C_{sj}\big|_{w=b}$, and in the surrounding fluid phase, C_{fj}.

Thus,

$$R_j' = R_j'(\overrightarrow{C_s}, T_s) = R_j''(\overrightarrow{C_{fo}}, C_{fj}, C_{sj}, C_{sj}\big|_{w=b}, T_s)$$

The final step involves the combination of the energy equation and the single independent conservation of mass equation for the particulate phase. Multiplying the conservation of mass equation by $(-\Delta H_j)$, the relevant equations may be written as,

$$K_p\left(\frac{\partial^2 T_s}{\partial w^2} + \frac{2}{w}\cdot\frac{\partial T_s}{\partial w}\right) - (-\Delta H_j).R_j''(\overrightarrow{C_{fo}}, C_{fj}, C_{sj}, C_{sj}\big|_{w=b}, T_s)=0 \qquad \text{(A1.21)}$$

$$(-\Delta H_j).D_j\left(\frac{\partial^2 C_{sj}}{\partial w^2} + \frac{2}{w}\cdot\frac{\partial C_{sj}}{\partial w}\right) + (-\Delta H_j).R_j''(\overrightarrow{C_{fo}}, C_{fj}, C_{sj}, C_{sj}\big|_{w=b}, T_s)=0 \qquad \text{(A1.22)}$$

Adding equations (A1.21) and (A1.22), integrating twice the resulting differential equation subject to boundary conditions (3.18) and (A1.8) gives

$$T_s = T_s\big|_{w=b} + \frac{(-\Delta H_j).D_j}{K_p}.(C_{sj}\big|_{w=b} - C_{sj}) \qquad \text{(A1.23)}$$

Differentiating equation (A1.23) with respect to w, putting w=b

$$\frac{\partial T_s}{\partial w}\Big|_{w=b} = -\frac{(-\Delta H_j)D_j}{K_p}.\frac{\partial C_{sj}}{\partial w}\Big|_{w=b} \qquad \text{(A1.24)}$$

From equations (3.7), (A1.9) and (A1.24), it follows that

$$T_s\Big|_{w=b} = T_f + \frac{(-\Delta H_j)k_j}{h}.(C_{fj}-C_{sj}\Big|_{w=b}) \qquad (A1.25)$$

Substituting equation (A1.25) into (A1.23) leads to the relationship

$$T_s = f_2(T_f, C_{fj}, C_{sj}, C_{sj}\Big|_{w=b})$$

$$= T_f + \frac{(-\Delta H_j)k_j}{h}.C_{fj} - \frac{(-\Delta H_j)D_j}{K_p}.C_{sj} + (-\Delta H_j)\left(\frac{D_j}{K_p}-\frac{k_j}{h}\right)C_{sj}\Big|_{w=b} \qquad (A1.26)$$

Using equation (A1.26) it is possible to eliminate T_s from the reaction rate, R''_j, appearing in equation (A1.22)

Thus,

$$R''_j = R''_j(\vec{C_{fo}}, C_{fj}, C_{sj}, C_{sj}\Big|_{w=b}, T_s) = R'''_j(\vec{C_{fo}}, C_{fj}, C_{sj}, C_{sj}\Big|_{w=b}, T_f)$$

Equations (A1.21) and (A1.22) may be replaced by the single differential equation

$$D_j.\left(\frac{\partial^2 C_{sj}}{\partial w^2} + \frac{2}{w}.\frac{\partial C_{sj}}{\partial w}\right) + R'''_j(\vec{C_{fo}}, C_{fj}, C_{sj}, C_{sj}\Big|_{w=b}, T_f)=0 \qquad (A1.27)$$

and the algebraic equation given by (A1.26).

Summary

The final design problem can be expressed in terms of 3 differential equations; a conservation of energy equation for the fluid phase and two conservation of mass equations for species j, one for the fluid phase and one for the particulate phase. Associated with the independent equations are (2N-1) linear dependent algebraic equations. The pertinent equations are summarised below:

Fluid

$$-G_o c_f.\frac{\partial T_f}{\partial x} + K_f.\left(\frac{\partial^2 T_f}{\partial r^2} + \frac{1}{r}.\frac{\partial T_f}{\partial r}\right) - (-\Delta H_j)(1-e)\eta_j R^o_j(\vec{C_{fo}}, C_{fj}, T_f)=0 \qquad (A1.28)$$

$$-V_o.\frac{\partial C_{fj}}{\partial x} + D_f.\left(\frac{\partial^2 C_{fj}}{\partial r^2} + \frac{1}{r}.\frac{\partial C_{fj}}{\partial r}\right) + (1-e)\eta_j R^o_j(\vec{C_{fo}}, C_{fj}, T_f)=0 \qquad (A1.29)$$

$$C_{fi} = C_{fio} + (a_i/a_j)(C_{fj}-C_{fjo}) \; ; \; (i=1,2,\ldots N \; ; \; i\neq j) \qquad (A1\ 19)$$

where $R_j'(\overrightarrow{C_f}, T_f) = R_j^o(\overrightarrow{C_{fo}}, C_{fj}, T_f)$ from equation (A1.19).

Solid

$$D_j\left(\frac{\partial^2 C_{sj}}{\partial w^2} + \frac{2}{w}\cdot\frac{\partial C_{sj}}{\partial w}\right) + R_j''(\overrightarrow{C_{fo}}, C_{fj}, C_{sj}, C_{sj}\big|_{w=b}, T_f)=0 \qquad (A1.27)$$

$$T_s=T_f+\frac{(-\Delta H_j)k_j}{h}\cdot C_{fj}-\frac{(-\Delta H_j)D_j}{K_p}\cdot C_{sj}+(-\Delta H_j)\left(\frac{D_j}{K_p}-\frac{k_j}{h}\right)C_{sj}\Big|_{w=b} \qquad (A1.26)$$

$$C_{si}=C_{fio}-(a_i/a_j)\cdot C_{fjo}+(a_i/a_j)\left(1-\frac{k_j}{k_i}\right)C_{fj}+(a_i/a_j)\frac{D_j}{D_i}\cdot C_{sj}$$

$$+(a_i/a_j)\cdot\left(\frac{k_j}{k_i}-\frac{D_j}{D_i}\right)\cdot C_{sj}\Big|_{w=b} \; ; \; (i=1,2,\ldots.N \; ; \; i\neq j) \qquad (A1.20)$$

A reduced set of boundary conditions is

$$T_f = T_{fo} \; ; \; ; \quad x=0 \; ; \quad 0 \leq r \leq ro. \qquad (3.11)$$

$$C_{fj} = C_{fjo} \; ; \quad x=0 \; ; \quad 0 \leq r \leq ro. \qquad (A1.30)$$

$$\left.\begin{array}{ll} \partial T_f/\partial r = 0 \; ; & r = 0 \\ -K_f\cdot\partial T_f/\partial r = U\cdot(T_f-T_a) \; ; & r = ro \end{array}\right\} \; 0 \leq x \leq L \qquad \begin{array}{l}(3.13)\\(3.14)\end{array}$$

$$\left.\begin{array}{ll} \partial C_{fj}/\partial r = 0; & r = 0 \\ & r = ro \end{array}\right\} \; 0 \leq x \leq L \qquad \begin{array}{l}(A1.31)\\(A1.32)\end{array}$$

$$\left.\begin{array}{ll} \partial C_{sj}/\partial w = 0 & w=0 \\ D_j\cdot\partial C_{sj}/\partial w = k_j(C_{fj}-C_{sj}) \; ; & w=b \end{array}\right\} \; \begin{array}{l}0 \leq x \leq L, \\ 0 \leq r \leq ro\end{array} \qquad \begin{array}{l}(A1.33)\\(A1.34)\end{array}$$

The choice of the species to follow in the equations is arbitrary. In accordance with convention, the choice of A_j is that species present stoichiometrically in least amount in the reaction mixture

APPENDIX 2

NUMERICAL METHODS OF SOLUTION FOR THE SINGLE PARTICLE PROBLEM

Two methods of solving a coupled system of non-linear ordinary differential equations of the two point boundary-value type are considered in connection with the work reported in Chapter 4 on simultaneous heat and mass transfer with chemical reaction in a porous catalyst particle. The first method is perhaps the most obvious one to try initially, i.e. the so-called boundary iteration approach. A summary of this method is given in Section 4.3.2(a).

A2.1 The boundary-iteration approach

A2.1.1 The iteration scheme

Suppose conditions for the unknowns c and t at y = 0 are assumed, i.e.

$$\left.\begin{aligned} c &= p \\ t &= q \end{aligned}\right\} \qquad \text{(A2.1)}$$

The concentration and temperature profiles within the particle may be written as functions of the radial co-ordinate y and the assumed conditions, p and q:

$$c = c\,(y,\ p,\ q)$$

$$t = t\,(y,\ p,\ q).$$

Functions f_1 and f_2 are defined as

$$f_1 = f_1(y,p,q) = \frac{dc}{dy}(y,p,q) - \frac{Sh'}{2}\left[1 - c(y,p,q)\right] \qquad \text{(A2.2)}$$

$$f_2 = f_2(y,p,q) = \frac{dt}{dy}(y,p,q) - \frac{Nu'}{2}\left[1 - t(y,p,q)\right] \qquad \text{(A2.3)}$$

If p^* and q^* are the correct values of c and t, at y = 0, then from equations (4.5), (4.6), (A2.2) and (A2.3)

$$f_1(1,p^*,q^*) = 0 \qquad \text{(A2.4)}$$

$$f_2(1,p^*,q^*) = 0 \qquad \text{(A2.5)}$$

For p and q close to p^* and q^*, the following truncated Taylor series expansions are used to approximate the functions $f_1(1,p^*,q^*)$, $f_2(1,p^*,q^*)$ of equations (A2.4) and A2.5)

$$f_1(1,p^*,q^*) = 0 = f_1(1,p,q) + (p^*-p)\frac{\partial f_1}{\partial p}(1,p,q) + (q^*-q)\frac{\partial f_1}{\partial q}(1,p,q) \qquad \text{(A2.6)}$$

$$f_2(1,p^*,q^*) = 0 = f_2(1,p,q) + (p^*-p)\frac{\partial f_2}{\partial p}(1,p,q) + (q^*-q)\frac{\partial f_2}{\partial q}(1,p,q) \qquad \text{(A2.7)}$$

By rearranging (A2.6) and (A2.7) it is possible to deduce the iteration formulae:

$$p^{i+1} = p^i + \left[\frac{f_2 \cdot \partial f1/\partial q - f_1 \cdot \partial f2/\partial q}{\partial f2/\partial q \cdot \partial f1/\partial p - \partial f1/\partial q \cdot \partial f2/\partial p}\right]^i_{y=1} \qquad \text{(A2.8)}$$

$$q^{i+1} = q^i + \left[\frac{f_1 \cdot \partial f2/\partial p - f_2 \cdot \partial f1/\partial p}{\partial f2/\partial q \cdot \partial f1/\partial p - \partial f1/\partial q \cdot \partial f2/\partial p}\right]^i_{y=1} \qquad \text{(A2.9)}$$

Note that equations (A2.8) and (A2.9) are analagous to the Newton iteration process generalized to two unknowns, p^* and q^*.

The partial derivatives in (A2.8) and (A2.9) may be estimated from solutions of the material and energy balance equations (4.1) and (4.2) for different values of p and q. This would require <u>three</u> trial solutions with initial conditions (p,q), (p+h,q) and (p,q+j) where h and j are small in relation to p and q respectively. It is possible, however, to generate the partial derivatives exactly by solving additional equations derived from (4.1) and (4.2).

<u>A2.1.2 The derived equations</u>

Define functions $u_1 = \frac{\partial c}{\partial p}(y,p,q)$, $v_1 = \frac{\partial c}{\partial q}(y,p,q)$, $u_2 = \frac{\partial t}{\partial p}(y,p,q)$ and $v_2 = \frac{\partial t}{\partial q}(y,p,q)$.

Equations (4.1) and (4.2) are differentiated in turn with respect to p and q to produce four differential equations:

$$d^2u_1/dy^2 + {}^2/_y \cdot du_1/dy + r^*(c,t) \cdot \left[n.u_1 + \frac{\gamma_c}{t^2}.u_2 \right] = 0 \qquad \text{(A2.10)}$$

$$d^2v_1/dy^2 + {}^2/_y \cdot dv_1/dy + r^*(c,t) \cdot \left[n.v_1 + \frac{\gamma_c}{t^2}.v_2 \right] = 0 \qquad \text{(A2.11)}$$

$$d^2u_2/dy^2 + {}^2/_y \cdot du_2/dy - \beta r^*(c,t) \cdot \left[n.u_1 + \frac{\gamma_c}{t^2}.u_2 \right] = 0 \qquad \text{(A2.12)}$$

$$d^2v_2/dy^2 + {}^2/_y \cdot dv_2/dy - \beta r^*(c,t) \cdot \left[n.v_1 + \frac{\gamma_c}{t^2}.v_2 \right] = 0 \qquad \text{(A2.13)}$$

where $r^*(c,t) = a_A \cdot \phi^2 \exp\left\{\gamma(1 - {}^1/t)\right\} c^{n-1}$.

Initial conditions on equations (A2.10) to (A2.13) follow from the definitions of u_1, v_1, u_2 and v_2, equations (4.3), (4.4) and (A2.1), i.e.

$$\left.\begin{aligned} u_1 &= 1, \; {}^{du_1}/_{dy} = 0 \\ v_1 &= 0, \; {}^{dv_1}/_{dy} = 0 \\ u_2 &= 0, \; {}^{du_2}/_{dy} = 0 \\ v_2 &= 1, \; {}^{dv_2}/_{dy} = 0 \end{aligned}\right\} \quad y = 0 \qquad \begin{aligned} &\text{(A2.14)} \\ &\text{(A2.15)} \\ &\text{(A2.16)} \\ &\text{(A2.17)} \end{aligned}$$

The partial derivatives of equations (A2.8) and (A2.9) are found in terms of the functions u_1, v_1, u_2 and v_2 by differentiating equations (A2.2) and (A2.3) in turn with respect to p and q, setting y = 1. It follows that

$$\frac{\partial f_1(1,p,q)}{\partial p} = \frac{du_1(1,p,q)}{dy} + \frac{Sh'}{2}.u_1(1,p,q) \qquad \text{(A2.18)}$$

$$\frac{\partial f_1(1,p,q)}{\partial q} = \frac{dv_1(1,p,q)}{dy} + \frac{Sh'}{2}.v_1(1,p,q) \qquad \text{(A2.19)}$$

$$\frac{\partial f_2(1,p,q)}{\partial p} = \frac{du_2(1,p,q)}{dy} + \frac{Nu'}{2}.u_2(1,p,q) \qquad \text{(A2.20)}$$

$$\frac{\partial f_2(1,p,q)}{\partial q} = \frac{dv_2(1,p,q)}{dy} + \frac{Nu'}{2}.v_2(1,p,q) \qquad \text{(A2.21)}$$

It is possible to effect considerable simplification in the calculations by decoupling the pairs of equations (A2.10) and (A2.12), (A2.11) and (A2.13). The relationships which result are given by

$$u_2 = \beta(1 - u_1) \qquad \text{(A2.22)}$$

$$v_2 = 1 - \beta v_1 \qquad \text{(A2.23)}$$

Substituting equations (A2.22) and (A2.23) into equations (A2.10) and (A2.11) respectively, the <u>four</u> equations may be reduced to <u>two</u>:-

$$d^2u_1/dy^2 + {}^2/y \cdot du_1/dy + r^*(o,t).\left[nu_1 + \frac{\gamma\beta_o}{t^2}.(1-u_1)\right] = 0 \qquad \text{(A2.24)}$$

$$d^2v_1/dy^2 + {}^2/y \cdot dv_1/dy + r^*(o,t).\left[nv_1 + \frac{\gamma_o}{t^2}.(1-\beta v_1)\right] = 0 \qquad \text{(A2.25)}$$

The partial derivatives $\partial f_2/\partial p$ and $\partial f_2/\partial q$ of equations (A2.20) and (A2.21) are simply found in terms of u_1, v_1 and their derivatives du_1/dy and dv_1/dy from equations (A2.22) and (A2.23), i.e.

$$\frac{\partial f_2}{\partial p}(1,p,q) = \beta\left[\frac{Nu'}{2}\left\{1 - u_1(1,p,q)\right\} - \frac{du_1}{dy}(1,p,q)\right] \qquad \text{(A2.26)}$$

$$\frac{\partial f_2}{\partial q}(1,p,q) = -\beta\frac{dv_1}{dy}(1,p,q) + \frac{Nu'}{2}\left\{1 - \beta.v_1(1,p,q)\right\} \qquad \text{(A2.27)}$$

<u>A2.1.3 The computational procedure</u>

The computational procedure is relatively straightforward:

(i) Assume values for p and q.

(ii) Starting from y = 0, integrate simultaneously the material and energy balance equations given by (4.1) and (4.2), subject to the boundary conditions (4.3) and (4.4) and the assumed conditions (A2.1), together with equations (A2.24) and (A2.25), subject to the initial conditions (A2.14) and (A2.15) respectively.

(iii) At the boundary, y = 1, compute the functions f_1 and f_2 and their partial derivatives $\partial f_1/\partial p$, $\partial f_1/\partial q$, $\partial f_2/\partial p$ and $\partial f_2/\partial q$ from the solutions of the differential equations and equations (A2.2), (A2.3), (A2.18), (A2.19), (A2.26) and (A2.27) respectively.

(iv) Use the iteration formulae (A2.8) and (A2.9) to obtain new estimates of p and q.

(v) Repeat the foregoing until the boundary conditions given by equations (4.5) and (4.6) are satisfied.

The system of equations (4.1), (4.2), (A2.24) and (A2.25) is readily integrated by the fourth-order Runge-Kutta-Merson method, a version of which is available at Leeds University, which has provision for step length adjustment.

A2.1.4 The starting equations

In order to propagate the integration away from y = 0, it is necessary to apply a set of starting equations over the first integration step, as a consequence of the indeterminate terms $^2/y \cdot dx/dy$ ($x = c, t, u_1, v_1$). It may be shown that

$$\lim_{y \to 0} \frac{2}{y}\cdot\frac{dx}{dy} \longrightarrow 2\frac{d^2x}{dy^2} \quad (x = c, t, u_1, v_1),$$

with the result that equations (4.1), (4.2), (A2.24) and (A2.25) take the form (at y = 0)

$$d^2c/dy^2 + \frac{1}{3}r^*(c,t).c = 0$$

$$d^2t/dy^2 - \frac{\beta}{3}r^*(c,t).c = 0$$

$$d^2u_1/dy^2 + \frac{r}{3}^*(c,t).\left[n.u_1 + \frac{\gamma\beta c}{t^2}(1-u_1)\right] = 0$$

$$d^2v_1/dy^2 + \frac{r}{3}^*(c,t).\left[n.v_1 + \frac{\gamma c}{t^2}(1-\beta v_1)\right] = 0$$

A2.2 The finite difference method

A relatively simple approach to the solution of equations (4.1) and (4.2) is based on the principle of replacing the derivatives by their central difference approximations, and including the boundary conditions in differenced form in the respective matrix of finite difference equations. Two sets of equations arise, each having a tri-diagonal coefficient matrix. Such matrices may be readily inverted by the Thomas[57] method.

A2.2.1 Iterative procedure

The treatment of the non-linearities by this method is somewhat crude, but this is compensated to some extent by the efficiency of the Thomas method.

Equation (4.1) is written in the form

$$d^2c/dy^2 + {}^2/y \cdot dc/dy + r^*(c,t).c = 0 \qquad \text{(A2.28)}$$

where $r^*(c,t) = a_A \phi^2 \exp\left\{\gamma(1 - {}^1/t)\right\} c^{n-1}$.

Suppose the radius is divided into P equal increments Δy, so that P. $\Delta y = 1$. Let $c_{i+1}(p)$ and $t_{i+1}(p)$ represent the discretized forms of c and t at the radial node p with subscript i+1 representing the $(i+1)^{'}$th iteration. The use of central difference approximations for the derivatives leads to the following set of equations

$$M_i(0).c_{i+1}(0) + c_{i+1}(1) = 0 \qquad \text{(A2.29)}$$
" "

$$\left(\frac{p-1}{p}\right).c_{i+1}(p-1) + M_i(p).c_{i+1}(p) + \left(\frac{p+1}{p}\right)c_{i+1}(p+1) = 0 \qquad \text{(A2.30)}$$
" "

$$2.c_{i+1}(P-1) + M_i^{'}(P).c_{i+1}(P) = -\frac{Sh^{'}}{P^2}.(P+1) \qquad \text{(A2.31)}$$

with $M_i(0) = -\left[1 - \frac{r^*}{6P^2}\left[c_i(0),\ t_i(0)\right]\right]$

$$M_i(p) = -\left[2 - \frac{r^*}{P^2}\left[c_i(p),\ t_i(p)\right]\right]$$

$$0 < p < P$$

$$M_i'(P) = M_i(P) - \frac{Sh}{P^2}'.(P+1);$$

and where the non-linear term $r^*(c,t)$ is included in the coefficient matrix by allowing it to lag 1 iteration.

The boundary conditions are included in equations (A2.29) and (A2.31), while equation (A2.30) applies at the internal points, $0 < p < P$. For example, at $y = 0$, the limiting form of equation (A2.28) is given in Section (A2.1.4) as

$$d^2c/dy^2 + \frac{r^*}{3}(c,t).c = 0 \qquad (A2.32)$$

The central difference approximation of (A2.32) is given by

$$c_{i+1}(1) - \left[2 - \frac{r^*}{3P^2}\left[c_i(0),\ t_i(0)\right]\right].c_{i+1}(0) + c_{i+1}(-1) = 0 \qquad (A2.33)$$

Noting from the central difference approximation of equation (4.3) that $c_{i+1}(-1) = c_{i+1}(1)$, equation (A2.33) simplifies to

$$c_{i+1}(1) - \left[1 - \frac{r^*}{6P^2}\left[c_i(0),\ t_i(0)\right]\right] c_{i+1}(0) = 0$$

The boundary condition (4.5) is incorporated in the manner indicated in Section (8.3.2).

Similarly, equation (4.2) is replaced by the set of equations

$$-t_{i+1}(0) + t_{i+1}(1) = Q_{i+1}(0) \qquad (A2.34)$$

$$\left(\frac{P-1}{p}\right).t_{i+1}''(p-1) - 2.t_{i+1}''(p) + \left(\frac{p+1}{p}\right).t_{i+1}''(p+1) = Q_{i+1}(p) \qquad (A2.35)$$

$$2\ t_{i+1}''(P-1) - \left[2 + \frac{Nu}{P}'.\left(1 + \frac{1}{P}\right)\right].t_{i+1}''(P) = Q_{i+1}(P) - \frac{Nu}{P}'.\left(1 + \frac{1}{P}\right) \qquad (A2.36)$$

where $Q_{i+1}(0) = \frac{\beta}{6P^2} \cdot r^*\left[c_{i+1}(0),\ t_i(0)\right] \cdot c_{i+1}(0)$

and $Q_{i+1}(p) = \frac{\beta}{p^2} \cdot r^*\left[c_{i+1}(p),\ t_i(p)\right] \cdot c_{i+1}(p)$

for $0 < p \leq P$

A2.2.2 The computational procedure

Solution of the equations (A2.29) to (A2.31) and (A2.34) to (A2.36) is obtained by assuming an initial value for the profiles c(y) and t(y) and iterating upon the assumed conditions. The M(p) of equations (A2.29) to (A2.31) are computed from the assumed c(y) and t(y) with i set equal to zero. Next equations (A2.29) to (A2.31) are solved to make known c(y), i=1. The resulting c(y) is used with the assumed t(y) to compute Q(y); equations (A2.34) to (A2.36) are solved for the new t(y), i=1. The procedure is then repeated, starting with the new set of c(y) and t(y) values. Convergence of the solution is assumed when each element of the c(y) and t(y) differs in relative value from its corresponding number in the previous iteration by less than some difference, ξ.

Note for the first order reaction the $r^*(c,t)$ of equation (A2.28) is independent of c and only an initial assumption of the temperature profile is required to start the iterative cycle.

APPENDIX 3

COMPARISON OF NUMERICAL METHODS OF SOLUTION OF THE SINGLE PARTICLE PROBLEM

A3.1 Two special cases

Consideration is given first to two special cases which have received considerable attention in the literature, namely

(i) $Nu' = Sh' = \infty$

(ii) $Sh'/Nu' = 1.$

PRATER[40] showed for case (i) that temperature and concentration are related by the equation

$$t = 1 + \beta (1-c); \qquad (A3.1)$$

a relationship independent of particle geometry and reaction order. The same equation is derived for case (ii) by putting $Sh'/Nu' = 1$ in equation (4.8). Substituting equation (A3.1) in (4.1), the material and energy balance equations may be decoupled to give the differential equation

$$\frac{d^2c}{dy^2} + \frac{2}{y}\frac{dc}{dy} + a_A \phi^2 \exp\left\{\frac{\gamma\beta (1-c)}{(1+\beta (1-c))}\right\} c^n = 0 \qquad (A3.2)$$

subject to the boundary conditions:

<u>case (i)</u> $dc/dy = 0$, $y = 0$ (4.3)

$c = 1$, $y = 1$ (A3.3)

<u>case (ii)</u> $dc/dy = 0$, $y = 0$ (4.3)

$dc/dy = \frac{Sh'}{2}(1-c)$, $y = 1$ (4.5)

Using the boundary iteration method, described in Appendix 2, it is only necessary to assume a single condition at the particle centre, i.e. $c = p$ at $y = 0$, and iterate upon this estimate until either boundary condition (A3.3) or (4.5) is satisfied. The finite difference method requires an estimate of the concentration profile.

Some results for the two special cases are presented in Figs. A3.1 and A3.2.

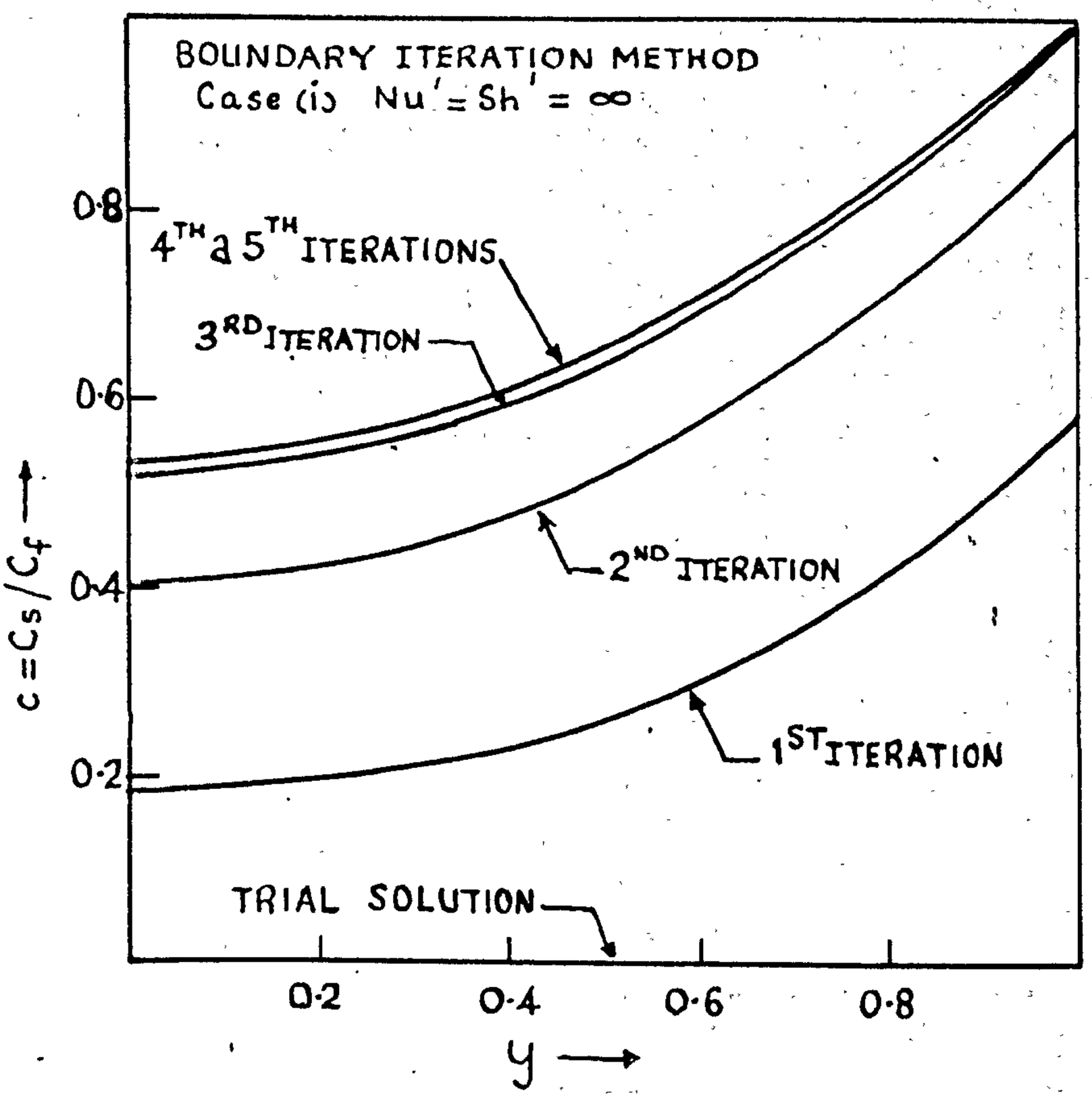

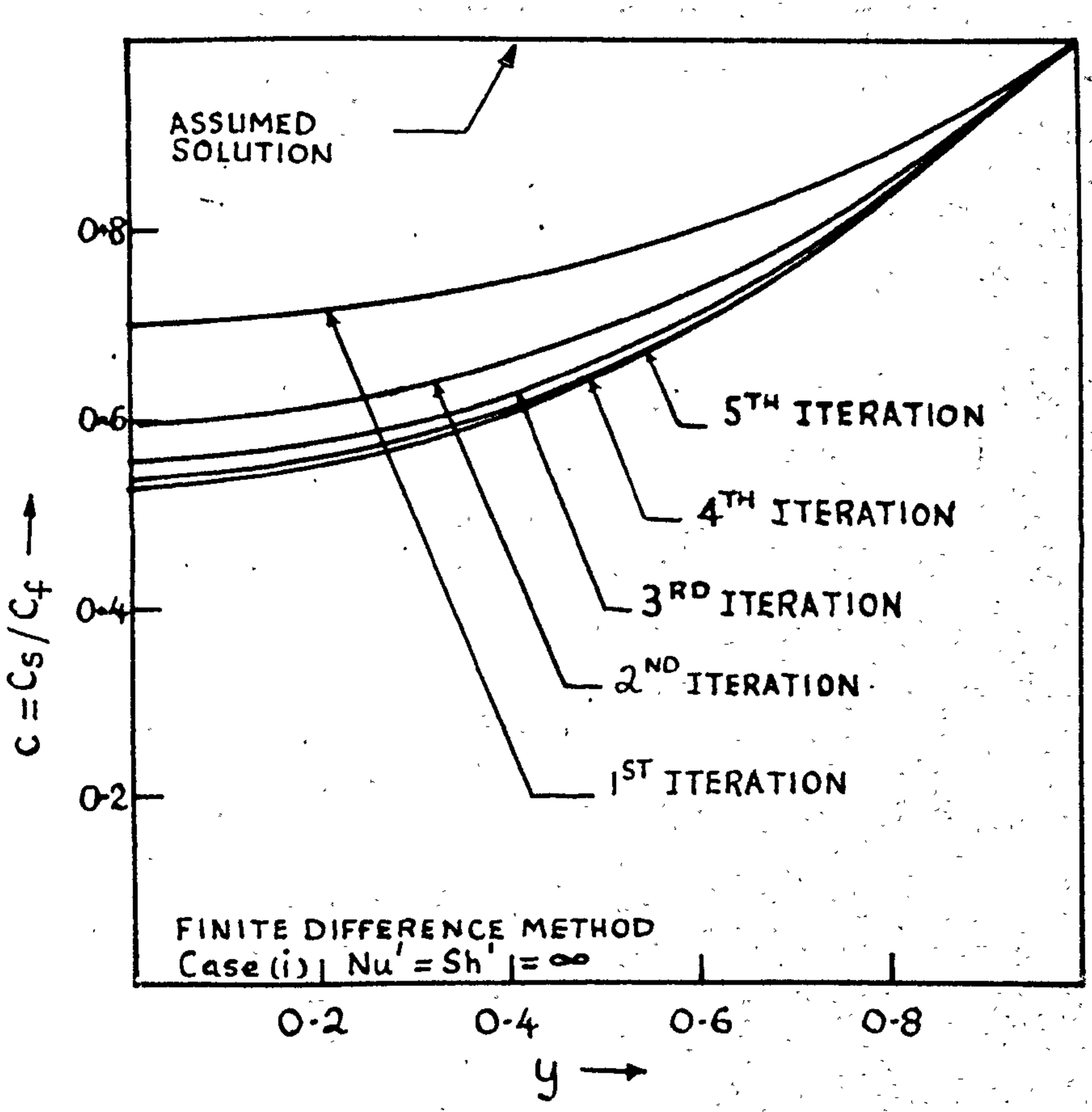

FIG. A3.1 The single particle problem. Rate of convergence of the boundary iteration and finite difference methods.

$A \rightarrow B$ ($n=1$).

$\varphi = 1{\cdot}5$, $\gamma = 20$, $\beta = 0{\cdot}1$, $Sh' = Nu' = \infty$.

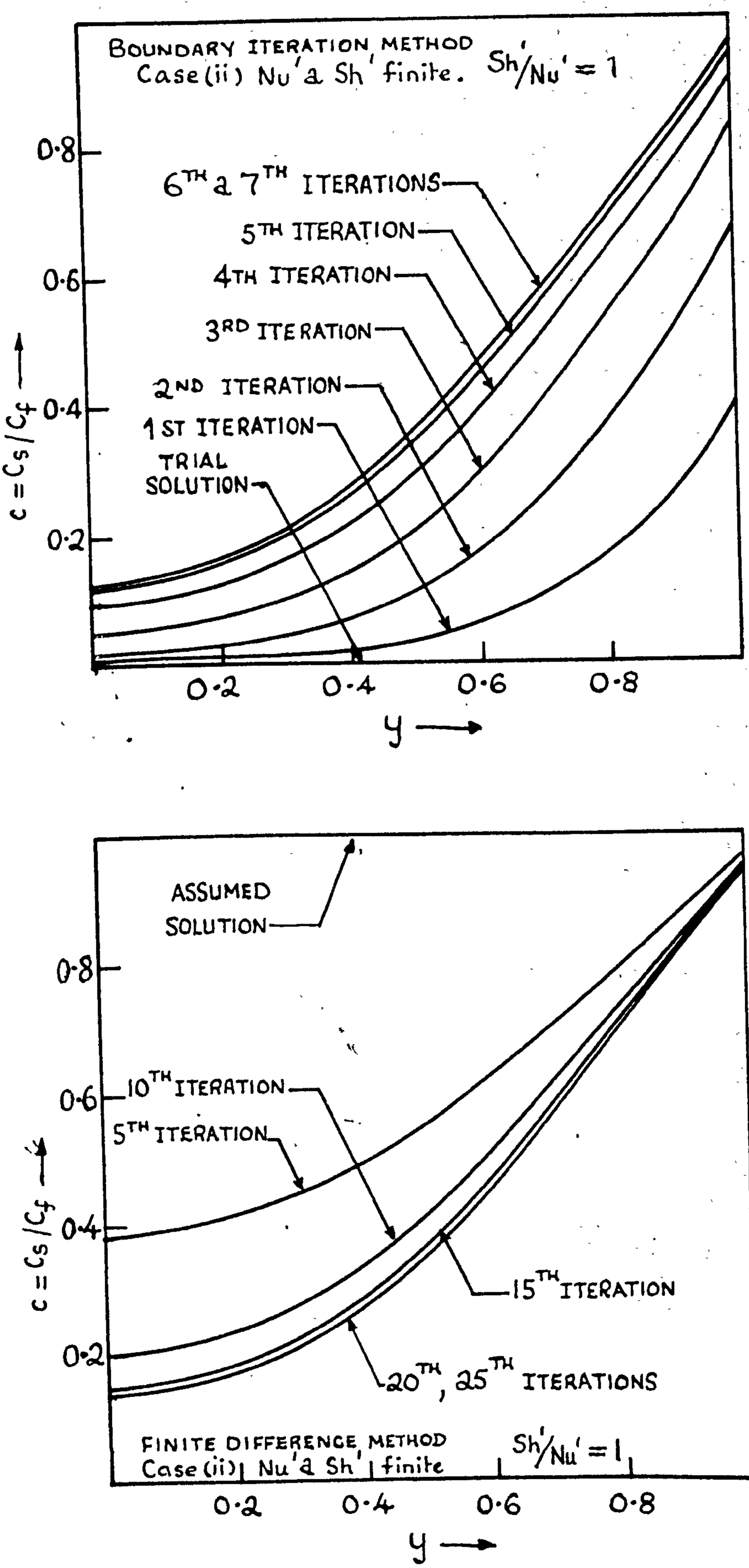

FIG A3.2 The single particle problem. Rate of convergence of the boundary iteration method and the finite difference method.

$A \rightarrow B$ $(n=1)$

$\varphi = 1{\cdot}2$, $\gamma = 40$, $\beta = 0{\cdot}1$, $Sh' = Nu' = 50$.

The boundary iteration method shows rapid convergence even from a poor trial solution. In all cases considered, convergence occurred providing the initial estimate p was less than the true value, say p^*. Convergence did not always occur for $p > p^*$. With the computer program using single precision floating point arithmetic, the least value of p which can be held is 10^{-37}. Generally, this figure is considerably less than the true value p^*. For $p^* < 10^{-37}$, the simple extrapolation procedure used by WEISZ and HICKS[46] allows an estimate of the effectiveness factor to be obtained. In the majority of cases an integration step Δy of 0.01 was employed. No stability problem was encountered with this step size. Approximately 5 seconds of computer time are required per iteration using $\Delta y = 0.01$.

The finite difference method also proved satisfactory in providing solutions, but was generally slower to converge than the boundary iteration method. This disadvantage is offset by a lighter computational load/ iteration. Convergence was faster for case (i) where the assumed solution c(y) = 1 satisfies the boundary conditions (4.3) and (A3.3). No instability was encountered even for $\Delta y = 0.1$. However, to maintain accuracy Δy was usually set equal to 0.01. Computing time/iteration is roughly 0.5 seconds.

A3.2 The general case, $Sh'/Nu' \neq 1$

The more relevant cases arise for $Sh'/Nu' \neq 1$. In this situation it is impossible to decouple the material and energy balance equations to produce a single differential equation analogous to (A3.2). The boundary iteration method now requires initial estimates of both c and t at y = 0, and the finite difference approach utilises, in general, initial assumptions of both the concentration and temperature profiles.

Considering first the boundary iteration method, it was found that this type of approach suffers acute stability restrictions. There were

no values of c and t at y = 0 which would produce solutions. Small changes in these conditions caused the iterations to oscillate violently, as shown in Fig. A3.3. It should be mentioned that the effect of increment size has been removed from these calculations. FOX [87] discusses this phenomenon in some detail and notes that the probability of non-convergence may increase rapidly with the size of the differential system, even for linear systems.

On the other hand, this problem was not encountered using the finite difference method. Even for initial distributions of concentration and temperature far removed from the final solution, no instabilities developed (Fig. A3.4). Convergence of the solution outside the multiple solution region is independent of the choice of starting conditions. In region I of the schematic diagram (4.4), ten integration steps proved satisfactory and roughly 4 iterations were required to establish convergence ($\xi = 10^{-4}$) starting from c(y) = t(y) = 1. Compute time was of the order of $^1/_5$th second/iteration. One hundred integration steps were used in region II and, in general, between 6 and 10 iterations were required; the compute time/iteration being 1 second. The finite difference scheme, as described in Appendix 2, proved unsatisfactory in region III because of the very steep gradients near to the external surface of the particle. A simple refinement was used in order to obtain more accurate results. The domain $0 \leq y \leq 1$ was divided into two intervals, $0 \leq y \leq y_1$ and $y_1 \leq y \leq 1$, where generally $y_1 \geq 0.9$. In the domain $y_1 \leq y \leq 1$, a small integration step was used ($\Delta y = 0.01$), whereas in the domain $0 \leq y \leq y_1$ a larger step ($\Delta y = 0.05$) could be employed. Convergence of the iterations was accelerated by starting from c(y) = 0, $t(y) = 1 + \beta . \frac{Sh'}{Nu}$.

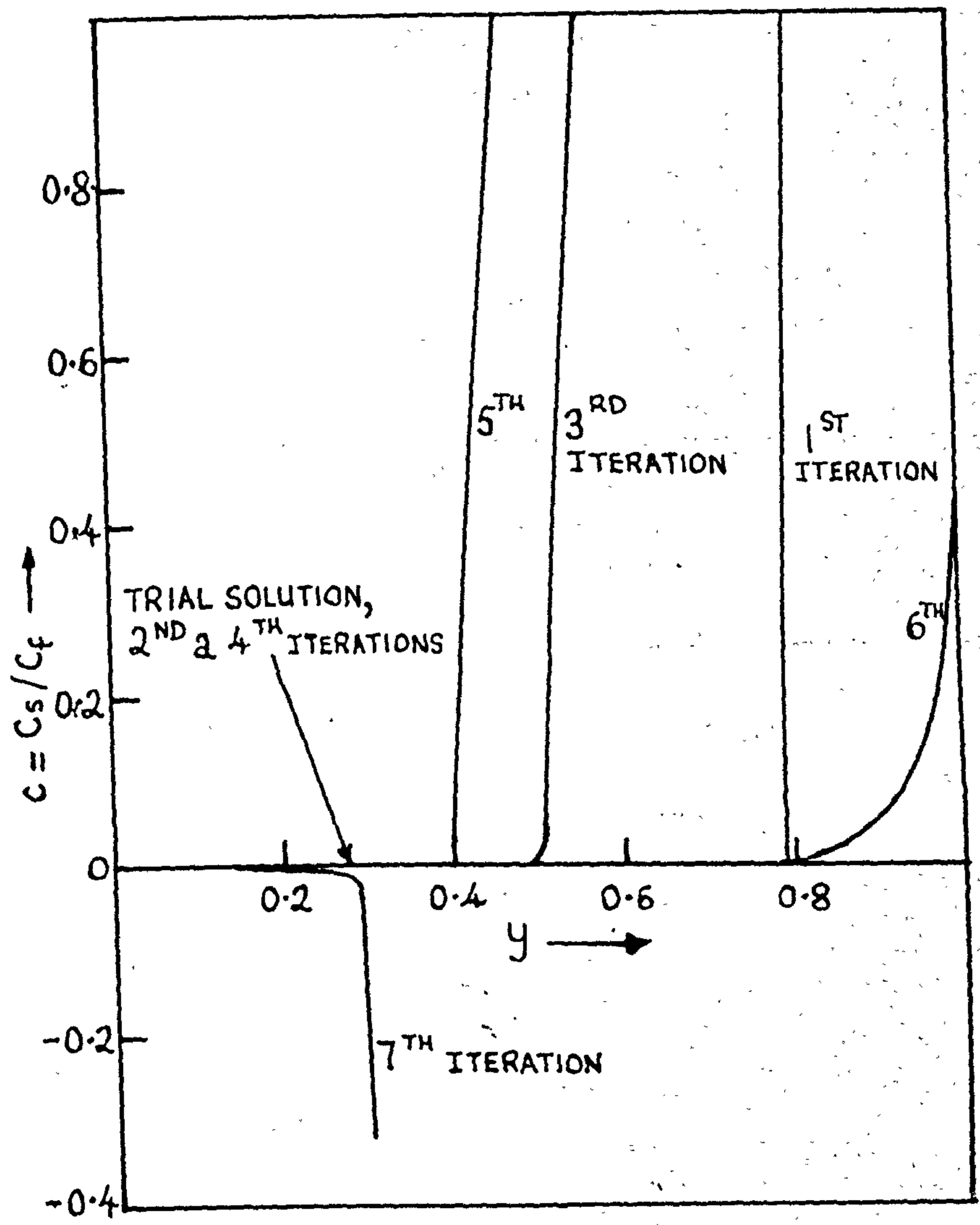

FIG. A3.3 The general case, $Sh'/Nu' \neq 1$. Instability of the boundary iteration method.

$A \rightarrow B$ $(n=1)$.

$\varphi = 5$, $\gamma = 40$, $\beta = 0.1$, $Sh' = 50$, $Nu' = 25$.

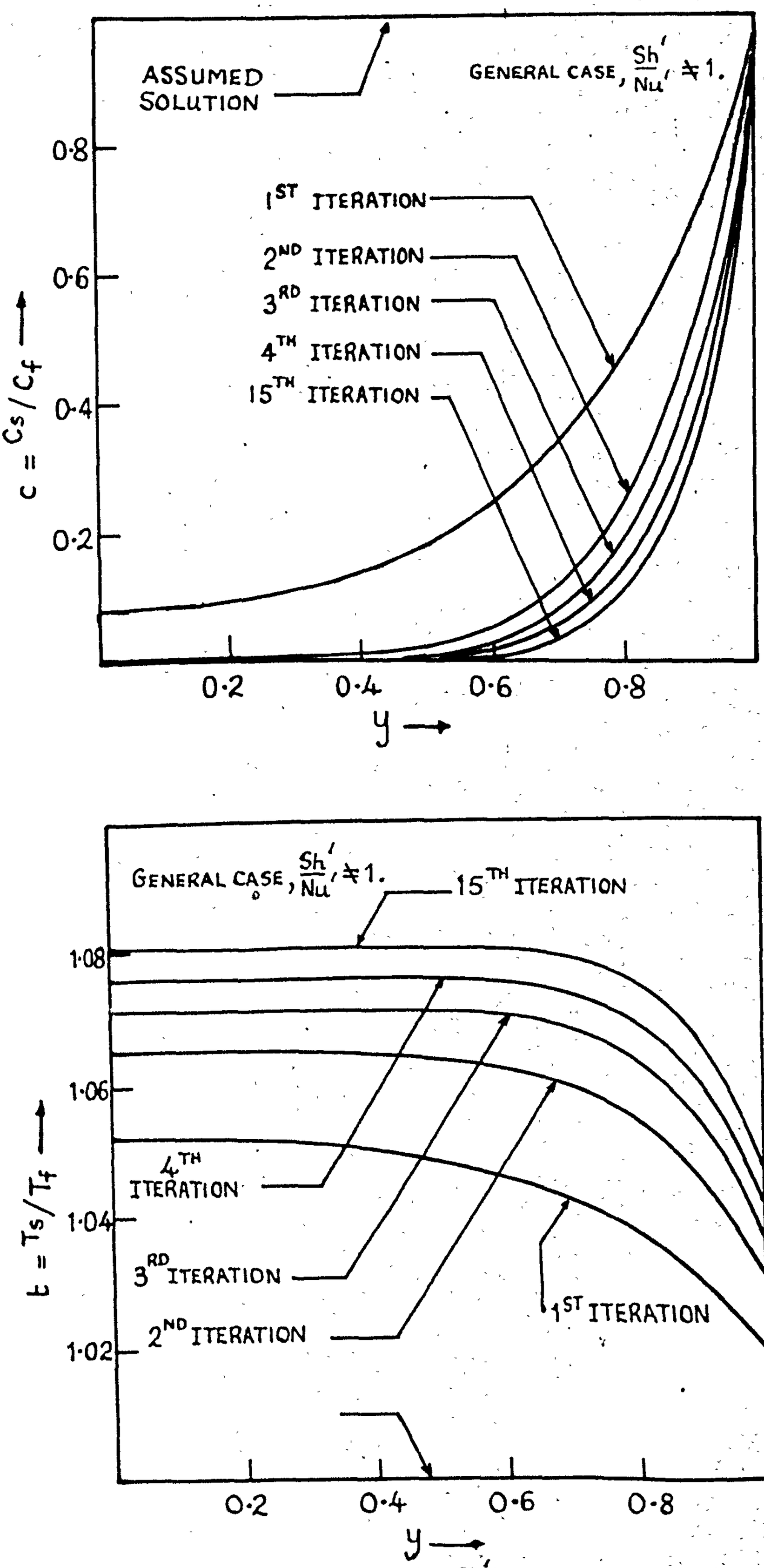

FIG. A3.4 The general case, $Sh'/Nu' \neq 1$. Finite difference method.

A → B (n=1)

$Q = 4.75$, $\gamma = 28.9$, $\beta = 0.037$, $Sh' = 415$, $Nu' = 14.4$

APPENDIX 4

THE ISOTHERMAL PELLET MODEL : A MODIFIED HEAT TRANSFER COEFFICIENT

Allowing for the existence of a temperature gradient within the catalyst pellet, the mean temperature is defined by

$$\bar{t} = 3\int_0^1 y^2 t(y)\, dy \quad , \qquad (A4.1)$$

employing the nomenclature of Chapter 4. Equation (A4.1) may be integrated twice by parts to give

$$\bar{t} = t(y=1) - \frac{1}{4}\left(\frac{dt}{dy}\right)_{y=1} + \frac{1}{4}\int_0^1 y^4 \cdot \left(\frac{d^2t}{dy^2}\right) dy \qquad (A4.2)$$

The rate of heat release to the surroundings is given by

$$Q = -K_p \cdot 4\pi b^2 \left(\frac{dT_s}{dw}\right)_{w=b} = h \cdot 4\pi b^2 \left(T_s\Big|_{w=b} - T_f\right) \qquad (A4.3)$$

from equation (3.7), where h is the fluid film heat transfer coefficient.

It is also possible to relate Q to the mean temperature difference between the catalyst pellet and the surrounding fluid, i.e.

$$Q = h_{ov} \cdot 4\pi b^2 \cdot (\bar{T} - T_f) \qquad (A4.4)$$

where h_{ov} is no longer a fluid film heat transfer coefficient. Rather, it is an overall coefficient which is, as yet, an undefined function of the 'true' film heat transfer coefficient, h, and the particle thermal conductivity, K_p.

Noting from equations (A4.3) and (A4.4) the following relationships

$$\left(dt/dy\right)_{y=1} = \frac{Nu}{2}''(1-\bar{t}) \qquad A4.5)$$

and $t(y=1) - 1 = \frac{h_{ov}}{h} \cdot (\bar{t}-1)$, equation (A4.2) may be simplified to give

$$\frac{Nu}{Nu'}'' + \frac{Nu}{8}'' + \frac{1}{4(\bar{t}-1)}\int_0^1 y \cdot^4 \left(\frac{d^2t}{dy^2}\right) \cdot dy = 1 \qquad (A4.6)$$

where Nu'' contains the modified heat transfer coefficient, h_{ov}, and is defined as $Nu'' = \frac{2h_{ov}b}{K_p}$. In order to evaluate the integral appearing in equation (A4.6) it is necessary to make an assumption of the form of the temperature profile, t(y). The simplest form which fits the boundary conditions (4.4) and (4.6) is a parabola

$$t = a\,y^2 + b, \qquad \text{(A4.7)}$$

where a and b are constants.

Differentiating equation (A4.7), setting y = 1, it follows that

$2a = (dt/dy)_{y=1}$, and further differentation leads to

$$d^2t/dy^2 = 2a = (dt/dy)_{y=1} \qquad \text{(A4.8)}$$

From (A4.5) and (A4.8)

$$d^2t/dy^2 = \frac{Nu''}{2}(1-\bar{t}) \qquad \text{(A4.9)}$$

After substituting equation (A4.9) in the integral of equation (A4.6) and evaluating, it can be shown that

$$Nu'' = \frac{10\,Nu'}{(10 + Nu')}$$

The same result is obtained from analysis of the transient heat conduction problem, irrespective of the form of the temperature profile.

APPENDIX 5

A5.1 Semi-Analytic Method

An alternative technique of solution is developed here primarily for two reasons:-

(i) to allow an examination of the validity of the results from numerical integration.

(ii) to give some insight into the type of strategy best suited to solving problems of the kind involving fluid flow, diffusion and chemical reaction.

The method, which is of necessity only semi-rigorous, is based upon the most general separable linear form of the kinetic rate expression which retains the coupling between the continuity and energy equations. To facilitate development consideration is given to the special case of the 2-dimensional "surface reaction" model. The descriptive equations for the interstitial fluid are given by (7.5) and (7.6) with boundary conditions (7.9) to (7.14). For the reaction scheme

$$a_A\ A \rightarrow B \quad (a_A = 1,2,..)$$

with kinetics given by equations (3.8) and (3.9), the more general forms of (7.1) and (7.2) are written in dimensionless units as

$$C_f^* - C_s^* = \delta . r^*(C_s^*, T_s^*) \qquad (A5.1)$$

$$T_f^* - T_s^* = \beta_2 . \delta r^*(C_s^*, T_s^*) \qquad (A5.2)$$

where the nomenclature is identical to that employed in Section (7.4), except that now C_s^* is constant within the catalyst volume and equal to the value at the external surface of the particle.

The parameter δ represents the ratio of the specific chemical rate at the inlet, based on interstitial fluid environment, to the mass transfer rate across the interface i.e., $\delta = k_{vfo}\ C_{fo}^{n-1} / (\frac{3}{b}\ k_A)$. β_2 is given by $\beta_2 = \dfrac{(-\Delta H)\ C_{fo}\ k_A}{h\ (T_a - T_{fo})}$. From the definition of effectiveness

factor in Section (2.2.1),

$$\eta = \frac{(C_f^* - C_s^*)}{\int .r^*(C_f^*, T_f^*)} \qquad (A5.3)$$

A5.2 The linear rate equation

Analytical integration of the system is made very difficult by the non-linear reaction rate term, r^*. An attempt is made here to overcome this difficulty by expressing r^* in the form

$$r^* = a + b\, C_s^* + c\, T_s^* \qquad (A5.4)$$

where a, b and c are suitably defined constants. Although the method presented here is necessarily based upon a linear rate expression, the form suggested by (A5.4) is the most general linear form which permits analytical integration. The linearization of r^* is effected by expressing r^* as a Taylor series about $r^*(C_f^*, T_f^*)\big|_{z=0}$. Carrying out the required algebra leads to an assessment of the constants a, b and c:-

i.e.,

$$\left.\begin{aligned} a &= r^*(C_f^*, T_f^*)\big|_{z=0} &&= a_A \\ b &= \partial r^*/\partial C_f^*\big|_{z=0} &&= -n.a_A \\ c &= \partial r^*/\partial T_f^*\big|_{z=0} &&= \gamma.\theta.a_A \end{aligned}\right\} \qquad (A5.5)$$

The approximation given by (A5.4) is generally a poor one, and its range of application is restricted on two counts. Firstly, the assumption with regard to concentration dependence is restrictive, although by no means as strong as the assumption of pseudo-first order kinetics. Secondly, and more important, the range of variation in temperature which can be covered is very limited for rarely does the reaction rate bear a linear dependence on temperature. Consequently, the semi-analytic solution developed here is likely to prove of quantitative value only over a region in the neighbourhood of the bed inlet. It is, of course, difficult to predict this region, a priori. Nevertheless, it is in the

entrance region where numerical integration is seemingly unattractive. This approach does offer, therefore, a basis for assessing the suitability of numerical exploration of the bed inlet and offers itself as a starting policy in the event of the latter proving unsatisfactory.

Putting the results of (A5.5) into (A5.4) and substituting the expression for r^* into the right hand sides of (A5.1) and (A5.2) two linear equations arise, simultaneous in C_s^* and T_s^*. These may be solved with ease to give

$$C_s^* = (1 + \delta.a').C_f^* + \delta.b'.T_f^* + \delta.c' \qquad (A5.6)$$

$$T_s^* = \delta.\beta_2 a'.C_f^* + (1 + \delta.\beta_2 b')\, T_f^* + \delta.\beta_2 c' \qquad (A5.7)$$

where $a' = -n/X$, $b' = \gamma\theta/X$, $c' = 1/X$

and $X = \delta.n - \gamma.\theta\beta_2.\delta - 1/a_A$

From (A5.3) and (A5.6)

$$\eta.r^*(C_f^*, T_f^*) = \frac{(C_f^* - C_s^*)}{\delta} = -(a'C_f^* + b'T_f^* + c') \qquad (A5.8)$$

Substitution of equation (A5.8) into (7.5) and (7.6) produces a pair of linear but coupled parabolic equations:-

$$\frac{\partial T_f^*}{\partial z} = c_1\left(\frac{\partial^2 T_f^*}{\partial s^2} + \frac{1}{s}.\frac{\partial T_f^*}{\partial s}\right) + A.C_f^* + B.T_f^* + D \qquad (A5.9)$$

$$\frac{\partial C_f^*}{\partial z} = c_3\left(\frac{\partial^2 C_f^*}{\partial s^2} + \frac{1}{s}.\frac{\partial C_f^*}{\partial s}\right) + E.C_f^* + F.T_f^* + H \qquad (A5.10)$$

where A, B, D, E, F and H are constants given by

$$A = c_2 a', \; B = c_2 b', \; D = c_2 c'$$

$$E = c_4 a', \; F = c_4 b', \; H = c_4 c',$$

and the boundary conditions on (A5.9) and (A5.10) follow from equations (7.9) to (7.14).

A5.3 Method of solution

The pair of equations given by (A5.9) and (A5.10) is susceptible to

analytical integration but the solutions are not easily evaluated. Basically, the approach is relatively straightforward (c.f., FROMENT[37]). At the outset solutions to (A5.9) and (A5.10) are assumed in terms of two Dini series which are made to fit the boundary conditions (7.9) to (7.14). Two transcendental equations arise for the determination of the discrete but infinite set of respective eigenvalues. Substitution of the assumed solutions in the system (A5.9) and (A5.10) leads to a doubly infinite set of differential equations for the eigenfunctions.

Let the assumed solutions be

$$C_f^*(z,s) = \sum_{n=0}^{n=\infty} h_n(z).\, J_o(\alpha_n s)/J_o(\alpha_n) \qquad \text{(A5.11)}$$

and

$$1-T_f^*(z,s) = \sum_{n=0}^{n=\infty} g_n(z).J_o(\mu_n s) \qquad \text{(A5.12)}$$

$$(n=0,1,2,\ldots\ \infty)$$

where $h_n(z)$ and $g_n(z)$ are as yet unknown sets of eigenfunctions. α_n and μ_n are corresponding eigenvalues.

(a) <u>determination of eigenvalues</u>

Partially differentiating equations (A5.11) and (A5.12) with respect to s and setting s=0 leads to the satisfaction of conditions (7.13) and (7.11) respectively. At the tube wall (s=1) the following transcendental equations arise for the determination of the sets of roots α_n, μ_n needed in (A5.11) and (A5.12).

$$J_1(\alpha_n) = 0 \qquad \text{(A5.13)}$$

$$\mu_n.J_1(\mu_n) = \lambda.J_o(\mu_n) \qquad \text{(A5.14)}$$

Those equations follow from the partial derivatives of (A5.11) and (A5.12) at s=1, and the boundary conditions (7.14) and (7.12) respectively.

Roots of (A5.13) and (A5.14) for integer values of λ are to be found in the literature[104]. Generally speaking it is necessary to set up an iterative scheme to extract the roots of (A5.13) and (A5.14).

(b) <u>determination of eigenfunctions</u>

From (A5.11) and (A5.12), written at z=0, and the conditions (7.10) and (7.9) it follows that

$$h_n(0) = 0 \qquad \text{(A5.15)}$$

$$\text{and} \qquad 1 = \sum_{n=0}^{n=\infty} g_n(0).J_o(\mu_n.s) \qquad \text{(A5.16)}$$

Introducing the Dini expansion of unity,

$$1 = 2.\lambda. \sum_{n=0}^{n=\infty} J_o(\mu_n.s)/\left[(\mu_n^2 + \lambda^2)\ J_o(\mu_n)\right] \qquad \text{(A5.17)}$$

and using (A5.17) in (A5.16) gives

$$g_n(0) = 2\lambda/\left[(\mu_n^2 + \lambda^2).\ J_o(\mu_n)\right]$$

Defining a new function $G_n(z)$ by

$G_n(z) = g_n(z)/g_n(0)$, equation (A5.12) may be written as

$$T_f(z,s) = 1 - 2\lambda \sum_{n=0}^{n=\infty} \frac{G_n(z).J_o(\mu_n s)}{(\mu_n^2+\lambda^2)J_o(\mu_n)} \qquad \text{(A5.18)}$$

where $$G_n(0) = 1 \qquad \text{(A5.19)}$$

The determination of the eigenfunctions now follows by substituting equations (A5.11) and (A5.18) into the system (A5.9) and (A5.10). To illustrate the procedure consider the evaluation of the $h_n(z)$.

Writing down the required partial derivatives of (A5.11) and using the results, together with (A5.11) and (A5.18), in equation (A5.10) leads to

$$\sum_{n=0}^{n=\infty} \frac{J_o(\alpha_n . s)}{J_o(\alpha_n)} . \left[\frac{dh_n(z)}{dz} + (\alpha_n^2 . c_3 - E) . h_n(z) \right] = (F+H)$$

$$- 2F . \lambda . \sum_{p=0}^{p=\infty} \frac{G_p(z) J_o(\mu_p . s)}{(\mu_p^2 + \lambda^2) . J_o(\mu_p)} \qquad (A5.20)$$

where, for convenience, index p is introduced in the right hand side.

Multiplying both sides of (A5.20) by $s . J_o(\alpha_x . s)$ and integrating over the range $0 \leq s \leq 1$ gives

$$\sum_{n=0}^{n=\infty} \frac{1}{2} . \frac{J_o^2(\alpha_x)}{J_o(\alpha_n)} . \delta_{nx} \left[\frac{dh_n(z)}{dz} + (\alpha_n^2 c_3 - E) h_n(z) \right] = \frac{(F+H)}{2} . \delta_{x0}$$

$$- 2F\lambda \sum_{p=0}^{p=\infty} \frac{G_p(z) . \lambda J_o(\alpha_x)}{(\mu_p^2 + \lambda^2)(\mu_p^2 - \alpha_x^2)} \qquad (A5.21)$$

where the Kronecker δ is given by

$$\left.\begin{aligned} \delta_{nx} &= 0 \quad n \neq x \\ \delta_{nx} &= 1 \quad n = x \end{aligned}\right\}, \qquad \left.\begin{aligned} \delta_{x0} &= 1 \quad x = 0 \\ \delta_{x0} &= 0 \quad x \neq 0 \end{aligned}\right\}$$

Define a new function $H_n(z)$ by

$$H_n(z) = h_n(z) + \frac{(F+H)}{E} . \delta_{n0} \qquad (A5.22)$$

From (A5.22), at z=0, and (A5.15)

$$H_n(0) = \frac{(F+H)}{E} . \delta_{n0} \qquad (A5.23)$$

Substituting (A5.22) into (A5.21), putting x identical to n, and equating coefficients of $J_o(\alpha_n)$ gives the system of differential equations for the unknown functions $H_n(z)$ - i.e.,

$$dH_n(z)/dz + (\alpha_n^2 c_3 - E) . H_n(z) = -4F\lambda^2 \sum_{p=0}^{p=\infty} \frac{G_p(z)}{(\mu_p^2 + \lambda^2)(\mu_p^2 - \alpha_n^2)}$$

$$(n=0,1,2,\ldots\infty) \qquad (A5.24)$$

with initial conditions given by equation (A5.23).

A similar series of steps leads to the system of differential equations for the functions $G_n(z)$.

The final result is

$$dG_n(z)/dz + (\mu_n^2 c_1 - B).G_n(z) = K - A\mu_n^2 \sum_{p=0}^{p=\infty}{}' \frac{H_p(z)}{\mu_n^2 - \alpha_p^2}$$

$$(n=0,1,2,\ldots\infty) \qquad (A5.25)$$

where $K = \frac{A}{E}.(F+H) - (B+D)$. Initial conditions on equation (A5.25) are given by (A5.19).

Integrated radial values of C_f^* and T_f^* follow directly from the equations

$$\bar{C}_f^*(z) = 2\int_o^1 s.C_f^*(z)ds \quad , \quad \bar{T}_f^*(z) = 2\int_o^1 s.T_f^*(z)ds$$

and (A5.11), (A5.22), (A5,18).

The final results are

$$\bar{C}_f^*(z) = \left[H_o(z) - \left(\frac{F+H}{E}\right)\right] / J_o(\alpha_o) \qquad (A5.26)$$

$$\bar{T}_f^*(z) = 1 - 4\lambda^2 \sum_{n=0}^{n=\infty}{}' \frac{G_n(z)}{\mu_n^2(\mu_n^2+\lambda^2)} \qquad (A5.27)$$

A5.4 Practical difficulties

For practical purposes it is necessary to truncate the system of equations (A5.24) and (A5.25).

The question may now be asked: To what extent is the system truncated? It is impossible to give a quantitative answer a priori. However, an appreciation of some of the issues involved is forthcoming from the following numerical experiment:-

A = 0.6265	E = -0.5824
B = 2.8278	F = -2.6287
D = -0.6265	H = 0.5824

For $\lambda = 3$ the first 6 eigenvalues of equations (A5.13) and (A5.14) are[104]

n	α_n	μ_n
0	0	1.7887
1	3.8317	4.4634
2	7.0156	7.4103
3	10.1735	10.4566
4	13.3237	13.5434
5	16.4706	16.6499

At the tube wall it follows from (A5.11), (A5.22) and (A5.18) that

$$C_f^*(z,1) = \sum_{n=0}^{n=\infty} H_n(z) - \frac{(F+H)}{E} \qquad \text{(A5.28)}$$

and $$T_f^*(z,1) = 1 - 2\lambda \sum_{n=0}^{n=\infty} \frac{G_n(z)}{(\mu_n^2+\lambda^2)} \qquad \text{(A5.29)}$$

For practical purposes the accuracy in computing $C_f^*(z,1)$ and $T_f^*(z,1)$ is only influenced by the degree of truncation of the infinite series appearing in (A5.28) and (A5.29). It is true that extraneous error is introduced as a result of numerical integration of the truncated system of ordinary differential equations for the $H_n(z)$ and $G_n(z)$. However, this may be made small by using a standard low truncation error integration formula.

Tables A5.1 and A5.2 reflect the influence of the degree of truncation of the infinite series upon the accuracy of the computed solutions for $C_f^*(z,1)$ and $T_f^*(z,1)$ over the initial tenth of the bed. It is apparent that even for 6-term Dini series, which amounts to a system of 12 simultaneous differential equations for the $H_n(z)$ and $G_n(z)$, the solutions for conversion and temperature at the tube wall have not

converged during the initial period of the integration. This is particularly noticeable for the case of conversion where the spread in magnitude of the eigenfunctions, $H_n(z)$, is narrow. This behaviour is typical of that found in the operating systems discussed in Chapters 9 and 10. As the computation progresses away from the inlet fewer terms can be used in the series: the result being that the size of the system of differential equations is considerably reduced.

<u>% Conversion</u>

	No. of terms in series				
z	(2)	(3)	(4)	(5)	(6)
0.01	0.478	0.508	0.513	0.510	0.504
0.02	0.929	0.963	0.953	0.929	0.903
0.04	1.75	1.74	1.65	1.56	1.49
0.06	2.48	2.34	2.15	2.00	1.89
0.08	3.10	2.80	2.50	2.29	2.17
0.10	3.64	3.14	2.73	2.49	2.35

Table A5.1 Influence of truncation upon $C_f^*(z,1)$

<u>Temperature</u>

	No. of terms in series				
z	(2)	(3)	(4)	(5)	(6)
0.01	0.307	0.223	0.181	0.159	0.147
0.02	0.314	0.237	0.204	0.189	0.182
0.04	0.327	0.265	0.244	0.237	0.235
0.06	0.340	0.291	0.278	0.276	0.275
0.08	0.352	0.315	0.308	0.307	0.308
0.10	0.365	0.336	0.333	0.334	0.335

Table A5.2 Influence of truncation upon $T_f^*(z,1)$

The solution of a system of this kind is a standard problem for which use is made of the Runge-Kutta-Merson formula, with provision being made for step length adjustment. Integration of the truncated versions of (A5.24) and (A5.25) is combined with calculation of Bessel functions in the radial space dimension to make known point values of C_f^* and T_f^*. Solid phase values, C_s^* and T_s^*, are then evaluated from (A5.6) and (A5.7), and integrated mean radial values, $\bar{C}_f^*$ and $\bar{T}_f^*$, are found from equations (A5.26) and (A5.27). To overcome the difficulties involved in determining accurately Bessel functions of large argument from ascending series, the polynomial approximations for $J_o(x)$ and $J_1(x)$ suggested by ALLEN[105] are utilized. These are of the form

$$J_o(x) = x^{-\frac{1}{2}} f_o \cos \theta_o$$

$$J_1(x) = x^{-\frac{1}{2}} f_1 \cos \theta_1$$

where the f's and θ's form polynomials in $(3/x)$. Absolute accuracies are given by ABROMOWITZ and STEGUN[66] as 1.6×10^{-8} and 4×10^{-8} respectively.

The first 20 roots of equation (A5.13) are tabulated[66] together with the first 6 roots of equation (A5.14) for certain integer values of λ.[104] For non-integer λ the roots of (A5.14) are extracted successively by iteration using the Newton-Raphson method. Initial estimates of the roots are suitably based on the values corresponding to the nearest tabulated integer value of λ. The approximation

$$\mu_{n+1} = \mu_n + \pi \quad (n=6,7,.....)$$

proved a suitable starting value for determining the 7th and subsequent roots.

Since the main purpose of pursuing this alternative approach is to furnish a check on the results from numerical analysis of the non-linear system, the rather delicate issue of improving the computing

efficiency, by logically reducing the size of the system of differential equations as the integration is propagated away from the entrance, is not investigated. Rather, the size of the system is specified at the outset and fixed throughout the integration.

APPENDIX 6

DETAILS OF SOME NUMERICAL EXPERIMENTS ON THE MATHEMATICAL MODELS OF THE REACTOR

A study is made here of the effects of increment size, type of finite difference scheme and convergence criterion upon the accuracy and speed of computation of the numerical solution given in detail in Chapter 8.

A6.1 Increment sizes : type of finite difference scheme

Some results, shown in Table A6.1, demonstrate the influence of the axial space increment Δz on the convergence of the numerical solution of MODEL 3 for the data presented in Table 9.1. For these particular data the values of C_f^* do not vary appreciably with radial position so the mean radial value $\overrightarrow{C_f^*}$ can be used to study the effect of increment size in the longitudinal direction. Two types of finite difference scheme are considered in Table A6.1 - i.e., the Crank Nicolson type ($\Theta = \frac{1}{2}$) and the Laasonen or fully implicit type ($\Theta = 1$). The values given for $\Theta = \frac{1}{2}$, $\Delta z = 0.01$, $\Delta s = 0.1$ represent converged values. Reducing the step sizes further produces no noticeable effect on the results for $\overrightarrow{C_f^*}$.

It is evident that much larger increments can be taken in the z-direction for a given accuracy of integration by using the Crank Nicolson scheme rather than the fully implicit version. Thus, the accuracy obtained with Crank and Nicolson's method using $\Delta z = 0.1$ is similar to that of the fully implicit scheme with $\Delta z = 0.01$. This result is to be expected on the basis of the analysis of truncation error presented in Section 8.3.3.

No restriction on the axial step length due to the convergence requirements on the starting policy of integration at each z-step was experienced with any of the cases investigated. However, Table A6.1 does not indicate an important consideration which leads to serious restrictions in the allowable axial step compared with that incurred by truncation

z	ⓗ = ½		ⓗ = 1	
	Δz = 0.1	Δz = 0.01	Δz = 0.1	Δz = 0.01
0.1	1.17	1.13	0.955	1.11
0.2	1.96	1.92	1.66	1.89
0.3	2.55	2.49	2.20	2.46
0.4	3.00	2.94	2.63	2.91
0.5	3.37	3.31	3.00	3.27
0.6	3.69	3.62	3.31	3.59
0.7	3.96	3.90	3.60	3.86
0.8	4.21	4.15	3.85	4.11
0.9	4.45	4.38	4.09	4.35
1.0	4.66	4.60	4.32	4.57

TABLE A6.1 Effect of axial increment size Δz upon % mean radial conversion for MODEL 3.

error alone. Notably, the discontinuity in $\partial T^*_f / \partial s$ at (0,1). Fig. A6.1 shows the effects of increment size and ⓗ on the fluid temperature profile at the tube wall. For the step sizes Δz = 0.01, Δs = 0.05, the results for the cases ⓗ = ½ and ⓗ = 1 are virtually indistinguishable save for a slight oscillation over the first tenth of the reactor for ⓗ = ½. Reducing the axial and radial step sizes produced little effect except to damp out completely the slight oscillation.

A rather interesting result is found when the increment sizes are increased, particularly the axial step, Δz. Increasing Δz for the Crank Nicolson scheme caused the onset of appreciable oscillation in the wall temperature profile. In all cases considered the error was damped as the computation proceeded away from z = 0, but for Δz = 0.1 significant error still persisted by the end of the computation at z = 1. This type of behaviour was observed by PARKER and CRANK[82] and subsequently by KEAST and MITCHELL[83] for the linear parabolic equation. The latter authors

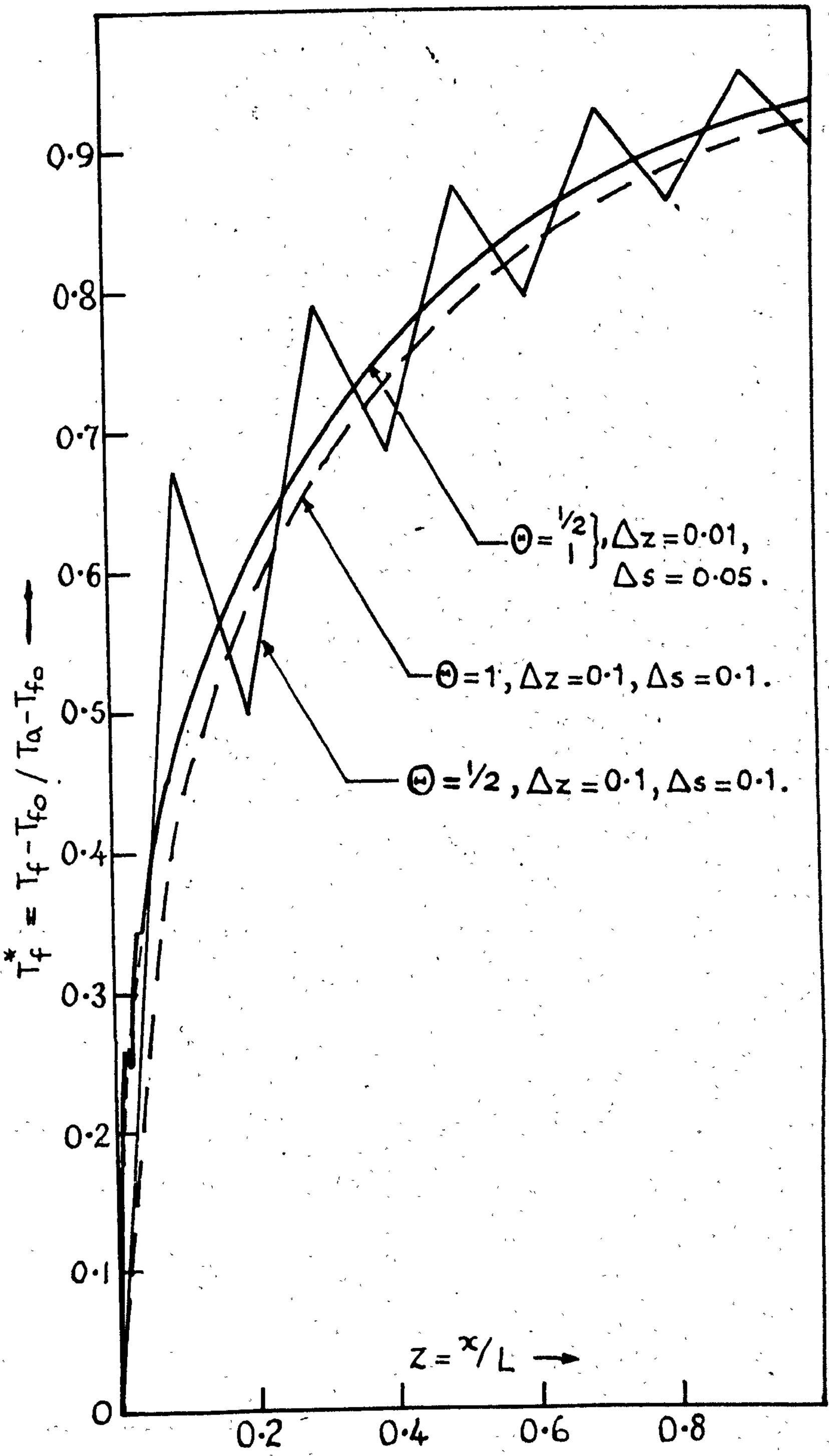

FIG. A6.1 Effect of Θ and increment size on longitudinal temperature profile at the tube wall.

showed that persistent errors could arise with Crank and Nicolson's formula under certain boundary conditions even though discontinuities were absent. Reference to Fig. A6.1 shows the oscillations are removed if Ⓗ = 1, even for the course grid with $\Delta z = 0.1$. However, the accuracy suffers to some extent by virtue of the larger truncation error, $O(\Delta z)$, in the axial direction. For the more non-linear case considered in Chapter 10, the use of increment sizes $\Delta z = 0.01$, $\Delta s = 0.05$ proved satisfactory for Crank and Nicolson's method, even for MODEL'S 1 and 2 in which steep gradients were present in both axial and radial directions.

The effect of integration step size on computing times for MODEL 2, employing the data of Chapter 10, is summarized in Table A6.2.

Δz	Δs	No. of mesh points	Computing time (seconds)
0.1	0.1	100	28
0.05	0.05	400	63
0.025	0.05	800	76
0.01	0.05	2000	129
0.005	0.025	8000	337

TABLE A6.2 Influence of integration step sizes on computing time for MODEL 2 with Ⓗ = $\frac{1}{2}$.

Improvement of the existing numerical technique is envisaged by

(a) increasing the size of the Δz step as the solution progresses away from the discontinuity,

and possibly

(b) using the Crank Nicolson integration method in the domain $0 < z \leq 1$, $0 \leq s < 1$, with a fully implicit scheme on the boundary, $s = 1$.

A6.2 Tolerence criterion

The tolerence criterion employed to test for convergence of the iterations is of a relative error type given by equation (8.36). Some experiments are reported here on the influence of the magnitude of the ξ of equation (8.36) on the accuracy of the numerical solutions and the speeds of computation, so that an "optimum" value might be chosen which leads to satisfactory convergence of the iterations in a reasonable time. The data of Chapter 10 are used in conjunction with MODEL 2 to investigate a highly non-linear system, in which it is reasonable to expect any effects due to an excessively large value of ξ to show up to the greatest extent.

Results are reported over a range of 1% relative error down to 0.01%, using integration step sizes $\Delta z = 0.01$ and $\Delta s = 0.05$ with $\textcircled{H} = \frac{1}{2}$. The convergence tests on the dependent variables were carried out at 6 equally spaced radial positions, s = 0(0.2) 1, and at each axial step. Table A6.3 shows the effect of ξ on the computing time. It is interesting to note that reducing the magnitude of ξ one hundredfold only leads to a relative increase of 1.2 in the computing time. An indication of the quadratic

100 x ξ	Computing time (seconds)
1	112
0.5	113
0.1	129
0.05	131
0.01	138

TABLE A6.3 Influence of ξ on computing time for MODEL 2 employing the data of Chapter 10.

rate of convergence of the quasilinearization scheme is provided in Fig. A6.2 which shows how rapidly the radial fluid conversion profile converges to the final value for $\xi = 10^{-4}$ in a region of the bed in which

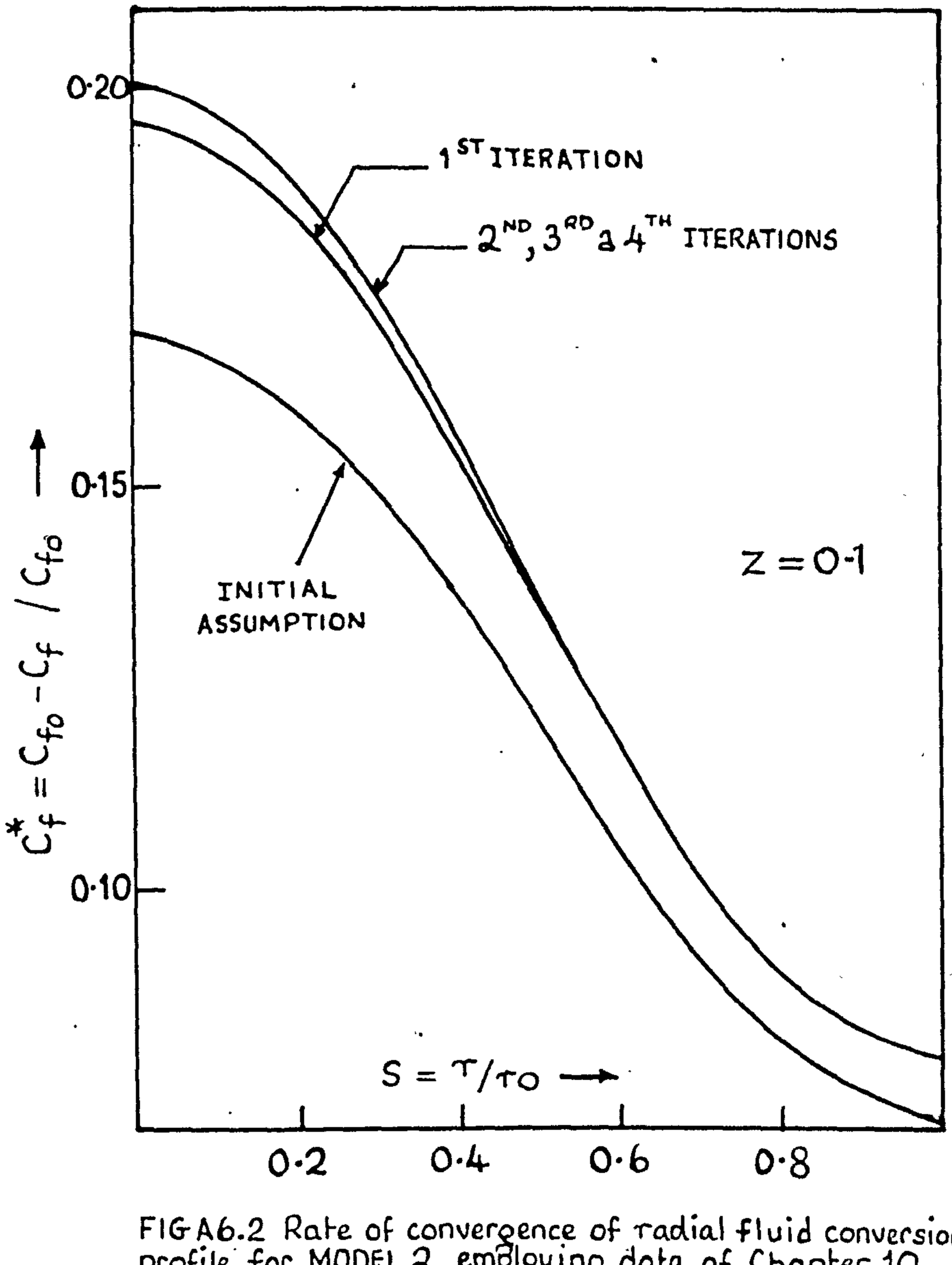

FIG A6.2 Rate of convergence of radial fluid conversion profile for MODEL 2 employing data of Chapter 10.

the initial assumed profile is not particularly accurate. Further, the numerical results for the two extreme cases, $\xi = 10^{-2}$ and $\xi = 10^{-4}$, show no disagreement at least up to the fourth decimal place of the output format employed in the computer program.

It would seem that the problem of choosing a suitable value for ξ is not a particularly difficult one. Even for a value as low as 10^{-4}, convergence of the iterative process is extremely rapid from relatively inaccurate estimates of the radial fluid conversion and temperature profiles.

A6.3 The discontinuity : its influence on the numerical solution

An attempt is made here to gain some insight into the difficult problem concerning the influence of a discontinuity in $\partial T^*_f / \partial s$ at $z = 0$, $s = 1$ on the solution of the finite difference equations.

Methods of obtaining solutions to partial differential equations based on finite differences are inaccurate in the region of a discontinuity. Nevertheless, until recently, it was widely believed for equations of parabolic type that the errors die away fairly rapidly in a step by step process. Evidence to the contrary is presented by PARKER and CRANK[82] and KEAST and MITCHELL[83] for the linear parabolic equation. Indeed, the latter authors showed that serious instability may arise with apparently stable difference formulae (e.g., Crank/Nicolson) for certain boundary conditions, even with no discontinuity present.

In relation to the problem at hand there seems little that can be achieved in the way of conventional numerical stability analyses. Instead, results from numerical integration are compared with those from the semi-analytic method presented in Appendix 5. It should be remembered that solutions from the semi-analytic method only approximate those of the non-linear partial differential equations in the entrance region, so that the comparison can only be legitimately carried to relatively small bed depths. Besides providing a partial check on the numerical solution, the use of the

semi-analytic approach also yields valuable information on the utility of a linearized rate expression for exploratory design purposes.

Results from MODEL 2 for the data of Chapter 9 are examined, and the relevant groups appearing in the semi-analytic method are summarized below:

A = 0.927, B = 1.784, D = -0.927, E = -0.155, F = -0.298, H = 0.155.

Experiments showed that 6-term Dini series for concentration and temperature were sufficient to establish convergence. The first 6 roots of the transcendental equations

$$\mu_n J_1(\mu_n) = 2 J_o(\mu_n)$$

$$J_1(\alpha_n) = 0$$

are[104]

n	μ_n	α_n
0	1.5994	0
1	4.2910	3.8317
2	7.2884	7.0156
3	10.3658	10.1735
4	13.4719	13.3237
5	16.5910	16.4706

Figs. A6.3 and A6.4 compare axial profiles of fluid temperature and conversion from the numerical and semi-analytic methods. Good agreement is obtained for bed depths up to z = 0.1. Some discrepancy in the fluid temperature profile at the tube wall, as determined numerically, is in evidence. The error is dependent on the axial step length and can be removed providing a sufficiently small axial step is used. Table A6.4 demonstrates this effect. For the mild operating conditions considered here, the assumption of a linear dependence of reaction rate on temperature is satisfactory. Even at a bed depth, z = 0.5, the semi-analytic method predicts the radial temperature profile to within 5°K of the result from numerical integration. The prediction of conversion is not so satisfactory,

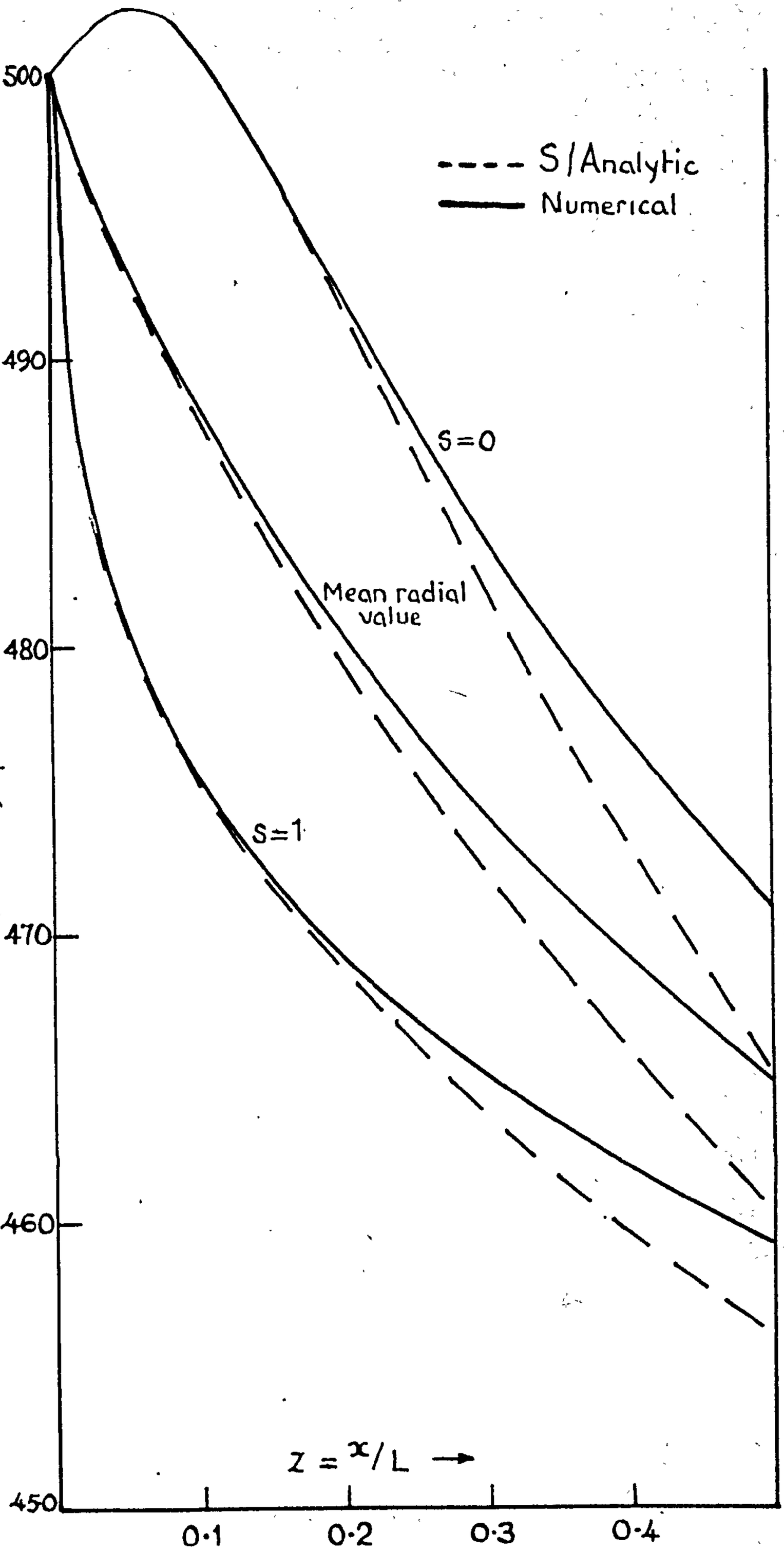

FIG. A6-3 Comparison of numerical and semi-analytic methods. Longitudinal fluid temperature profiles for MODEL 2 employing data of Chapter 9.

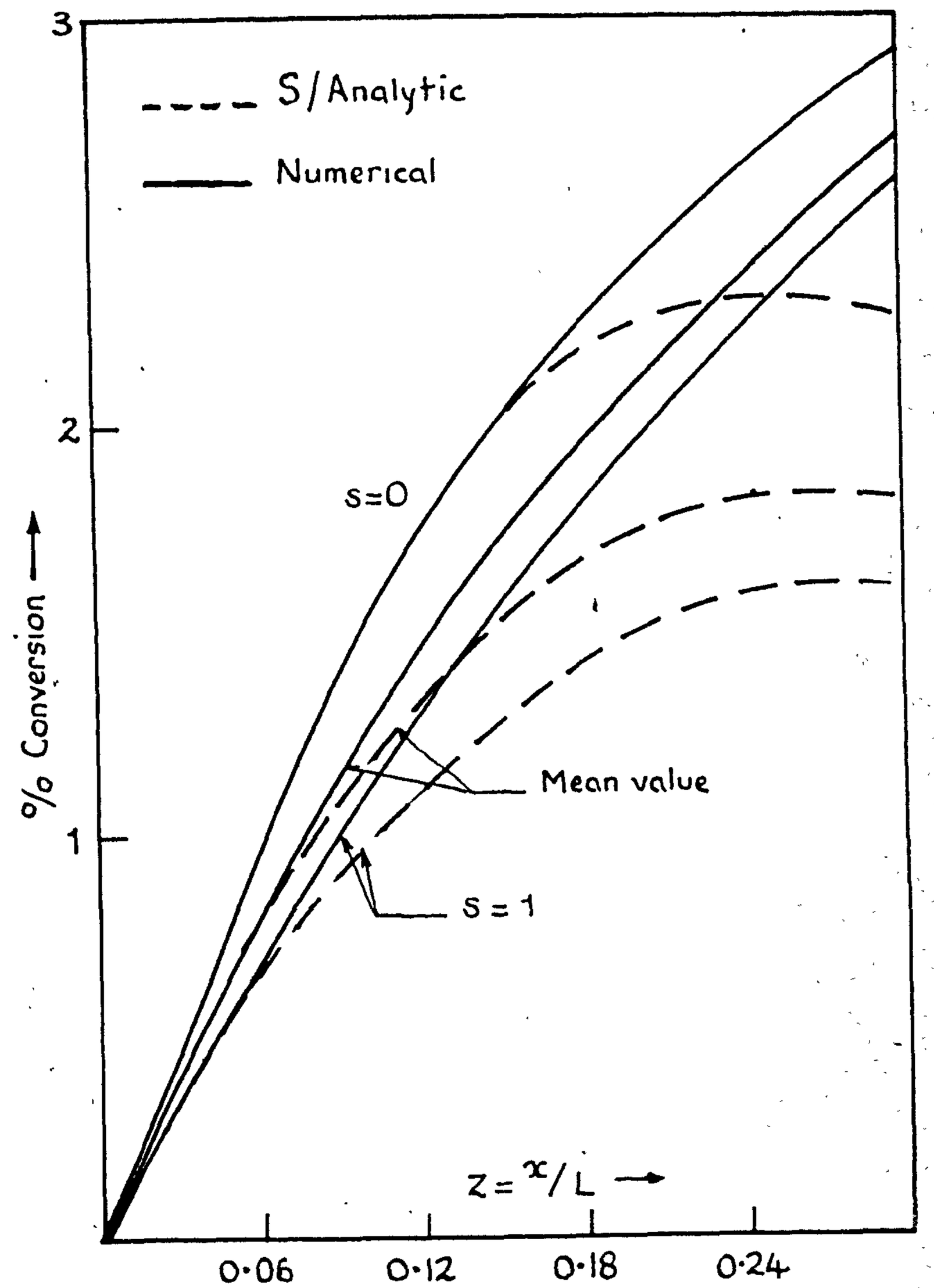

FIG. A6.4 Comparison of numerical and semi/analytic methods. Longitudinal fluid conversion profiles (%) for MODEL 2 employing the data of Chapter 9.

		Numerical Solution ($\mathcal{H} = \frac{1}{2}$)		
z	S/Analytic method	$\Delta s = .05$ $\Delta z = .001$	$\Delta s = .05$ $\Delta z = .01$	$\Delta s = .1$ $\Delta z = .02$
0.01	0.208	0.207	0.259	
0.02	0.276	0.275	0.249	0.338
0.03	0.323	0.322	0.344	
0.04	0.360	0.359	0.345	0.333
0.05	0.390	0.389	0.400	
0.06	0.416	0.414	0.407	0.433
0.07	0.439	0.436	0.443	
0.10	0.496	0.491	0.488	0.498
0.20	0.625	0.609	0.609	0.609

TABLE A6.4 Comparison of numerical and semi-analytic methods. Fluid temperature profile at the wall (s = 1), $T_f^*(z;1)$.

particularly near the tube wall where an appreciable temperature gradient is present. However, as far as z = 0.05 radial conversion profiles from the two methods agree to within 10%. Along the axis (s = 0) agreement is better, as shown in Table A6.5.

	S/Analytic		Numerical ($\mathcal{H} = \frac{1}{2}$)	
z	6-term	12-term	$\Delta s = .05$ $\Delta z = .001$	$\Delta s = .05$ $\Delta z = .01$
0.01	0.177	0.157	0.156	0.156
0.02	0.326	0.316	0.315	0.315
0.03	0.480	0.477	0.476	0.476
0.05	0.800	0.801	0.801	0.800
0.07	1.11	1.11	1.11	1.11
0.10	1.51	1.51	1.52	1.52
0.12	1.72	1.73	1.75	1.75
0.15	1.98	1.98	2.03	2.03
0.20	2.23	2.23	2.40	2.40
0.30	2.26	2.26	2.92	2.92

TABLE A6.5 Comparison of numerical and semi-analytic methods. Fluid conversion (%) at the axis (s = 0).

Separating the rate expression into the form of the sum of terms linear in concentration and temperature can cause a maximum to exist in the axial conversion profiles (cf., Fig. A6.4). It is, of course, now possible for the reaction rate to be large when the temperature is high, even though the concentration is zero. An improvement of the representation of the rate is envisaged by giving it as a product of terms linear in concentration and temperature. However, it is difficult to take advantage of the improvement because this description of the rate is not linear in the concentration and temperature taken together and so cannot be incorporated into the analysis. Alternatively, the point about which the reaction rate is linearized might be updated successively as the calculation proceeds along the reactor, but this method would be of little use in cases where appreciable radial gradients are present. In its present form the semi-analytic method cannot be regarded as a serious competitor to the more flexible and very much faster (a factor of 10 in computing time) numerical method. The usefulness of the latter method also lies in its easy extension to the more complex situation in which "pore" diffusion is present (cf. Chapter 7). It is difficult to envisage the same ease of adaptation of the semi-analytic method.

The results presented here show that the numerical scheme can be made to converge to the solution of the partial differential equations at least in the inlet region of the bed, providing the axial step Δz is made sufficiently small. Little can be inferred about the numerical solution for large bed depths except to say that the computed results approximately satisfy the material and energy balance equations at a number of examined points.

Further, the commonly used criterion for establishing convergence by gradually reducing the mesh size until the solution stops changing is adhered to, although there is no guarantee that this is the correct answer[85].

NOMENCLATURE

a_i	stoichiometry coefficient ($a_i < 0$ is a reactant)
a_k	coefficient appearing in the linearization process (equation 8.8
$a_k'(j,m)$	discretized form of a_k ($j\Delta z$, $m\Delta s$)
a_v	surface to volume ratio of a catalyst particle (3/b)
A	reactant
$\underline{A}_{1,k}$, $\underline{A}_{2,k}$	tridiagonal matrices (given on pages 119 and 121 respectively)
A_p	external surface area of a catalyst pellet
b	particle radius
b_k	coefficient appearing in the linearization process (eqn. 8.8)
$b_k'(j,m)$	discretized form of b_k ($j\Delta z$, $m\Delta s$)
B	product
$\underline{B}_{1,k}$, $\underline{B}_{2,k}$	diagonal matrices (see pages 120 and 121)
$\underline{B}_3$, $\underline{B}_4$	diagonal matrices (page 126)
c	dimensionless concentration, (C_s/C_f)
c_f	mean specific heat of reaction mixture
c_{fi}	concentration fluctuation
c_o, c_s	value of c at y=0, 1 respectively
c_1, c_2	coefficients in equation (7.5), (see page 100)
c_3, c_4	coefficients in equation (7.6), (see page 100)
C_{fi}	point molar concentration of reactant i in the fluid phase (on volume fluid basis)
C_{fo}	inlet fluid concentration of reactant A, (x=0)
$\overline{C}_{fi}$, $\overline{C}_{s,i}$	space-averaged concentrations of component i in the fluid and particulate phases
$\vec{\overline{C}}_s$	vector of scalar intensive space-averaged concentrations in the particulate phase
C_f^*, C_s^*	dimensionless fluid and solid concentrations respectively, $C_{fo} - C_f(C_s) / C_{fo}$
$C_{f,k}^*$	the value of C_f^* at the k'th iteration

d_k	coefficient appearing in the linearization process, (8.8)
$d'_k(j,m)$	discretized form of d_k ($j\Delta z$, $m\Delta s$)
d_p	particle diameter
$\underline{d}_{1,k}$, $\underline{d}_{2,k}$	column vectors (equations (8.28) and (8.29))
$\underline{d}_1(j)$, $\underline{d}_2(j)$	column vectors (page 125)
D	fluid molecular diffusivity
D_f	radial mass diffusivity
D_i	"effective" diffusivity of species i in the particulate phase
D^*_A	"effective" diffusivity of reactant A in the particulate phase
$D_{K,eff}$	Knudsen diffusion coefficient (eqn. 9.5)
D_{12}	molecular binary diffusion coefficient (9.7)
$D_{12,eff}$	"effective" bulk diffusion coefficient (9.6)
$\underline{D}_{1,k}$, $\underline{D}_{2,k}$	column vectors (pages 120 and 122)
$\underline{D}_3$	a column vector (page 126)
e	bed voidage
E	Arrhenius activation energy
E:	modified activation energy
$E_1(\alpha)$	exponential integral, $E_1(\alpha) = \int_\alpha^\infty \frac{\exp(-v)}{v}\, dv$
$g_n(z)$	a set of functions appearing in the Dini expansion of temperature (A5.12)
G (x)	function defined by equation (6.1)
$G_n(z)$	$g_n(z) / g_n(0)$
G_o	superficial mass flow rate
$\vec{G}$	actual mass flow rate vector at any point in the fluid field
h	film heat transfer coefficient between solid and fluid
h_o	outside film wall heat transfer coefficient
h_{ov}	overall heat transfer coefficient between fluid and solid based on mean temperature difference
h_w	apparent wall heat transfer coefficient
$h_n(z)$	a set of functions appearing in the Dini expansion of conversion (A5.11)

$H_n(z)$ $h_n(z) + \frac{(F + H)}{E} \cdot \delta no$ (A5.22)

$I(c_s)$ exact form of integral of eqn. (5.27)

$I^*(c_s)$ approximate form of integral, eqn. (5.36)

j node value, z direction.

j_H j-factor for heat transfer, $\frac{eh}{G_o c_f}(Pr)^{2/3}$

j_M j-factor for mass transfer, $\frac{e\rho_f k_A}{G_o}(Sc)^{2/3}$

J number of axial increments

k' molecular thermal conductivity of fluid

k_A mass transfer coefficient of reactant A between fluid and solid

k_e effective rate constant (MODEL 3)

k_E effective rate constant (MODEL 2)

k_i mass transfer coefficient of component i between fluid and solid

k_s surface reaction rate constant

k_v intrinsic reaction rate constant per unit gross volume of catalyst pellet

K constant characteristic of the packing only

K_f radial "effective" thermal conductivity

K_p "effective" thermal conductivity of porous solid

K_w thermal conductivity of tube wall

l characteristic pellet dimension

l tube wall thickness

L reactor length

m node value, s-direction

M number of radial bed increments

n order of reaction

$\vec{n}$ unit vector

Nu' modified Nusselt number, $h\ dp/K_p$

Nu" Nusselt number based on mean temperature difference between solid and fluid, $h_{ov} \cdot d_p/K_p$

Pe_H	Peclet number for heat transfer, $G_o c_f dp/K_f$
Pe_M	Peclet number for mass transfer $V_o dp/D_f$
Pr	Prandtl number (Table 9.2)
r	reactor radial co-ordinate
ro	reactor inside radius
Rg	gas constant
R_{k+1}	a separable function of $T^*_{f,k+1}$ and $C^*_{f,k+1}$ (8.15)
R^*_i, R^*_j	pseudo-rates of production of species i and j per unit mass of catalyst
Re'	Reynolds number based on interstitial flow rate, $G_o dp/e.\mu$
s	dimensionless reactor radial co-ordinate, r/ro
S_v	available pore surface per unit volume of porous solid
Sc	Schmidt number (Table 9.2)
Sh'	modified Sherwood number, $k_A dp/D^*_A$
t	dimensionless temperature, T_s/T_f
t_s	value of t at $\xi = 0$
T_a	coolant temperature
T_f	fluid temperature
T_{fo}	inlet fluid temperature
$\bar{T}_f$	space-averaged fluid temperature
$\bar{T}_s$	space-averaged solid temperature
T^*_f, T^*_s	dimensionless fluid and solid temperatures, $T_f(T_s) - T_{fo} / T_a - T_{fo}$
$T^*_{s,k}$	the value of T^*_s at the k'th iteration
U	overall heat transfer coefficient between coolant and fluid adjacent to tube wall
$U_{k+1}(j,m)$	discretized form of $C^*_{f,k+1}$ $(j\Delta z, m\Delta s)$
$\underline{U}_{k=0}(j+1)$	a "starting policy" vector (eqns. 8.33 and 8.35)
$\underline{U}_{k+1}(j+1)$	a column vector (page 120)

v_l	average of the absolute values of the lateral velocity fluctuations
V_o	superficial velocity
V_p	volume of a catalyst pellet
$V_{k+1}(j,m)$	discretized form of $T^*_{f,k+1}(j\Delta z,\ m\Delta s)$
$\vec{v}$	fluctuating velocity vector
$\vec{V}$	actual velocity vector at any point in the fluid
$\vec{V}_o$	superficial velocity vector
$\underline{v}_{k=0}(j+1)$	a "starting policy" vector (eqns. 8.34 and 8.35)
$\underline{v}_k(j+1)$	a column vector (page 125)
$\underline{V}_{k=0}(j+1)$	a "starting policy" vector, (eqns. 8.33 and 8.35)
$\underline{V}_{k+1}(j+1)$	a column vector (page 120)
w	radial particle co-ordinate
x	reactor axial co-ordinate
y	dimensionless particle radial co-ordinate ($^{w}/b$)
z	dimensionless reactor axial co-ordinate, $^{x}/L$.

Greek Symbols

α Arrhenius frequency factor.

α_n set of positive zeros of the Bessel function $J_1(x)$.

$(\alpha S_v)'$ modified pre-exponential factor.

β thermicity group, $C_f(-\Delta H)D_A^*/K_p T_f$.

β_1 dimensionless group defined on page 100.

β_2 dimensionless group of MODEL 2 (A21).

γ $= E/R_g T_f$ (Chapter 4).

γ $= E/R_g T_{fo}$ (Chapter 7).

δ central difference operator.

δ dimensionless group of MODEL 2 (page A21)

δ_{nx} Kronecker δ $\begin{cases} 1 \text{ for } n = x \\ 0 \text{ for } n \neq x \end{cases}$

$\Delta = \phi \exp\left\{\frac{\gamma}{2}\left(1 - \frac{1}{t}\right)\right\}$, Chapter 5.

$\Delta = \overline{\Phi}_o \exp\left\{\frac{\gamma\theta}{2} T_s^*/(1 + \theta T_s^*)\right\}$, Chapter 7.

$-\Delta H_j$ heat of reaction.

Δs grid size for numerical solution (Fig. 8.2).

Δt_{ex} dimensionless film temperature rise, $t(y=1) - 1$.

Δt_{ov} dimensionless overall temperature rise, $t(y=0) - 1$.

Δt_{max} maximum temperature rise permissible between pellet and fluid, $\frac{\beta}{Nu'} Sh'$.

$\Delta t'_{max}$ max^m. temperature rise for special case, $Sh' = Nu' = \infty$ β,

Δz grid size for numerical solution (Fig. 8.2).

ε relative change between successive iterations.

η effectiveness factor.

θ time co-ordinate.

Θ = $T_a - T_{fo}/T_{fo}$.

Θ a weighting factor, $0 \leq \Theta \leq 1$.

λ a suitable mean free path.

λ dimensionless group, $\beta Sh'/Nu'$.

λ a Nusselt number, Uro/K_f.

μ_n set of positive roots of the transcendental equation (A5.14).

ψ ratio of Nu' and Sh' groups.

ϱ fluid density.

ϱ_B mass of catalyst/volume of bed.

ϱ_p apparent density of a catalyst pellet.

τ a correction factor for the effects of pore geometry on diffusion rate inside a catalyst pellet.

ϕ Thiele modulus, $b\sqrt{k_{vf} C_f^{n-1}/D_A^*}$

Ω_o a reaction-diffusion modulus, $b\sqrt{k_{vfo} C_{fo}^{n-1}/D_A^*}$

ξ dimensionless co-ordinate, $\phi(1-y)$.

ζ_r' "effective" radiation constant.

REFERENCES

1. Baron, T., C.E.P. (1952) 48 118.
2. Bakhurov, V.G., Boreskov, G.K., J.Appl.Chem. (U.S.S.R.) (1947) 20 721.
3. Ranz, W.E., C.E.P. (1952) 48 247.
4. Singer, E., Wilhelm, R.H., C.E.P. (1950) 46 343.
5. Beek, J., Advances in Chemical Engineering, (1962) 3 204.
6. Aris, R., Amundson, N.R., A.I.Ch.E.J. (1957) 3 280.
7. Kramers, H., Alberda, G., C.E.S. (1953) 2 173.
8. Cairns, E.J., Prausnitz, J.M., C.E.S. (1960) 12 20.
9. Converse, A.O., A.I.Ch.E.J. (1960) 6 344.
10. Carberry, J.J., Wendel, M., A.I.Ch.E.J. (1963) 9 129.
11. Carberry, J.J., Can.J.Chem.Eng. (1958) 36 207.
12. Deans, H.A., Lapidus, L., A.I.Ch.E.J. (1960) 6 656, 663.
13. Thiele, E.W., I.E.C. (1939) 31 916.
14. Zeldowitsch, J.B., Acta Physicochim. U.S.S.R. (1939) 10 583.
15. Satterfield, C.N., Sherwood, T.K., The Role of Diffusion in Catalysis, (1963) Addison-Wesley (Mass).
16. Wheeler, A., "Catalysis" II, Reinhold, New York (1956).
17. Wakao, N., Smith, J.M., C.E.S. (1962) 17 825.
18. Foster, R.N., Butt, J.B., A.I.Ch.E.J. (1966) 12 180.
19. Mingle, J.O., Smith, J.M., A.I.Ch.E.J. (1961) 7 243.
20. Harriott, P., unpublished paper (1961). Cornell University.
21. Carberry, J.J., A.I.Ch.E.J. (1962) 8 557.
22. Carberry, J.J., C.E.S. (1962) 17 675.
23. Dacey, J.R., I.E.C. (1965) 57 No. 6 27.
24. Rivarola, J.B., Smith, J.M., I.E.C. Fund. (1965) 3 308.
25. Foster, R.N., Bliss, H., Butt, J.B., I.E.C. Fund. (1966) 5 579.
26. Foster, R.N., Butt, J.B., I.E.C. Fund. (1967) 6 481.
27. Petersen, E.E., "Chemical Reaction Analysis", Prentice-Hall New Jersey (1965).
28. Wheeler, A., Advances in Catalysis, (1951), III, 250.
29. Acrivos, A., Chambre, P.L., I.E.C. (1957) 49.2 1025.
30. Frank-Kamenetskii, D.A., "Diffusion and Heat Exchange in Chemical Kinetics", (1955), Princeton Press.
31. McHenry, K.W., Wilhelm, R.H., A.I.Ch.E.J. (1957) 3 83.
32. Bernard, R.A., Wilhelm, R.H., C.E.P. (1950) 46 233.
33. Latinen, G.A., Dissertation, Princeton University, Princeton, New Jersey (1951).

34. Morales, M., Spinn, C.W., Smith, J.M., I.E.C. (1951) 43 225.

35. Schwartz, C.E., Smith, J.M., I.E.C. (1953) 45 1209.

36. Dorweiler, V.P., Fahien, R.W., A.I.Ch.E.J. (1959) 5 139.

37. Froment, G.F., C.E.S. (1962) 17 849.

38. McGreavy, C., Nussey, C., Cresswell, D.L., I.Chem.E. Symposium Series No. 23 (1967).

39. McGuire, M.L., Lapidus, L., A.I.Ch.E.J. (1965) 11 85.

40. Prater, C.D., C.E.S. (1958) 8 284.

41. Cunningham, R.A., Carberry, J.J., Smith, J.M., A.I.Ch.E.J. (1965) 11 636.

42. Miller, F.W., Deans, H.A., A.I.Ch.E.J. (1967) 13 45.

43. Irving, J.P., Butt, J.B., C.E.S. (1967) 22 1859.

44. Tinkler, J.D., Metzner, A.B., I.E.C. (1961) 53 663.

45. Carberry, J.J., A.I.Ch.E.J. (1961) 7 350.

46. Weisz, P.B., Hicks, J.S., C.E.S. (1962) 17 265.

47. Hougen, O.A., I.E.C. (1961) 53 509.

48. Crosser, O.K., Fulton, J.W., A.I.Ch.E.J. (1965) 11 513.

49. Hutchings, J., Carberry, J.J., A.I.Ch.E.J. (1966) 12 30.

50. Schilson, R.E., Amundson, N.R., C.E.S . (1961) 13 226.

51. Liu, Shean-Lin., C.E.S. (1967) 22 871.

52. Bellman, R.E., Kalaba, R.E., "Quasilinearization and Nonlinear boundary-value problems", Elsevier, New York, (1965).

53. Lee, E.S., C.E.S . (1966) 21 183.

54. Coste, J., Rudd, D., Amundson, N.R., Can.J.Chem.Eng., (1961) 39 149.

55. McGinnis, P.H. Jr., C.E.P. Symp.Ser. (1965) 61 2.

56. Butt, J.B., C.E.S. (1966) 21 275.

57. Bruce, G.H., Peaceman, D.W., Rachford, H.H., Rice, J.D., Trans. A.I.M.E. (1953) 198 79.

58. Sehr, R.A., C.E.S. (1958) 9 145.

59. Mischke, R.A., Smith, J.M., I.E.C. Fund., (1962) 1 288.

60. Masamune, S., Smith, J.M., Jl.Chem.&.Eng.Data (1963) 8 54.

61. Beek, J., A.I.Ch.E.J. (1961) 7 337.

62. Carberry, J.J., A.I.Ch.E.J. (1960) 6 460.

63. Tinkler, J.D., Pigford, R.L., C.E.S. (1961) 15 326.

64. Petersen, E.E., C.E.S. (1962) 17 986.

65. Gunn, D.J., C.E.S. (1966) 21 383.

66. Abramowitz, M., Stegun, I.A., Handbook of Mathematical Functions, National Bureau of Standards Appl.Math.Series. 55 (1965)

67. Amundson, N.R., Raymond, L.R., A.I.Ch.E.J. (1965) 11 339.

68. McGreavy, C., Cresswell, D.L., C.E.S. to be published.
69. Hudgins, R.R., C.E.S. (1968) 23 93.
70. Weisz, P.B., Prater, C.D., Adv.Catalysis (1954) 6 143.
71. Petersen, E.E., C.E.S. (1965) 20 587.
72. Schneider, P., Mitschka, P., C.E.S. (1966) 21 455.
73. Schneider, P., Mitschka, P., C.E.S. (1966) 21 726.
74. Petersen, E.E., C.E.S. (1968) 23 94.
75. Liu, Shean-Lin., A.I.Ch.E.Symp. "Advances in Chemical Engineering Digital Computation", Part I, St. Louis, Missouri, February (1968).
76. Liu, Shean-Lin., Amundson, N.R., I.E.C. Fund. (1962) 1 201.
77. Liu, Shean-Lin., Aris, R., Amundson, N.R., I.E.C. Fund. (1963) 2 12.
78. Liu, Shean-Lin., Amundson, N.R., I.E.C. Fund. (1963) 2 183.
79. Lapidus, L., Digital Computation for Chemical Engineers", McGraw-Hill, New York (1962).
80. McGreavy, C., Cresswell, D.L., 4th European Symposium on "Chemical Reaction Engineering", Brussels, Sept. 1968.
81. Phelps, C.E., D.Phil. Thesis, Oxford, (1962).
82. Parker, I.B., Crank, J., The Computer Journal, (1964) 7 163.
83. Keast, P., Mitchell, A.R., The Computer Journal (1966) 9 110.
84. Crank, J., Nicolson, P., Proc.Camb.Phil.Soc., (1947) 43 50.
85. Fox, L., The Computer Journal, (1963) 6 69.
86. Rosenbrock, H.H., Storey, C., "Computational Techniques for Chemical Engineers", Pergamon Press, Oxford, (1966).
87. Fox, L., "Numerical Solution of Ordinary and Partial Differential Equations", Addison-Wesley, London (1962).
88. Laasonen, P., J.Assoc.Comput.Mach. (1958) 5 32.
89. von Rosenberg, D.U., Durrill, P.L., Spencer, E.H., Brit.Chem.E. (1962) 7 186.
90. Froment, G.F., I.E.C. (1967) 59 18.
91. Lee, E.S., C.E.S. (1966) 21 143.
92. Mickley, H.S., Letts, R.W.M., Can.J.Chem.Eng. (1963) 41 273. (1964) 42 21.
93. Douglas, J., Trans.Am.Math.Soc., (1958) 89 484.
94. Douglas, J., Numerische Mathematik, (1962) 4 41.
95. Douglas, J., Jones, B.F., J.S.I.A.M. (1963) 11 195.
96. Rothenberger, B.F., Lapidus, L., A.I.Ch.E.J. (1967) 13 114, 972, 982.
97. Lee, E.S., A.I.Ch.E.J. (1967) 13 1043.
98. Lee, E.S., I.E.C. Fund. (1968) 7 152.
99. Lee, E.S., "Quasilinearization and Invariant Imbedding", Academic Press, New York, in press (1968).

100. Lee, E.S., A.I.Ch.E.J. (1968) 14 490.

101. Saul'yev, V.K., "Integration of Equations of Parabolic Type by the Method of Nets", Macmillan, New York, (1964).

102. Larkin, B.K., Math.Comput. (1964) 18 196.

103. Kalaba, R., J.Math.Mech. (1959) 8 519.

104. Carslaw, M.S., Jaeger, J.C., "Conduction of Heat in Solids", 2nd Edn. Oxford Univ. Press (1960).

105. Allen, E.E., Math. Tables Aids. Comp. (1954) 8 240.

106. Barker, J.J., I.E.C. (1965) 57 43.

107. Fulton, J.W., Ph.D. Thesis, Univ. of Oklahoma, Norman, Oklahoma, (1964).

108. Ramaswami, D., Ph.D. Thesis, Univ. of Wisconsin, Madison, Wisconsin (1961).

109. Rowe, P.N., Claxton, K.T., Lewis, J.B., T.I.C.E. (1965) 43 7.14.

110. Gillespie, B.M., Crandall, E.D., Carberry, J.J., A.I.Ch.E.J. (1968) 14 483.

111. Mixon, F.O., Carberry, J.J., C.E.S. (1960) 13 30.

112. Argo, W.B., Smith, J.M., C.E.P. (1953) 49 443.

113. Yagi, S., Wakao, N., A.I.Ch.E.J. (1959) 5 79.

114. Steisel, N., Butt, J.B., C.E.S. (1967) 22 469.

115. Bird, R.B., Stewart, W.L., Lightfoot, E.N., "Transport Phenomena", Wiley, New York (1960).

116. Scott, D.S., Dullien, F.A.L., A.I.Ch.E.J. (1962) 8 113.

117. Pollard, W.G., Present, R.D., Phys.Rev. (1948) 73 762.

118. Butt, J.B., A.I.Ch.E.J. (1965) 11 106.

119. Luss, D., Amundson, N.R., C.E.S. (1967) 22 253.

120. Kuo, J.C.W., Amundson, N.R., C.E.S. (1967) 22 1185.

121. Gavalas, G.R., C.E.S. (1967) 22 997.

122. Carberry, J.J., I.E.C. (1966) 58 40.

123. Nussey, C., Ph.D. Dissertation, University of Leeds (1968).

124. Paris, J.R., Stevens, W.F., 4th European Symposium on "Chemical Reaction Engineering", Brussels, Sept. 1968.

125. Calderbank, P.H., Caldwell, A., Ross, G., ibid.

126. Thomas, J.M., Thomas, W.J., "Introduction to the principles of heterogeneous catalysis", Academic Press, London (1967).

127. Barkelew, C.H., C.E.P. Symp. Ser. (1959) 55 (25) 37.

128. Bilous, O., Amundson, N.R., A.I.Ch.E.J. (1956) 2 117.

129. Vanderveen, J.W., Luss, D., Amundson, N.R., A.I.Ch.E.J. (1968) 14 636.

130. Luss, D., C.E.S. (1968) 23 1249.

131. Heggs, P.J., Ph.D. Dissertation, University of Leeds (1967).